SEISMIC-WAVE ATTENUATION AND THE STATE OF THE UPPER MANTLE

by

SEAN CARL SOLOMON

B.S., California Institute of Technology
(1966)

SUBMITTED IN

PARTIAL FULFILLMENT

OF THE REQUIREMENTS FOR THE

DEGREE OF DOCTOR OF PHILOSOPHY

at the

MASSACHUSETTS INSTITUTE OF TECHNOLOGY
June, 1971

Signature of Author.....
Department of Earth and Planetary Sciences, February 25, 1971

Certified by.....
Thesis Supervisor

Accepted by.....
Chairman, Departmental Committee on Graduate Students

Abstract

Seismic-wave Attenuation and the state of the upper mantle

by

Sean Carl Solomon

Submitted to the Department of Earth and Planetary Sciences on February 25, 1971 in partial filfillment of the requirements for the degree of Doctor of Philosophy

Seismic-wave attenuation, as represented by the specific quality factor Q, is strongly controlled by the state of the propagation medium. If the dependence of Q on temperature, pressure, and phase in materials of the earth's mantle were known, then measurements of attenuation might be inverted to estimate the mantle's physical properties. In lieu of hard fact, a theory, generalized from the work of Walsh, for attenuation in partially melted rock due to viscous dissipation in the fluid phase has been used to interpret determinations of Q in a region thought to be partially molten: the asthenosphere of western North America. The theory, supported by limited laboratory studies of attenuation in solid-fluid composites, predicts that over at least some portion of the frequency band of seismic waves, attenuation in a partially melted asthenosphere will be large and both velocity and Q will be frequency-dependent. As long as the 'effective' concentration of melt is less than a critical value, the dissipation mechanism is adequately described as one or more thermally-activated relaxation processes; the parameters of the relaxations are related to properties of the melt.

Attenuation in the upper mantle of North America shows a strong regional dependence. Body-wave differential attenuation, obtained using a spectral-ratio technique, is high in western United States, between the Rocky Mountains and the Sierra Nevada - Cascade ranges, and in northeast U.S. In support of the hypothesis that these lateral variations in Q are controlled by temperature and/or partial melting, the differential attenuation of P waves is attributable entirely to losses in shear and is strongly frequency-dependent. Surface-wave attenuation both confirms that most

of the dissipation of seismic waves occurs in the mantle rather than the crust and highlights differences in the Q structure between western and east-central U.S. The lithosphere (high Q) is thinner in the west than east (60 to 90 km versus 100 to 120 km) and the asthenosphere (low Q) is more pronounced in the west (Q, at the frequencies of surface waves, is lower in the asthenosphere of western than in east-central U.S. by a factor of 3).

A relaxation model of Q^{-1}, based on the theory for attenuation in partially melted rock, is proposed for the mantle of western North America. The asthenosphere (or low-Q zone) is 300 km thick in the model and must be vertically inhomogeneous. The model is consistent with a wide assortment of attenuation and velocity data, in all spanning approximately three decades in frequency. Estimates of the viscosity and volume concentration of melt may be made from the relaxation parameters. Further, if lateral changes in these parameters, determined from the differential attenuation and travel-time delays of P and S waves, are attributed to temperature variations, then these temperature differences in the asthenosphere may be calculated. The highest temperatures, appropriate to a depth of several hundred kilometers, determined in this fashion are beneath the Rocky Mountain and Pacific Border regions.

Thesis Supervisor: M. Nafi Toksöz

Title: Associate Professor of Geophysics

Acknowledgements

This work is the product of roughly two years of thought, much of which was shaped by the probing questions and helpful suggestions of others. I owe particular thanks to Professor M. Nafi Toksöz, who put up with my cynicism and bad jokes and whose ideas and comments both clarified my thinking and improved this manuscript. Also constructive were discussions with Drs. Christoper Goetze, David Jackson, Bruce Julian, Amos Nur, and Joseph Walsh. I appreciate the assistance of David Johnston, who performed some of the selection, digitization, and processing of the surface waves used for measuring attenuation. Lastly I extend especial gratitude to my wife Nancy, whose patience, understanding, and cheer lasted considerably longer than mine.

During the course of the research reported in this work, I was fortunate to be a Fellow of the Fannie and John Hertz Foundation, to whom I am deeply grateful.

This investigation was supported by the Advanced Research Projects Agency and monitored by the Air Force Office of Scientific Research under contract AF 49(638)-1632.

Table of Contents

Page

Page

List of Figures

Page

Page

List of Tables

Chapter 1. Introduction and Review

The materials that constitute the earth are not perfectly elastic. This is fortunate in many ways, for the earth's anelasticity can be put to good use. Such anelastic properties as seismic attenuation, effective shear viscosity, and yield strength under shearing stress, while notoriously difficult to measure accurately, are highly sensitive to temperature, microstructure, and the presence of fluid phases. Knowledge of how these properties vary within the crust and upper mantle would thus greatly improve our understanding of the interior state and tectonic history of the earth.

Toward such an end, the present work reports a study of the attenuation of seismic waves in the upper mantle of North America, and is concerned in particular with the magnitude and causes of regional variation of this attenuation. While the accurate determination of seismic absorption in the earth is of considerable importance in itself to real-earth problems of wave propagation such as the study of earthquake source-mechanisms and the discrimination of earthquakes from underground nuclear explosions, we seek the answers to more basic questions. By relating measured values of attenuation to plausible theoretical models for dissipation, we shall test the hypothesis of partial melting in the upper mantle, estimate many of the properties such a partial melt must have, and deduce how

these properties (including temperature) vary laterally beneath North America.

There are several measures of attenuation commonly used in seismology. In a linear, perfectly elastic medium, the amplitude of a stress wave propagating in one dimension (x) is proportional to exp [i(kx- ωt)], where ω is the angular frequency, k is the wave number, and t is time. In a linearly, viscoelastic medium, the wave number of a travelling wave may be considered complex, so that the wave amplitude is proportional to exp [-k*x + i (kx- ωt)]. The imaginary part of the wave number, k*, is called the (spatial) attenuation coefficient. If the medium is non-dispersive and losses are small ($k^* \ll k$), then the attenuation coefficient obeys the relation

$$k^* = \frac{\omega}{2Qv} = \frac{\pi f}{Qv} \qquad (1.1)$$

where Q is the well-known dimensionless quality factor (2π /Q equals the fractional elastic energy dissipated per cycle), v is the wave velocity in the medium, and f is the frequency. When the medium is heterogeneous, we might wish to speak only of the <u>total</u> attenuation of the wave amplitude along the entire propagation-path. A convenient parameter for such purposes is the quantity

$$t^* = \frac{1}{f} \int_{\substack{\text{entire} \\ \text{path}}} k^*(x)\, dx. \qquad (1.2)$$

The notation t* is derived from the formal similarity of (1.2) to the definition of travel time. Note that if k* is proportional to frequency then t* is a constant. Throughout the discussion to follow we shall have recourse to use each of the three indices of attenuation mentioned above: k*, Q^{-1} and t*.

Studies of the variation, particularly laterally, of Q in the earth provided some of the stimulus to the theories of the new global tectonics (Isacks et al., 1968; and many others). These theories dictate that lithospheric plates, several tens of kilometers thick, slide over a much weaker asthenosphere in response to yet ill-defined forces. The boundary between lithosphere and asthenosphere is often estimated by the different rates at which seismic-wave amplitudes attenuate in the two regions: Q in the asthenosphere is a factor of at least ten less than in the cooler, presumably stronger lithosphere. The interface between the high-Q lithosphere and the low-Q asthenosphere, while usually horizontal, is more complicated in those regions where the lithosphere is thought to descend deep into the mantle.

Such regions, principally island arcs, were sites of the earliest observations of the lateral variation of Q.

Katsumata (1960) and Utsu (1966b) in Japan concluded that the amplitudes of seismic waves which propagate along the zone of deep earthquakes beneath the Japanese arc attenuate less rapidly than do the amplitudes of waves that travel through the neighboring mantle. Interest in the Q structure of island arcs was stimulated in this country by the work of Oliver and Isacks (1967), who introduced the concept of a downthrust lithosphere for the Tongan arc. To date, many additional details of the three-dimensional Q distribution beneath island-arc regions have been established for Japan (Wadati and Hirono, 1956; Asada and Takano, 1963; Tsujiura, 1966; Utsu, 1967; Nagamune et al., 1967; Utsu and Okada, 1968; Wadati et al., 1969; Kanamori, 1970b), Tonga (Mitronovas et al., 1969; Barazangi and Isacks, 1970), New Zealand (Mooney, 1970), Kuril-Kamchatka (Gorshkov, 1958; Fedotov, 1963; Fedotov and Boldyrev, 1969), South America (Sumner, 1967; Sacks, 1969), Novaya Zemlya, the Aleutians, and New Guinea (Tsujiura, 1969).

Recently Molnar and Oliver (1969) qualitatively characterized, on the basis of efficiency of S_n wave propagation, upper-mantle attenuation over much of the earth's surface. In general, they found that S_n propagates efficiently across shields, deep ocean basins and other stable regions of the earth, but inefficiently across mid-ocean ridges and the concave sides of island-arcs, both of which represent discontinuities

in the high-Q lithosphere.

Less pronounced, but no less important, lateral variations of Q occur within the lithosphere and asthenosphere. The best documented of these regional differences in crustal and upper-mantle Q are in North America. Romney et al. (1962) noticed that P_n and L_g waves from the GNOME explosion near Carlsbad, New Mexico, appeared to attenuate more rapidly along paths to the west of the test site than along paths to the east. Ichikawa and Basham (1965) and Utsu (1966a), from spectral amplitude curves in the frequency range 0.5 to 3 Hz, have suggested that the P-wave absorption is greater beneath Resolute, Canada, than beneath neighboring seismograph stations in the Canadian Arctic. Cleary (1967) showed that the station amplitude A/T (A is the amplitude of the first peak and T is the wave period), after correcting for distance and source, shows considerable lateral variation for 1-second P waves recorded at North American stations. A/T is low beneath mountainous regions and in the western U.S. in general; A/T is particularly high in the northern Great Plains. Sutton et al. (1967) measured the apparent Q of short period P_g and L_g phases for a dozen different paths in the United States from the spacing of contours in the seismic-energy radiation-patterns from several explosions and earthquakes. Their determinations of Q, appropriate for the crust and that portion of the mantle above the low velocity zone, ranged from near 200

in the western U.S. to 1000 in east-central U.S. These values include large contributions from scattering and must be assigned large uncertainties due to their assumption of symmetrical radiation-patterns at the sources and to their difficulty in separating modes. Molnar and Oliver (1969) found S_n attenuation high west of the Rocky mountains and relatively low attenuation to the east. McGinley and Anderson (1969), from differences in the unified magnitude and the ratio of S amplitude to P amplitude at several stations in the U.S., concluded that upper mantle attenuation beneath the Basin and Range province is higher than for other areas.

Isolated estimates of attenuation for short-period P waves propagating in the shallow mantle beneath North America suggest that Q may be laterally inhomogeneous. For P waves recorded 200 to 350 km from underwater explosions in the Gulf of Maine, Frantti (1965) found Q_α increased from 104 at 2 Hz to 252 at 5 Hz and 510 at 10 Hz. In the Lake Superior region, Dorman (1968) concluded $Q_\alpha = 475$ for reflected P waves, bottoming at a depth of about 126 km, in the frequency range 1 to 5.5 Hz. Julian (1970) concluded that Q must be greater than 3000 for P waves of frequency 2 Hz propagating in the upper 180 km of the Canadian shield between Lake Superior and Yellowknife, N.W.T. Roller and Jackson (1966) noted the "extremely low" attenuation of P waves, roughly in the frequency range 1-3 Hz, which had propagated through the

upper mantle of the Central Lowlands and Great Plains, compared with the attenuation of P_n waves in the Basin and Range province. From an examination of refracted P waves observed at distances of 100 to 600 km from the GNOME and SHOAL nuclear explosions, Long and Berg (1969) estimated that for the uppermost mantle of eastern New Mexico $Q_\alpha = 169$ at 5 Hz, while east of the Nevada Test Site Q_α at the top of the mantle equals 116 at 4 Hz. Archambeau et al. (1969), after studying P_n amplitudes from the BILBY and SHOAL events, obtained somewhat higher Q values: in the frequency range 0.75 to 1.5 Hz, Q_α in the crust equals 1000, while Q_α in the uppermost mantle increases with frequency from 300 at $f \simeq .875$ Hz to 400 at $f \simeq 1.25$ Hz. Johnson and Couch (1970) obtained a Q_α of 383 ± 41 at a frequency of 3 Hz for P_n waves beneath the northern Cascade range in Washington and British Columbia. In southern Alberta, Q_α in the frequency range 5 to 25 Hz is about 300 (with considerable fine structure) in the uppermost 2 km (sediments) of crust and 1500 (increasing with depth) in the lower 40 km of crust (Clowes and Kanesewich, 1970).

It appears likely, for reasons discussed in the next chapter, that low values of Q in the upper mantle are associated with partial melting in the asthenosphere. It is therefore imperative, if measured values of Q are to be correctly interpreted, that we understand the

various physical processes which contribute to the absorption of elastic waves in partially molten systems. These processes are considered, from both theoretical and experimental viewpoints, in Chapter 2. It is concluded that viscous damping in thin films of melt is most likely the dominant mechanism of seismic attenuation in a partially melted mantle. This mechanism may be characterized as a relaxation process; all losses are associated with the shearing component of stress and both attenuation and shear modulus are functions of wave frequency.

One approach to determining the lateral variation of Q^{-1} in the North American mantle is developed in Chapter 3. The P- or S-wave 'differential attenuation', obtained from a suitably corrected spectral ratio, is a rough measure of vertically averaged Q^{-1} in the upper mantle. In North America, the differential attenuation of long-period P and S waves shows systematic regional variations, with particularly high attenuation in the western United States between the Rocky mountains and the Sierra Nevada-Cascade ranges. Comparison both of the relative magnitudes of P and S differential attenuation and of relative P-wave amplitudes in two distinct frequency bands lends considerable support to the hypothesis that at least the laterally varying component of attenuation in the upper mantle is controlled by partial melting in the asthenosphere.

An independent measure of Q^{-1} in the upper mantle is provided by the attenuation of surface waves, considered in Chapter 4. Surface-wave absorption, though not particularly sensitive to detailed lateral changes in structure, is more readily interpreted in terms of the distribution of Q^{-1} with depth than is body-wave attenuation. In particular, the much greater absorption of surface waves of period 40-80 sec in western United States than in east-central United States implies anomalously low Q (in that period range) at depths as shallow as 60 to 80 km in the upper mantle of western North America. Several quite different models of Q^{-1} can explain the observed surface-wave attenuation to within the rather large measurement-error. Thus the Q^{-1} structure, even within a single region, cannot be resolved by surface-wave data alone.

An integration of all available information to deduce a simple, plausible model of attenuation for western North America is made in Chapter 5. The proposed model is based on the hypothesis that the asthenosphere is partially melted. Attenuation and velocity measurements of various sorts, spanning a frequency band roughly three decades in width, are all approximately satisfied. From the considerations of Chapter 2, the parameters of the model can give some idea of the physical properties of the partially melted upper-mantle. Further, the lateral variation of attenuation reported in Chapter 3 may be

intepreted in terms of laterally varying temperature and melt concentration in the asthenosphere.

Those of you, faithful readers, who at this point are too impatient to pore over fascinating detail may skip immediately to Chapter 6, in which all of the important conclusions of this work are summarized. Particular emphasis is placed on suggestions for testing, by further measurement, the several hypotheses made in earlier chapters and for extending some of the techniques used to other regions and to other problems.

Chapter 2. On Partial Melting and Q

If it were known how such variables as pressure, temperature, composition, and phase affect the elasticity and anelasticity of possible mantle-materials, then complete specification of seismic velocity and attenuation in the earth could (in principle) determine the physical and chemical state of the mantle. Neither the elastic and anelastic properties in the earth nor their simultaneous dependence on all of the independent variables are sufficiently well-determined for such an interpretation yet to be made. Fortunately, however, most of the attenuation of seismic waves appears to take place in the asthenosphere, where it is thought the mantle may be partially melted. Thus if we knew the form and controlling parameters for attenuation in a partial melt, then measurement of attenuation in the mantle could be used both to test the hypothesis of partial melting and to estimate some of the properties of the melt.

For our purposes, a partial melt consists of a solid matrix which contains a small but non-zero fraction (by mass and by volume) of a fluid (i.e. incapable of sustaining shear stresses in an equilibrium state) phase which is in chemical equilibrium with the solid phase or phases. It will be assumed that the melt forms in thin films at the boundaries between solid grains. While such a melt configuration has been observed for granites melted in

the presence of water and subjected to effective confining pressures of about a kilobar (Unger, 1967), it is not known to what degree partial melt will 'wet' the grain boundaries in mantle rocks. The wetting properties of the melt depend upon the (unknown) relative surface energies of the solid and liquid phases (Smith, 1948).

In this chapter, after a quick review of the geophysical evidence pertinent to the existence of partial melting in the upper mantle, we shall examine the mechanical behavior (in particular the attenuation) to be expected of partially molten rock, as indicated by both experimental and theoretical considerations. The ultimate goal, to be pursued in later chapters, is the specification of the physical state of the asthenosphere from measurements of elastic and anelastic properties of the upper mantle.

2.1 Partial melting in the asthenosphere

What governs the strength of the asthenosphere? Why is Q in the asthenosphere lower than in the mantle immediately above or below? Current geophysical opinion leans heavily toward the opinion that the asthenosphere, defined by low seismic velocities, low Q, or both, is partially molten. In the context of sea-floor spreading, the top of a partially melted asthenosphere is thought to serve as a lubricated surface over which lithospheric plates may readily ride (Press, 1959; and others) and as the source of magma-filled cracks which might provide a driving mechanism for symmetrical spreading at mid-ocean ridges (Lliboutry, 1969). Certainly some melt exists in the mantle; there must be a source of basaltic magma beneath volcanoes and ridges. Whether there is a laterally continuous zone of partial melting in the upper mantle of oceanic and tectonically active continental regions is a question currently debated. The arguments in favor of such a zone, however, are fairly persuasive.

The low-velocity layer, which for shear waves appears to be present in some form throughout the entire earth, has for many years been regarded by seismologists as implying temperatures near the solidus at depths between about 50 and 150 km in the upper mantle (e.g. Gutenberg, 1945a; Press, 1959). Shimozuru (1963a,b) suggested that oblate-spheroidal pockets of melt, with minor axis vertical, could

explain the low-velocity zone and the phase velocities of surface waves in tectonic regions as well as serve as the source of rock magma. Anderson and Sammis (1970) combined published velocity models for the upper mantle with ultrasonic measurements of the temperature and pressure derivatives of velocity in laboratory minerals to conclude that temperature alone cannot produce the observed low-velocity zones in oceanic and tectonic regions. They further argued that possible phase changes cannot account for the low velocities; nor is a compositional change likely the complete answer, particularly in view of the low Q associated with the low-velocity zone (cf. Birch, 1970). If the velocities in the upper mantle are assumed to be a function of temperature and pressure only, then (Anderson and Sammis, 1970): (1) the temperature gradient in the low-velocity zone required by P-wave velocities is greater than that required by S-wave data; (2) the temperature gradient required in the low-velocity zone is a factor of two greater than the gradient in the overlying 'lid'; (3) "unacceptably high" heat flow is required through the low-velocity zone; and (4) computed temperature-depth curves intersect the dry-pyrolite solidus at depths less than 100 km. In short, partial melting of mantle material, probably in the presence of small amounts of free water (Kushiro et al., 1968; Lambert and Wylie, 1968; Ringwood, 1969; Anderson and Sammis, 1970), provides a simple and consistent explanation of the region of low seismic

velocities between 50 and 150 km depth. Lambert and Wylie (1970) have concluded, in fact, that if there is any water present in the upper mantle, partial melting is a necessary consequence.

The tectonically active region of western North America has attracted particular attention as an area where partial melting is likely in the shallow mantle. From the relative magnitudes of P- and S-wave travel time anomalies in North America, Hales and Doyle (1967) concluded that the shear modulus in the upper mantle varies laterally while the bulk modulus remains nearly constant. Their interpretation was that upper-mantle temperatures beneath the western U.S. must be near the melting point. In an effort to explain a decrease in the electrical conductivity at a depth of 40 to 55 km beneath the North American Cordillera, Caner et al. (1967) suggested (with no particular enthusiasm) that partial melting may begin at such depths. Temperature models calculated (with some initial prejudice) by Roy et al. (1970) from heat-flow observations indicated partial melting in the shallow mantle beneath the Basin and Range province and the Northern and Southern Rocky Mountains.

We shall adopt as a working hypothesis in all discussion to follow that large portions of the upper mantle in tectonic regions, and in western North America in particular, are partially melted and that the depth at which melting begins constitutes the top of the asthenosphere.

2.2 Attenuation in a partial melt: the Walsh model

If the occurrence of partial melting in the upper mantle beneath tectonic regions is accepted, it is then logical to attempt to determine the physical properties, which in general vary both laterally and with depth, of the fluid phase. Such quantities as melt concentration and viscosity not only yield information on the temperatures and composition of the upper mantle, but also serve as vital input to the problems of magma generation and mantle dynamics.

The most detailed knowledge of the earth's deep interior has traditionally come from seismology. Can the measured velocity and attenuation of seismic waves in the low-velocity zone be related to properties of a melt phase? This clearly cannot be done with confidence until laboratory measurements of velocity and attenuation, at seismic frequencies and strains, have been made on partially molten mantle-rocks (or likely candidates for mantle rocks). Such measurements have not yet been performed. As an alternative, somewhat inferior, approach, we can formulate a theory for the elastic and anelastic behavior of two-phase media, test the theory against the limited laboratory-data on velocity and attenuation in solid-liquid composites, and choose <u>reasonable</u> values for the physical parameters of partially molten rock such that all the seismic observations are satisfied.

A theoretical model for attenuation of a sinusoidally varying elastic wave due to viscous dissipation in partially melted material, in which the melt appears in thin films along grain boundaries, has been developed in some detail by Walsh (1968, 1969). As this model has had considerable success in qualitatively describing the results of recent elastic-wave velocity and attenuation measurements in two-phse (or two-component) materials designed to approximate partially molten rock (Nur and Simmons, 1969; Walsh, 1969; Goetze, 1969; Nur, 1971; Anderson and Spetzler, 1970), we shall use Walsh's theory a starting point in our considerations.

A useful concept in the discussion to follow is that of stress relaxation in a standard linear solid (Zener, 1948), which is a material obeying the most general linear, homogeneous relation among stress σ, strain ε, and their first time derivatives. Ignoring the tensor character of stress and strain (or, equivalently, considering only one-dimensional problems), in a standard linear solid

$$\sigma + \tau_\varepsilon \frac{d\sigma}{dt} = M_R \left(\varepsilon + \tau_\sigma \frac{d\varepsilon}{dt} \right) \qquad (2.1)$$

where τ_ε and τ_σ are, respectively, the times of relaxation of stress under constant strain and of strain under constant stress, and M_R is an elastic modulus.

Figure 2.1 Modulus and attenuation, standard linear solid. Both M and Q^{-1} (normalized by the unrelaxed modulus M_U and the minimum Q, respectively) depend strongly on angular frequency ω . A 'relaxation' occurs when $\omega\tau = 1$, where τ is the relaxation time.

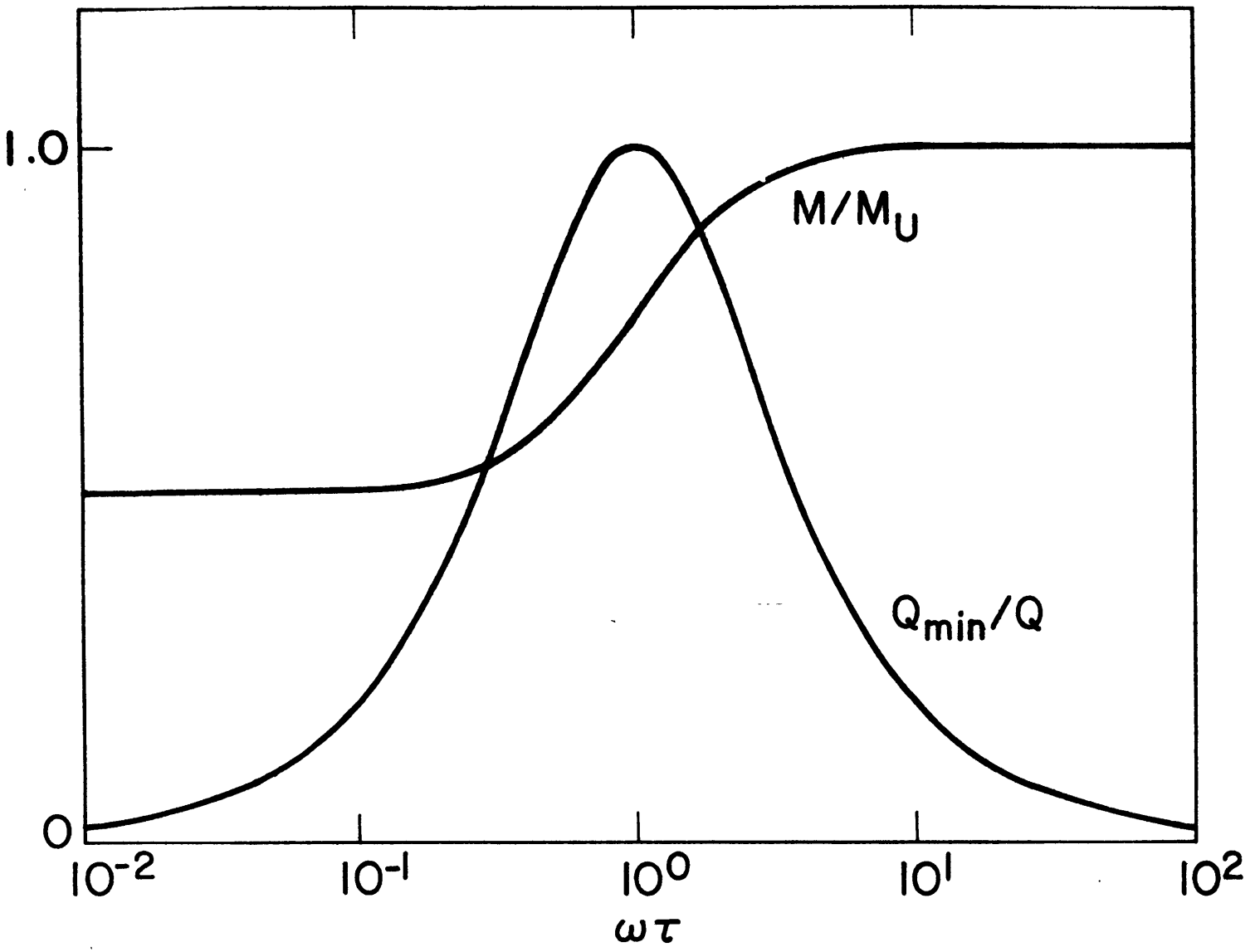
1.0
0
M/M_U
Q_min/Q
10^-2
10^-1
10^0
10^1
10^2
ωτ

When stress and strain are periodic (with period $2\pi / \omega$) in time, the effective modulus is complex:

$$\tilde{M} = \frac{1 + i\omega\tau_\sigma}{1 + i\omega\tau_\varepsilon} M_R \qquad (2.2)$$

Then the real modulus, which governs the rate of energy propagation, and the attenuation (when losses are small) are given by Zener (1948)

$$M = M_U \left[1 - \frac{\Delta M}{1 + (\omega\tau)^2} \right] \qquad (2.3)$$

$$Q^{-1} = \frac{\Delta M}{(1-\Delta M)^{1/2}} \frac{\omega\tau}{1 + (\omega\tau)^2}$$

where $\Delta M = 1 - \frac{M_R}{M_U}$, $M_U = M_R \tau_\sigma / \tau_\varepsilon$ and $\tau = (\tau_\sigma \tau_\varepsilon)^{1/2}$. The dependence on frequency of both M and Q^{-1} is shown in Figure 2.1. From the figure, and by inspection of equations (2.3), it may be seen that for large frequencies ($\omega\tau >> 1$) the modulus is equal to M_U and Q^{-1} is negligibly small. At frequencies such that $\omega\tau$ is comparable to or less than unity, a portion of the stress 'relaxes' and M, the ratio of stress to that part of the strain in phase with the stress, is reduced. (Clearly $M_U \leq M_R$ for a physically realizable material.) In addition, at $\omega\tau = 1$ there is a 'peak' in the attenuation. For small frequencies ($\omega\tau << 1$), $M = M_R$. Generally, M_U and M_R are called, respectively, the

unrelaxed and relaxed elastic modulus and ΔM is sometimes called the relaxation strength or modulus defect. (Often the latter terms are used for the quantity $\frac{M_U}{M_R} - 1$.) For convenience, we introduce the following notation to be used in all subsequent discussion: $Rx(\Delta M, \tau)$ shall represent the relaxation process described by relations (2.3). The two quantities ΔM and τ completely describe the behavior of M (normalized to M_U) and Q^{-1} as functions of frequency.

2.2.1 Walsh's formulation

The Walsh model of attenuation in a partial melt is based on the following important assumptions: (i) the fluid phase is confined to a set of isolated, randomly oriented, non-interacting, oblate-spheriodal (penny-shaped) inclusions of uniform aspect-ratio; (ii) the matrix, or solid phase, is isotropic and linearly elastic, while the liquid is elastic in dilatation and Newtonian viscous in shear; (iii) wave lengths are large compared to the dimensions of the liquid inclusions; and (iv)

$$c,\ \alpha,\ Q^{-1},\ \frac{\omega\mu}{\mu} \ll 1$$

where c is the volume concentration of melt, α is the aspect ratio (ratio of minor axis to major axis) of the liquid inclusion, Q^{-1} is the internal friction or specific

attenuation factor, ω is the angular frequency, η is the dynamic shear viscosity of the fluid, and μ is the effective shear modulus of the composite.

Using the theories of Eshelby (1957) and Wu (1966) for the effective elastic moduli of a body with ellipsoidal inclusions, together with the viscoelastic correspondence principle, Walsh demonstrated that the dynamic response of a partially melted material is completely specified by the bulk and shear moduli (K and μ , respectively) of the solid and liquid phases and by the quantities ω , c, η , and α . At frequencies less than a critical frequency, attenuation due to the hydrostatic component of stress is negligible (as long as bulk moduli of solid and liquid are not too different) and the response of the medium to shearing stress is that of a standard linear solid; i.e. a relaxation Rx ($\Delta\mu$, τ), where

$$\Delta\mu = \frac{A}{1 + A}$$

$$\tau = \frac{4\eta}{3\pi\alpha\mu_1} \frac{3K_1 + 4\mu_1}{3K_1 + 2\mu_1} \frac{1}{(1+A)^{1/2}} \qquad (2.4)$$

$$A = \frac{8}{15\pi} \frac{c}{\alpha} \frac{3K_1 + 4\mu_1}{3K_1 + 2\mu_1}$$

The subscript 1 denotes the solid matrix; the subscript 2 is used below for the fluid inclusion. Note that the shear modulus and attenuation do not depend directly on the melt concentration, but rather on a much larger 'effective

concentration' c/α which, if the major axis of the fluid inclusion is held fixed, is proportional to the density of melting sites (Walsh, 1969). When the attenuation is small ($A<<1$), then $\Delta\mu$ is proportional to c/α and τ is proportional to η/α. If α and A depend only weakly on temperature and if $\eta = \eta_o e^{H/RT}$, where H is a constant (with units of energy) and R is the gas constant, then (2.3) and (2.4) are of the form of a 'thermally-activated relaxation process'. From (2.4), it is clear that measurement of velocity (i.e. modulus) and attenuation in a partial melt can never uniquely determine the three quantities c, η, and α unless one of the three is known a priori.

To test both Walsh's and any competing theory, we shall compare predicted with observed behavior for two liquid-solid composites which are thought to be fair models of partially molten rock: (i) granite saturated with glycerol (Nur and Simmons, 1969) and (ii) ice-brine (Spetzler and Anderson, 1968). The first test is included because the experimenters succeeded in measuring velocity and attenuation for shear and compressional waves over a wide range of $\omega\mu$. The second test is the more crucial for whatever theory we adopt for partial melting in rock, inasmuch as the careful work of Spetzler and Anderson constitutes perhaps the most complete observations to date of velocity and attenuation in a system undergoing partial melting.

2.2.2 Granite-Glycerol

In Figure 2.2 is plotted the shear modulus measured by Nur and Simmons (1969) for Barre granite with glycerol-filled microcracks; log η is the ordinate. Velocity was measured over the temperature range -80 to 160°C; then ignoring the slight dependence of elastic moduli on temperature, the transformation

$$\eta_{fluid} = F(1/T)$$

where F is known from experiment, allows μ to be calculated as a function of fluid viscosity. It is important to note that, since in Walsh's theory viscosity and frequency appear only as powers of $\omega\eta$, varying η with ω fixed is equivalent to changing frequency with viscosity held constant.

Let us now apply Walsh's (1969) theory to the granite-glycerol experiment. The elastic moduli of solid and liquid components, the total concentration of liquid, fluid viscosity and frequency are all known (see Table 2.1); the parameter α is the only unknown. Suppose all cracks have the same aspect ratio. Following Nur and Simmons we choose α so as to match the relaxation peak in attenuation and the inflection point in the modulus curve at $\log \mu \simeq -0.5$. This gives $\alpha = 4 \times 10^{-9}$. With α thus determined, equations (1) of Walsh (1969) give

Figure 2.2 Shear modulus, granite-glycerol system, versus viscosity of glycerol. Measured values (circles) are those of Nur and Simmons (1969). Theoretical models, fit to various features of the data, are those of the Walsh theory (dashed line) and the generalized Walsh theory (solid line). Parameters used in the fit of these models are given in Table 2.1.

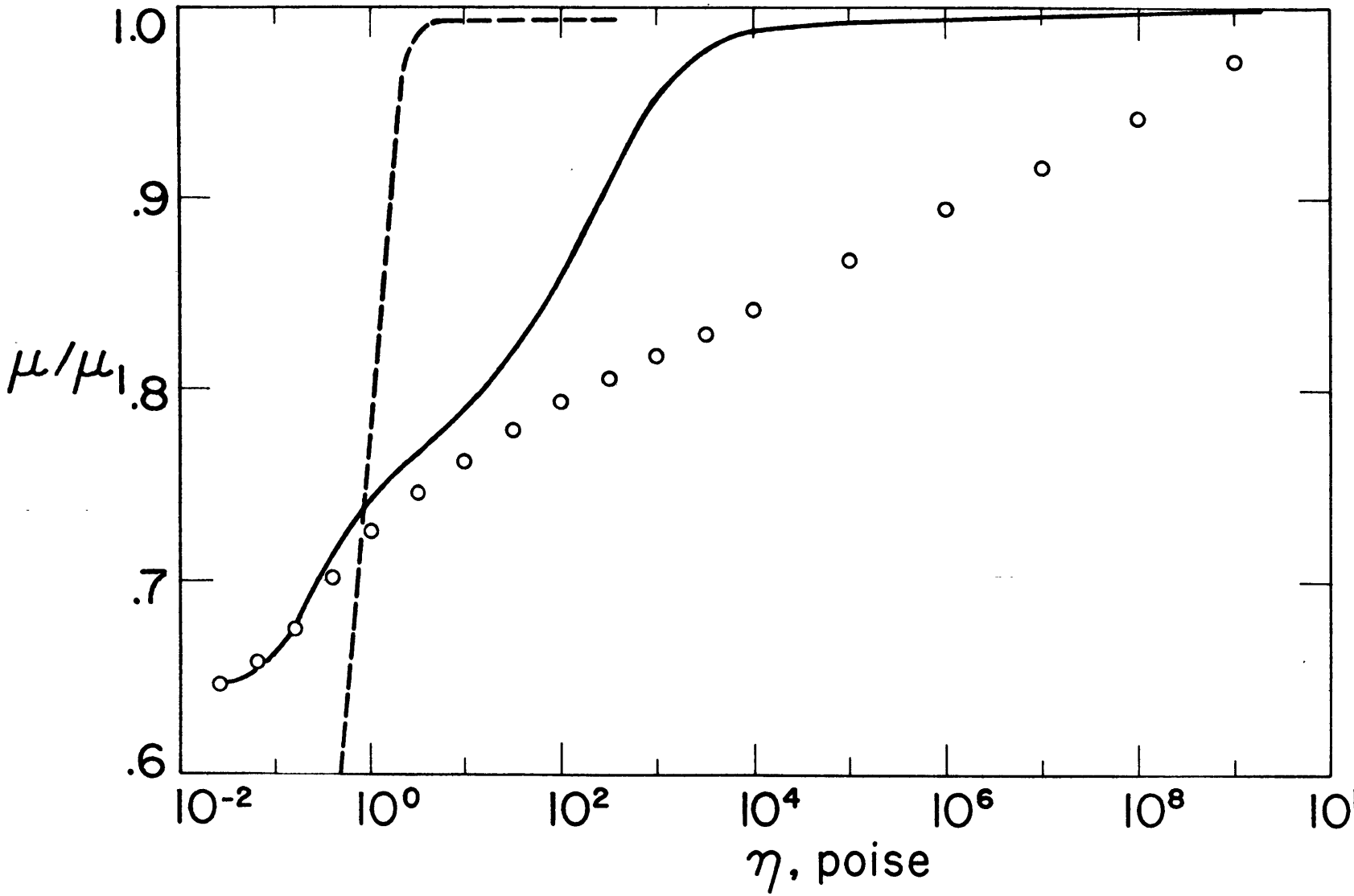
1.0
.9
.8
.7
.6
μ/μ1
10-2
100
102
104
106
108
1010
η, poise

Table 2.1. Parameters used in fitting partial-melt models to granite-glycerol experiment

1. Assumed parameters

Solid (granite)

K_1, 10^4 bar	44.0	(T=25°C)
$\frac{1}{K_1}\frac{dK_1}{dT}$, 10^{-4} °C^{-1}	2.2[a]	
μ_1, 10^4 bar	28.5	(T=25°C)
$\frac{1}{\mu_1}\frac{d\mu_1}{dT}$, 10^{-4} °C^{-1}	1.1[b]	

Fluid (glycerol)

c (total	.006
c ('cracks' only)	.003

2. Parameters derived from fit of theoretical models to data

i) Walsh model (roughly a single relaxation)

K_2, 10^4 bar	3.93[c]	(T≈80°C)
μ, poise	.32	(T≈80°C)
α	4×10^{-9}	
τ, 10^{-7} sec	3.2	
$\Delta\mu$	1.00	

ii) Generalized Walsh model (roughly a distribution of relaxations)

$$K_2 = K_R + \frac{i\omega\eta}{1 + i\omega\eta/(K_U - K_R)}$$

given in Nur and Simmons (1969)

$$\mu_2 = \frac{i\omega\eta}{1 + i\omega\eta/\mu_U}$$

K_R, 10^4 bar[c]	4.94-.012T	[T] = °C
K_U, 10^4 bar[c]	8.41-.011T	
μ_U, 10^4 bar[c]	2.72-.018T	

Distribution of inclusion shapes

c(α)	α
2×10^{-3}	1
1×10^{-3}	1×10^{-1}
2.2×10^{-3}	1×10^{-2}
5×10^{-4}	2×10^{-3}
2.5×10^{-4}	1×10^{-3}
4.5×10^{-5}	2×10^{-4}
4×10^{-6}	2×10^{-5}
1×10^{-6}	2×10^{-6}

All assumed values are taken from Nur and Simmons (1969) unless otherwise noted.

[a] From Birch (1943) and Skinner (1966)

[b] From Birch (1966)

[c] Piccirelli and Litovitz (1957)

$\mu(\eta)$ and $Q_\mu^{-1}(\eta)$, if parameters other than η are held constant. The shear modulus calculated in this manner is plotted in Figure 2.2.

It is immediately apparent that μ determined in the above fashion from Walsh's theory does not give a satisfactory fit to observation. In fact we find the model inadequate on three counts:

(1) The predicted aspect ratio is too small. If the major axis of fluid inclusions were assumed to equal the upper limit of 7 mm required by the quasi-homogeneous assumption (iii), then an aspect ratio of 4×10^{-9} gives for the crack thickness (minor axis) the absurd value of 3 Å. Even if the major axis were set equal to the sample thickness (3 cm), we would conclude that the crack thickness is of the same order as the dimensions of a glycerol molecule. It is unreasonable to imagine that a rock with such cracks could be 'saturated'. From the increase of compressional velocity with pressure in Barre granite (Birch, 1960), Nur and Simmons (1969) estimated the average aspect ratio of cracks in their sample to be about 10^{-4}.

(2) The relaxation strength is too large. The theory gives a ratio of unrelaxed (high-frequency) to relaxed (low-frequency) modulus of 10^5, and predicts $Q^{-1} = 200$ at the relaxation peak. Such a value for the internal friction clearly violates the assumption (iv) that $Q^{-1} \ll 1$.

(3) The theory fails to account for the marked increase of μ with log η (or $^1/T$) which is superimposed on the relaxation near $\eta = 10^{-1}$ poise. This increase is more rapid than that for the dry rock (Nur and Simmons, 1969).

Many of the above objections disappear if the cracks are not uniform in shape and if only a small volume-fraction of cracks of small aspect-ratio contribute to the attenuation peak. In that case α need be no smaller than about 10^{-6}. Several of the other assumptions implicit in the Walsh scheme, however, are inappropriate for the granite-glycerol experiment: (a) the effective fluid concentration is sufficiently great that account should be made of the interaction between inclusions; (b) glycerol undergoes both dilatational and shear relaxations when $\omega\eta$ becomes greater than about 10^{10} c.g.s. (Piccirelli and Litovitz, 1957); (c) $\omega\eta/\mu$ is obviously not $\ll 1$ for $\eta > 10^4$ poise. A more general model which takes these considerations into account is developed in a later section.

2.2.3 Ice-brine

Spetzler and Anderson (1968) measured the frequency and half-power width (attenuation) of longitudinal- and shear-mode resonance peaks, as functions of temperature, for cylinders of the mixture H_2O plus NaCl-$2H_2O$. The system is partially molten at temperatures above -21.3°C.

In Figure 2.3 are shown their results (open symbols) at three temperatures: the partially relaxed modulus and the attenuation for the first three harmonics in the longitudinal mode for H_2O plus 2% NaCl by weight. As given in Figure 2.3, attenuation (Q^{-1}) in the partial melt was 'normalized' by subtracting from it the Q^{-1} observed in the solid prior to melting. Such normalized values of Q^{-1}, should represent only that part of the total attenuation which is associated with the melting phenomenon.

The data in Figure 2.3 are adequately described by a single relaxation at each temperature. We assume that the elastic constants of the solid and fluid are known, as well as the total concentration of fluid (Table 2.2). Note that because of the marked anisotropy of the ice-brine rods (Spetzler and Anderson, 1968; Anderson and Spetzler, 1970), we must assume values for K_1 and K_2 rather than obtain them from the observed shear-wave and longitudinal-wave velocities. The fluid viscosity and melt-pocket aspect-ratio (assumed uniform) are considered unknown.

The parameters η and α in Walsh's (1969) theory (roughly equivalent to a single relaxation) may then be varied until a fit to the data, at each of the three temperatures, is achieved. The values of η and α necessary for such fits are given in Table 2.2. The attenuation and Young's modulus, both functions of

Figure 2.3 Attenuation and modulus, partially melted H_2O-2% NaCl. Data (open symbols) are from Spetzler and Anderson (1968): circles, T=-18°C; triangles, T=-14°C; squares, T=-8°C. Theoretical models, fit to the data at each temperature, are those of the Walsh (1969) theory (dashed lines) and the generalized Walsh theory (solid lines). Parameters used in the fit of these models are given in Table 2.2 (a) 100/Q, longitudinal mode, versus frequency. (b) Young's modulus, normalized by the modulus of the (sub-solidus) solid, versus frequency.

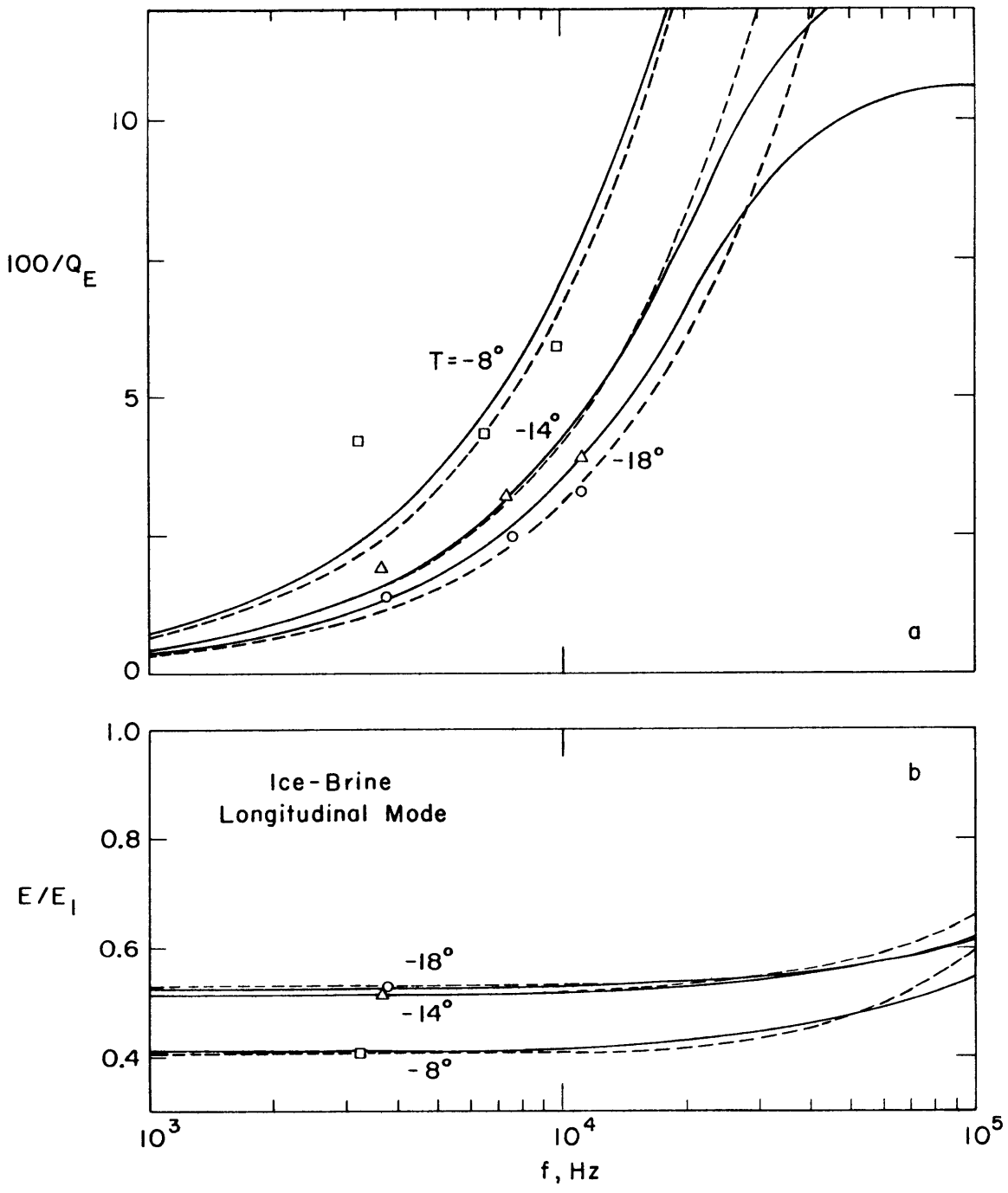
10
5
0
100/Q_E
T=-8°
-14°
-18°
a
1.0
0.8
0.6
0.4
E/E_1
Ice-Brine
Longitudinal Mode
b
-18°
-14°
-8°
10^3
10^4
10^5
f, Hz

Table 2.2 Parameters used in fitting partial-melt models to ice-brine system (H_2O-2% NaCl, longitudinal mode)

Temperature, ^oC	-18	-14	-8
1. Assumed parameters			
Solid (ice)			
K_1, 10^4 bar	8.33[a]	8.33[a]	8.33[a]
E_1, 10^4 bar	9.26	9.22	9.15
Fluid (brine)			
c (total)	.073	.090	.142
K_2, 10^4 bar	1.65[b]	1.73[b]	1.84[b]
2. Parameters derived from fit of theoretical models to data			
i) Walsh model (roughly a single relaxation)			
η, 10^3 poise	1.3	2.2	2.6
α	.017	.021	.020
τ, 10^{-6} sec	.82	1.13	1.23
$\Delta\mu$	.492	.495	.618
ii) Generalized Walsh model (roughly two relaxations)			
η, poise	.035	.032	.024
Distribution of inclusion shapes	$c(\alpha)$ α	$c(\alpha)$ α	$c(\alpha)$ α
	73×10^{-2} 6×10^{-2}	9×10^{-2} 1×10^{-1}	14×10^{-1} 2×10^{-1}
	4×10^{-7} 4×10^{-7}	5×10^{-7} 4×10^{-7}	7×10^{-7} 4×10^{-7}

All assumed values are taken from Spetzler and Anderson (1968) unless otherwise noted.

[a] Birch (1966): pure H_2O solid, roughly -16 to -7 °C

[b] Kell (1970): pure H_2O liquid

frequency, calculated from these models are shown (dashed lines) in Figure 2.3. The agreement with the observations is quite satisfactory. However, although the values for aspect ratio are very reasonable and agree with those determined by Anderson and Spetzler (1970) using only the relaxation strengths, the predicted melt-viscosity is about five orders of magnitude greater than the viscosity of pure water at similar temperatures (as given, say, in the Handbook of Chemistry and Physics). It is not likely that the addition of even 20 percent NaCl (by weight) to water would increase the viscosity that much. Furthermore, the predicted viscosity appears to increase with increasing temperature, contrary to what we expect for most fluids and to what is observed for water. Clearly a somewhat more realistic model is needed of a partially molten system.

2.3 Attenuation in a partial melt: a generalized Walsh model

2.3.1 Some theoretical considerations

Let us assume, following Walsh (1968, 1969), that partially molten rock consists of a solid matrix containing isolated pockets of melt, and that these pockets are in the shape of oblate spheriods oriented at random throughout the matrix. Wu (1966) has solved the elastic problem for a composite material in which spheroidal inclusions of one phase are embedded in a continuous second phase. He has shown that the bulk modulus K and shear modulus μ of the composite are given by

$$\frac{1}{K} = \frac{1}{K_1}\left[1 + \frac{c_2}{3} T_{iijj} \left(\frac{K_1-K_2}{K}\right)\right]$$

$$\frac{1}{\mu} = \frac{1}{\mu_1}\left[1 + \frac{c_2}{15} (3T_{ijij}-T_{iijj}) \left(\frac{\mu_1-\mu_2}{\mu}\right)\right] \qquad (2.5)$$

where subscripts 1 and 2 denote, respectively, the matrix and inclusion materials, c_2 is the volume concentration of the inclusion phase, and T_{iijj} and T_{ijij} (summation convention implied) are the scalar forms of a fourth-order tensor defined by Wu (1966). Explicit expressions for T_{iijj} and T_{ijij}, functions only of the elastic moduli of the two phases and the aspect ratio of the inclusions, are given in Appendix 1. It should be mentioned in passing that if we had no preconception of the geometrical arrangement of the fluid phase in partially

melted rock, then we would have to use an approach such as that of Kröner (1967) rather than the one we have followed here.

Note that equations (2.5) do not yield K and μ explicitly. This is a consequence of the 'self-consistent assumption' (i.e. the inclusions 'see' their surroundings as having the elastic moduli of the composite, rathr than of the matrix phase), which Wu employed so that his theory might still be useful at relatively high concentrations of the inclusion phase. Walsh (1968, 1969) removed the self-consistent assumption in order that (2.5) might be algebraically tractable. If (2.5) is to be applied to systems where the volume concentration of inclusions is as high, say, as in the ice-brine experiment of Spetzler and Anderson (1968), the self-consistent approximation must probably be retained.

If the spheroidal inclusions are not of uniform shape, then c is a function of α (the actual dimensions of the inclusions do not enter into relations 2.5). In that case equations (2.5) become

$$\frac{1}{K} = \frac{1}{K_1}\left\{1 + \frac{1}{3}\int_o^1 d\alpha\ c(\alpha)\ T_{iijj}(\alpha)\ \left(\frac{K_1-K_2}{K}\right)\right\} \qquad (2.6)$$

$$\frac{1}{\mu} = \frac{1}{\mu_1}\left\{1 + \frac{1}{15}\int_o^1 d\alpha\ c(\alpha)\left[3T_{ijij}(\alpha)-T_{iijj}(\alpha)\right]\ \left(\frac{\mu_1-\mu_2}{\mu}\right)\right\}$$

Again following Walsh, apply the viscoelastic correspondence principle; i.e. substitute for μ_2 (and possibly for K_2) the complex modulus suitable to a particular phenomenological model for the fluid phase. Then if the elastic (or viscoelastic) parameters of the two phases and the volume distribution $c(\alpha)\, d\alpha$ of melt-pocket shapes are specified, we may solve (2.6) using an iterative scheme. That is, in the first iteration set $K = K_1$ and $\mu = \mu_1$ in the right-hand side of (2.6) and evaluate. Then substitute the resulting values for K and μ (which should closely approximate those determined using Walsh's treatment) back into the right-hand side of (2.6), re-evaluate the expressions and repeat the process until the solutions from successive iterations converge. A useful test of convergence is the relative change in the shear modulus after an iteration step.

In using equation (2.6), with μ_2 complex and frequency-dependent, in preference to (2.3) and (2.4), we sacrifice the elegance of algebraic simplicity and risk loss of an intuitive 'feel' for the partial-melt model. In return, we obtain a more general model, presumably applicable at relatively large volume concentrations of melt and able to include such non-Newtonian effects as stress relaxations in the fluid phase. It should be emphasized that this generalized model shares several of the assumptions made by Walsh: (1) wavelengths are large compared to the inclusion dimensions; (2) the

inclusions, for every value of α such that $c(\alpha) \neq 0$, are isolated and randomly oriented, so that the composite may be treated as isotropic; and (3) losses are small enough so that equating Q to the ratio of the real and imaginary parts of the complex modulus of the composite is valid.

A comparison of the self-consistent model with the simple relaxation is shown in Figure 2.4. The normalized shear modulus and attenuation for a hypothetical Poisson-solid containing spheroidal melt pockets of uniform shape ($\alpha = 10^{-4}$) are plotted as functions of frequency for several values of c/α. The melt is assumed to be a Newtonain fluid ($\eta = 1$ poise). Also shown are the frequency $(2\pi\tau)^{-1}$ of the relaxation peak and the relaxed modulus predicted by relations (2.4) For $c/\alpha = 0.1$, the modulus and attenuation are virtually indistinguishable from that given by (2.3) and (2.4). In other words, the self-consistent assumption does not alter the conclusions of Walsh (1969). For $c/\alpha = 1$, it may be seen from the figure that the frequency of the peak in attenuation and the relaxed modulus are both somewhat over-estimated by (2.4). Both the attenuation peak and the decrease in modulus are spread over a somewhat broader range of frequency than is a single relaxation. For $c/\alpha = 5$, the attenuation peak in the self-consistent model is centered at a frequency almost a decade lower than that predicted by (2.4) and no longer coincides with the

Figure 2.4 Modulus and attenuation in the self-consistent, or generalized Walsh, model of a partial melt for several values of c/α. All melt is assumed to be contained in isolated spheroids of uniform aspect ratio $\alpha = 10^{-4}$. Viscosity of the melt equals 1 poise. Shown for comparison (dashed lines) are the relaxed shear-modulus and the frequency of the relaxation peak predicted by the single-relaxation theory of Walsh.

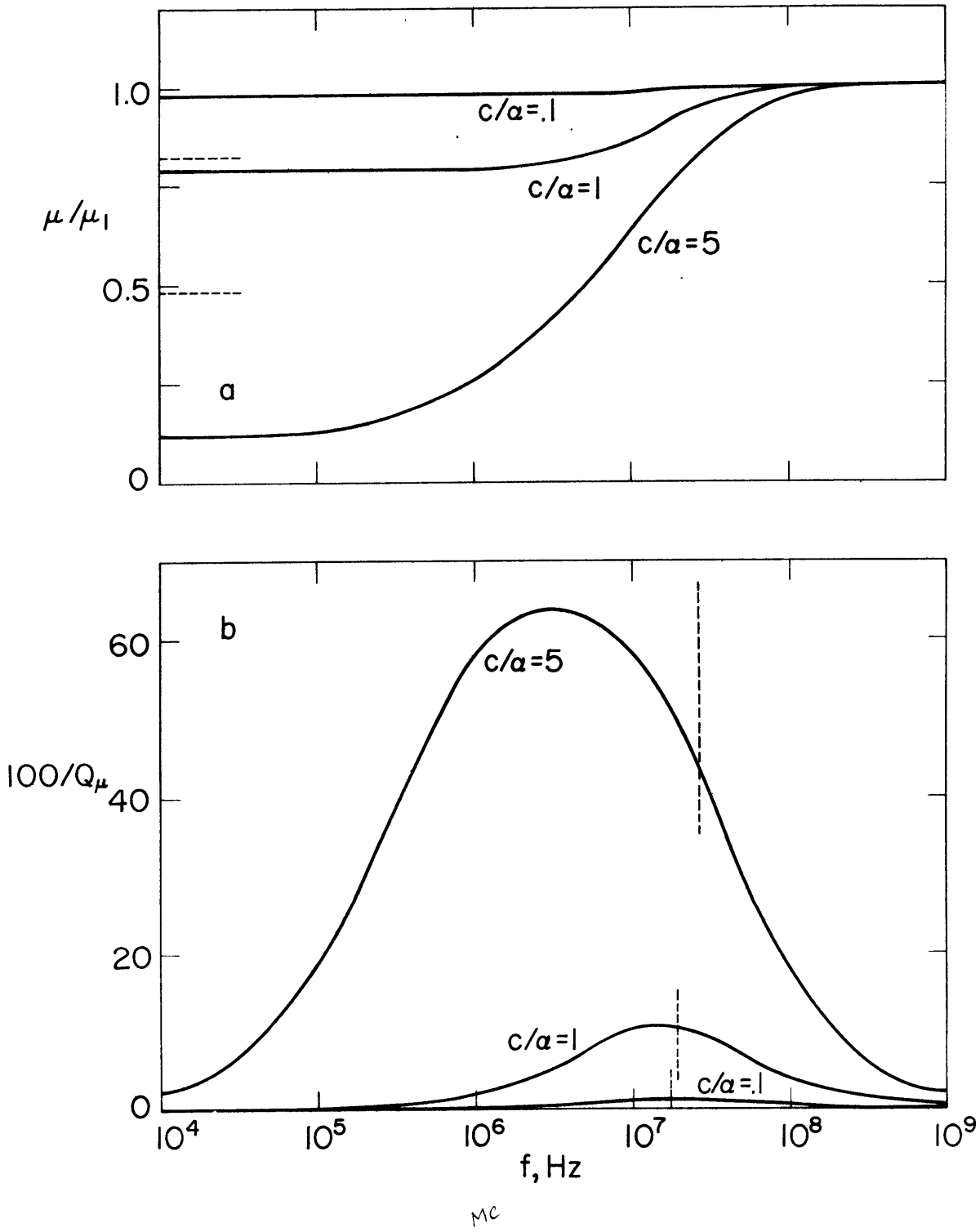
1.0
0.5
0
μ/μ1
c/a=.1
c/a=1
c/a=5
a
60
40
20
0
100/Qμ
b
c/a=5
c/a=1
c/a=.1
10^4
10^5
10^6
10^7
10^8
10^9
f, Hz

MC

frequency at which the modulus has an inflection point; the peak half-width spans a factor of 400 in frequency (the half-width of a single relaxation peak spans a factor of about 14 in frequency); and the relaxed modulus is less than one-fourth that given by (2.4).

That the behavior of a solid with fluid inclusions should depart, when c/α equals 1 or greater, from that predicted by (2.3) and (2.4) is quite reasonable. Consider a sphere of composite material just enclosing a single inclusion (i.e. the sphere's radius equals the major semi-axis of the oblate spheroid). Clearly the volume of the sphere equals $1/\alpha$ times the volume of the enclosed spheroid. If the total composite is made up entirely of such spheres (i.e. if the spheres come in a sufficiently wide range of sizes that they may be packed to completely fill any desired volume of space), then $c/\alpha = 1$ for the composite. Each sphere, containing a single inclusion, must then just touch against several other similar spheres. It is obvious that the elastic energy computed for such a composite must include the energy of interaction between touching spheres or alternatively, a scheme such as the self-consistent assumption must be employed. As c/α is made greater than unity, interaction between nearby inclusions further relaxes the stress (beyond the relaxation of the non-interacting model) and spreads the single characteristic time of relaxation into a band of relaxation times. For c/α greater than about 5, the shear modulus relaxes

completely.

2.3.2 Application to experiment

Let us see how well the mechanical behavior of the partially-molten-rock analogues can be matched by the generalized Walsh-theory, using estimates for all parameters that are as realistic as possible. For the granite-glycerol system of Nur and Simmons (1969), the following input is considered known: Glycerol behaves as a standard linear solid in response to pure compression and as a Maxwell fluid in response to shear (Piccirelli and Litovitz, 1957). The elastic moduli of the solid component, the shear viscosity of glycerol and the wave frequency are as indicated by Nur and Simmons. All assumed values are listed in Table 2.1. (Note that K_2 and μ_2 as given are each the result of a single relaxation, whereas Piccirelli and Litovitz have shown that a spectrum of relaxation times is required. This distinction does not seriously affect the discussion below.)

It then remains to choose a distribution of inclusion shapes so as to approximate as closely as feasible the measured shear modulus (Figure 2.2) with that predicted from equations (2.6). Additional constraints are that total pore concentration equals .003 and total 'crack' concentration equals .003 (Nur and Simmons, 1969). To the extent that a fit is possible, the determination of the distribution $c(\alpha)$ is merely an exercise in curve

fitting. The fine structure of such a distribution is unimportant. What should concern us is how good a fit can be obtained and what features the data seem to require of $c(\alpha)$.

One such distribution $c(\alpha)$ is given in Table 2.1; the predicted shear modulus is shown in Figure 2.2. Basically, for $\eta < 10^3$ poise we are at liberty to choose $c(\alpha)$ so as to match any curve of μ that increases monotonically with $\log \eta$. In particular, an inflection point in $\mu(\log \eta)$ near $\log \eta = -0.5$ may be obtained by allowing a small concentration ($c \leq 10^{-6}$) of cracks of aspect ratio about 2×10^{-6}. However, the data of Nur and Simmons cannot be matched by the theory over the entire viscosity range. Namely, the roughly linear increase of μ with $\log \eta$ indicated in their data cannot be reproduced for $\eta > 10^3$ poise. The reason may be seen by appealing to equation (2.4). The slope of $\mu(\log \eta)$ would imply, if we are to fit the entire length of the curve, that $c(\alpha) \geq 0.1\,\alpha$ over a range of α in excess of 11 orders of magnitude. From the total concentration of fluid, however, the greatest α such that $c(\alpha)$ can be as great as $0.1\,\alpha$ is less than 10^{-1}. Using (2.4), this corresponds to $\eta \simeq 10^4$ poise. The concentration of cracks of lower aspect ratio only affects the curves in Figure 2.2 at values of η less than 10^4 poise.

It is probable that the linear increase of μ with

log η reported by Nur and Simmons is not a consequence of viscous forces in the fluid component. This is certainly true at the highest viscosities studied. In a Maxwell fluid, the ratio of the real to the imaginary part of the shear modulus is given by $\omega\eta/\mu_U$, where μ_U is the (real) value of the shear modulus in the high-frequency limit (i.e. the unrelaxed modulus). For glycerol, when η is greater than about 10^4 poise the quantity $\omega\eta/\mu_U$ (for $\omega / 2\pi = 5 \times 10^5$ Hz) exceeds unity; that is, glycerol behaves more like a solid than a liquid. Thus viscous damping in glycerol does not contribute significantly to the shear-modulus defect observed by Nur and Simmons (1969) at viscosities in excess of 10^4 poise. We shall not speculate on other possible causes of this phenomenon. It is of more than casual interest, however, that Nur (1971), in graphically citing his earlier results, apparently removed most of the linear change of μ with log η before plotting his graph.

Observed longitudinal-mode attenuation and modulus in the ice-brine system of Spetzler and Anderson (1968) can be well fit by equations (2.6) using values for fluid viscosity similar to those of super-cooled water (i.e. about 3×10^{-2} poise). The primary distinction between the 'Walsh model' and the 'generalized Walsh model' is that in the latter there is a bimodal distribution of melt-pocket shapes. This produces what we may consider as two relaxations (the difference between a true relaxation

and the broader 'relaxation' predicted by the self-consistent approximation is unimportant here). Thus, unlike the model which assumes uniform aspect ratio, the attenuation peak apparently centered between 10^4 and 10^5 Hz may be fit without requiring an unreasonable value for the viscosity. The particular values of η and $c(\alpha)$ used to fit the experimental data (see Figure 2.3, solid lines) at three temperatures are given in Table 2.2. About half of the modulus defect at each temperature is attributable to inclusions of aspect ratio near 0.1 (and increasing slightly with temperature) and half to a very small volume-concentration of exceedingly narrow ($\alpha = 4 \times 10^{-7}$) inclusions.

A common feature of the generalized Walsh-models for ice-brine and granite-glycerol is the presence of fluid inclusions of very small aspect-ratio (near 10^{-6}). Even if the major axis of these inclusions is 1 cm in length (this is an overestimate by about a factor of 20 for ice-brine unless several interconnected melt-pockets of similar thickness act as a single 'long' pocket), the minor axis is 10^{-6} cm or 100 Å. A somewhat smaller major axis would make the inclusions reminiscent of viscous grain boundaries in metals. Kê (1947, 1948) found that if he assumed the grain boundaries in aluminum and alpha-brass to have a thickness on the order of one atomic diameter (i.e. a few Angstroms, giving $\alpha = 10^{-6}$), that the grain-boundary viscosity calculated at temperatures

near melting from the relaxation-peak frequency closely approximated the viscosity of the molten metal at similar temperatures (see also Goetze, 1969). It is thus plausible that the inclusions of small aspect ratio indicated by the fit of the generalized Walsh-model may be grain boundaries at which no appreciable melt has formed. Such an interpretation receives some support in the case of the ice-brine data from the observation by Spetzler and Anderson (1968) that pure ice at temperatures between -28^{o} and -12^{o} C has a shear-stress relaxation-peak at a frequency in the range 10^{4} to 10^{5} Hz. Attributing the attenuation peaks implied in Figure 2.3 to viscous 'grain-boundaries', however requires that there be more such boundaries (by a factor of about 3 per unit volume) in the temperature range of partial melting than at sub-solidus temperatures.

Another point worth considering is that our phenomenological description of the fluid breaks down when inclusion thicknesses are small enough so that the effects of short-range order in the fluid are important. Water molecules, for instance, form 'flickering clusters' of quasi-crystalline structure that average about 90 molecules per cluster at $T = 0^{o}$ C (Nemethy and Scheraga, 1962). Thus even if we retain the notion of Newtonian viscosity, the value of the viscosity appropriate for water in very thin cracks (i.e. thickness comparable to cluster dimensions, or a few tens of Angstroms) might be somewhat larger than the value determined from macroscopic measurements. It is relevant

that liquids for which hydrogen bonding is important (such as water and glycerol) readily form clusters (Ubbelohde, 1965, ch. 10). Thus extrapolating experiments made using such liquids to conditions in the upper mantle of the earth may be quite hazardous, and the need for laboratory measurements of velocity and attenuation in partially molten rocks appears even more painfully obvious.

2.4 Other possible dissipation mechanisms

It should be mentioned that physical processes other than viscous damping in the fluid phase can contribute to the total attenuation in a partial melt. (Note that when several mechanisms contribute to the total attenuation, the effective Q^{-1} is the sum of the Q_i^{-1} values arising individually from each mechanism as long as all losses are relatively small.) The solid phase will attenuate some seismic energy; the loss mechanisms for solid, polycrystalline materials are many and diverse (e.g. Jackson and Anderson, 1970). It is sufficient in the discussion to follow, however, to assume that attenuation associated with the presence of a fluid component is much greater than absorption within the solid phase. [This assumption is reasonable for all dissipation mechanisms in solids except for viscous grain-boundary damping (Kê, 1947), a phenomenon which is mathematically indistinguishable from Walsh's (1969) treatment of attenuation in a partial melt except perhaps for somewhat different values of c, α, and η. For our purposes the distinction between an actual melt-phase and a grain boundary that, though of uncertain molecular structure, behaves in all important respects as a fluid is academic and need not greatly concern us further.] Secondly, if the solid matrix is permeable (i.e. if the melt pockets are interconnected), there may be attenuation arising from flow of the fluid relative to the solid (Biot, 1956 a,b). Finally, changes in pressure associated with

wave propagation may shift the phase-change boundary: the resulting reaction acts to absorb elastic-wave energy. (Vaišnys, 1968). We shall discuss the latter two mechanisms somewhat more thoroughly.

The theory of elastic-wave propagation in a porous, permeable solid saturated with a viscous, compressible fluid has been developed in detail by Biot (1956 a,b). In response to inertial forces, relative motion of fluid in the pores gives rise to friction. Below a critical frequency f_t (determined by the conditions for non-turbulent flow and given by

$$f_t = \frac{\pi\eta}{4\rho_2 d^2} \tag{2.7}$$

where d is a characteristic pore diameter or thickness), the composite behaves as a standard linear solid in response to purely shearing stresses (Biot, 1956a); i.e. the material may be characterized by a relaxation $R_x(\Delta\mu, \tau)$ where

$$\Delta\mu = \frac{c^2\rho_2^2}{\rho(c\rho_2+\rho_a)}$$

$$\tau = \frac{\rho k}{\mu c^2}\left\{\frac{(c\rho_2+\rho_a)\ [(1-c)c\rho_2\rho_1 + \rho_a\rho]}{\rho^3}\right\}^{1/2}. \tag{2.8}$$

In (2.8), c is the 'effective' concentration of the fluid (i.e. the volume concentration of interconnecting, fluid-

filled channels); ρ_1 , ρ_2 and ρ are, respectively, the density of the solid, fluid, and composite; k is the permeability of the solid matrix; and ρ_a represents an apparent mass which accounts for a coupling of solid and fluid displacements in the equations of motion. The ratio ρ_a/ρ is typically small. Thus we may write, for those materials for which $\rho_1 \simeq \rho_2 \simeq \rho$ holds,

$$\Delta\mu \simeq c$$
$$\tau \simeq \frac{\rho k(1-c)}{\eta} \qquad (2.9)$$

For dilatational waves (' of the first type' in Biot's terminology), the expressions for attenuation and modulus are somewhat more complicated. The modulus may increase or decrease with frequency; in the particular case when a certain 'dynamic compatibility' condition is satisfied, there is no relative motion between fluid and solid so that the modulus is frequency-independent and there are no losses. In the numerical examples given by Biot, the ratio $Q_\alpha^{-1}/Q_\beta^{-1}$ (i.e. the ratio of attenuation of dilatational waves to that of shear waves) varies from about 5 to 0.

To what extent does such an attenuation mechanism contribute to the experimental results considered above? For the granite-glycerol experiment of Nur and Simmons (1969), the important point to note is the very low permeability of most granites. If we adopt $k = 10^{-14}$ cm^2 (10^{-6}d) as a reasonable value(see Brace et al., 1968), then even for

η as low as 10^{-2} poise, τ must be less than 10^{-11} sec (i.e. the peak frequency must be greater than 10^{10} Hz), outside the range of importance for the Nur-Simmons work. At the lower end of the viscosity range studied, the condition $f < f_t$ does not hold for cracks thicker than about 1 micron. From Biot's (1956b) work, however, the conclusion that significant attenuation occurs only for frequencies much greater than 5×10^5 Hz remains unaltered.

Whether or not the Biot theory is important for the ice-brine system examined by Spetzler and Anderson (1968) depends upon the permeability, largely unknown, of their samples. Friction due to relative motion of fluid and solid might contribute to the attenuation peaks shown in Figure 2.3 if $k \simeq 10^{-8}$ cm^2 (1 d), a figure appropriate to the most permeable oil-bearing sands. This is unlikely; a value several orders of magnitude lower is probably more reasonable. In any event, because the relaxation strength is roughly equal to the fluid concentration, the large decrease in shear modulus upon first appearance of melt reported by Spetzler and Anderson (1968) cannot be exclusively the result of the shear relaxation given by equations (2.9).

Vaišnys (1968) has demonstrated that a partial melt may dissipate elastic-wave energy through irreversible reactions toward thermodynamic equilibrium, such equilibrium having been disturbed by the wave. The loss mechanism may be characterized as a relaxation process,

with the modulus defect and relaxation time depending in a complicated fashion on the volume change associated with the reaction and the reaction rate. An important aspect of this dissipation mechanism is that losses associated with the hydrostatic component of stress are comparable to and probably greater than losses due to the shearing component. (The precise ratio depends upon the geometrical arrangement of the fluid within the solid matrix.)

2.5 The attenuation mechanism in the asthenosphere

Which of the several mechanisms of absorption discussed above might dominate seismic attenuation in a partially molten asthenosphere? Consider viscous losses in isolated pockets of melt, i.e. equations (2.3) and (2.4) or (2.6). Viscosities of molten rock, measured in the laboratory and *in situ* in lava flows, fall in the range 10^1 to 10^6 poise (Clark, 1966), with the precise value dependent on temperature and the amount of water and other volatiles present. It is presumed that the viscosity of the melt phase in a partially molten asthenosphere will fall within or somewhat above (due to the effect of pressure) this range of values. Thus, if all other parameters implicit in relations (2.4) or (2.6) are similar to those in either the ice-brine or granite-glycerol experiments, we would almost certainly expect significant relaxation of shear stress in the upper mantle for waves of frequency somewhere in the range 10^{-3} to 10^2 Hz. Viscous dissipation in the fluid phases will therefore be an extremely important mechanism of seismic-wave attenuation, over at least a portion of the siesmic-wave frequency-band, wherever the upper mantle is partially molten.

Fluid flow through interconnecting melt channels is probably not a significant source of seismic attenuation in the asthenosphere. If all parameters in partially melted mantle-rock other than fluid viscosity are similar to those

in the granite-glycerol or ice-brine experiments, then because of the presumably higher values of viscosity appropriate to molten rock, the relaxation time (equation 2.9) is many orders of magnitude less than the periods of seismic waves. We therefore need not concern ourselves further with this mechanism of attenuation.

Attenuation due to perturbations of a phase-change boundary by the elastic wave cannot be ruled insignificant on theoretical grounds; and Vaišnys (1968) has, in fact, suggested that such a mechanism in a partially molten mantle might peak at a frequency within the range relevant to seismic waves. The finding, to be reported in section 3.5.2, that most of the attenuation of long-period P waves in the western United States can be attributed entirely to losses in shear, however, makes this mechanism relatively unimportant.

Thus the most likely cause of seismic attenuation in a partially molten athenosphere appears to be viscous damping in thin films of fluid. An important facet of this mechanism is that shear modulus and Q^{-1} are dependent on frequency. (We might note that for <u>all</u> dissipation mechanisms considered in this chapter, whenever Q^{-1} is relatively large it is also a strong function of frequency.) Such properties as the concentration and viscosity of the fluid may be estimated by fitting the generalized model of Walsh (equations 2.6) to the measured velocities and attenuation in the zone of partial melt. In fact, from the

considerations of section 2.3.1, when $c(\alpha)/\alpha$ is less than 1 or so for all values of α then the 'generalized Walsh-model' is not significantly different from a superposition of several relaxations (i.e. the interaction between inclusions may be neglected). This is very convenient, for we may therefore attribute all observed attenuation to one or more relaxation processes, and obtain the (approximate) parameters of the relaxation from equations (2.4). We shall do precisely that in Chapter 5.

Chapter 3. Lateral Variation of Body-Wave Attenuation

How may we begin to determine the complete, three-dimensional description of seismic-wave absorption in the earth? The classical technique for obtaining the attenuation of a travelling wave is to measure the wave amplitude (or energy) at two successive points in the wave's propagation-path. The difference in amplitudes can then be related directly to the attenuation averaged along the path between the two sampling sites. For seismic body-waves which sample the mantle, this technique is obviously limited to waves which have been reflected at least once from the earth's surface. The paths for which this method have been used to determine the attenuation are generally long (e.g. the thickness of the mantle), and thus the details of the spatial variation of Q cannot be resolved.

If the variation of seismic-wave amplitude with propagation direction at an earthquake source is assumed, then the spatial variations in attenuation may be determined by comparing amplitudes of waves which have traveled somewhat different paths. Though several such schemes have been proposed, each requiring that somewhat different assumptions be satisfied, the most plausible is the technique of eliminating unknown source- or propagation-parameters by forming ratios of Fourier-amplitude spectra.

The method of spectral amplitude ratios was first used for body waves to determine vertically averaged values of

Q for the upper and lower mantle (Kovach and Anderson, 1964; Kanamori, 1967a,b,c; Sato and Espinosa, 1967). A major step in the inversion of body wave amplitudes to obtain Q as a function of depth was made by Teng (1966, 1968), who attempted to explain changes in the relative attenuation of P waves with epicentral distance in terms of a radially varying Q_α in the mantle. Similar calculations have since been made by Sumner (1967), Hirasawa and Takano (1966), and Mikumo and Kurita (1968).

Both Teng (1968) and Mikumo and Kurita (1968) measured the P-wave spectra at many stations spread over a wide range of epicentral distances. The smoothly varying attenuation-versus-distance curves predicted by spherically symmetric Q-distributions fit the observations only in a crude fashion; much scatter is evident. In this chapter some of the 'scatter' in the reported P-wave amplitude data, together with new measurements of the differential attenuation of shear waves, are examined for systematic regional trends in North America. An earlier version of this work has appeared elsewhere (Solomon and Toksöz, 1970). If the relative attenuation between two stations, after correcting for a reasonable variation of Q with depth, is similar for many earthquakes at different distances and azimuths, then there must be a corresponding difference in the upper-mantle or crustal Q beneath the two stations. It is expected that observations of lateral variations in Q will aid in determining regional differences in the temperature, phase, and composition of the upper mantle.

3.1 Formulation

To isolate the effect of anelasticity on the spectrum of a seismic signal, the effects of source, station crustal structure, and instrument must be eliminated. We employ for this purpose the technique of body-wave equalization, as set out by Ben-Menahem et al. (1965) and Teng and Ben-Menahem (1965), and as first used for attenuation measurements by Teng (1966, 1968). Assume that geometric-ray theory is valid for wave propagation through the mantle and that both the elasticity and anelasticity of the earth are linear (i.e. independent of stress, or strain, amplitude). (These and other assumptions made in this section are discussed in the section immediately following.) Then the observed amplitude-spectrum of a body wave from an earthquake may be written:

$$A(f) = A_0 (f, \theta, \phi) \; A_M(f) \; A_C(f) \; A_I(f) \qquad (3.1)$$

A_0 is the source spectrum, in general a function of frequency, f, and propagation direction (θ, ϕ). A_M is the mantle transfer-function, and includes the effects of attenuation and geometrical spreading. A_C is the crustal transfer-function, approximately equal to the transform of the impulse response convolved with the transform of the time window used in calculating A(f) (Kanamori, 1967b). A_I is the instrumental transfer-function.

Let us make the additional assumptions that (1) the

earthquake in question acts like a point source, i.e. for the bundle of rays reaching stations confined to a relatively small portion of the globe such as the United States, A_0 is separable into the product of a term depending only on frequency and a term depending only on the direction of ray propagation; (2) the crustal transfer-functions for the stations considered are only weakly dependent on frequency; and (3) the instrumental transfer-function is correctly specified by the theoretical response-function (Hagiwara, 1958) once the appropriate instrumental constants are known. Then (3.1) simplifies to

$$A(f) = a\, S(f)\, A_M(f)\, A_I(f) \tag{3.2}$$

where a is a constant (independent of frequency), S(f) is the (direction-independent) source spectrum, and $A_I(f)$ is known.

Consider the ratio of the spectra of a given body-wave phase recorded at two stations (i and j, say). Define

$$R_{ij}(f) \quad \frac{A_{I_j}(f)\, A_i(f)}{A_{I_i}(f)\, A_j(f)} .$$

Clearly

$$R_{ij}(f) = b_{ij} \frac{A_{M_i}(f)}{A_{M_j}(f)} \tag{3.3}$$

where b_{ij} is a constant.

At each station we factor $A_M(f)$ into three components:

$$A_M(f) = G \cdot \exp[-f \cdot t^*] \cdot \exp[-f \cdot \delta t^*] \quad . \tag{3.4}$$

G is the geometrical-spreading factor and is independent of frequency. Further

$$t^* = \pi \int_S Q^{-1}(s,f) \; v^{-1}(s) \, ds \tag{3.5}$$

where v is the wave velocity and the integration is performed along the ray path S (in general a function of the five parameters which describe the location of the station and the event); and

$$\delta t^* = \pi \int_S \delta Q^{-1}(s,f) \; v^{-1}(s) \; ds \quad . \tag{3.6}$$

δQ^{-1}, by which we mean $\delta(Q^{-1})$, is the departure of the true anelasticity, at some point along the ray path, from a radially symmetric distribution $Q^{-1}(r)$. For small attenuation,

$$Q^{-1}_{\text{true}} = Q^{-1} + \delta Q^{-1} \quad . \tag{3.7}$$

In writing equation (3.6) it has been assumed that variations in v^{-1} are small relative to δQ^{-1}. We have not restricted

δQ^{-1} to any particular spatial dependence, though we shall normally assume δQ^{-1} is nonzero only in the upper mantle. For a station at an epicentral distance (Δ) in the range 40 to 75 degrees, t* and δt^* may be treated as independent of Δ to within an error of about ten percent (see Teng, 1969).

Using expression (3.4), (3.3) may be rewritten:

$$f(\delta t^*_j - \delta t^*_i) + c_{ij} = \ln R_{ij}(f) + f(t^*_i - t^*_j) \qquad (3.8)$$

where c_{ij} is a constant. Hereafter, the quantity ($\delta t^*_i - \delta t^*_j$), or sometimes simply δt^*_i when no confusion will result, will be called the differential attenuation. This differs from the definitions of Teng (1968) and of Ward and Toksöz (1971). If Q^{-1} (or δQ^{-1}) depends on frequency, then so may t* (or δt^*). In the treatment below we have made the assumption, not completely justifiable, that t* and δt^* are frequency-independent over the frequency band considered. This will be discussed more fully in section 3.5.3.

Equation (3.8) is our working relation. In practice we fix j, and for a given i measure $\ln R_{ij}(f)$, add $f(t^*_i - t^*_j)$, and to the sum fit a straight line of the form a + bf. If δt^*_j is arbitrarily set to zero, the coefficient b then equals - δt^*_i. The set $\{\delta t^*_i\}$ constitutes a measure of the lateral variation of ray-path-averaged attenuation. It is important to remember that δt^*_j, the departure of the real attenuation at the reference station to that given by equation

(3.5) for a particular model of $v(r)$ and $Q^{-1}(r)$, is unknown, and may vary for different earthquakes. Thus the set $\{\delta t_i^*\}$ can be known only to within addition by a constant.

3.2 Some discussion of assumptions

a) Losses are amplitude-independent.

Seismic strains are small, except in the immediate vicinity of the earthquake-source rupture. For earthquakes of magnitude 6, roughtly the size of events considered in this study, Duda (1970) has recently shown, for instance, that the strains associated with P waves are less than 10^{-6} at all distances greater than a few kilometers from the focus. Jackson and Anderson (1970) concluded that the most likely mechanisms contributing to seismic attenuation in the mantle are linear. For both of these reasons, treating Q^{-1} in the earth as independent of strain amplitude is probably an excellent approximation except perhaps for the outer crust, where attenuation is probably controlled by frictional dissipation along cracks (Walsh, 1966).

b) Earthquakes may be treated as point sources.

As long as wavelengths are large compared to the dimensions of the equivalent-dislocation source of an earthquake, the effects of finite rupture-velocity and rise-time will not be manifested in the source spectrum. For two of the three deep earthquakes studied in the following sections, Berckhemer and Jacob (1968), using a spreading-disk dislocation model for the earthquake source, estimated the areas of the dislocation surfaces to be 20 and 34 km^2. The fault radius (2.5 and 3.3 km, respectively) for

each of the two earthquakes, therefore, is much less than the shortest wavelength (about 35 km) of waves considered below. The same may almost certainly be said of any deep earthquake of magnitude about 6 or less.

c) Geometric-ray theory is approximately valid.

A requirement of geometric-ray theory is that wavelengths are shorter than characteristic lengths associated with changes in the elastic properties. This requirement usually does not strictly hold for long-period body waves in the crust and some parts of the mantle.

The most obvious region where ray theory is often inadequate for body waves is the crust, a fact implicit in equation (3.1). If the crust is considered to be a sequence of plane layers, then the pulse shape of a wave recorded at the surface differs from the shape of the original wave incident from the mantle because of frequency-dependent interference from later arrivals reflected from the various discontinuities in the crust. The crustal transfer-function $A_C(f)$ is strongly dependent on frequency for periods shorter than 5 or 10 seconds and for SV waves incident at angles greater than the critical angle (Haskell, 1962). For longer periods, and short time-windows, however, the variation with frequency of the ratio of crustal responses at two different stations is slight and may be considered negligible. Kanamori (1967b) and Berckhemer and Jacob (1968) have discussed this assumption for incident P-waves.

A further consideration is that the crustal structure beneath most seismograph sites is poorly known; the uncertainty in the correction term which would account for differences in crustal transfer functions at different stations is probably similar in magnitude to the correction itself.

A further potential complication introduced by the presence of a crust is the contamination of SV waves by S-coupled PL waves (Oliver, 1961). (This possibility was kindly brought to my attention by Dr. Gary Boucher.) An SV wave, of period greater than about 20 sec and of horizontal phase-velocity less than P_n velocity, incident on a continental-crust wave guide will generate a PL wave, of roughly the same period and phase velocity, that may propagate distances as great as 30° (Oliver, 1961). From published phase-velocity curves for fundamental-mode PL waves (Oliver, 1961; Chander et al., 1968), it may be concluded that for the combinations of epicentral distance and frequency band used in this study, probably no potentially interfering PL waves were generated within about 10° of any of the stations considered. This distance is sufficiently great that, judging from PL-wave group velocities (Oliver, 1961) for the appropriate periods, the time windows chosen for the spectral measurements reported below should not include PL-wave energy in the relevant frequency bands. The possibility exists that other leaking modes, coupled to SV or SH waves, contribute to the measured spectra; such

contributions are assumed to be small.

Laterally inhomogeneous velocity or density in the crust or upper mantle (e.g. a 'step' in the crust-mantle interface) can also affect the shape of the body-wave amplitude spectrum (Aki and Larner, 1970; Larner, 1970), particularly for variations with dimensions comparable to the wavelength of the incident waves (roughly 30 to 400 km for the waves used in this study). At any arbitrary station site, there is no means of predicting the magnitude or form of such inhomogeneities. We can, however, determine the effect on δt^* measurements of a known Moho irregularity, that beneath the Large Aperture Seismic Array in Montana (Greenfield and Sheppard, 1969; Aki and Larner, 1969; and others). Using SH waves from the 1 December 1967, Kuril Islands earthquake (U.S.C.G.S. magnitude 5.9, depth 136 km), the following values of δt^*_{SH} (.02 to .12 Hz frequency band) were observed at the four seismograph sites in the outermost LASA ring: 0 at F1 (reference station), -1.5 ± 0.3 sec at F2, 0.7 ± 0.3 sec at F3, -1.0 ± 0.4 sec at F4.

Some of the differences in δt^*_{SH} might be attributable to genuine attenuation-variations (site F3, for instance, is the closest station of the four to Blackwell's (1969) Cordilleran thermal-anomaly zone, which would be expected to show large positive values of δt^*). The fact that δt^* at F1 and F3, the two stations nearer the postulated 'step' in the Moho (Greenfield and Sheppard, 1969), however, is noticeably larger than at F2 and F4 suggests that the

anomalous crust-mantle interface may be the principal cause of the observed differences in δt^*_{SH}. While it is debatable whether Moho 'steps' of a size comparable to that under LASA (crustal thickness changes 25% over a lateral distance of 20 km in the Aki-Larner model) are commonplace in North America, the above discussion suggests that little significance should be attached to variations in δt^*_S less than about 2 sec.

For propagation through the mantle, the use of geometric ray theory is questionable probably only if the wave bottoms in the immediate vicinity of a transition zone. Waves which arrive at distances of 40 to 75 degrees (the range considered in the present study) from the epicenter, bottom in the mantle at depths of about 1000 to 2200 km. From P-wave studies, it appears likely that there are at least two or three 'discontinuities' (increased velocity gradients) over this depth range (e.g. Chinnery and Toksöz, 1967; Johnson, 1969), corresponding to epicentral distances (for focal depth equal to 33 km) of roughly 35-43°, 50-52°, and 70-71°. (These distances should be lowered by 3 to 4° when considering very deep earthquakes.) Such lower mantle 'transition zones' are not as well documented for shear waves, though it has been suggested there are second-order discontinuities in $dT/d\Delta$ at 42° (Hales and Roberts, 1970) and near 70° (Fairborn, 1969). The effect on δt^* determinations of anomalously steep velocity gradients in the lower mantle is uncertain.

Values of δt^* obtained from waves which bottomed near a presumed transition zone should be used with care.

3.3 S-wave differential attenuation

The shear waves used in this study are from the four earthquakes shown in Table 3.1, as recorded on long-period horizontal seismographs at stations of the World-Wide Standard Seismograph Network. Origin time, magnitude, and hypocenter information is from the United States Coast and Geodetic Survey and the International Seismological Centre. WWSSN Stations in the conterminous United States, together with physiographic-province boundaries (assumed to roughly separate distinct tectonic provines), are shown in Figure 3.1. The two deep South-American earthquakes have almost the same hypocenter, and their wave-forms are very much alike. These events were chosen to test the repeatability of differential-attenuation observations from two presumably similar sources. The third event, a deep earthquake in the Kuril island-arc region, was included to examine the possibility of azimuth dependence of attenuation measurements. The fourth event, an earthquake on the mid-Arctic ridge, was selected to investigate whether lateral variations of Q in the source region of shallow earthquakes in tectonic areas can be observed using teleseismic, long-period body waves. During 1964, all WWSSN long-period seismographs had a pendulum period of 30 seconds and a galvanometer period of 100 seconds. By late 1965, most stations (and all stations used for the two South American earthquakes) had switched to a pendulum period of 15 seconds.

Table 3.1

Earthquakes used to measure S-wave differential attenuation

Date	Origin Time (GMT) h m s	Latitude	Longitude	Region	Focal Depth km	Magnitude
15 Feb 1967	16 11 11.8	9.0°S	71.3°W	Peru-Brazil border	597	6.2
3 Nov 1965	01 39 03.2	9.0°S	71.3°W	Peru-Brazil border	587	5.9
18 Mar 1964	04 37 25.7	52.6°N	153.7°E	Kuril island-arc	424	5.6
25 Aug 1964	13 47 19.3	78.2°N	126.6°E	Laptev Sea, on mid-Arctic ridge	34	6.2
Other earthquakes for which P-wave differential attenuation has been measured						
9 Nov 1963	21 15 30.4	9.0°S	71.5°W	Peru-Brazil border	600	5.9
28 Aug 1962	10 59 59.0	38.0°N	23.1°E	Greece	120	6.8

Figure 3.1 WWSSN seismograph stations, conterminous United States. Station locations are indicated by circles. Physiographic provinces of the United States, after Fenneman (1931, 1938), are delineated by solid lines.

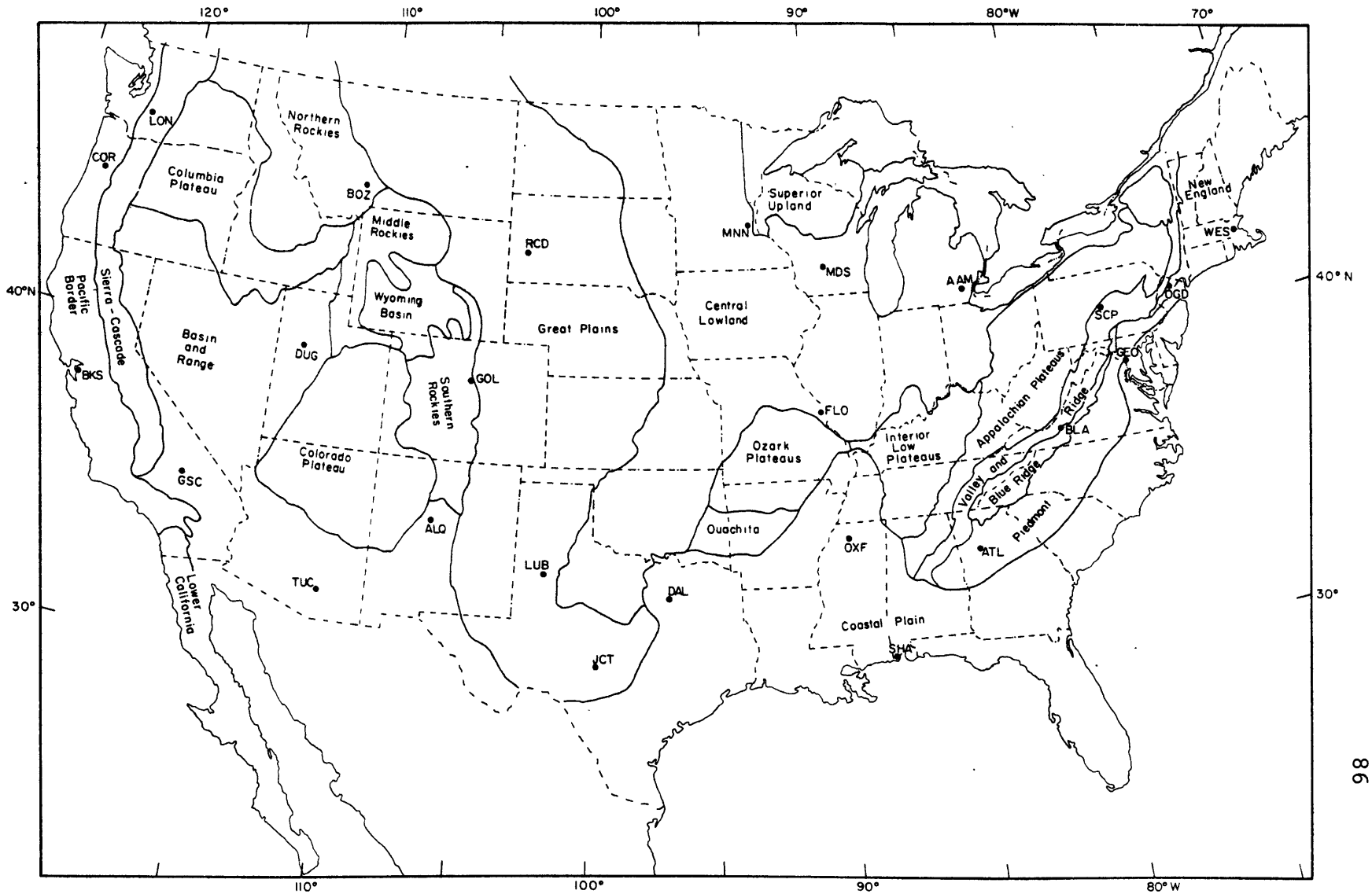
120°
110°
100°
90°
80°W
70°
40°N
30°
LON
COR
BOZ
Northern Rockies
Columbia Plateau
Middle Rockies
Wyoming Basin
RCD
MNN
Superior Upland
MDS
AAM
New England
WES
OGD
SCP
GEO
Pacific Border
Sierra - Cascade
BKS
Basin and Range
DUG
GOL
Southern Rockies
Great Plains
Central Lowland
FLO
Appalachian Plateaus
Ridge
BLA
Valley and
Blue Ridge
Piedmont
Interior Low Plateaus
Ozark Plateaus
Colorado Plateau
GSC
ALQ
Ouachita
OXF
ATL
LUB
TUC
DAL
Lower California
Coastal Plain
SHA
ICT

In all, a total of 96 shear wave components were analyzed. Records were digitized at an interval of about 0.7 seconds. N-S and E-W components were rotated to give SV and SH waves, which were then bandpass filtered to correct small digitizing errors and to isolate the desired frequency range from the effects of interference. The cutoff frequencies of the bandpass, a linear-termination filter, and the time windows applied to each trace are given in Tables 3.2 to 3.5. The SV and SH components were fast-Fourier transformed to give the amplitude spectra. Prior to forming the spectral ratio, each individual spectrum was smoothed by applying a moving-average window of width about .02 Hz. Selected waveforms and spectral ratios are shown in Figure 3.2. Extremes both in the amount of attenuation and in the quality of the straight-line fit to the spectral ratio are included. Figures 3.2a and 3.2c demonstrate the similarity of SV waveforms from the two South American earthquakes (e.g. ATL, WES).

The stations at which clear S waves were observed for each of the four earthquakes are listed in Tables 3.2 to 3.5, along with distance and azimuth information. The reference station used in calculating ratios is indicated. (Differences between δt^* determinations are not particularly

Figure 3.2 Selected S waveforms and spectral ratios. (a) SV waves from Peru-Brazil earthquake of 15 February 1967. (b) SH waves from earthquake of 15 February 1967. (c) SV waves from Peru-Brazil earthquake of 3 November 1965. (d) SV waves from Arctic earthquake of 25 August 1964.

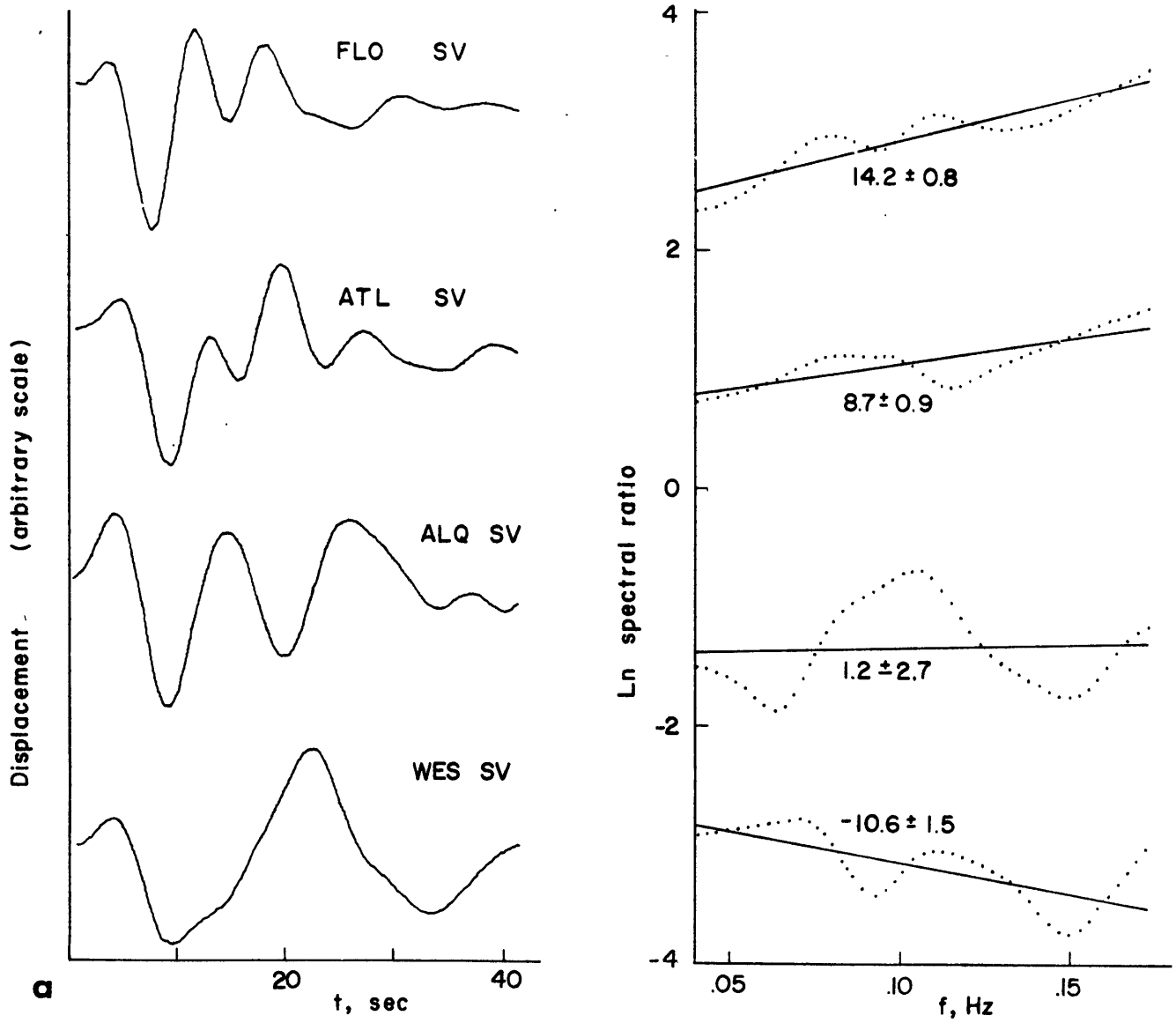
FLO SV
ATL SV
ALQ SV
WES SV
Displacement (arbitrary scale)
a
20
40
t, sec
4
2
0
-2
-4
14.2 ± 0.8
8.7 ± 0.9
1.2 ± 2.7
-10.6 ± 1.5
Ln spectral ratio
.05
.10
.15
f, Hz

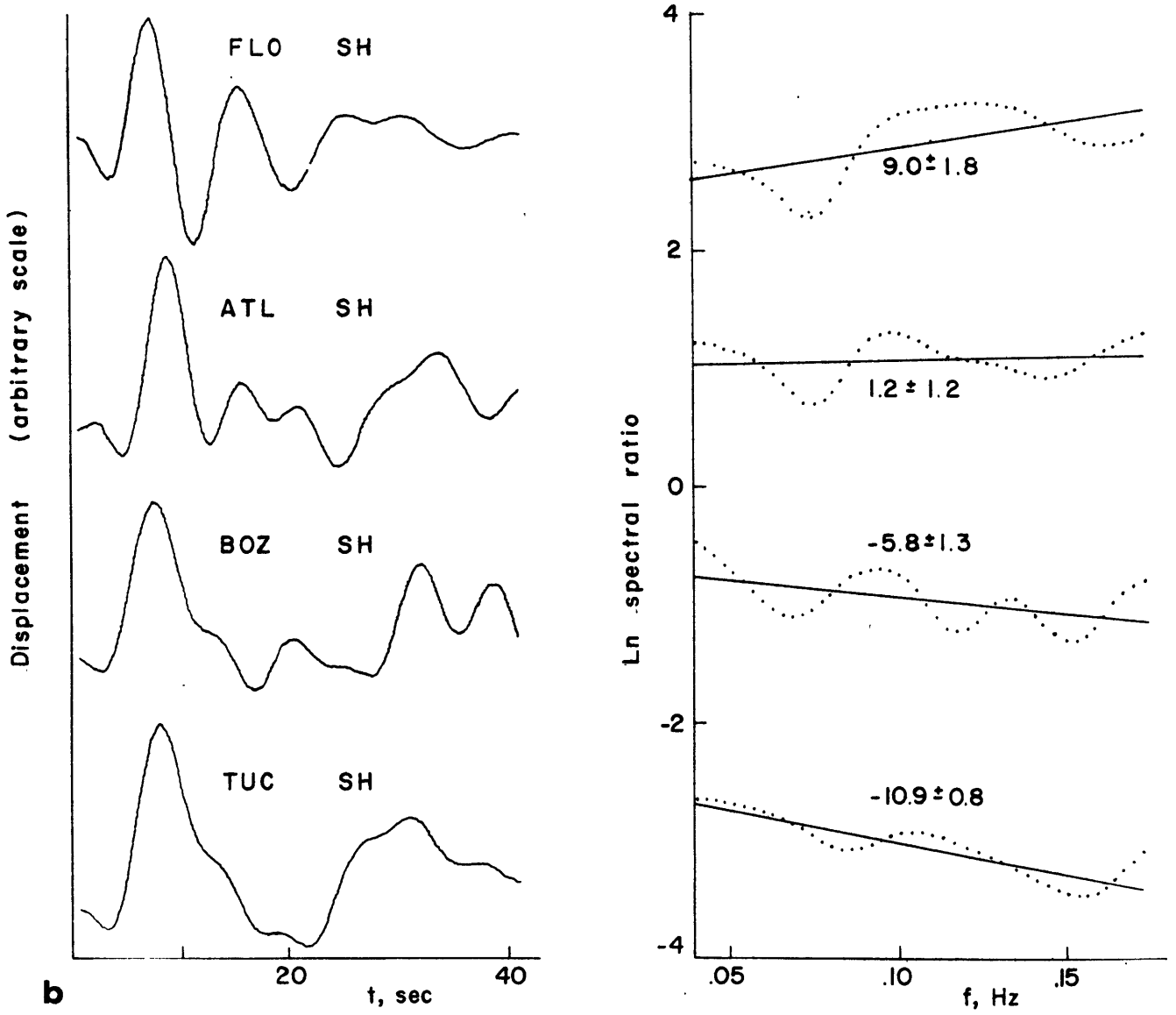
FLO SH
ATL SH
BOZ SH
TUC SH
Displacement (arbitrary scale)
20
40
t, sec
b
4
2
0
-2
-4
9.0 ± 1.8
1.2 ± 1.2
-5.8 ± 1.3
-10.9 ± 0.8
Ln spectral ratio
.05
.10
.15
f, Hz

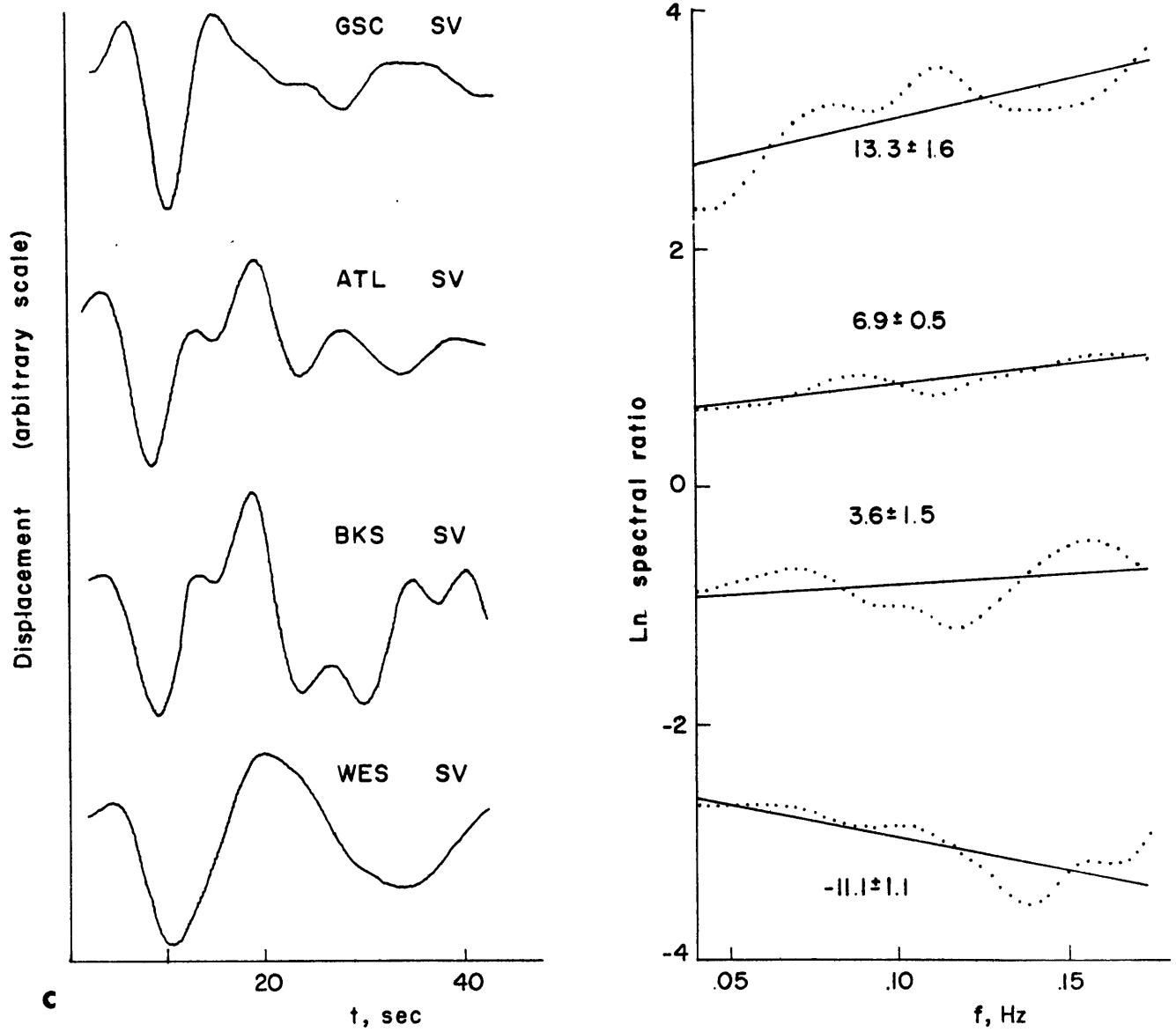
GSC SV
ATL SV
BKS SV
WES SV
Displacement (arbitrary scale)
20
40
t, sec
c
4
2
0
-2
-4
13.3 ± 1.6
6.9 ± 0.5
3.6 ± 1.5
-11.1 ± 1.1
Ln. spectral ratio
.05
.10
.15
f, Hz

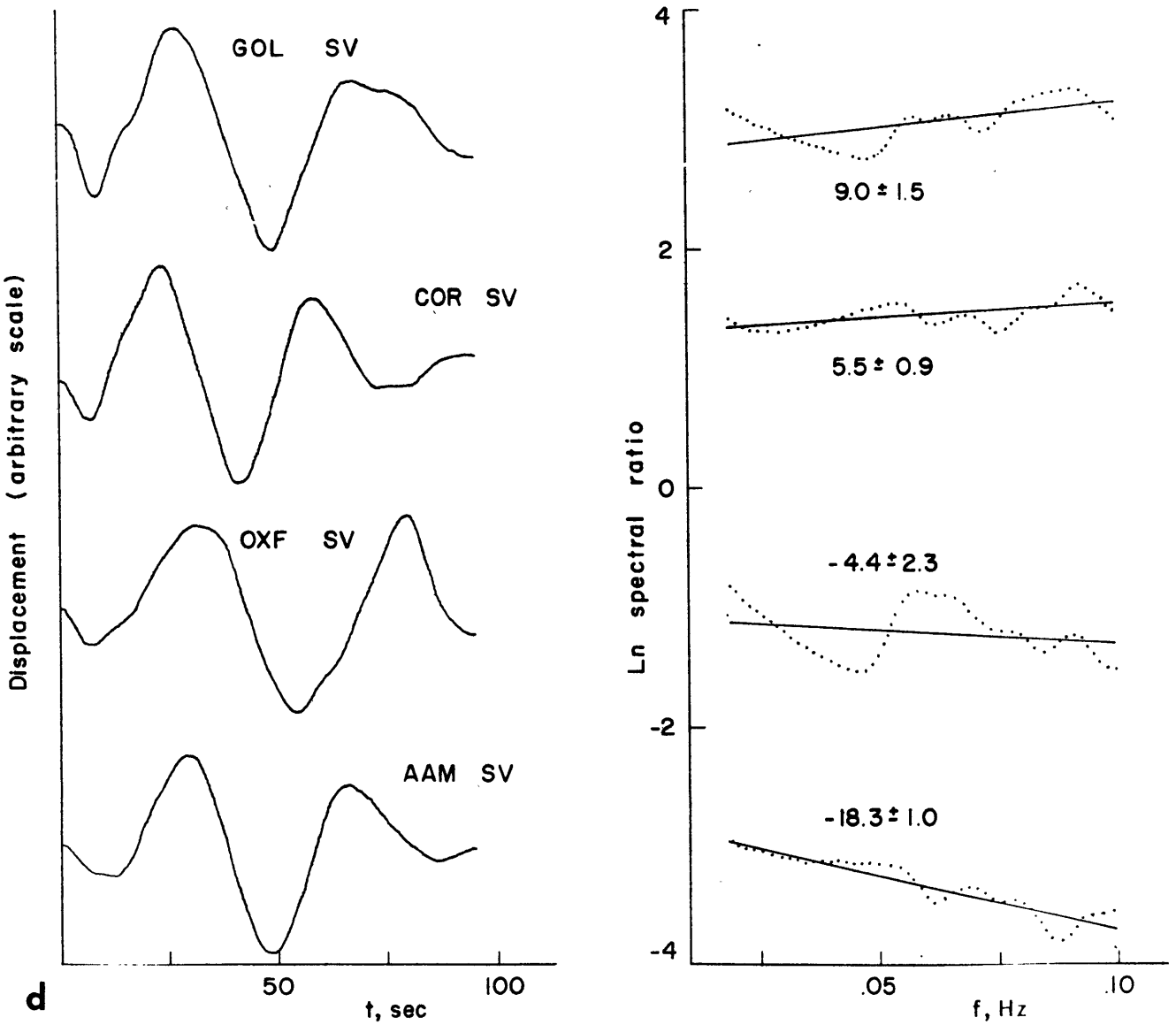
GOL SV
COR SV
OXF SV
AAM SV
Displacement (arbitrary scale)
50
100
t, sec
d
4
2
0
-2
-4
9.0 ± 1.5
5.5 ± 0.9
-4.4 ± 2.3
-18.3 ± 1.0
Ln spectral ratio
.05
.10
f, Hz

sensitive to the choice of reference station.) The differential attenuation is obtained by fitting a straight line to the right-hand side of equation (3.8) by the method of least squares. The t^*'s are calculated from equation (3.5); the integral is evaluated using the numerical scheme outlined by Julian and Anderson (1968), with the MM8 Q_β - distribution (Anderson et al., 1965) and the shear wave velocity distribution given by Ibrahim and Nuttli (1967) above 750 km and by Fairborn (1969) in the lower mantle. We have assigned a Q_β of 2000 to the lower mantle (MM8 is only given for the upper 1000 km). This gives values for $(t_i^* - t_j^*)$ of less than 1 second for shear waves recorded in the epicentral distance range given in Tables 3.2 to 3.5. A non-attenuating lower mantle would make the maximum value of $(t_i^* - t_j^*)$ about 1.5 seconds. As we shall see from the magnitude of the quantities δt_i^*, the uncertainty in the Q_β distribution for the lower mantle does not introduce serious error.

The measured values of differential attenuation for SV and SH waves, with corresponding standard deviations for the least-squared-error fit, are presented in Tables 3.2 to 3.5. The data are not of uniform quality. Less reliable determinations are at stations with poor film records, low signal-to-noise ratios, or waveforms distinctly different from average. Such values are enclosed in parentheses in the tables and are not used in the subsequent analysis. The standard deviations shown range from

0.4 to 3.3 seconds and indicate how closely individual spectral ratios may be approximated by straight lines, though in most cases they probably underestimate the total uncertainty.

3.3.1 South American events

SV waveforms were very similar for the deep earthquakes of 15 February 1967 and 3 November 1965, though there was some difference in the degree of SH-wave excitation and in the SH-waveform shapes. The ratio of peak amplitudes of SV to SH at U.S. stations was commonly 2 for the 15 February 1967 shock, and was 4 or more for the 1965 event.

The spectra (uncorrected for instrumental response) peaked at periods from 9 to 22 seconds, with the average peak-period 16 seconds for SV and 15 seconds for SH. Fault-plane solutions for the two earthquakes (Khattri, 1969; Chandra, 1970a), determined from the spectra of long-period P waves, imply for both events that an SH nodal plane intersects the earth's surface very nearly along the eastern boundary of North America. Thus for the 3 November 1965 shock in particular, low SH amplitudes are not unexpected at WES, GEO, SCP and possibly AAM. None of the other U.S. stations recording the two South American earthquakes lie near nodal planes for either SV or SH waves.

Many of the S waveforms for both events appeared to consist of two pulses of opposite polarity separated in

Table 3.2

Differential attenuation of S waves,
South American event of 15 February 1967

Station		Distance (deg)	Azimuth (deg)	δt^*_{SV} (sec)	δt^*_{SH} (sec)
AAM	Ann Arbor, Mich.	52.3	348.4	+0.6±2.0	+5.1±1.3
ALQ	Albuquerque, N. Mex.	54.9	324.7	-1.2±2.7	+1.7±1.3
ATL	Atlanta, Ga.	44.0	344.2	-8.7±0.9	-1.2±1.2
BKS	Berkeley, Calif.	66.6	318.0	-6.5±1.0	-1.5±1.0
BOZ	Bozeman, Mont.	65.3	330.0	-0.5±2.3	+5.8±1.3
COR	Corvallis, Ore.	71.0	323.4	-1.9±1.6	-3.3±1.2
DUG	Dugway, Utah	62.2	325.0	-0.7±1.6	+9.0±1.0
FLO	Florissant, Mo.	50.8	340.8	-14.2±0.8	-9.0±1.8
GSC	Goldstone, Calif.	61.5	318.4	(+0.1±2.2)[a]	(+6.2±1.1)[a]
JCT	Junction, Tex.	47.9	326.2	+2.3±1.6	+6.9±2.1
OXF	Oxford, Miss.	46.6	339.3	-6.0±0.7	-3.0±1.6
SCP†	State College, Pa.	49.9	353.5	0	0
SHA	Spring Hill, Ala.	42.6	338.4	-10.8±0.9	(-1.4±0.9)[a]
TUC	Tucson, Ariz.	55.7	319.3	-3.9±1.9	+10.9±0.8
WES	Weston, Mass.	51.1	0.0	+10.6±1.5	+8.2±1.7

† reference station

a film record poor; waveform uncertain

Time window used: 40.6 sec

Band-pass filter cutoffs: 0.040 - 0.173 Hz

Table 3.3

Differential attenuation of S waves,
South American event of 3 November 1965

Station		Distance (deg)	Azimuth (deg)	δt_{SV}^* (sec)	δt_{SH}^* (sec)
AAM	Ann Arbor, Mich.	52.4	348.5	+1.6±2.0	(+9.8±2.0)[b]
ATL	Atlanta, Ga.	44.1	344.4	-6.9±0.5	+4.0±1.1
BKS	Berkeley, Calif.	66.6	318.0	-3.6±1.5	-2.2±0.8
COR	Corvallis, Ore.	71.0	323.5	-6.6±1.3	+5.3±1.2
DUG	Dugway, Utah	62.2	325.1	-5.1±2.2	+9.1±0.4
FLO	Florissant, Mo.	50.8	340.9	(-6.5±1.1)[a]	(+0.2±1.9)[a]
GEO	Georgetown Univ.	48.0	354.1	+4.0±1.1	(+0.6±1.4)[b]
GSC	Goldstone, Calif.	61.5	318.5	-13.3±1.6	-8.6±1.8
LON	Longmire, Wash.	71.4	326.4	+3.0±2.8	+14.3±1.1
LUB	Lubbock, Texas	51.4	327.2	-8.9±0.9	+3.7±1.5
RCD	Rapid City, S. Dak.	60.3	334.1	-9.3±1.5	+0.5±1.1
SCP†	State College, Pa.	50.0	353.6	0	(0)[b]
SHA	Spring Hill, Ala.	42.7	338.5	-9.6±1.1	(+12.3±1.8)[b]
TUC	Tucson, Ariz.	55.8	319.5	-5.7±1.6	+10.1±1.3
WES	Weston, Mass.	51.2	0.1	+11.1±1.1	(+7.4±1.9)[b]

† reference station

a film record poor; waveform uncertain

b low s/n on E-W trace; station near SH nodal plane

Time window used: 40.6 sec

Bandpass filter cutoffs: 0.040 - 0.173 Hz

time by some 12 to 16 sec. While deep earthquakes in South America are often considered multiple events (e.g. Berckhemer and Jacob, 1968; Chandra, 1970b), the variability of observed pulse separation with distance and azimuth and the shorter though similar separation between double P-pulses suggests that the second pulse may be a reflection of the first from a mantle discontinuity. A conceivable candidate for such a reflector is the discontinuity at depths between 490 and 560 km that Whitcomb and Anderson (1970) observed beneath the Atlantic-Indian rise and the Ninety-East ridge. Another intriguing possibility is that the reflection occurs at the upper boundary (somewhat deeper than 500 km) of the discontinuous piece of lithosphere currently thought to be delimited by the isolated zone of very deep earthquakes beneath the Peru-Brazil region (e.g. Isacks, 1970). Whatever their cause, the double-pulse nature of the S waves produced pronounced troughs in the spectra at those periods, and was the motivation for smoothing spectra before forming ratios.

In general, the agreement between the two determinations of δt^*_{SV} and δt^*_{SH} for the 11 stations with well-recorded S waves for both earthquakes is good. The exceptions reflect the differences between the two events discussed above. For δt^*_{SV}, differences between values in Tables 3.2 and 3.3 for a single station vary between 1 and slightly more than 4 sec, well within the total range of almost 25 sec covered by the data. For δt^*_{SH}, the agreement

is not so satisfactory, primarily a result of the lower amplitude of SH waves from the 1965 earthquake.

Average values of δt_S^* for the stations given in Tables 3.2 and 3.3 are listed in Table 3.7 and plotted on a map of the United States in Figure 3.3 The averages were obtained as follows: For each column of numbers δt_k^* (k = SV or SH), we find the average value of δt_k^* for the 11 stations common to Tables 3.2 and 3.3. This average is subtracted from each member of the column, and we call the difference the adjusted differential attenuation. We could just as well have assumed that $\delta t_{k,SCP}^* = 0$ for all earthquakes and for both SV and SH but the predominance of positive values in the δt_{SV}^* columns and negative values in the δt_{SH}^* columns suggests that $\delta t_{SV,SCP}^* \neq \delta t_{SH,SCP}^*$. The average δt_S^* for a station is the mean of the average adjusted values of δt_{SV}^* and δt_{SH}^*. Data in parentheses were not included.

The differential shear-wave attenuation divides the U.S. into four regions, as can be seen in Figure 3.3. There is a broad zone of low attenuation (negative δt_S^*) in the central and much of the eastern U.S. And, not surprisingly, there is a wide band of high attenuation (positive δt_S^*) in the western U.S., including stations in the Basin and Range province (TUC, ALQ, DUG), the Cascade range (LON), the northern Rocky mountains (BOZ), and southern Texas (JCT). This region of high attenuation roughly coincides with the western heat-flow province of

Figure 3.3 Lateral variation of S-wave differential attenuation, United States. δt_S^* is the average of attenuation measurements for two deep earthquakes in South America. The dashed lines separate (approximately) regions of positive and negative δt_S^*

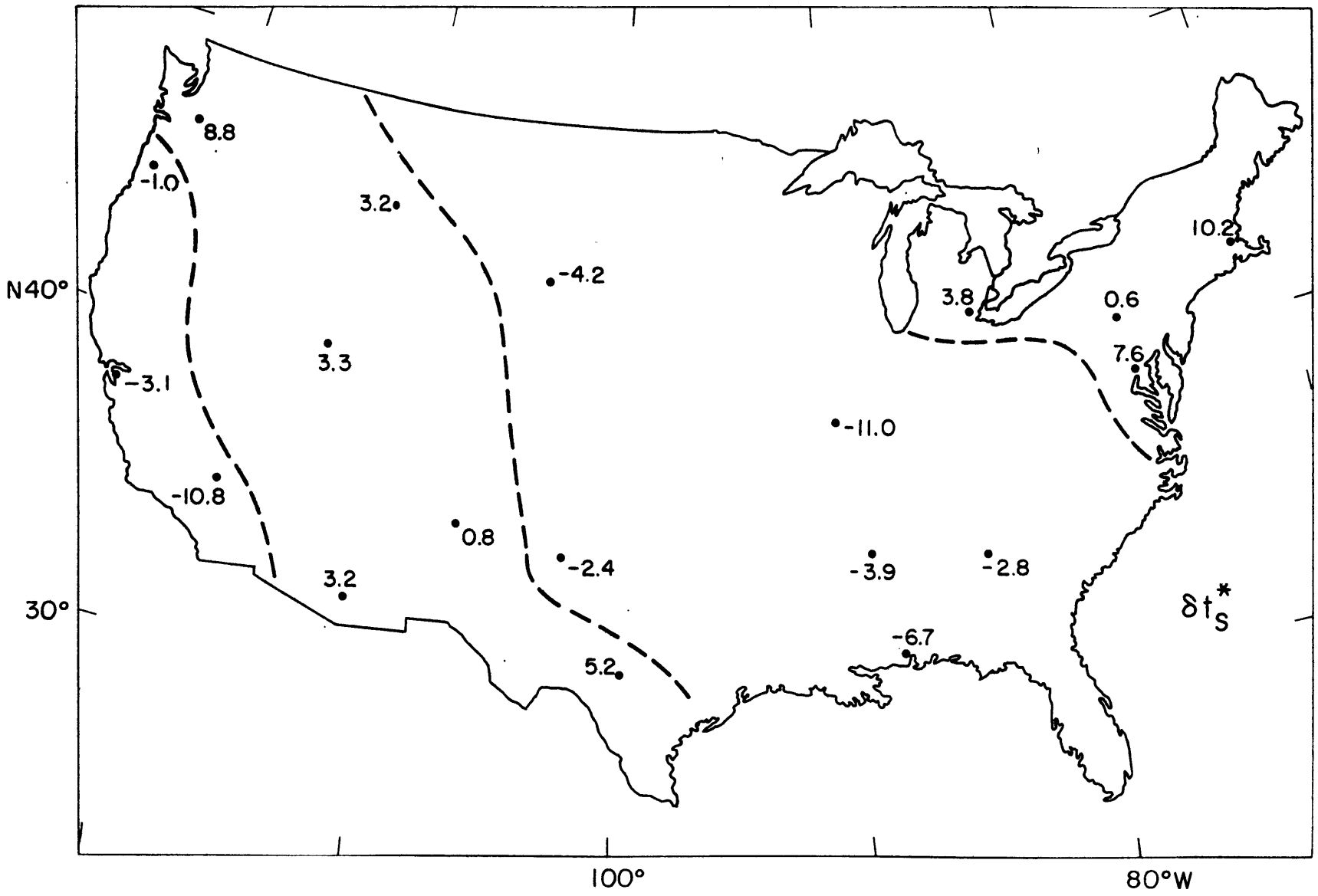
8.8
-1.0
3.2
-4.2
10.2
3.8
0.6
7.6
3.3
-3.1
-11.0
-10.8
0.8
-2.4
-3.9
-2.8
3.2
-6.7
5.2
δt_s^*
N40°
30°
100°
80°W

100

Simmons and Roy (1969). Finally, there are two smaller areas that stand out from the broad pattern: a zone of low attenuation in California and western Oregon, and a region of above-average attenuation in the northeast. WES and GEO have particularly large values of δt_S^*.

It must be emphasized that these values of differential attenuation are averages of differences in attenuation along the mantle ray-path. It seems probable that for ray paths from deep earthquakes the variations δQ_β^{-1} are largest where Q^{-1} is the greatest (i.e. in the low velocity, 'low Q' zone). But spatial fluctuations in attenuation near the source cannot be ruled out as an explanation, for example, of the unexpectedly high attenuation at stations in the northeast U.S. (azimuths greater than 345°), unless δt_S^* is shown to be independent of source region.

3.3.2 Kuril event

Of the WWSSN stations in the United States located within 70° of the epicenter of the Kuril event of 18 March, 1964, six (see Table 3.4) recorded S waves suitable for spectral analysis. Almost all of the S-wave energy was in the SH mode, a consequence of the focal mechanism (Berckhemer and Jacob, 1968), which produced an SV nodal plane whose intersection with the earth's surface passed through the United States. Also well-recorded at all six stations were ScS waves (transverse component); these were included in the analysis, although use of ScS waves in the spectral-

Table 3.4

Differential attenuation of S waves, Kuril Islands event of 18 March 1964

Station		Distance (deg)	Azimuth (deg)	δt^*_{SH} (sec)	δt^*_{ScS} (sec)
BKS	Berkeley, Calif.	57.7	68.6	+2.8±0.8	-2.9±1.5
COR	Corvallis, Ore.	52.6	63.2	-2.5±1.4	-5.7±1.0
DUG†	Dugway, Utah	61.3	60.7	0	0
MNN	Minneapolis, Minn.	67.2	45.1	+9.1±0.6	-5.4±0.7
RCD	Rapid City, S. Dak.	63.3	51.8	-6.7±0.6	-7.8±0.7
TUC	Tucson, Ariz.	68.2	65.2	+2.0±0.4	-1.5±0.5

† reference station

Time window used: 47.8 sec for S

37.5 sec for ScS

Band-pass filter cutoffs: 0.023 - 0.177 Hz

ratio scheme outlined in section 3.1 requires the additional assumption that the SH-wave reflection coefficient at the core-mantle boundary, if frequency-dependent, does not depend significantly on epicentral distance.

The computed differential attenuation values are given in Table 3.4. That the errors shown for this event are generally lower than those obtained for the South American events (Tables 3.2 and 3.4) may be due to the simpler wave-forms for the Kuril event (i.e. no double pulses), a characteristic that may be typical of all deep earthquakes from the Kuril arc (Berckhemer and Jacob, 1968). The absolute amplitudes of SH and ScS waves, after correcting for focal mechanism and geometric spreading, are roughly consistent with the differential-attenuation measurements at all stations but one (ScS at TUC). That is, at each station other than DUG (the reference station), if δt^* is positive (negative) then over much, if not all, of the frequency band, the corrected spectral amplitude is less than (greater than) the amplitude of the same wave recorded at DUG.

If we adjust the δt^* values in the table by requiring that the average of δt^* at the five stations BKS, COR, DUG, RCD, and TUC equal the average δt_S^*, for the same five stations, from the South American earthquakes (this amounts to adding 0.5 sec to the δt_{SH}^* column and 3.2 sec to the δt_{ScS}^* column), then the two adjusted determinations

agree reasonably well (to within 3 sec) at every station except MNN. The large discrepancy ($\delta t^*_{SH} = 9.6$, $\delta t^*_{ScS} = -2.2$) at MNN is difficult to explain; it may be related to the likelihood that the S wave to MNN bottoms very near a suggested lower-mantle transition zone mentioned earlier. It is intuitively more reasonable that the positive δt^*_{SH}, rather than the negative δt^*_{ScS}, value is in greater error in view of the large negative travel-time delay observed at MNN (e.g. Hales and Roberts, 1970).

The mean, for each station except MNN, of the two adjusted δt^* values is given in Table 3.7. The agreement between δt^*_S determinations using events from two different azimuths is quite good (within 1.5 sec) for four of the five stations at which both measurements could be made. This suggests that (1) most of the contributions to δt^*_S arise in the upper mantle or crust, and that (2) for these four stations at least, δt^*_S is not strongly dependent on the <u>particular</u> path through the upper mantle along which the wave has travelled; i.e. attenuation varies slowly with lateral position in the mantle beneath these stations.

The exceptional station is BKS, at which shear waves from the northwest appear to be more attenuated, relative to the North-American norm, than do shear waves which have propagated from the southeast. This is probably related to the fact that BKS lies near the continental margin; the S wave from the Kurils passes through

a predominantly oceanic mantle, whereas the ray path from South America intersects the upper mantle beneath central California. Nuttli and Bolt (1969) have recently suggested that lateral variations in the depth to the top and bottom of the low-velocity zone may explain the azimuthal dependence of P-wave travel-time residuals at California stations near BKS. Such a structure would probably make δt_S^* azimuth-dependent as well. Alternatively, there is a growing body of evidence implying the prior existence of a zone of oceanic-lithosphere subduction near the California coast perhaps as recently (near BKS) as 6 million years ago (Atwater, 1970). If there is a fossil 'plate', thermally distinct from the surrounding asthenosphere, beneath California then attenuation of body waves in that region may be nearly as strongly path-dependent as in the vicinity of active island-arcs. (The difference is δt_S^* at BKS for events in South America and the Kurils is of the correct sign for the notion of a relatively 'cool' plate dipping toward the east or northeast.) It is conceivable that measurement of δt_S^* as a function of path direction to California stations can distinguish between the model of Nuttli and Bolt and the hypothesis that a remnant lithospheric plate lies beneath western North America.

It is not unreasonable that at all stations situated near boundaries betwen distinct tectonic or structural

provinces, δt^* should vary with azimuth. Thus, for example, δt_S^* at COR for wave propagating from the northeast or at RCD for waves from the southwest might be significantly different from the corresponding value in Table 3.7. The careful determination of δt^* as a function of azimuth might prove to constrain powerfully the possible lateral variations of attenuation beneath a station. The requirement that large, deep-focus earthquakes be uniformly distributed in azimuth, however, rules out most portions of the world (except perhaps Hawaii) as candidate sites for such an experiment.

3.3.3 Mid-Arctic ridge event

The earthquake of 25 August 1964, a shallow event near the continental shelf of Siberia, produced S waves of much longer period than those from the deep earthquakes. SV spectra (uncorrected for instrument) were dominated by peaks of width .03 to .04 Hz, with maximum Fourier amplitudes occurring between 40 and 50 sec periods. SH waves were of shorter duration and wavelength, and correspondingly their spectra were smoother and on the average peaked at periods shorter than 40 sec. A time window of about 90 sec was required for the SV waves; the shorter wavetrains and the more likely possibility of ScS contamination at distances greater than 60° dictated a shorter time window for SH waves.

Table 3.5

Differential attenuation of S waves,
Arctic event of 25 August 1964

Station		Distance (deg)	Azimuth (deg)	δt^*_{SV} (sec)	δt^*_{SH} (sec)
AAM	Ann Arbor, Mich.	58.4	26.0	+18.3±1.0	-0.1±0.6
ALQ	Albuquerque, N. Mex.	62.8	47.6	-3.7±2.8	-4.9±1.7
BOZ	Bozeman, Mont.	51.6	49.6	(-11.9±1.5)[a]	-4.9±0.5
COR	Corvallis, Ore.	50.6	60.2	-5.5±0.9	(-17.4±1.0)[c]
DAL	Dallas, Tex.	66.3	39.2	(-19.1±2.5)[b]	(-17.2±1.8)[b]
FLO	Florissant, Mo.	61.2	32.4	-1.3±2.4	-0.8±1.1
GOL	Golden, Colo.	58.3	45.6	-9.0±1.5	-17.6±1.7
LON	Longmire, Wash.	48.8	58.2	+0.2±2.0	(-6.4±3.0)[c]
MNN	Minneapolis, Minn.	54.8	33.8	-4.4±1.6	-4.5±3.3
OXF	Oxford, Miss.	65.5	32.2	+4.4±2.3	-0.1±0.9
SCP†	State College, Pa.	60.3	21.2	0	0
TUC	Tucson, Ariz.	64.7	52.1	-6.2±2.4	-11.4±1.2

† reference station

a film record poor; waveform uncertain

b spurious high frequency modulation of waveform

c irregular waveform; station near SH nodal plane

Time window used; 90.8 sec for SV

61.0 sec for SH

Band-pass filter cutoffs; 0.019 - 0.100 Hz

The calculated values of differential attenuation for this earthquake are given in Table 3.5. It is immediately apparent that the attenuation pattern is different than that for the deep South-American events. One complication is the source radiation-pattern (Sykes, 1968), which indicates that COR and LON lie near an SH-wave nodal plane, an explanation of their unusual SH waveforms. More significant is that the stations with the five highest values of δt^*_{SH} (in order: SCP, AAM, OXF, FLO, MNN) are all in the eastern U.S. and, in fact, all record arrivals which left the source at azimuths less than 35°. These five stations are among those with the seven largest values of δt^*_{SV}. The fact that FLO and OXF show very little attenuation for S waves from the south implies either a strong azimuthal dependence of δt^*_S at those stations or, more likely, that in the source area the attenuation depends greatly on the direction of ray propagation.

The earthquake occurred on what the seismicity (Sykes, 1965) and linear magnetic-anomalies (Demenitskaya and Karasik, 1966, and others) indicate is an active mid-ocean ridge. It is thus reasonable that the seismic attenuation is large in the immediate vicinity of the earthquake source. We might expect that the angle the projection of an S-wave ray-path onto the earth's surface makes with the ridge axis is related to the amount of near-source attenuation that the wave suffers. Further, it may be

Figure 3.4 Lateral variation of near-source attenuation: the mid-Arctic ridge earthquake. The difference between δt_S^* determined at U.S. stations from the Arctic event and δt_S^* (S. Am.) determined from the South American events (i.e. Table 3.7) is shown (right) as a function of propagation direction (azimuth, measured clockwise from north) from the source. The projections onto the earth's surface of several S-wave propagation-paths to North America are plotted (left) on a map of the Arctic region (Lambert equal-area projection). The Lomonosov ridge is well-defined by the 2-km isobath (simplified from Vogt and Ostenso, 1970), while the deeper mid-Arctic (also Nansen) ridge follows the trend of earthquake epicenters (crosses; from National Earthquake Information Center, 1970).

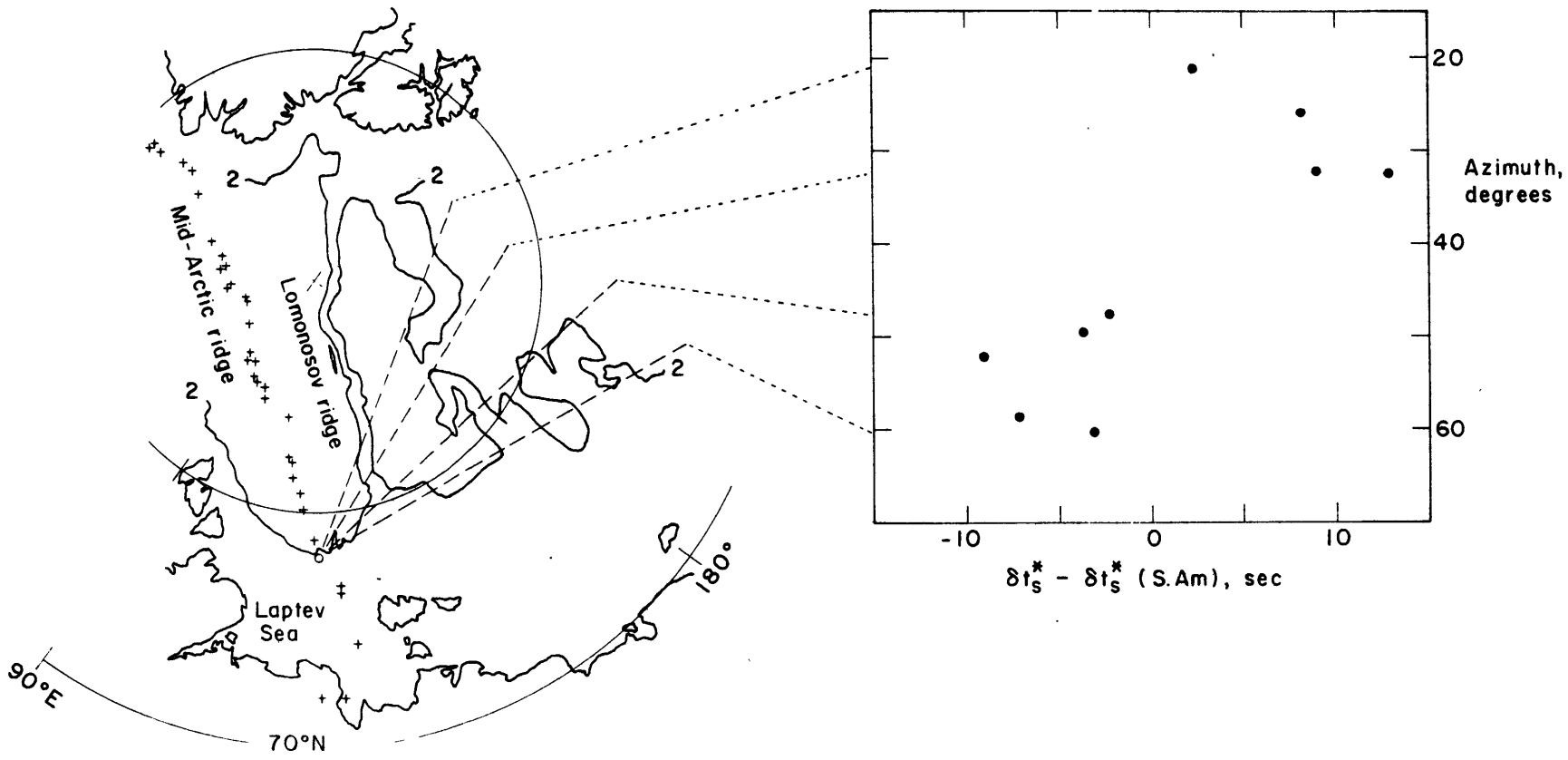
Mid-Arctic ridge
Lomonosov ridge
Laptev Sea
2
2
2
2
90°E
180°
70°N
20
40
60
Azimuth, degrees
-10
0
10
$\delta t_s^* - \delta t_s^*$ (S.Am), sec

no more than coincidental that rays leaving the earthquake focus at azimuths less than 35^{o} or 40^{o} must pass beneath the aseismic Lomonosov ridge, a feature that appears to be associated with uniformly high heat-flow (e.g. Lyubimova, 1970), whereas those at greater azimuths do not. This is shown graphically in Figure 3.4, where we have plotted the difference between δt_S^* as determined for the Arctic event from that obtained for the South American earthquakes as a function of propagation direction at the epicenter of the Arctic event. It should be cautioned that the determinations of δt_S^* for the two source regions were made over somewhat different frequency-intervals.

The notion that the lateral heterogeneity of attenuation near a mid-ocean ridge strongly might affect the spectra, observed teleseismically, of long-period shear waves from earthquakes on that ridge is potentially very useful. Ward and Toksöz (1971) observed similar lateral variations of attenuation of short-period P waves near the crest of the mid-Atlantic ridge. While conclusive support for such a hypothesis has not been demonstrated, the possibility that spatial variations of Q^{-1}, and hence of the material properties which affect Q^{-1}, in the vicinity of active ridges might be deduced from body-wave spectra of ridge earthquakes deserves considerable study.

In spite of the fact that both near-source and near-receiver attenuation influence the δt^* values in Table 3.5,

we may still check some of the small-scale patterns of Figure 3.3 by looking at the relative value of δt^* for stations at nearly the same azimuth from the source. Thus FLO appears less attenuating than OXF, LON is more attenuating than COR, and BOZ and ALQ have similar spectral ratios. This is in good qualitative agreement with Figure 3.3. In addition we can predict that if we analyzed records at GOL and MNN for South American earthquakes, δt_S^* would be less than -5 sec for GOL and less than -10 sec for MNN.

3.4 P-wave differential attenuation

To determine the P-wave differential attenuation δt_P^*, we use values of relative attenuation reported in the literature. Table 3.6 lists values of δt_P^* obtained from Teng (1968) and Mikumo and Kurita (1968) for the earthquakes indicated. Both sets of authors measured P-wave spectral ratios and used a relation such as equation (7) with $\delta t_j^* = \delta t_i^* \equiv 0$, to obtain the quantities $(t_j^* - t_i^*)$, which were assumed to depend only on epicentral distance and the focal depth of the source. We subtracted from their reported values of $(t_j^* - t_i^*)$ the attenuation predicted by equation (3.5) for a CIT-11A velocity distribution (e.g. Anderson, 1967) and Teng's (1968) model-F Q_α-distribution. The differences were then assumed to equal $(\delta t_j^* - \delta t_i^*)$.

Table 3.6 includes two independent determinations of δt_P^* for the Peru-Brazil border earthquake of 3 November 1965. The differences between the two determinations are greater than 3 sec for three stations (BKS, OXF, WES). The two values at the remaining stations agree to within 0.1 to 2.8 sec. The reason for the discrepancies may lie in the slightly different forms of analysis used by the two sets of authors.

Teng's (1968) method of obtaining $\delta A_i = t_j^* - t_i^*$ is the one we have followed in this paper: equations (3.1), (3.4) and (3.8). He smoothed all spectra and spectral ratios by averaging over a window of width .02 Hz. The

Table 3.6
P-wave differential attenuation

		δt_P^* (sec)			
		Teng (1968)		Mikumo & Kurita(1968)	
		9 Nov 65	3 Nov 65	3 Nov 65	28 Aug 62
AAM	Ann Arbor, Mich.	2.06		-2.10	
ALQ	Albuquerque, N. Mex.		1.33	4.14	(14.75)[a]
ATL	Atlanta, Ga.	1.87	-1.47	-1.66	
BKS	Berkeley, Calif.		1.80	-8.18	
BLA	Blacksburg, Va.	-0.94			
BOZ	Bozeman, Mont.		-0.04		
COR	Corvallis, Ore.		-0.55	-0.42	(0.43)[a]
DAL	Dallas, Tex.				(0.95)[a]
DUG	Dugway, Utah	1.05			
FLO	Florissant, Mo.	-0.68		-3.35	(1.41)[a]
GEO	Georgetown Univ.		1.72	0.36	3.54
GOL	Golden, Colo.	-0.48	1.45	-1.27	(6.54)[a]
LON	Longmire, Wash.			3.41	(7.55)[a]
LUB	Lubbock, Tex.			-0.75	(5.21)[a]
MDS	Madison, Wis.				(6.43)[a]
MNN	Minneapolis, Minn.				(4.72)[a]
OGD	Ogdensburg, N.J.		-0.10	-2.32	
OXF	Oxford. Miss.	1.92	0.22	3.80	
PLM	Palomar , Calif.			-3.24	
RCD	Rapid City, S. Dak.		1.43	1.02	(3.52)[a]
SCP †	State College, Pa.	0.0	0.0	0.0	0.0
TUC	Tucson, Ariz.	1.94		6.52	
WES	Weston, Mass.		-0.98	4.68	4.57

† reference station

a $\Delta > 75^\circ$, core diffraction effects important

frequency bandwidth for which his attenuation measurements are appropriate is .01 to 0.2 Hz. Teng has estimated that scatter in the data and errors in assumed crustal structure each introduce uncertainties in δA_i of about ± 1 sec.

Mikumo and Kurita (1968) define a new quantity

$$F(\omega) = \ln[R_{ij}(\omega)/R_{ij}(\omega_0)]$$

where $\omega = 2\pi f$ and ω_0 is a reference frequency. They fit a straight line through the origin to $F(\omega)$, and equate $\frac{dF}{d\omega}$ with $(t_j^* - t_i^*)/2\pi$. (Dr. Mikumo kindly provided his values of $\frac{dF}{d\omega}$ in tabulated form.) Because of the narrower frequency band (.03 to 0.13 Hz) and the simpler crustal model (a single layer, uniform for all stations) used in their calculations and the greater spread in their reported attenuation-values, the δt_P^* values obtained from Mikumo and Kurita (1968) are considered somewhat less reliable than those calculated from Teng's (1968) work.

Teng measured the attenuation for a second South American shock with a hypocenter very close to that of the 3 November 1965 event. The agreement in the values of δt_P^* for the two earthquakes is not any better than that between the two determinations of δt_P^* for 3 November 1965. Shown also in Table 3.6 are δt_P^* calculated from the attenuation measurements of Mikumo and Kurita (1968) for

an intermediate depth shock in Greece. Unfortunately, all U.S. stations are at least 68° from the epicenter. Beyond 75° or 80°, the effects of core diffraction become important. Since these effects were not considered by Mikumo and Kurita, δt_P^* for all stations at epicentral distances greater than 75° are not of much value except for comparing stations at similar epicentral distances. These values are enclosed in parentheses in the table.

Mean values of δt_P^* at each station for deep South American earthquakes, adjusted so that the average δt_P^* for the U.S. equals zero, are listed in Table 3.7 and plotted on a map of the U.S. in Figure 3.5. Similarities between Figures 3.3 and 3.5 are readily apparent. The wide zone of high attenuation west of the Rockies and the low attenuation on the Pacific coast and throughout the central and much of the eastern parts of the country duplicate similar features in the δt_S^* map. Some differences emerge. RCD and BOZ, the latter near the border between two physiographic provinces, have δt_P^*, respectively, greater than and less than zero, but δt_S^*, respectively, less than and greater than zero. WES and GEO show both P and S waves highly attenuated, though the continuous zone of high attenuation in the northeast is less well outlined in the δt_P^* data. OGD, in particular, has a low value of δt_P^*, though unfortunately no δt_S^* for that station has been yet measured. The P-wave differential

Table 3.7
Comparison of average differential attenuation for P and S waves at U.S. stations

Station	From South America δt_P^* (sec)	From South America δt_S^* (sec)	From Kuril arc δt_S^* (sec)
AAM	-0.3	3.8	
ALQ	2.5	0.8	
ATL	-0.7	-2.8	
BKS	-3.4	-3.1	1.7
BLA	-1.2		
BOZ	-0.3	3.2	
COR	-0.7	-1.0	-2.3
DUG	0.8	3.3	1.8
FLO	-2.3	-11.0	
GEO	0.8	7.6	
GOL	-0.4		
GSC		-10.8	
JCT		5.2	
LON	3.1	8.8	
LUB	-1.0	-2.4	
OGD	-1.5		
OXF	1.7	-3.9	
PLM	-3.5		
RCD	1.0	-4.2	-5.6
SCP	-0.3	0.6	
SHA		-6.7	
TUC	4.0	3.2	2.0
WES	1.6	10.2	

Figure 3.5 Lateral variation of P-wave differential attenuation, United States. δt_P^* is the average of attenuation measurements for two deep earthquakes in South America. Dashed lines separate (approximately) regions of positive and negative δt_P^*.

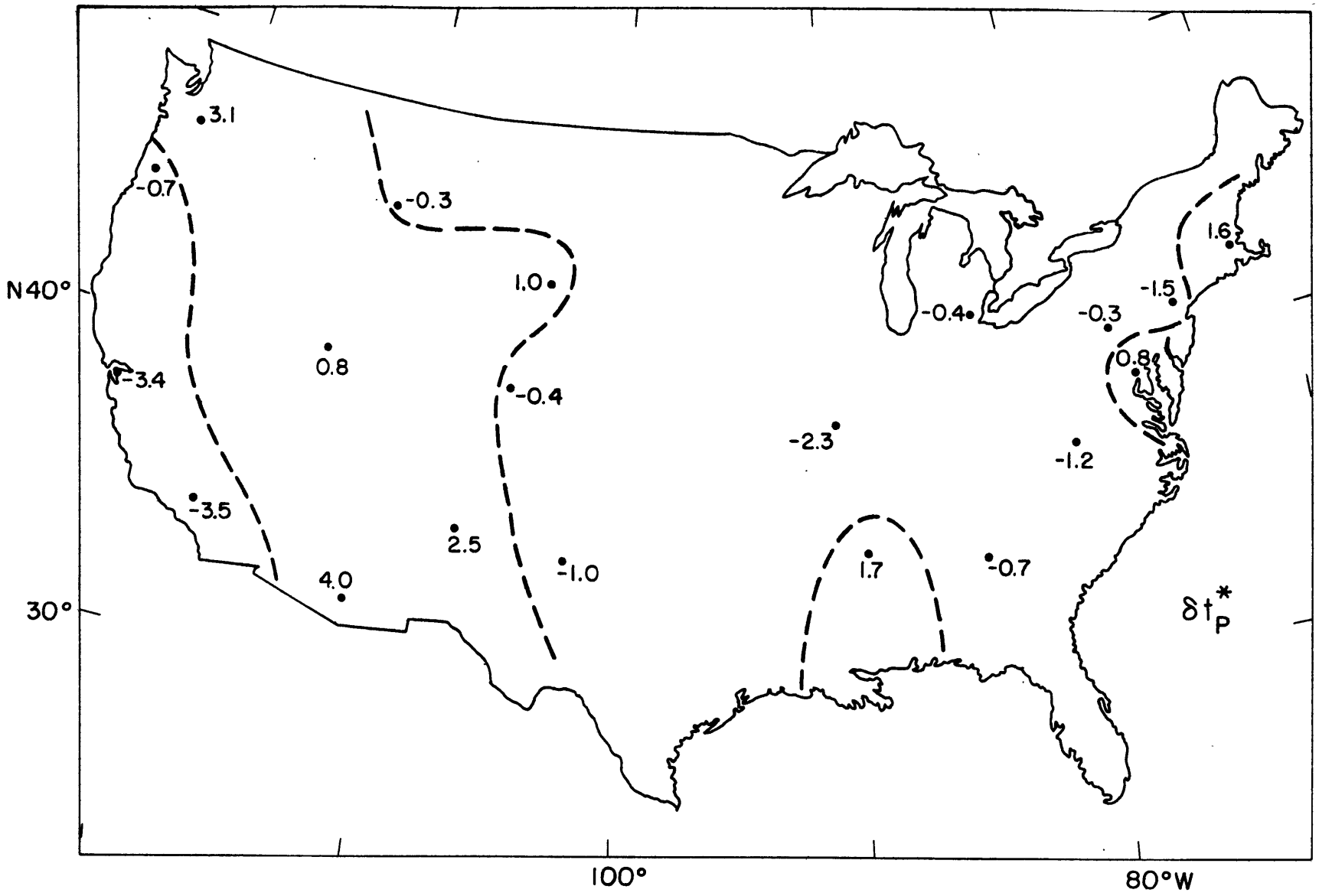
3.1
-0.7
-0.3
1.0
N40°
0.8
-3.4
-0.4
-0.4
-0.3
1.6
-1.5
0.8
-2.3
-1.2
-3.5
2.5
4.0
-1.0
1.7
-0.7
30°
δt_p^*
100°
80°W

attenuation also points to relatively high absorption for waves arriving at stations in the Gulf coastal plain (OXF), though this is not indicated by S-wave data. In general, however, qualitative agreement between the patterns of S and P attenuation is fairly good. A more quantitative comparison is made in the next section.

3.5. Constraints on the mechanism of attenuation

The data of the preceding section do not, by any means, completely define the Q-structure beneath North America. Nonetheless, several important results pertaining to the physical mechanism of dissipation (at least of the laterally-varying component of dissipation) may be obtained by comparing the relative attenuation of SV and SH waves and of P and S waves. A convincing case may also be made that Q^{-1} must be frequency-dependent.

3.5.1 Possible anisotropy of attenuation

If the mantle is everywhere isotropic, then δt^*_{SV} and δt^*_{SH} for a given station provide independent estimates of a single quantity. To the extent that shear-wave attenuation is anisotropic in some region of the mantle, that region will show different values of δt^* for SH and SV components. With the aim of investigating the possibility of attenuation isotropy in the upper and lower mantle, we have examined 'adjusted' values of δt^*_{SV} and δt^*_{SH} for all combinations of stations and events for which we have reliable estimates of both quantities. 'Adjustment' for the 25 August 1964 earthquake was satisfied by requiring that at the set of stations common to Tables 3.5 and 3.7, the average value of δt^* (SV or SH) in Table 3.5 equal the average value, for the same station set, of δt^*_S in Table 3.7.

We suppose that if the difference $\delta t^*_{SH} - \delta t^*_{SV}$ (adjusted values), at a given station and for a given event, departs significantly from zero then anisotropic attenuation is indicated. The term 'significantly' deserves more than passing note. We are subtracting two quantities, each with considerable uncertainty (due both to errors in obtaining the slopes of the spectral ratio and to incorrectly accounting for the baseline differences used in comparing various sets of data). Thus conclusions derived from the quantities $\delta t^*_{SH} - \delta t^*_{SV}$ should be treated with a healthy skepticism. With that note of gloom we press on.

Vvedenskaya and Balakina (1959) have invoked anisotropy of attenuation at certain depths in the lower mantle to explain decreased amplitudes of SH waves, relative to those of P and SV waves, within five epicentral distance ranges. As a test of their suggestion, we plot in Figure 3.6 the quantity $\delta t^*_{SH} - \delta t^*_{SV}$ as a function of epicentral distance. Vvedenskaya and Balakina (1959) found the ratio of SH amplitude to SV amplitude to be anomalously low for epicentral distances in the range 51-53° and near 70°. (These figures are appropriate to shallow sources; for deep earthquakes the corresponding values will be several degrees lower). While there is no readily discernible trend in Figure 3.6, the scatter indicating that either upper mantle properties or data errors dominate the effect of the lower mantle, the absence of obvious peaks

Figure 3.6 Relative differential attenuation of SH and SV waves. The quantity $\delta t^*_{SH} - \delta t^*_{SV}$, assumed here to be a function of epicentral distance only, has been determined using two deep earthquakes (solid circles) and one shallow event (open circles). The two shaded regions indicate ranges of epicentral distance (for a shallow focus) over which SH-wave amplitudes are reputed (Vredenskaya and Balakina, 1959) to be anomalously low relative to SV and P amplitudes.

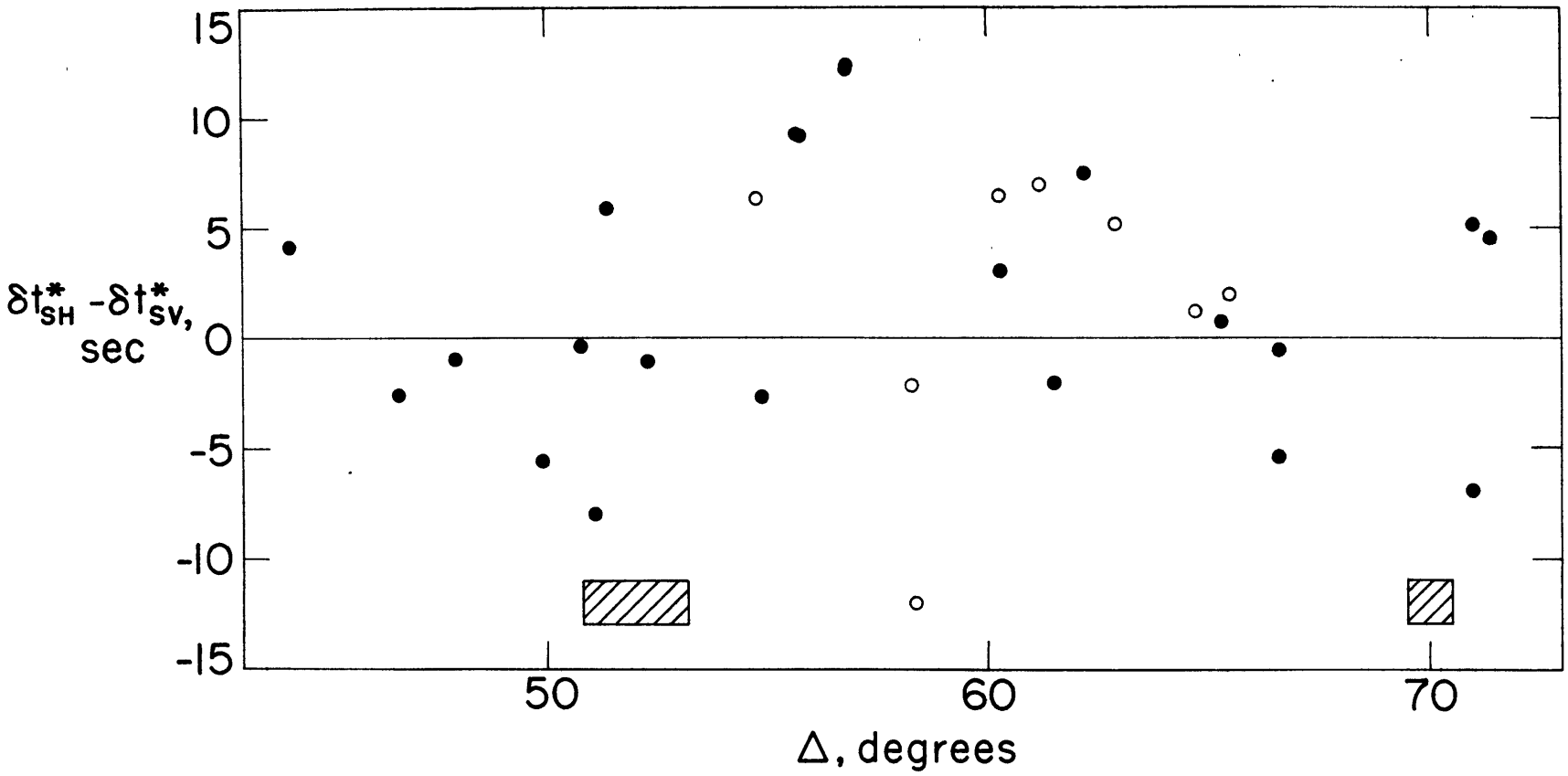
15
10
5
0
-5
-10
-15
$\delta t^*_{SH} - \delta t^*_{SV}$, sec
50
60
70
Δ, degrees

in $\delta t^*_{SH} - \delta t^*_{SV}$ near 47^o or 66^o (for the South-American data) provide no encouragement for Vvedenskaya's and Balakina's hypothesis. It may be concluded that the amplitude anomalies they observed either are regional in character or are not the result of attenuation.

A look at the quantity $\delta t^*_{SH} - \delta t^*_{SV}$, averaged for the two South American earthquakes, at individual stations is also illuminating. The absolute value of the difference between SH and SV attenuation is greater than 3 sec at 6 (out of 17) stations. At LON, DUG, TUC, and LUB in the western U.S., $\delta t^*_{SH} - \delta t^*_{SV}$ equals +5 to +9 sec (i.e. SH waves appear more attenuated than SV waves); while at WES and SCP in the northeast U.S., $\delta t^*_{SH} - \delta t^*_{SV}$ equals -8 and -6, respectively (i.e. SH waves are apparently less attenuated than SV waves). The notion that such differences imply anisotropic Q^{-1} (presumably the result of non-hydrostatic stresses) in the upper mantle has not been verified, of course, since the effects of attenuation along remaining parts of the ray path have not been eliminated. Nonetheless, the idea is an intriguing one that deserves further attention.

3.5.2 Relative magnitude of P and S differential-attenuation

Consider the relative magnitudes of δt^*_P and δt^*_S obtained from records of South American earthquakes. The δt^*_P values in Table 3.7 vary over a range of 7.5 sec, whereas the range of δt^*_S values is 22.2 sec or almost three

Figure 3.7 Comparison of S and P differential attenuation at U.S. stations. Vertical and horizontal error bars delimit the range of calculated values for each station. The straight line drawn through the data points is the least-squared-error fit.

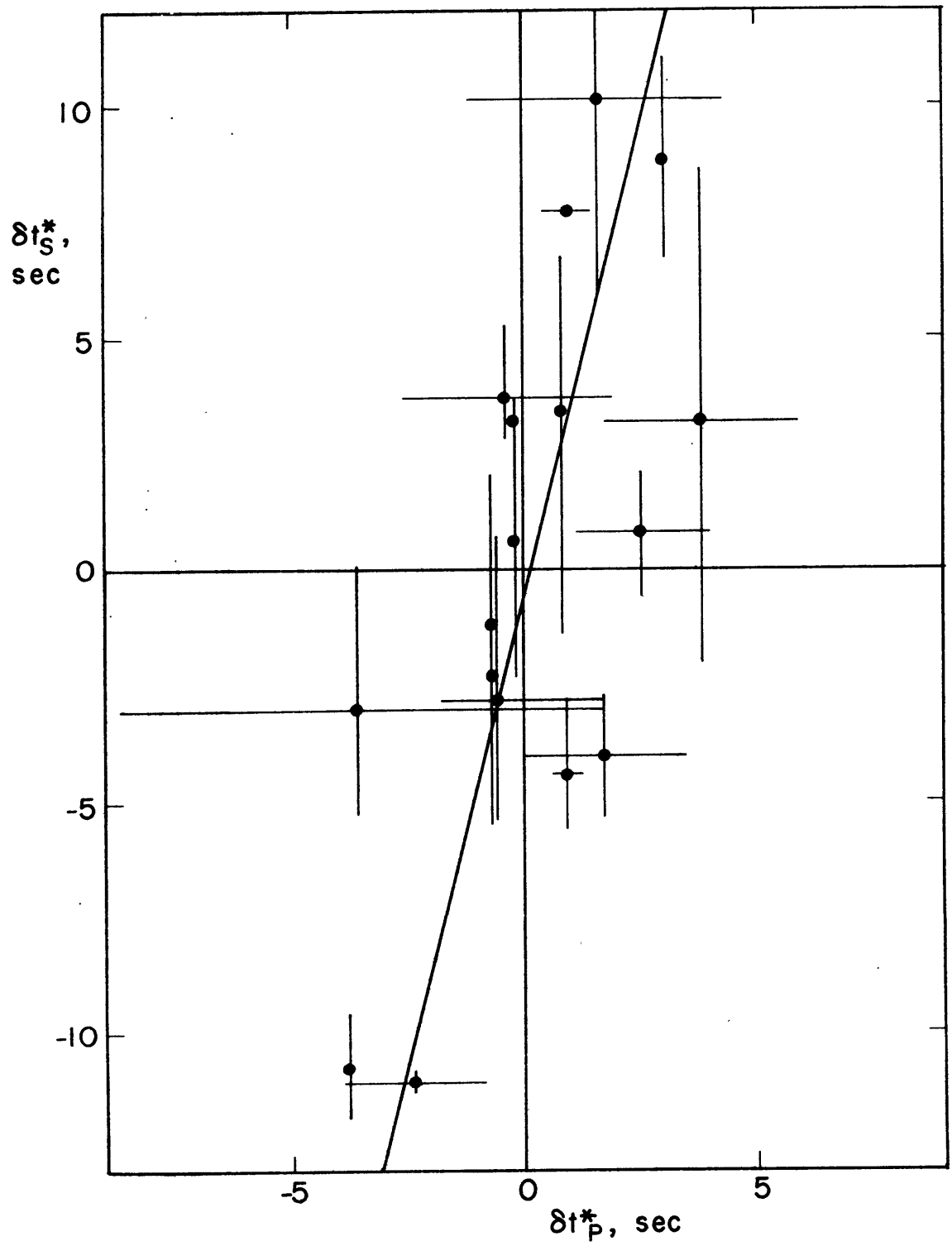
10
5
0
-5
-10
δt_S^*, sec
-5
0
5
δt_P^*, sec

times as great. This implies that contributions to the differential attenuation due to losses in shear are greater than those due to losses in pure compression. This conclusion may be stated more quantitatively.

In Figure 3.7 is a comparison of average δt_S^* and δt_P^* at U.S. stations for ray paths from South America. (GSC and PLM are treated as a single point.) Error bars indicate the range of individual values. The correlation coefficient for the two sets of data is 0.65. This correlation coefficient is significantly greater than zero at the 99 percent confidence level. The straight line satisfying the requirement that the sum of the squares of the perpendicular distances of the points from this line be a minimum (e.g. York, 1966) is given by

$$\delta t_S^* = -0.6 \pm 1.6 + (4.1 \pm 0.8)\, \delta t_P^* .$$

(The uncertainties indicated are the standard deviations.)

From the slope of the straight-line fit, an estimate may be made of the relative contributions to observed differential attenuation of losses in shear and in compression. Let us write δQ_μ^{-1} (equal to δQ_β^{-1}) in the following form (Anderson and Archambeau, 1964), valid for most attenuation mechanisms when losses are small.

$$\delta Q_\mu^{-1} = \frac{\delta \mu''}{\mu'} \qquad (3.9)$$

where the complex shear modulus is given by

$$\mu = \mu' + i\,(\mu'' + \delta\mu'') \ .$$

For S waves at normal incidence, assuming lateral attenuation-variations (i.e. $\delta\mu''$) are confined to a zone of thickness h in which μ' and μ'' do not vary, equations (3.6) and (3.9) give

$$\delta t_S^* = h\rho^{1/2} \frac{\delta\mu''}{(\mu')^{3/2}} \tag{3.10}$$

where ρ is the density, assumed constant. Similarly

$$\delta t_P^* = h\rho^{1/2} \frac{\delta K'' + \frac{4}{3}\delta\mu''}{(K' + \frac{4}{3}\mu')^{3/2}} \tag{3.11}$$

where $K = K' + i(K'' + \delta K'')$ is the complex bulk modulus. Then

$$\frac{\delta t_S^*}{\delta t_P^*} = \frac{\delta\mu''}{\delta K'' + \frac{4}{3}\delta\mu''} \left(\frac{K' + \frac{4}{3}\mu'}{\mu'}\right)^{3/2} \tag{3.12}$$

$$= 4.1 \pm 0.8 \ .$$

Taking $(K' + \frac{4}{3} \mu')/ \mu' = 3$ in equation (3.12) gives

$$\frac{\delta\mu''}{\delta\mu'' + \frac{3}{4}\delta K''} = 1.0 \pm 0.2 \qquad (3.13)$$

which implies $\delta K'' = 0$. Even if we take $\delta t_S^* / \delta t_P^* = 3.3$, one standard deviation less than the calculated value, we find

$$\frac{\delta K''}{\delta\mu''} = 0.24 \qquad \text{or} \qquad \frac{\delta Q_K^{-1}}{\delta Q_\mu^{-1}} = 0.14 .$$

Thus compressional losses are considerably less important than shear losses in governing regional differences in attenuation, and the relative magnitudes of S- and P-wave differential attenuation are consistent with all contributions to δQ_α^{-1} being due to losses in rigidity. This is in line with the finding by Hales and Doyle (1967) that travel-time residuals in the U.S. are most simply explained by regional differences only in the shear modulus.

(A word of qualification should be interjected. Figure 3.7 shows considerable scatter. This is due in large part to random errors, but may also reflect real lateral differences in the contributions of compressional losses. At ALQ and TUC, for instance, δt_P^* is greater than

δt_S^*)

The conclusion that all regional variations of attenuation in North America may be attributed entirely to losses in shear is of immense importance. A viscous dissipation-mechanism, such as would be appropriate to a partial melt (see Chapter 2), is strongly indicated. Further support for such a hypothesis comes from the fact that most of the regions of high attenuation are areas where near-solidus temperatures in the upper mantle are indicated by other geophysical studies. Thus upper-mantle attenuation mechanisms for which compressive losses are comparable to or greater than shear losses (i.e. those which involve changes in volume), such as interface inelasticity at fluid-filled cracks (Gordon and Davis, 1968) or acoustic-wave propagation through a phase change with reaction rate comparable to wave frequency (Vaišnys, 1968), contribute negligibly to the lateral variations of attenuation.

3.5.3 Frequency dependence of Q^{-1}

It is now widely accepted that for rocks at pressures less than a few kilobars, the intrinsic Q is substantially independent of frequency (see Knopoff, 1964 , or Attewell and Ramana, 1966, for reviews of recent measurements). Much more in doubt is the frequency dependence of Q in the earth's mantle. Elaborate theories have been worked out for a myriad of attenuation mechanisms, and various functional

dependencies of Q^{-1} on f have been proposed. Unfortunately most seismic evidence is ambiguous at best.

Gutenberg (1945c,1958) was the first to make measurements of body-wave attenuation. He concluded that Q in the mantle is proportional to frequency for both P and S waves. Because he used data from many earthquakes, without regard to variations in source functions, instrument responses or station crustal structures, his findings have been lightly dismissed by subsequent workers.

That Q may increase with frequency for short-period P waves in the mantle is suggested by the high values of Q (greater than 1000) determined for the frequency range 1-10 Hz (Asada and Takano, 1963; Sumner, 1967). This contrasts with values an order of magnitude lower for the frequency range .01 to 1 Hz reported by other authors (Teng, 1966, 1968; Hirasawa and Takano, 1966; Kanamori, 1967a). More conclusively, Q_α proportional to frequency has been shown to be appropriate for P_n waves in the frequency range 1.5 to 20 Hz, in Maine (Frantti, 1965) and for direct P waves in the frequency range 0.3 to 1.3 Hz (Kurita, 1968). Furthermore, Fedotov and Boldyrev (1969) found that Q_α and Q_β at depths near 100 km beneath the southern Kuril Islands increase as $f^{0.8}$ for f in the range 1.25 to 20 Hz. From the attenuation of P_n waves in the western United States, Archambeau et al. (1969) also concluded that Q_α in the uppermost mantle increases with increasing frequency

over the frequency range 0.75 to 1.5 Hz.

After a study of the spectral ratios of shear waves multiply reflected at the core-mantle boundary and recorded over a wide epicentral-distance range, Sato and Espinosa (1967) concluded that Q_β in the mantle decreases with period, T, between periods of 25 and 90 sec. Their method consists of first computing Q for each independent spectral amplitude in the spectral ratio of a given (n+1) ScS/nScS or (n+1) sScS/nsScS pair for a single earthquake. Plots of Q versus T are then grouped into three epicentral-distance ranges. In each range, the Q's for a certain period are averaged. The resulting average Q's show a general decrease with increasing period for all three distance-ranges.

The results of Sato and Espinosa are suspect on several counts, however. For the smallest epicentral distances, spectral ratios with both Q increasing with T and Q decreasing with T are observed. For a given period, averaging the various values of Q^{-1} -- more physically reasonable than averaging the Q's -- would give a mean Q^{-1} that shows very little if any dependence on period. For greater epicentral distances, the drop in apparent Q with period appears to be real. This may not represent an intrinsic frequency dependence, however. Sato and Espinosa assumed that surface and core reflection coefficients, as well as station crustal response, are independent of period. Including the effects of layering

in the crust and near the core-mantle boundary may alter their conclusions.

More recently Tsai and Aki (1969) were forced to invoke a frequency-dependent Q to explain Love- and Rayleigh-wave attenuation in the frequency range .02 to .065 Hz. They proposed that Q for periods shorter than 20 seconds is lower than that for longer periods in the upper 30 km of the earth.

Let us suppose that for a sufficiently restricted frequency bandwidth we have for any given region of the earth three possible forms for the functional dependence of Q on frequency: (1) Q is independent of f, (2) Qf is independent of f, (3) Q/f is independent of f. (Clearly, for a frequency band as wide as a decade or more, these three choices do not exhaust all possible forms of frequency dependence; cf. Chapter 2.) If (3) holds everywhere in the earth, then all body-wave spectral ratios, after corrections for source and station effects had been made, would be constants, independent of frequency. This is not the case. If, on the other hand, Q in the mantle is everywhere inversely proportional to frequency (i.e. 2 holds), then appropriately corrected spectral ratios would vary as the square of frequency. In fact, the (n+1) ScS/nScS spectral ratios of Kovach and Anderson (1964) and the P/PcP ratios of Kanamori (1967c), as functions of frequency, show a downward curvature, indicating that in those studies the apparent Q may decrease with frequency.

As a test of whether δt_S^* (and therefore δQ^{-1}) proportional to frequency is appropriate for the S-wave spectral ratios discussed above, each ratio from the two South American earthquakes and from the Kuril arc event was fitted not only by a straight line of the form $a + bf$ but also by a square law of the form $a + bf^2$. The sum of the squared residuals was used as a test of the goodness of fit. Of the 57 spectral ratios (again omitting components with δt_K^* given in parentheses in Tables 3.2 through 3.4), 29 were fit slightly better by the second-power law than by the straight line. The opposite was the case for the remaining 28 ratios. This is hardly overwhelming evidence either for or against a frequency-dependent Q, and the question may be considered still unresolved. It is safe to say, however, that there is no strong reason to indicate the previous assumption of a frequency-independent δt^* is improper. (Note that the assumption that δt^* is frequency-independent, because δt^* is an integral over a ray path, is much weaker than requiring δQ^{-1} to be everywhere independent of frequency. See also Chapter 5.)

It is quite possible that the ambiguous results cited in the preceding paragraph are the result of the relatively narrow frequency band (less than a decade) over which spectral measurements were made. How may we extend our discussion, say, to higher frequencies? For P waves, we might compare values of δt_P^* (appropriate to $f \approx .10 \pm .09$ Hz) at U.S. stations to the measured station

Figure 3.8 Surface-wave magnitude versus body-wave magnitude for events in southwestern North America. M_S and m_b, measured at stations in the Canadian Network, are from Basham (1969). Earthquakes represented by solid symbols are located in regions of negative δt_P^* in Figure 3.5; those given by open symbols are located in areas of high attenuation (positive δt_P^*) in Figure 3.5. Straight lines are (lowest line) Basham's fit to nuclear-explosion data and (upper two lines) least-squared error fits to the two earthquake populations.

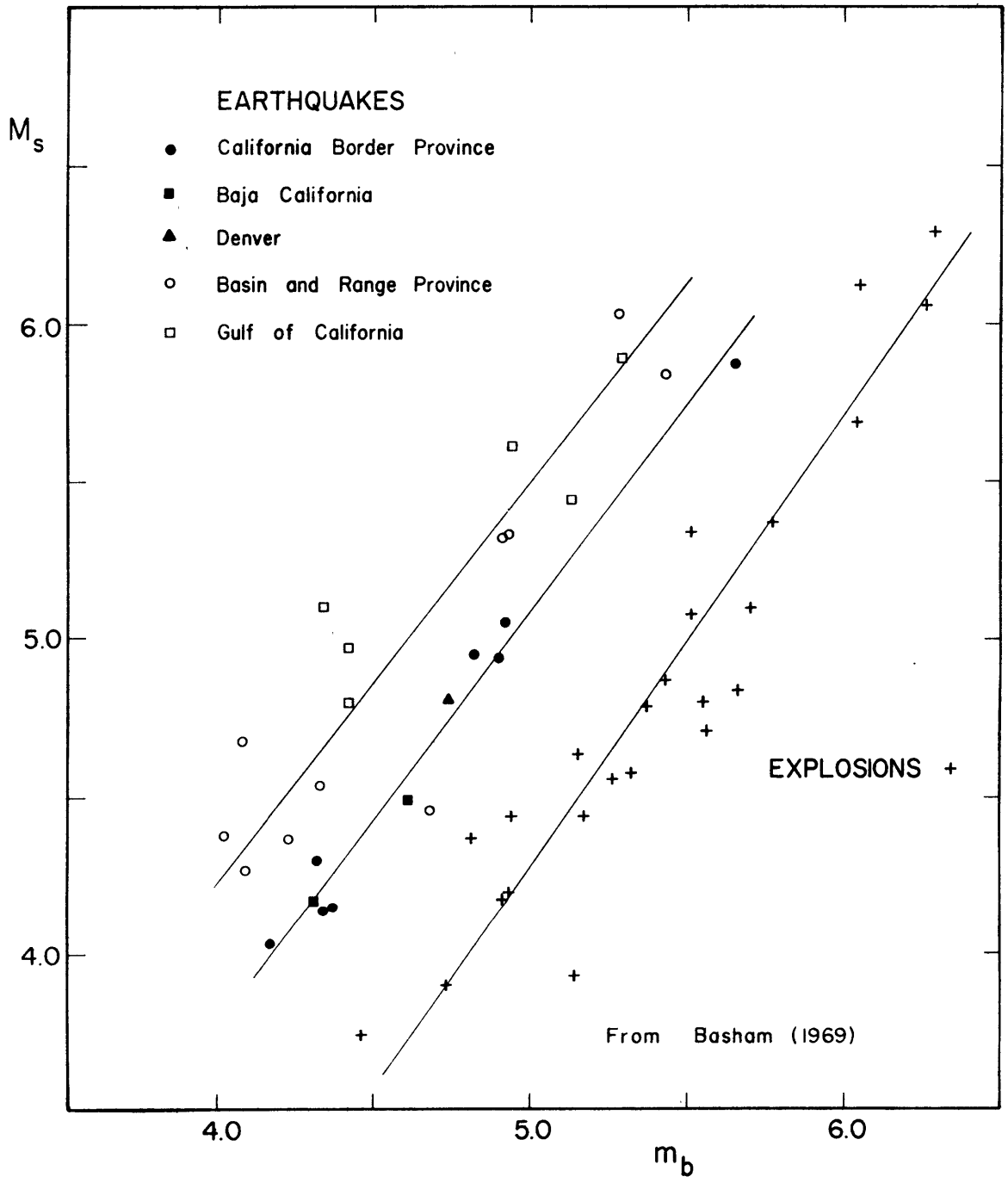
EARTHQUAKES
California Border Province
Baja California
Denver
Basin and Range Province
Gulf of California
EXPLOSIONS
From Basham (1969)
M_s
m_b
6.0
5.0
4.0
4.0
5.0
6.0

anomalies for body-wave magnitude, obtained from amplitudes of short-period (f ≃ 1 Hz) P waves (e.g. Guyton, 1964; Cleary, 1967). The body-wave magnitude at any single station may be at least as sensitive, however, to local geology (i.e. the presence of a sedimentary basin) as it is to upper-mantle attenuation. Thus we shall take an alternate (and, to some extent, reciprocal) approach: we compare δt_P^* at U.S. stations to the body-wave magnitude, m_b, of U.S. earthquakes of a given dimension (i.e. surface-wave magnitude).

From Figure 3.5 one can make two important hypotheses concerning body-wave magnitudes: (1) If the differences at long periods between δt_P^* for the Pacific Border province and that for the Basin and Range province persist at periods near 1 second, then body-wave magnitudes for California earthquakes, recorded at teleseismic distances, should be greater than those for Nevada-Arizona earthquakes of comparable surface wave magnitude M_s. (This presupposes that the effect on m_b of lateral variations in δt_P^* is much greater than the effect on M_s of lateral variations in Q_R^{-1} for 20-sec Rayleigh waves, an assumption supported by the results of Chapter 4.) (2) Because differences in m_b predicted from δt_P^* values obtained for long-period waves are less than those observed, Q_α^{-1} is frequency-dependent. Each of these statements merits closer scrutiny.

As a test of the first hypothesis above, we reproduce in Figure 3.8 Basham's (1969) measurements at Canadian

stations of m_b and M_S for earthquakes and explosions in south-western North America; we make, however, an additional important distinction. The earthquake population is segregated into two groups: (i) those that occur within the zone of high attenuation (10 in the Basin and Range Province and 6 in the Gulf of California), and (ii) those that occur outside the zone (8 in the California Border Province, 2 in western Baja California, and 1 near Denver). The earthquakes in group (ii) cluster very tightly about a straight line. With one exception, earthquakes in group (i) lie well above that line. From the fitting of straight lines, using a least-squared-error criterion, to the two populations, we conclude that in the m_b range 4.5 to 5.5 earthquakes of a given surface wave magnitude from the Basin and Range - Gulf of California region show apparent body wave magnitudes 0.3 to 0.4 less than do comparable earthquakes from adjacent areas (principally the San Andreas region of California). That this difference is due to lateral variations of Q^{-1} in the upper mantle is strongly suggested, though not proven. Differences in average depth of focus or source volume for earthquakes of the two areas is another possible explanation. The typically shallow depth of earthquakes throughout southwestern North America, however, and the findings by Wyss and Brune (1968) that source dimensions of earthquakes in the Nevada-Arizona region are similar to or smaller than those on the San Andreas fault-

system are compelling arguments that the latter explanation is not valid. Basham's (1969) measurements, therefore, lend considerable qualitative support to the results of Figure 3.5 for at least the western United States.

Thus the attenuative properties of a medium can significantly alter the $M_S - m_b$ relationship, used to discriminate underground nuclear explosions from earthquakes. The anomalous $M_S - m_b$ pattern in western North America is at least in part due to greater-than-average attenuation of P waves in the upper mantle of that region (cf. Ward and Toksöz, 1971). Even more importantly, by considering in Figure 3.8 only those earthquakes and explosions which occur in the same tectonic region (NTS is in the Basin and Range province), a more effective separation of explosion and earthquake populations is achieved than if all earthquakes from western North America are lumped into a single category.

Consider now the difference in body wave magnitudes for earthquakes of a given M_S in California and the Basin and Range province that we might predict from Figure 3.5. The average δt_P^* for California is -3.4; for the Basin and Range province δt_P^* is about 2.4. Using equations (3.3) and (3.4), we find that for P waves of 10-second period the amplitude observed from a California earthquake should be, on the average, a factor of 2 greater than the amplitude of an event of similar size (i.e. energy release) in the Arizona-Nevada region.

If δt_P^* is independent of frequency (i.e. if we make the questionable assumption that long-period spectral ratios may be extrapolated to higher frequencies), then for 1-second P waves we should predict amplitudes in California 300 times greater than in the Basin and Range area. This amounts to a magnitude difference of 2.5, clearly much larger than the difference of 0.3 to 0.4 indicated in Figure 3.8. Though the larger source volume of California earthquakes (Wyss and Brune, 1968) mentioned above may mask some of the effect of variations in upper-mantle attenuation, the conclusion that the differences in δt_P^* between the two regions decreases with increasing frequency is difficult to avoid.

A further interesting observation may be made by comparing Figure 3.5 with the results of Ward and Toksöz (1971). For long-period P waves, $\delta t^*_{TUC} - \delta t^*_{BOZ}$ equals 4.0 sec, indicating that P waves of frequency about 0.1 Hz are much more highly attenuated beneath southern Arizona than beneath the middle and northern Rockies. Ward and Toksöz (1971) measured the differential attenuation of short-period (f ≈1 Hz) P waves at the LASA and TFSO arrays in Montana and Arizona, respectively. They found $\delta t^*_{TFSO} - \delta t^*_{LASA}$ equal to -0.2 and -1.1 sec for two deep earthquakes (in South America and in the Kuril arc, respectively) equidistant from the two arrays. While the attenuation beneath LASA (TFSO) may not be identical to

that beneath BOZ (TUC), it appears that the lateral variation of Q^{-1} between Arizona and Montana is a strong function of frequency between 0.1 and 1.0 Hz.

Thus from the standpoint both of the physical mechanisms likely to dominate attenuation in the upper mantle (Chapter 2) and of a substantial number of amplitude measurements of various sorts, Q^{-1} in the upper mantle of such tectonic regions as western North America appears to be dependent on frequency over at least some portion of the frequency range appropriate to seismic waves. This fact must be considered in any scheme for inverting attenuation observations to obtain Q^{-1} within the earth. It is also probable that our assumption that δt^* for long-period P and S waves is independent of frequency over the frequency bands studied is incorrect. In that case, the values of δt_S^* and δt_P^* discussed above may be considered parameterizations of corrected spectral ratios which are somewhat more complicated than linear functions of frequency. The actual measured value of δt^* is then appropriate roughly to the midpoint of the frequency band, i.e. a frequency of about 0.1 Hz for the determinations given in this chapter.

Chapter 4. Regional Variation of Surface-Wave Attenuation

In the last chapter it was shown that the differential attenuation of body waves shows a strong and systematic regional variation, which was presumed to be due to a laterally inhomogeneous absorbing zone (low Q) in the upper few hundred kilometers of the mantle. If this zone is a locus of partial melting, then the discussion of Chapter 2 suggests that Q^{-1} at these depths is highly dependent on frequency over at least some portion of the frequency range appropriate to seismic waves. A crucial test of these two hypotheses is the determination of surface wave attenuation, in the period range roughly between 15 and 100 seconds, for individual tectonic provinces. Inversion of such measurements to yield Q^{-1} as a function of depth and frequency will determine the region of the mantle or crust in which the greatest attenuation occurs and whether Q^{-1} within that region can have the frequency dependence expected for a partial melt.

The obstacles involved in such a task are legion. The measurement of surface-wave dissipation over path lengths on the order of 1000 km is notoriously wrought with complications. Uncertainties in instrument calibrations, the effect of crustal-structure variations, often unknown, on wave amplitudes, and the frequent presence of interfering higher modes or laterally refracted multiple arrivals can make Q determinations meaningless.

Even if surface-wave attenuation were known with absolute accuracy along some path and over some period range, the technique of inversion is largely a matter of personal taste. There is, of course, no unique inverse, and the variation of surface wave Q^{-1} with frequency may be ambiguously interpreted as a variation of the material Q^{-1} with depth alone, with frequency alone, or with both depth and frequency.

The above difficulties notwithstanding, because the attenuation of surface waves with periods between 15 and 100 seconds is so highly sensitive to the state of the uppermost mantle, Q^{-1} for surface waves has been determined over two North American paths. Plausible models of $Q^{-1}(z,f)$ for the two paths fit both surface- and body-wave attenuation measurements and are consistent with the idea that the low-velocity, low Q zone is a region of partial melting.

4.1 Formulation

Most recent measurements of the attenuation of surface waves have been obtained from the spatial decay of Fourier amplitude spectra, a scheme introduced by Sato (1958). When two seismograph stations and an earthquake epicenter all lie on a common great-circle path, the ratio of the observed surface-wave spectral amplitude at station 1, at a frequency f, to that at station 2, may be written in the form:

$$R_{12}(f) \equiv \frac{A_1(f)}{A_2(f)} = \frac{a_1(f)\ I_1(f)}{a_2(f)\ I_2(f)} \left(\frac{\sin \Delta_2}{\sin \Delta_1}\right)^{1/2} e^{-(\Delta_1-\Delta_2)k^*(f)} \tag{4.1}$$

(e.g. Toksöz et al., 1964). In the above expression Δ_i is the epicentral distance to station i; $k^*(f)$ is the average attenuation-coefficient along the path between the two stations; $I_i(f)$ is the amplitude response of the seismograph at station i; and $a_i(f)$ is proportional to the theoretical amplitude, appropriate to the underlying layered structure, at the ith station. In the special case where the crust-mantle structure is constant along the two-station path, the ratio a_1/a_2 equals unity.

Consider a surface wave propagating from station 1 to station 2. Define

$$k^*_{12}(f) \equiv \frac{1}{\Delta_2-\Delta_1} \ln \left[R_{12}(f) \frac{I_2(f)}{I_1(f)} \left(\frac{\sin \Delta_1}{\sin \Delta_2}\right)^{1/2}\right]$$

$$= k^*(f) + \frac{1}{\Delta_2-\Delta_1} \ln \left[\frac{a_1(f)}{a_2(f)}\right] . \qquad (4.2)$$

Similarly, for a wave propagating from station 2 to station 1 we define

$$k^*_{21}(f) \equiv \frac{1}{\Delta_1-\Delta_2} \ln \left[R_{21}(f) \frac{I_1(f)}{I_2(f)} \left(\frac{\sin \Delta_2}{\sin \Delta_1}\right)^{1/2}\right] \qquad (4.3)$$

$$= k^*(f) + \frac{1}{\Delta_1-\Delta_2} \ln \left[\frac{a_2(f)}{a_1(f)}\right] .$$

Thus

$$2k^*(f) = k^*_{12}(f) + k^*_{21}(f) \qquad (4.4)$$

The specific quality factor Q is obtained from

$$Q^{-1}(f) = \frac{k^*(f)\ U(f)}{\pi f} \qquad (4.5)$$

where U (f) is the reciprocal of the average group slowness between the two stations.

If a_1/a_2 differs from unity, i.e. if the two stations lie in different structural provinces, then the above discussion is not valid in the immediate vicinity of the transition zone between the two provinces, where such effects as scattering and mode conversion are important.

For Love waves, Boore (1970) has shown that (4.1) is a valid approximation at distances greater than one wavelength from the transition region. This provides a useful criterion for judging whether relations (4.4) and (4.5) will yield an accurate estimate of Q.

4.2 Location of surface-wave paths

The two paths over which surface-wave attenuation has been determined lie in western and east-central United States. The first is between WWSSN stations at Longmire (LON), Washington, and Tucson (TUC), Arizona, and crosses the Basin and Range and Columbia Plateau provinces, with a short segment in the southwest corner of the Colorado Plateau. The LON-TUC path is relatively homogeneous, though anomalous, in many geophysical parameters; the P_n velocity is 7.8 to 7.9 km/sec (Herrin, 1969); travel-time residuals are generally large and positive (except at LON itself!) for both P (Clearly and Hales, 1966; Herrin and Taggart, 1968; and others) and S (Hales and Roberts, 1970) waves; δt_P^* and δt_S^* are large and positive (see Figures 3.3 and 3.5); heat flow is consistently greater than 1.5 $\mu cal/cm^2$-sec (Roy et al., 1968; Blackwell, 1969); and the electrical conductivity in the upper mantle is abnormally high (Caner et al., 1967; Reitzel et al., 1970).

The seismograph station at Longmire, Washington, is located in the Cascade mountain range at the foot of Mount Rainier and overlies a crust of some 25 to 35 km thickness. From local earthquake travel times, Dehlinger et al. (1965) found the crust west of the Cascades to be 5 to 10 km thinner than the crust to the east (roughly 35 km thick). Thus the crustal structure in the immediate vicinity of LON may vary laterally, a conclusion strengthened

by the pronounced negative Bouguer-anomaly closure southeast of the station site (Woolard and Rose, 1963). The Cascade range considered as a structural unit, however, has little or no crustal root (Johnson and Couch, 1970). Unreversed seismic-refraction profiles to LON from the coast of Oregon (Berg et al., 1966) and from British Columbia along the northern Cascades (Johnson and Couch, 1970) yielded crustal thicknesses of 16 and 32 km, respectively. For the path between LON and TUC, a good estimate for the crustal thickness at the LON end is therefore between 30 and 35 km.

The seismograph station at Tucson, Arizona, is located in the Sonoran Desert section of the Basin and Range province and sits atop a crust probably less than 25 km thick. Warren (1969) observed that the Mohorovicic discontinuity beneath central Arizona dips to the northeast, and the crustal thickness increases from 21 km in southwestern Arizona to about 40 km near the boundary of the Colorado Plateau. Extrapolating from Warren's results some 200 km along the strike of the M-discontinuity would indicate a crustal thickness beneath Tucson of 21 or 22 km.

It is clear that the structure of at least the crust beneath TUC is different from that under LON. The mantle velocity structure may also vary along the LON-TUC path, though Julian (1970) has indicated that the entire Basin and Range province may be represented by a single com-

pressional-velocity model. It is therefore imperative that the apparent attenuation be measured in both directions along the path. Then Q^{-1} may be determined from equations (4.4) and (4.5) as long as the transition zone between the two structural provinces is sufficiently far from either station. We anticipate that the transition is centered near the boundary between the Great Basin and the Colorado Plateau (see also Pakiser and Zietz, 1965), which along the path to TUC lies about 400 km southeast of LON. This distance, we shall see, is greater than one wavelength for all surface waves considered below.

The second surface-wave path examined in this study lies between WWSSN stations at Rapid City (RCD), South Dakota, and Atlanta (ATL), Georgia, and includes segments crossing the Great Plains, the Central Lowland, and the Appalachian provinces. Along the RCD-ATL path the P_n velocity is 8.1 to 8.2 km/sec (Herrin, 1969); travel-time residuals are generally negative (Cleary and Hales, 1966; Hales and Roberts, 1970); δt_S^* and δt_P^* are mostly negative (see Figures 3.3 and 3.5); heat flow, magnetic and electrical properties are generally normal. The only exceptional portion of the path is in the northern Great Plains near RCD, where heat flow greater than 2 $\mu cal/cm^2$-sec has been observed (Roy et al., 1968; Combs, 1970) and δt_P^* is positive.

The crustal structures beneath RCD and ATL are quite

similar (total thickness of crust is 40 to 45 km), and are not much different from those determined by refraction experiments at other locations near the RCD-ATL path (Steinhart and Meyer, 1961; James et al., 1968; Healy and Warren, 1969). Furthermore, recent upper mantle compressional-wave velocity models for various parts of central and eastern United States (Green and Hales, 1968; Julian, 1970) are alike in their broad characteristics, differing only in detail. We therefore assume that the surface wave attenuation between RCD and ATL may be determined by measuring the amplitude decay in a single direction only.

4.3 Events used in analysis

The earthquakes used as sources of surface waves for the measurement of attenuation in the western United States, after a reasonably exhaustive search of all possible events in the years 1964-1968, are given in Table 4.1. Those used to determine attenuation in east-central U.S. are listed in Table 4.2. The origin time, location, and magnitude are those supplied by the United States Coast and Geodetic Survey.

For the determination of surface-wave attenuation along a path between two stations, we should in principle use as sources of surface waves only earthquakes which lie precisely on the great circle connecting the two stations, guaranteeing that we are sampling a single bundle of energy at two points in space. This is practically impossible. We therefore must relax our requirements somewhat, and allow events that are very near to the two-station great circle. Nearness is a subjective entity, but we have quantified it in the form of two parameters given in Tables 4.1 and 4.2. The quantity $\Delta\phi$ is simply the difference in azimuth, at the source, between the actual paths to the two stations, and thus is a measure of the extent to which the source radiation-pattern can affect attenuation measurements. For most source mechanisms, $\Delta\phi$ less than 10^{o} is probably adequate. The quantity Δr is the greatest (perpendicular) distance between the paths to the two stations, i.e. the

Table 4.1

Earthquakes used to determine surface-wave Q^{-1}, western U.S.

Event Number	Date	Origin Time (G.M.T.) h m s	Latitude	Longitude	Region
1	3 Apr 1964	22 33 42.2	61.6°N	147.6°W	Southern Alaska
2	4 Apr 1964	09 10 55.1	56.9°N	152.7°W	Kodiak Island
3	20 Apr 1964	11 56 41.6	61.4°N	147.3°W	Southern Alaska
4	16 Apr 1965	23 22 18.6	64.7°N	160.1°W	Central Alaska
5	30 Aug 1966	20 20 54.0	61.3°N	147.5°W	Southern Alaska
6	18 Jan 1967	05 34 32.6	56.6°N	120.8°E	Southeastern Russia
7	30 Aug 1967	04 22 01.5	31.7°N	100.3°E	Szechwan Province, China
8	11 Apr 1966	17 17 33.8	18.4°N	102.3°W	Mexico
9	15 Nov 1967	21 31 51.5	28.7°S	71.2°W	Northern Chile
10	26 Apr 1968	17 48 02.3	18.7°N	103.3°W	Mexico

Table 4.1 cont.

Earthquakes used to determine surface-wave Q^{-1}, western U.S.

Event Number	Depth (km)	Magnitude	Distance (deg)		Azimuth (deg)		Modes Used	$\Delta\phi$ (deg)	Δr (km)
			to LON	to TUC	to LON	to TUC			
1	40	5.7	20.98	37.69	123.3	123.9	R	0.6	23
2	15	5.9	21.44	37.77	105.1	112.6	L	7.5	304
3	30	5.7	20.75	37.46	123.3	124.1	R,L	0.7	28
4	5	5.8	27.44	44.15	112.4	112.8	R,L	0.4	22
5	36	5.9	20.77	37.49	122.8	123.7	R	0.9	35
6	11	6.1	64.54	81.25	42.6	42.2	R	0.4	39
7	3	6.1	93.16	109.88	27.5	27.7	L	0.2	22
8	72	5.7	32.52	15.82	334.7	332.7	R,L	2.0	60
9	15	6.2	87.91	71.38	327.9	325.3	R,L	2.6	272
10	65	5.5	31.85	15.13	335.6	335.0	R,L	0.5	16

Table 4.2

Earthquakes used to determine surface-wave Q^{-1}, east-central U.S.

Event Number	Date	Origin Time (G.M.T.) h m s	Latitude	Longitude	Region
11	23 May 1965	23 46 12.0	52.2°N	175.0°E	Rat Islands
12	30 Dec 1965	02 06 29.0	54.1°N	164.3°W	Unimak Island
13	16 Apr 1966	01 27 15.3	57.0°N	153.6°W	Kodiak Island
14	19 May 1966	07 06 26.8	54.1°N	164.1°W	Unimak Island
15	7 Jun 1966	13 59 36.0	11.3°N	139.6°E	Caroline Islands
16	7 Aug 1966	02 13 5.1	50.6°N	171.3°W	Aleutian Islands

Table 4.2 cont.

Earthquakes used to determine surface-wave Q^{-1}, east-central U.S.

Event Number	Depth (km)	Magnitude	Distance (deg)		Azimuth (deg)		Modes Used	$\Delta\phi$ (deg)	Δr (km)
			to RCD	to ATL	to RCD	to ATL			
11	22	6.1	52.4	70.3	64.2	60.8	L	3.4	296
12	13	5.7	40.1	58.1	78.6	76.0	R,L	2.6	189
13	33	5.7	33.7	51.6	90.6	86.2	L	4.4	272
14	28	5.8	39.9	57.9	78.8	76.2	R,L	2.6	188
15	50	6.5	100.8	118.9	40.8	41.5	R	0.8	85
16	39	6.5	45.1	63.2	70.7	69.4	R	1.3	105

(perpendicular) distance of the nearer station to the (great-circle) path between the source and the farther station. If Δr is large, then lateral (i.e. perpendicular to the wave paths) changes in structure can significantly alter the apparent attenuation. An upper limit for allowable values of Δr is difficult to determine; such a limit will vary from one region to another and may be a function of wavelength. We may assume that Δr is sufficiently small for all earthquakes listed in Table 4.1, for instance, except possibly for events 2 and 9. The fact that velocities and attenuation calculated for the latter two earthquakes agree with those of other events in the table is a good argument for their inclusion in the compilation below.

4.4 Procedure

Long-period seismograms were digitized at a time interval of about 1.4 sec. After mean and linear trend were removed, N-S and E-W components were rotated to the radial and transverse directions. All components were then bandpass filtered (.01 to .067 Hz), appropriate group-velocity windows were applied, mean and linear trend were again removed, and Fourier amplitude and phase spectra were computed using a fast Fourier-transform technique. Both amplitude and phase spectra, the latter made a continuous function of frequency by removing jumps of ± 2 , were smoothed by averaging over a frequency interval of .0085 Hz. For the pair of stations 1 and 2, the ratio $R_{12}(f)$ of amplitude spectra and the difference

$\Delta\Phi(f) = [\, \Phi_2(f) - \Phi_1(f) \,] / 2\pi$ in phase spectra were determined and corrected for any differences in the theoretical-response curves of the two instruments (Hagiwara, 1958). The apparent attenuation-coefficient was obtained using equation (4.2), and the phase and group velocity were calculated from the relations

$$c(f) = \frac{\Delta_2 - \Delta_1}{t_2 - t_1 + (N - \Delta\Phi)/f}$$

$$U(f) = \frac{\Delta_2 - \Delta_1}{t_2 - t_1 - \frac{d\,\Delta\Phi(f)}{df}}$$

where t_i is the start time of the group velocity window at station i and N is an integer. The derivative of the tabulated function $\Delta\Phi$ (f) was approximated by the derivative of the Lagrangian interpolation-polynomial of degree 2.

Data in a particular frequency-band were considered acceptable when they satisfied the following constraints: (1) The arrival of energy for all frequencies in the specified band should be clearly visible on the seismograms (perhaps after suitable filtering)at both stations. (2) If all three components were available, then the Love and Rayleigh waves should separate upon rotation. This was checked by comparing the radial component with the $\pi/2$ phase-shifted vertical component. (3) Group velocities for the western U.S. path should be near (i.e. within perhaps 5 percent) those found by Alexander (1963) for fundamental-mode Love and Rayleigh waves in the same region. (4) For the western U.S. path, Rayleigh-wave phase velocities should be similar (i.e. within about 5 percent) to those found by Ewing and Press (1959) for the tripartite array of Reno, Boulder City, and Eureka, Nevada; and Love-wave phase velocities should be roughly similar to those computed by Chang (1968) for the path NTS-Houston. For the east-central U.S. path, phase velocities are expected to be close to those of McEvilly (1964). The above restrictions occasionally required combinations of

narrow band-pass filters and group-velocity windows. Failure of the above conditions was generally due to: (1) insufficient excitation at the source of waves in the particular frequency-band (e.g. longer periods), (2) interference due to multipathing (i.e. two or more waves of nearly the same frequency arrive simultaneously), or, in at least one case, (3) interference due to higher (Love) mode contamination.

4.5 Discussion of observations - qualitative

In Tables 4.3 through 4.6 are given the average values of phase velocity, group velocity, and attenuation (k* and Q^{-1}) for Love and Rayleigh waves along the two North American paths. (Individual determinations of velocity and attenuation for all events listed in Tables 4.1 and 4.2 are given in Appendix 2). The errors shown in the tables are statistical only. For each direction along a given path, mean and standard deviation are computed for $c^{-1}(f)$, $U^{-1}(f)$ and $k^*(f)$ at each f. (These are also included in Appendix 2). Attenuation and reciprocal velocities for the two directions are then averaged, with standard deviations obtained by assuming the determinations along the two opposite directions are independent. This use of the standard deviation as a measure of error is a gross simplification: firstly, departure from the mean of an individual observation is probably not a normally-distributed random variable; secondly, the sampling space is too small, for some frequencies it is only two observations; finally, velocity and attenuation in the two opposite directions may not be independent. Thus the errors given in Tables 4.3 through 4.6 are intended only as rough indicators of the precision of the measurements.

4.5.1 Western United States

$Q_L^{-1}(f)$ and $Q_R^{-1}(f)$ for the LON-TUC path are shown

Table 4.3

Love-wave propagation parameters, western United States

f Hz	T sec	c km/sec	U km/sec	k^* $10^{-4}km^{-1}$	100/Q	Q
.0121	82.52	4.475	4.12	2.31	2.50	40
.0135	73.84	4.439	4.11	2.57	2.48	40
.0150	66.80	4.400	4.10	2.65	2.31	43
.0164	60.99	4.320±.053[a]	4.02±.04[a]	2.58±.68[a]	2.01±.53[a]	50
.0178	56.12	4.292±.050	3.97±.02	2.65±.65	1.88±.46	53
.0192	51.96	4.257±.041	3.94±.04	2.90±.65	1.89±.42	53
.0207	48.38	4.231±.035	3.91±.05	3.02±.70	1.81±.42	55
.0221	45.26	4.208±.029	3.87±.07	3.02±.84	1.68±.41	59
.0235	42.51	4.185±.022	3.83±.09	2.88±.84	1.49±.44	67
.0249	40.08	4.161±.014	3.79±.11	2.65±.90	1.28±.44	78
.0264	37.92	4.136±.011	3.77±.08	2.65±.68	1.21±.31	83
.0278	35.97	4.113±.007	3.69±.11	2.38±.64	1.01±.27	99
.0292	34.22	4.088±.009	3.66±.12	2.18±.67	.87±.27	115
.0307	32.62	4.067±.015	3.65±.13	2.04±.87	.77±.33	129
.0321	31.18	4.045±.022	3.61±.18	1.9±1.2	.69±.43	144
.0335	29.85	4.024±.031	3.53±.22	1.1±2.0	.35±.68	283
.0349	28.63	4.013±.040	3.55±.23	0.9±2.4	.28±.76	360
.0364	27.51	3.992±.049	3.51±.22	0.7±2.7	.22±.81	450
.0378	26.47	3.969±.059	3.47±.21	0.5±2.9	.14±.85	700
.0392	25.51	3.923±.051	3.36±.13	-1.6±0.4		

a standard deviation

Table 4.3 cont.

Love-wave propagation parameters, western United States

f Hz	T sec	c km/sec	U km/sec	k^* $10^{-4}km^{-1}$	100/Q	Q
.0406	24.61	3.899±.055	3.34±.15	-1.8±0.9		
.0421	23.78	3.877±.059	3.34±.13	-1.9±1.6		
.0435	23.00	3.857±.059	3.36±.12	-1.9±2.1		
.0449	22.27	3.839±.057	3.39±.15	-1.8±2.3		
.0463	21.58	3.824±.056	3.40±.16	-1.6±2.3		
.0478	20.94	3.810±.054	3.40±.17	-1.2±2.1		
.0492	20.33	3.796±.054	3.39±.17	-0.7±2.0		
.0506	19.76	3.783±.053	3.39±.15	-0.1±1.9		
.0520	19.22	3.772±.052	3.39±.12	0.3±1.7	.06±.36	1600
.0535	18.70	3.728	3.38	0.15	.03	3400
.0549	18.22	3.717	3.34	0.27	.05	1900
.0563	17.76	3.706	3.33	0.36	.07	1500
.0577	17.32	3.696	3.33	0.44	.08	1230
.0592	16.90	3.686	3.34	0.52	.09	1070
.0606	16.50	3.677	3.35	0.66	.12	870
.0620	16.12	3.669	3.37	0.80	.14	730
.0634	15.76	3.662	3.39	0.88	.15	670
.0649	15.42	3.656	3.38	0.98	.16	615
.0663	15.08	3.649	3.35	1.16	.19	540

a standard deviation

Table 4.4

Rayleigh-wave propagation parameters, western United States

f Hz	T sec	c km/sec	U km/sec	k^* $10^{-4}km^{-1}$	100/Q	Q
.0235	42.51	3.744	3.55	1.62	.78	128
.0249	40.08	3.740±.010[a]	3.50±.03[a]	1.42±.96[a]	.63±.43[a]	158
.0264	37.92	3.726±.008	3.44±.04	1.22±.92	.51±.38	197
.0278	35.97	3.708±.007	3.41±.06	1.0±1.2	.37±.49	270
.0292	34.22	3.692±.008	3.40±.05	1.6±1.3	.58±.47	172
.0307	32.62	3.677±.008	3.36±.04	2.1±1.4	.72±.48	138
.0321	31.18	3.660±.007	3.32±.06	2.3±1.3	.75±.42	134
.0335	29.85	3.644±.008	3.29±.08	2.0±1.0	.64±.31	156
.0349	28.63	3.639±.024	3.28±.09	1.54±.62	.46±.19	217
.0364	27.51	3.625±.026	3.22±.12	0.84±.80	.24±.23	420
.0378	26.47	3.606±.031	3.20±.11	0.3±1.2	.08±.32	1200
.0392	25.51	3.590±.034	3.17±.11	0.08±1.4	.02±.37	5000
.0406	24.61	3.573±.037	3.13±.09	0.01±1.4	.00±.35	
.0421	23.78	3.554±.037	3.09±.07	0.2±1.5	.05±.35	2000
.0435	23.00	3.536±.038	3.06±.06	0.6±1.6	.13±.36	790
.0449	22.27	3.518±.039	3.00±.06	0.8±1.8	.16±.37	600
.0463	21.58	3.493±.039	2.93±.04	0.3±1.6	.07±.33	1500
.0478	20.94	3.473±.039	2.92±.07	0.9±1.6	.17±.31	580
.0492	20.33	3.453±.039	2.92±.09	1.4±1.4	.26±.27	380
.0506	19.76	3.436±.040	2.94±.10	1.6±1.3	.30±.24	340
.0520	19.22	3.420±.041	2.95±.11	1.7±1.1	.31±.20	320
.0535	18.70	3.406±.043	2.95±.12	1.83±.94	.32±.17	310

a standard deviation

Table 4.4 cont

Rayleigh-wave propagation parameters, western United States

f Hz	T sec	c km/sec	U km/sec	k^* $10^{-4}km^{-1}$	100/Q	Q
.0549	18.22	3.392±.046	2.94±.12	1.83±.71	.31±.12	320
.0563	17.76	3.379±.049	2.93±.12	1.78±.55	.29±.09	340
.0577	17.32	3.366±.051	2.92±.10	1.68±.42	.27±.07	370
.0592	16.90	3.354±.052	2.91±.09	1.51±.25	.24±.04	420
.0606	16.50	3.342±.052	2.88±.08	1.64±.41	.25±.06	400
.0620	16.12	3.329±.075	2.85±.09	1.80±.80	.26±.12	380
.0634	15.76	3.316	2.88	2.14	.31	320
.0649	15.42	3.305	2.91	2.27	.32	310
.0663	15.08	3.295	2.92	2.69	.38	270

a standard deviation

in Figures 4.1 and 4.2, respectively, along with several measurements of Q^{-1} (along other paths) published by other investigators. (Negative values of Q_L^{-1} in Table 4.3 are not included in Figure 4.1). Several interesting observations may be made.

For periods greater than 35 or 40 sec ($f < .03$ Hz), Q_L^{-1} (see Figure 1) is dramatically greater than values determined in the same period range for the Atlantic Ocean (Anderson et al., 1965) or for complete great-circle paths (Sato, 1958; Båth and López-Arroyo, 1962; Kaminuma and Hirasawa, 1964). The value $Q_L = 40$ for 70-80 sec Love waves, even with an uncertainty of 25 percent, is the lowest value of surface-wave Q yet reported. The rapid rise in Q_L^{-1}, as a function of period, between 30 and 50 seconds places a severe constraint on possible Q^{-1} models for western North America.

For periods less than 35 sec, Q_L^{-1} in the western U.S. closely resembles the values cited by Tsai and Aki (1969), who used a least-squares technique to fit attenuation along predominantly oceanic paths east from Parkfield, California. Most of the surface-wave energy in this period range (15-35 sec) propagates in the lithosphere, i.e. the crust and uppermost mantle. That Q_L^{-1} in a tectonic region such as the western U.S. is similar in this period range to Q_L^{-1} in more 'normal' regions of the earth confirms the notion that the most noticeable lateral variations of $Q_\beta^{-1}(z)$ occur in that part of the

Figure 4.1 Love-wave attenuation, $Q_L^{-1}(f)$, western United States (semi-log scale). Error bars, showing standard deviations for selected determinations, indicate the precision of the measurements. Several published values of $Q_L^{-1}(f)$, obtained for primarily oceanic paths, are included for comparison (Sato, 1958; Båth and López-Arroyo, 1962; Kaminuma and Hirasawa, 1964; Anderson et al., 1965; Tsai and Aki, 1969).

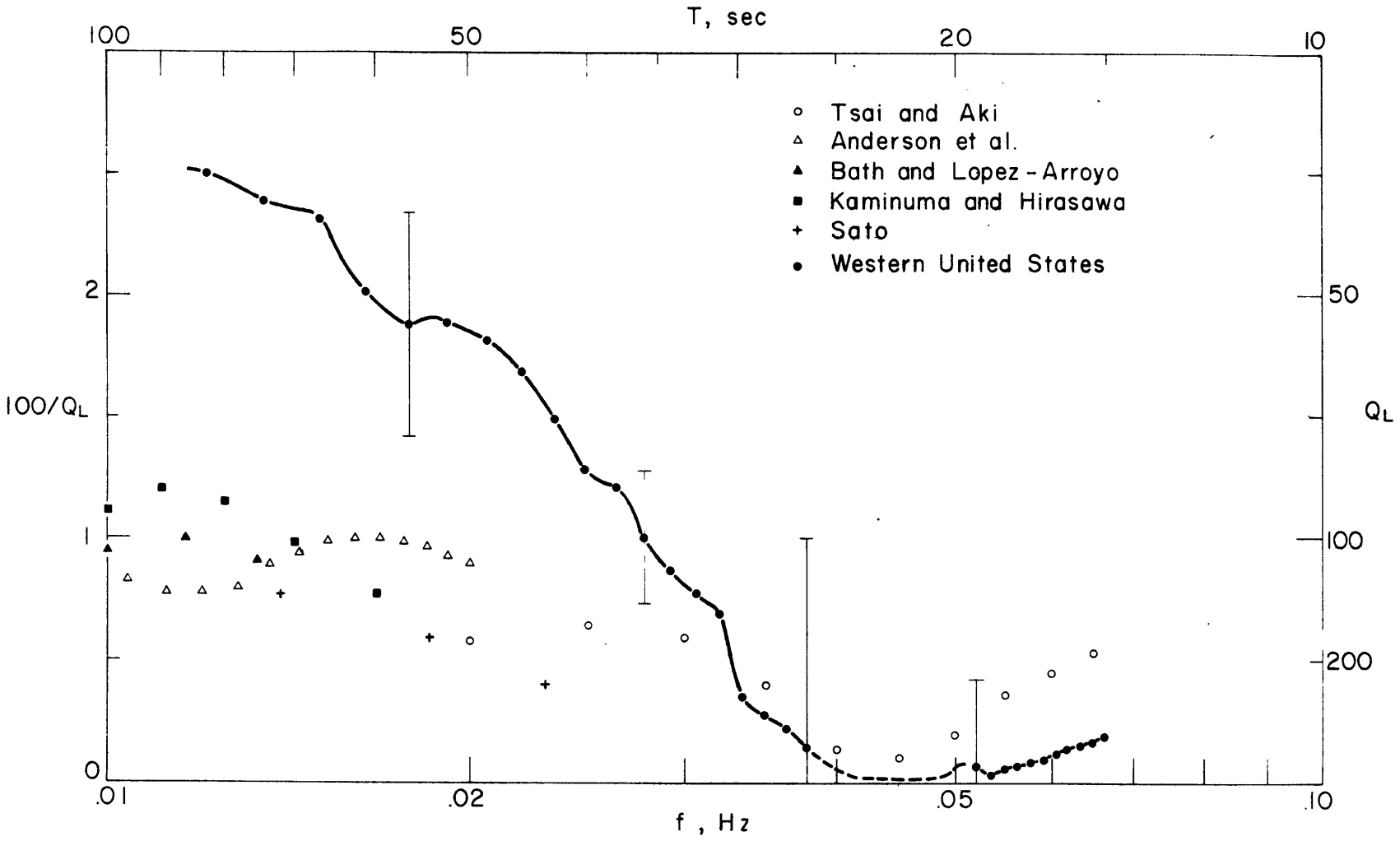
T, sec
100
50
20
10
Tsai and Aki
Anderson et al.
Bath and Lopez-Arroyo
Kaminuma and Hirasawa
Sato
Western United States
2
1
0
100/Q_L
50
100
200
Q_L
.01
.02
.05
.10
f , Hz

Figure 4.2 Rayleigh-wave attenuation, $Q_R^{-1}(f)$, western United States (semi-log scale). Errors bars are as in Figure 4.1. Published values of $Q_R^{-1}(f)$, also shown in the figure, are for primarily oceanic (open symbols) or purely continental (closed symbols) paths (Gutenberg, 1945b; Press, 1964; Tryggvason, 1965; Tsai and Aki, 1969).

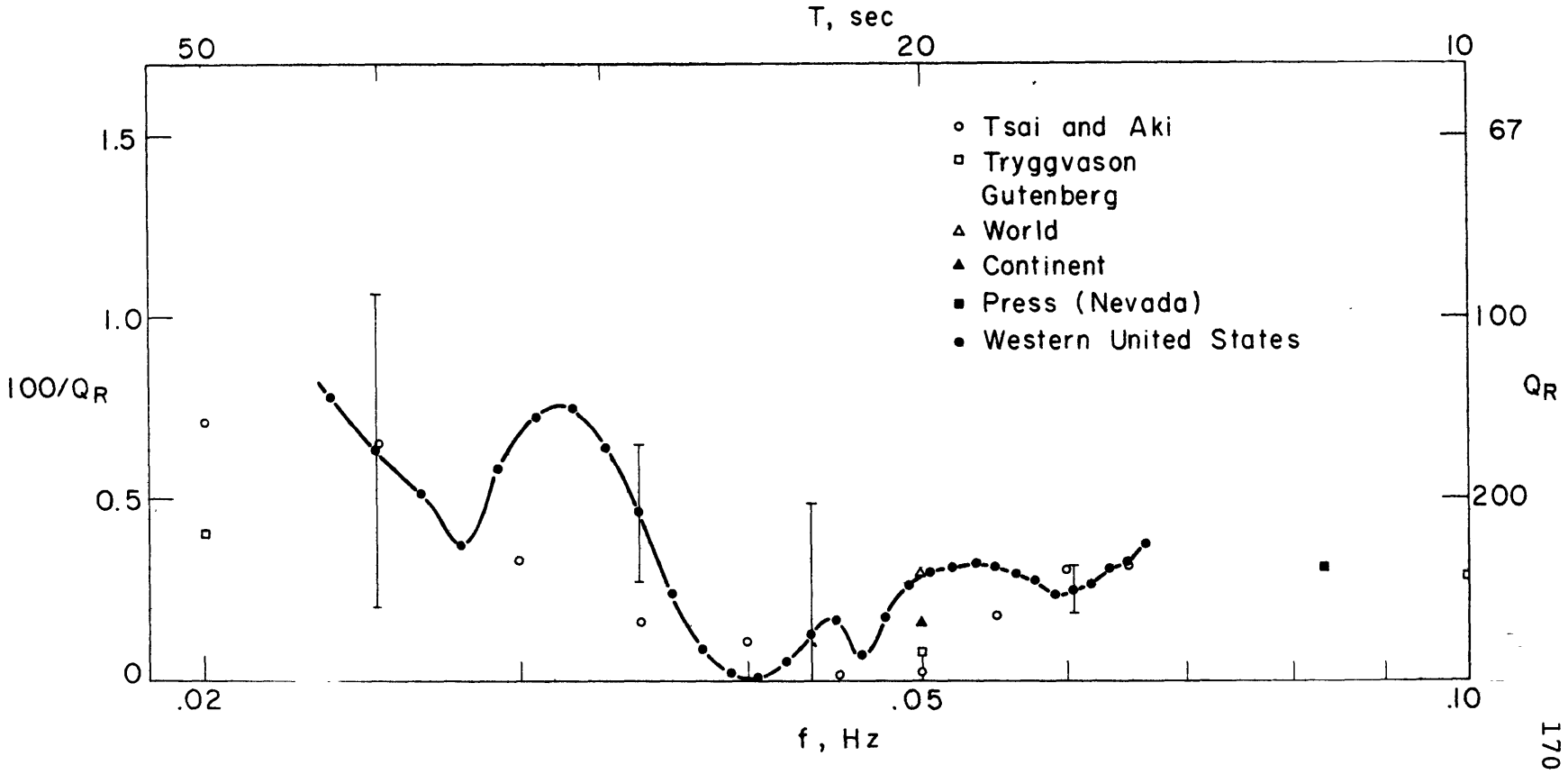
T, sec
50
20
10
1.5
1.0
0.5
0
100/Q_R
67
100
200
Q_R
.02
.05
.10
f, Hz
Tsai and Aki
Tryggvason
Gutenberg
World
Continent
Press (Nevada)
Western United States

mantle below the lithosphere (see also section 4.6).

Rayleigh-wave attenuation in the western U.S. (Figure 4.2) is not significantly different from attenuation in other areas (as measured by Gutenberg, 1945b; Tryggvason, 1965; Tsai and Aki, 1969), at least for the period range 15 to 40 sec, over which our measurements were made. (A possible exception is the apparent peak in attenuation for periods near 30 sec.) $Q_R^{-1}(f)$ in Figure 4.2 never exceeds .008, and in fact the line $Q_R^{-1} = .003$ (i.e. Q_R independent of frequency over the range shown) would intersect almost all of the error bars, a consequence of the considerable relative uncertainty attached to most determinations of attenuation, for both Rayleigh and Love waves, at the higher frequencies considered in this study. In the period range 15 to 32 sec, Q_R^{-1} is consistently greater than Q_L^{-1}, though for greater periods this relationship appears to be reversed.

The rapid increase in Q_L^{-1} with increasing period between 30 and 50 seconds is weakly mirrored by a similar, though considerably less pronounced rise in Q_R^{-1}. Of some interest is the single determination of $Q_R(325)$ for 12-second Rayleigh waves made by Press (1964) for the Nevada region, very near to the values (320-270) of Q_R given in Table 4.4 for periods between 15 and 16 seconds.

Both Love and Rayleigh waves show an apparent, but not statistically significant, minimum in Q^{-1} for periods between 20 and 25 seconds. This minimum has been noted previously by Tryggvason (1965) and by Tsai and Aki (1969). It appears to be the result of a decrease in Q_α^{-1} and Q_β^{-1} with depth in the lithosphere and may require a frequency-dependent Q^{-1} in this depth region (Tsai and Aki, 1969). This minimum in $Q_R^{-1}(f)$ is relevant to the well-known surface-wave magnitude (Gutenberg, 1945b), derived from Rayleigh waves with 20-second period. If such a minimum is a world-wide phenomenon, then lateral variations of Q_α^{-1} and Q_β^{-1} in the earth will not appreciably affect the surface-wave magnitude (a fact of which we made use in section 3.5.3).

We note in passing that the Love- and Rayleigh-wave group velocities given in Tables 4.3 and 4.4, over most of the frequency range considered, are lower (by .05 to .15 km/sec) than those measured by Alexander (1963) using paths from Montana and Utah to Pasadena, California. An interesting side-problem, one not considered here, would be to determine what changes in his preferred model (35CM2) are necessary to fit the velocities that are observed for the LON-TUC path.

4.5.2 East-central United States

$Q_L^{-1}(f)$ and $Q_R^{-1}(f)$ for the RCD-ATL path are shown in Figures 4.3 and 4.4, respectively. (Again, negative

Table 4.5

Love-wave propagation parameters, east-central United States

f Hz	T sec	c km/sec	U km/sec	k^* $10^{-4}km^{-1}$	100/Q	Q
.0164	60.99	4.55±.04[a]	4.00±.02[a]	1.13±.10[a]	.88±.08[a]	114
.0178	56.12	4.49±.03	3.95±.01	.76±.01	.54±.01	185
.0192	51.96	4.45±.03	3.92±.02	.55±.14	.36±.09	280
.0207	48.38	4.41±.02	3.92±.06	.16±.53	.10±.32	1000
.0221	45.26	4.38±.03	3.84±.04	0 ±.8		
.0235	42.51	4.34±.02	3.76±.02	-.05±.9		
.0249	40.08	4.30±.02	3.71±.02	.09±1.2	.04±.58	2400
.0264	37.92	4.26±.02	3.67±.02	.3 ±1.5	.13±.66	780
.0278	35.97	4.23±.02	3.63±.02	.5 ±1.7	.22±.70	460
.0292	34.22	4.19±.02	3.60±.02	.8 ±1.9	.30±.74	330
.0307	32.62	4.16±.02	3.57±.03	1.1±2.0	.39±.75	260
.0321	31.18	4.13±.02	3.55±.03	1.3±2.1	.47±.74	210
.0335	29.85	4.10±.01	3.54±.03	1.5±2.1	.51±.71	200
.0349	28.63	4.07	3.58	.2	.06	1700

a standard deviation

Table 4.6

Rayleigh-wave propagation parameters, east-central United States

f Hz	T sec	c km/sec	U km/sec	k^* 10^{-4}km^{-1}	100/Q	Q
.0192	51.56	4.077±.009[a]	3.80±.03[a]	1.6±1.2[a]	.98±.78[a]	102
.0207	48.38	4.059±.015	3.76±.07	1.1±1.4	.63±.79	160
.0221	45.26	4.036±.018	3.68±.04	1.0±1.3	.53±.69	190
.0235	42.51	4.010±.019	3.61±.04	.8±1.3	.40±.63	250
.0249	40.08	3.982±.019	3.54±.05	.7±1.2	.31±.54	320
.0264	37.92	3.953±.020	3.47±.05	.5± .9	.23±.40	440
.0278	35.97	3.923±.021	3.41±.04	.4± .7	.16±.28	610
.0292	34.22	3.893±.021	3.37±.02	.4± .6	.13±.22	760
.0307	32.62	3.865±.020	3.34±.01	.3± .8	.10±.28	970
.0321	31.18	3.837±.018	3.28±.04	.2±1.2	.05±.40	1900
.0335	29.85	3.807±.018	3.23±.07	.1±1.6	.02±.48	4500
.0349	28.63	3.778±.020	3.20±.10	.1±1.8	.03±.53	3900
.0364	27.51	3.752±.024	3.19±.12	.1±2.0	.04±.57	2400
.0378	26.47	3.713±.012	3.10±.06	.1±2.8	.03±.73	3400
.0392	25.51	3.686±.012	3.07±.04	.4±3.1	.10±.77	960
.0406	24.61	3.654±.013	3.04±.01	-1.1± .9		
.0421	23.78	3.629±.013	3.04±.02	-.7± .9		
.0435	23.00	3.607±.014	3.05±.02	-.3± .9		
.0449	22.27	3.586±.013	3.07±.01	.1± .9	.01±.19	7600

a standard deviation

Table 4.6 cont.

Rayleigh-wave propagation parameters,
east-central United States

f Hz	T sec	c km/sec	U km/sec	k^* $10^{-4}km^{-1}$	100/Q	Q
.0463	21.58	3.568±.013	3.08±.01	.4± .8	.09±.17	1150
.0478	20.94	3.552±.013	3.08±.01	.8± .6	.16±.13	610
.0492	20.33	3.544	3.06	1.5	.29	340
.0506	19.76	3.529	3.05	1.7	.33	310

a standard deviation

Figure 4.3 Love-wave attenuation, $Q_L^{-1}(f)$, east-central United States (semi-log scale). Error bars are as in Figure 4.1. For comparison, $Q_L^{-1}(f)$ in western U.S. and along paths crossing the Atlantic Ocean (Anderson et al., 1965; Tsai and Aki, 1969) are also shown.

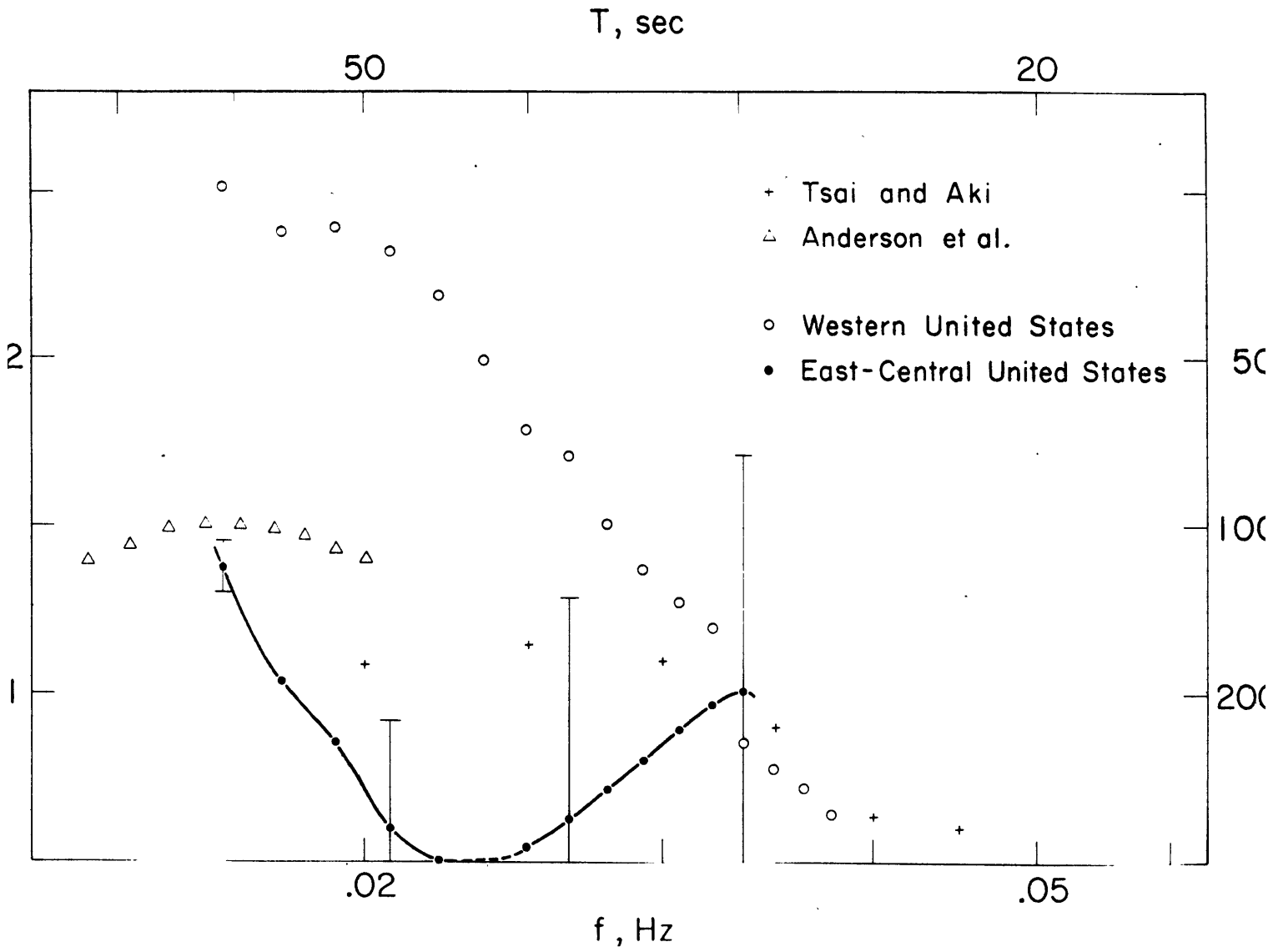
T, sec
50
20
Tsai and Aki
Anderson et al.
Western United States
East-Central United States
2
1
50
100
200
.02
.05
f , Hz

Figure 4.4 Rayleigh-wave attenuation, $Q_R^{-1}(f)$, east central United States (semi-log scale). Error bars are as in Figure 4.1. Also shown are $Q_R^{-1}(f)$ for western U.S. and for paths crossing the Atlantic Ocean (Anderson et al., 1965; Tsai and Aki, 1969).

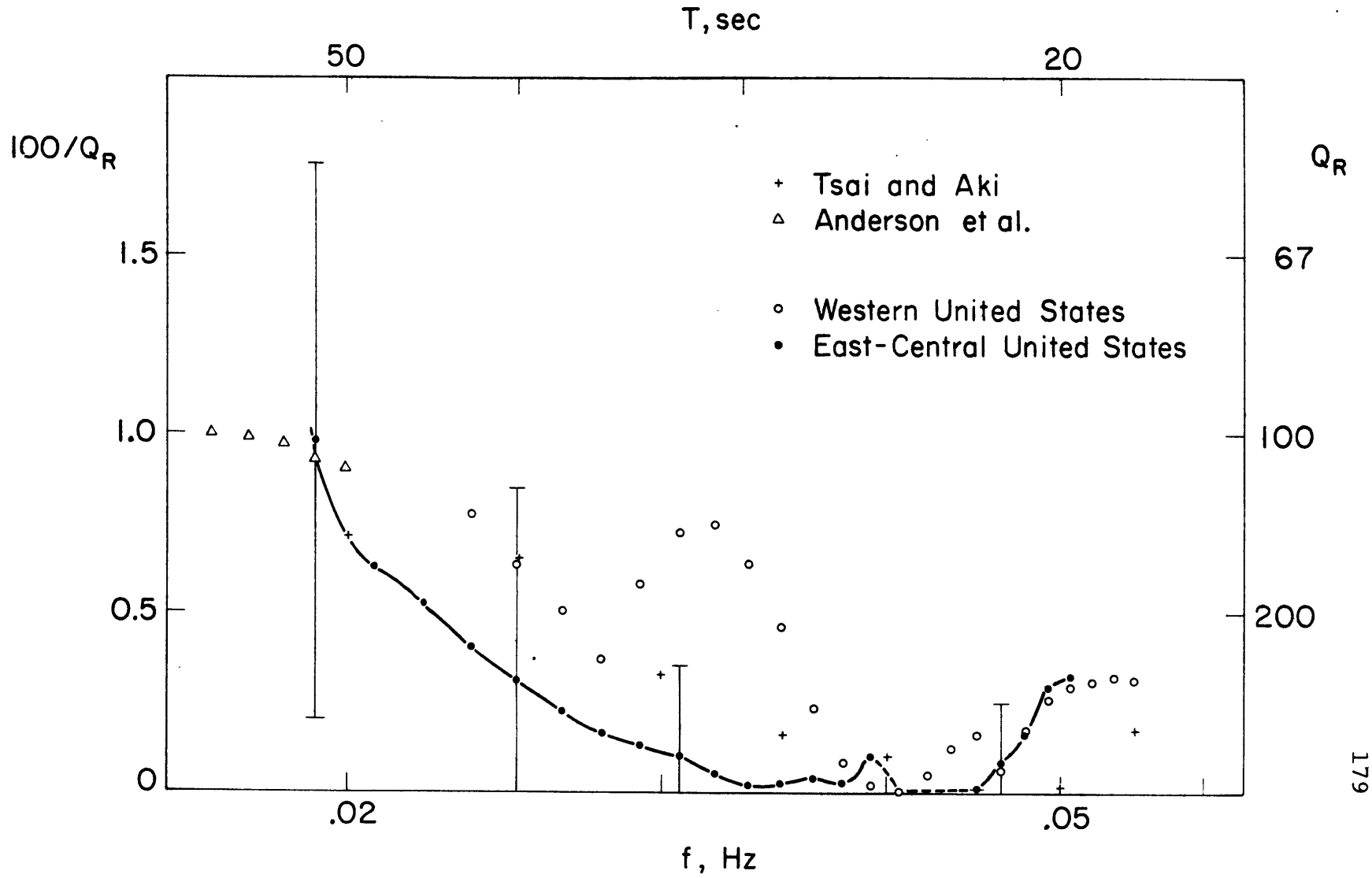
T, sec
50
20
100/Q_R
Q_R
1.5
1.0
0.5
0
67
100
200
+ Tsai and Aki
△ Anderson et al.
○ Western United States
• East-Central United States
.02
.05
f, Hz

values of Q^{-1}, attributable to interference affects or measurement error, are not included in the figures. It is presumed, however, that when the measured value of Q^{-1} is negative, the actual value is small.) Though the frequency range over which Q^{-1} could be measured was less, particularly for Love waves, than along the LON-TUC path, several conclusions can be made.

Love-wave attenuation (Figure 4.3), at periods between 40 and 60 sec, in east-central United States is much less than in western United States. In fact, in east-central United States Q_L^{-1} over the entire frequency range studied is comparable to or less than Q_L^{-1} determined for oceanic or great-circle paths (Sato, 1958; Anderson et al., 1965; Tsai and Aki, 1969).

At periods less than about 27 sec ($f > .038$ Hz), $Q_R^{-1}(f)$ in east-central United States (Figure 4.4) is very similar to Q_R^{-1} determined for the LON-TUC path. At longer periods, however, Q_R^{-1} is consistently lower in east-central than in western United States. (This difference is not statistically significant, though.) If surface-wave attenuation is interpreted as due to a Q_β^{-1} in the earth that varies with depth but not with frequency, then we might say that Q_β^{-1} (and Q_α^{-1}) is fairly uniform in the crust of eastern, central, and western North America but that Q_β^{-1} in the upper mantle of western United States is higher than in the mantle to the east.

An interesting point, of peripheral interest to the

present study, is that the phase velocities of Love waves (Table 4.5) for the RCD-ATL path are slightly lower than most of the values (at corresponding periods) reported by McEvilly (1964) for central United States, while the phase velocities of Rayleigh waves (Table 4.6) are generally higher (at corresponding periods) than the majority of McEvilly's values. The sense of these differences is such that an anisotropic mantle (such as that proposed by McEvilly) may not be required to fit the velocities within reasonable uncertainties.

4.6 Interpretation of observations - quantitative

Numerical inversion of the surface wave Q^{-1} observations, as mentioned earlier, may be accomplished using any of several diverse techniques. Because of the large uncertainties in measured Q^{-1}, it makes little sense to require a possible $Q_\beta^{-1}(z,f)$, $Q_\alpha^{-1}(z,f)$ model to fit the observations exactly. Our approach, rather, will be to seek simple but physically plausible attenuation-models which satisfy the data to within a reasonable estimate of the measurement error. By 'simple' we mean (1) losses under purely compressive stress are neglected (see section 3.5.2, also Anderson et al., 1965; Tsai and Aki, 1969), so that $Q_\alpha^{-1} = \frac{4}{3}\left(\frac{\beta}{\alpha}\right)^2 Q_\beta^{-1}$; and (2) $Q_\beta^{-1}(z,f)$ is completely determined by the specification of a small number of parameters. For historical reasons, we include mention of $Q_\beta^{-1}(z)$ models which are everywhere independent of frequency. Preferred models, for reasons discussed in Chapters 2 and 3, include at least one relaxation-type mechanism in the depth range of greatest attenuation.

4.6.1 Western United States

Even if the values of Q_L^{-1} and Q_R^{-1} in Tables 4.3 to 4.6 were known were no uncertainty, such a set of observations can give only the broad-scale features of the actual Q distribution in the earth. A formalism for quantitatively measuring the resolving power of a finite

set of exact earth-data has been developed in elegant detail by Backus and Gilbert (1968). If the material Q^{-1} is independent of frequency in the earth and if all losses are associated with the shear component of stress, then $Q_L^{-1}(f)$ and $Q_R^{-1}(f)$ are linear functionals on the linear space of all possible $Q_\beta^{-1}(r)$ models; i.e.

$$Q_{L,R}^{-1}(f_i) = \int_o^1 G_i(r)\, Q_\beta^{-1}(r)\, dr \qquad (4.6)$$

where r is the radius normalized to the radius R_0 of the earth and the kernel $G_i(r)$ may be determined from an assumed velocity-density model (Anderson and Archambeau, 1964). The resolving length of the data at radius r_o is given in the Backus-Gilbert treatment by the peak width of that unimodular, linear combination $A(r_o, r)$ of kernels $G_i(r)$ $(i=1,2,\ldots,N)$ which most nearly resembles the function $\delta(r-r_o)$; i.e. $A(r_o,r)$ satisfies a specified ' δ-ness' criterion subject to the constraint

$$\int_o^1 A(r_o,r)\, dr = 1 .$$

The optimum averaging kernel $A(r_o,r)$ corresponding to the set of attenuation observations for the western U.S. given in Tables 4.3 and 4.4 (using only positive values of Q_L^{-1}) was obtained as follows: A plane-layered velocity-density model was assumed (above 125 km depth, model 35CM2 of Alexander, 1963; below that depth, α from

model NTS N3 of Julian, 1970, β similar to model US 26 of Anderson and Julian, 1969). Then $G_i(r)$ at the midpoint of layer j was taken to be given by

$$G_i(r) = \frac{R_o}{H_j} \frac{\beta_j}{c_L(f_i)} \frac{\partial c_L(f_i)}{\partial \beta_j} \tag{4.7}$$

for Love waves and

$$G_i(r) = \frac{R_o}{H_j} \left\{ \frac{\beta_j}{c_R(f_i)} \frac{\partial c_R(f_i)}{\partial \beta_j} + \frac{4}{3} \left(\frac{\beta_j}{\alpha_j} \right)^2 \frac{\alpha_j}{c_R(f_i)} \frac{\partial c_R(f_i)}{\partial \alpha_j} \right\} \tag{4.8}$$

for Rayleigh waves (Anderson et al., 1965). In the above relations, H_j, β_j, and α_j are the layer thickness (in km), the layer shear-wave velocity, and the layer compressional-wave velocity; c_L and c_R are Love- and Rayleigh-wave phase velocities. The phase-velocity partial derivatives were calculated using computer programs written by D.G. Harkrider (Harkrider, 1964). Then following Backus and Gilbert (1968), the optimum unimodular function $A(r_o,r)$ is the linear combination of all $G_i(r)$ that minimizes the integral

$$\int_o^1 J(r_o,r)\ A(r_o,r)^2\ dr$$

where $J(r_o,r) = 2\sigma^2 \{1 - \exp [-(r-r_o)^2/2\sigma^2]\}$

and $2\sigma^2$ is taken equal to 10^{-2}.

Figure 4.5 The resolving power of surface-wave attenuation data, western United States. The resolving length of the data set, assumed to be error-free, of Tables 4.3 and 4.4 is given roughly (Gilbert and Backus, 1968) by the half-width of the optimum averaging kernel $A(r_o,r)$, shown as a function of r (or z) for several values of $z_o = R_o(1-r_o)$.

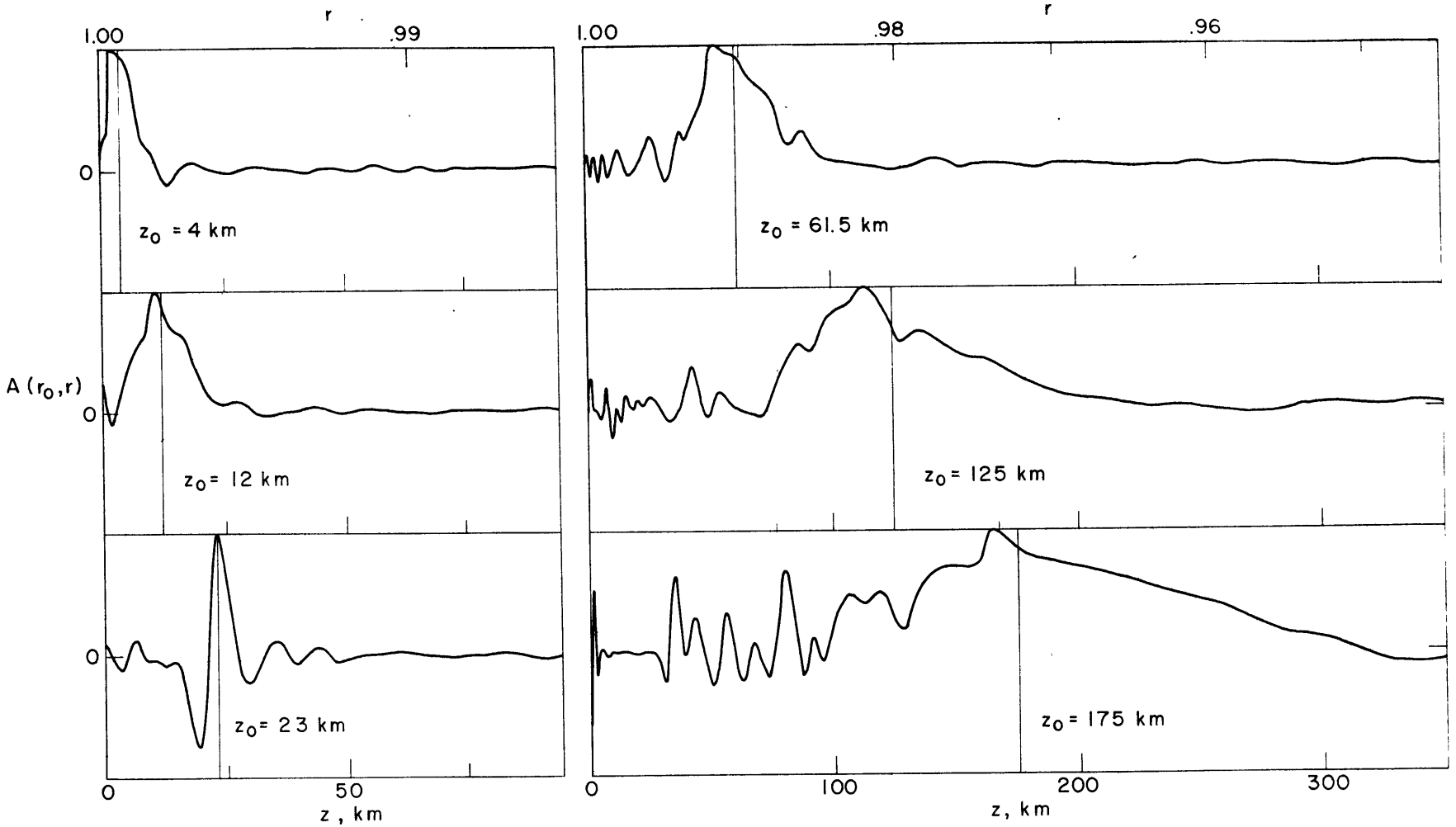
r
1.00
.99
.98
.96
0
z_0 = 4 km
z_0 = 61.5 km
A (r_0,r)
z_0= 12 km
z_0= 125 km
z_0= 23 km
z_0= 175 km
0
50
100
200
300
z, km

In Figure 4.5, $A(r_o,r)$ is shown for several values of r_o(i.e. several values of $z_o = R_o[1-r_o]$). For z_o between 20 and 150 km, the half-width of the optimum averaging kernel is not too different from $0.5\ z_o$. Consider a set of values of r_o(or z_o) such that the main peaks in the collection of kernels $A(r_o,r)$ do not appreciably overlap. Such a set contains at most about 8 values of r_o. In our inversion of Q_L^{-1} and Q_R^{-1} for the western U.S., we shall consider models of $Q_\beta^{-1}(r)$ that have at most 8 free parameters.

The attenuation observations, of course, are not free from error. If we had complete knowledge of the variance matrix of the errors of measurements, thenwe night wish to trade off resolving length against the resultant error in our weighted averages $\int_o^1 A(r_o,r)\ Q_\beta^{-1}(r)\ dr$ (Backus and Gilbert, 1970). From an earlier discussion, we conclude that the variance matrix of errors is poorly known. We thus note only that the actual resolving length of the Q^{-1} data in Tables 4.3 and 4.4 is at least as large at all depths as is indicated in Figure 4.5.

What are some possible models of shear-wave attenuation $Q_\beta^{-1}(z,r)$ which can explain the surface wave attenuation measurements for western United States (Tables 4.3 and 4.4)? We consider plane-layered structures, such that within each layer Q_β^{-1} either is a constant or has a functional dependence on frequency such as that discussed

in Chapter 2. A model is considered possible if $Q_\beta^{-1}(z,f) > 0$ everywhere and if the predicted values of $Q_L^{-1}(f)$ agree with the values given in Table 4.3 to within the cited error or, if no error is given, to within .004. (We might in addition require agreement with the $Q_R^{-1}(f)$ observations of Table 4.4 to within the cited error, though as we shall see, this leads to considerable difficulties.) Starting with an assumed model $Q_\beta^{-1}(z,f)$, the surface-wave attenuation is calculated using the scheme of Anderson and Archambeau (1964); i.e. equations (4.6) through (4.8). An iteration process described in Appendix 3 is used to obtain an acceptable model from the starting model.

Suppose $Q_\beta^{-1}(z)$ is independent of frequency at all depths. While this is not a particularly reasonable assumption, we discuss such models for the western U.S. primarily for comparison with frequency-independent Q_β^{-1} models that other workers (Anderson and Archambeau, 1964; Knopoff, 1964; Anderson et al., 1965; Tsai and Aki, 1969) have proposed to explain surface-wave attenuation in other regions. Typical of the layered models of Q_β^{-1} which fit the Love-wave attenuation data for western United States (see Figure 4.7) is model 1, shown in Figure 4.6a. Basically, $Q_\beta^{-1} < .004$ near the surface in model 1 while $Q_\beta^{-1} \geq .03$ below about 60 km depth. The details of the model are unimportant; the uncertainties in $Q_L^{-1}(f)$ allow considerable latitude in specifying the fine structure.

Figure 4.6 Some models of Q_β^{-1}, western United States. (a) In models 1 and 2, Q^{-1} is everywhere independent of frequency. (b) In models 3 and 4, a (frequency-dependent) relaxation of the shear stress takes place within the 'asthenosphere', but Q^{-1} is frequency-independent outside the asthenosphere. The parameters of the relaxations are $\Delta\mu = .1$, $\tau = 8$ sec in model 3; $\Delta\mu = .1$, $\tau = 20$ sec in model 4.

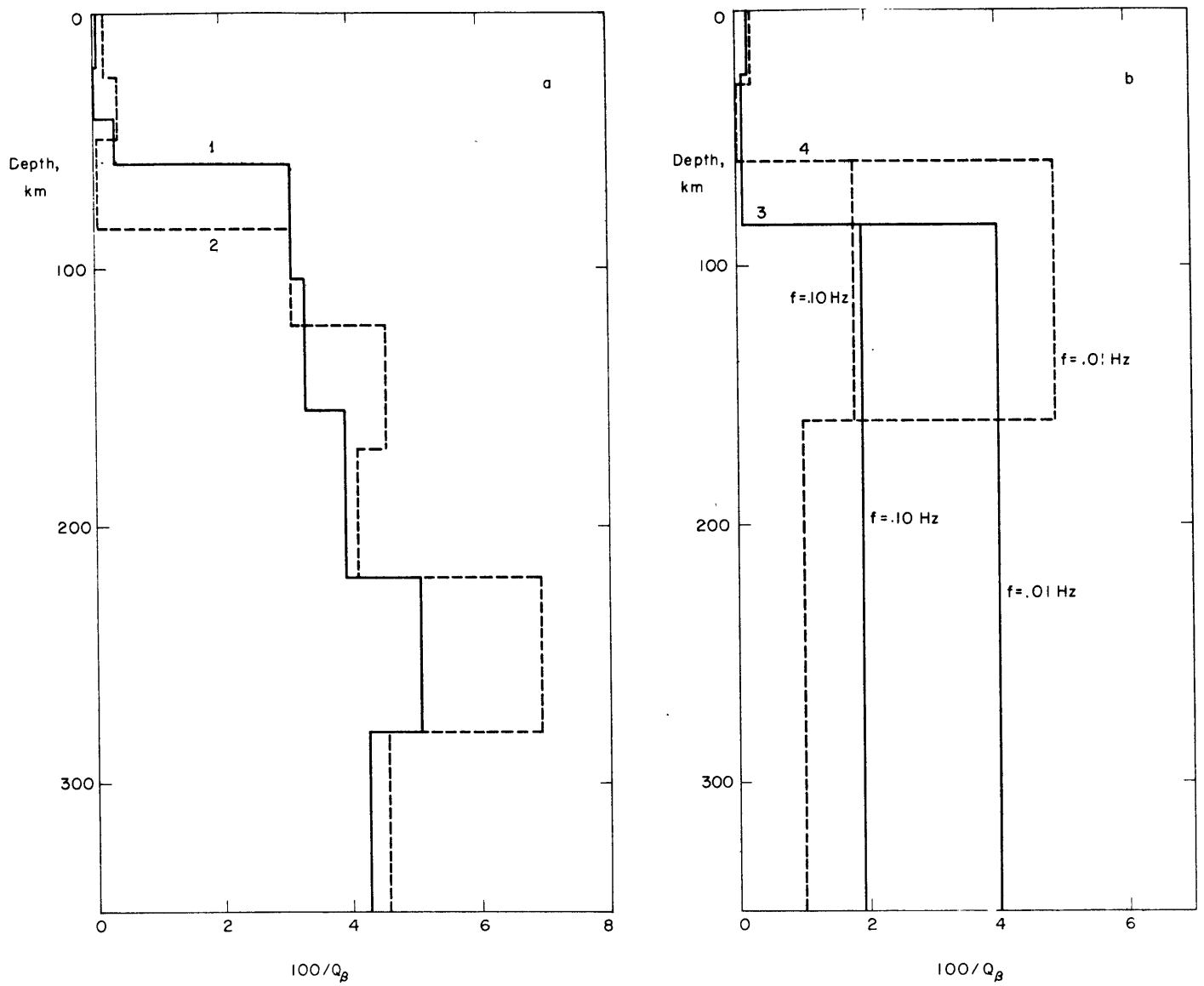
a
b
Depth, km
0
100
200
300
1
2
3
4
f=.10 Hz
f=.01 Hz
f=.10 Hz
f=.01 Hz
0
2
4
6
8
100/Qβ

Figure 4.7 Love-wave attenuation predicted by Q_β^{-1} models, western United States. Numbers next to theoretical (continuous) curves of $Q_L^{-1}(f)$ correspond to numbers of $Q_\beta^{-1}(z,f)$ models in Figure 4.6. Observed $Q_L^{-1}(f)$, with selected error bars, are included. Note semi-log scale.

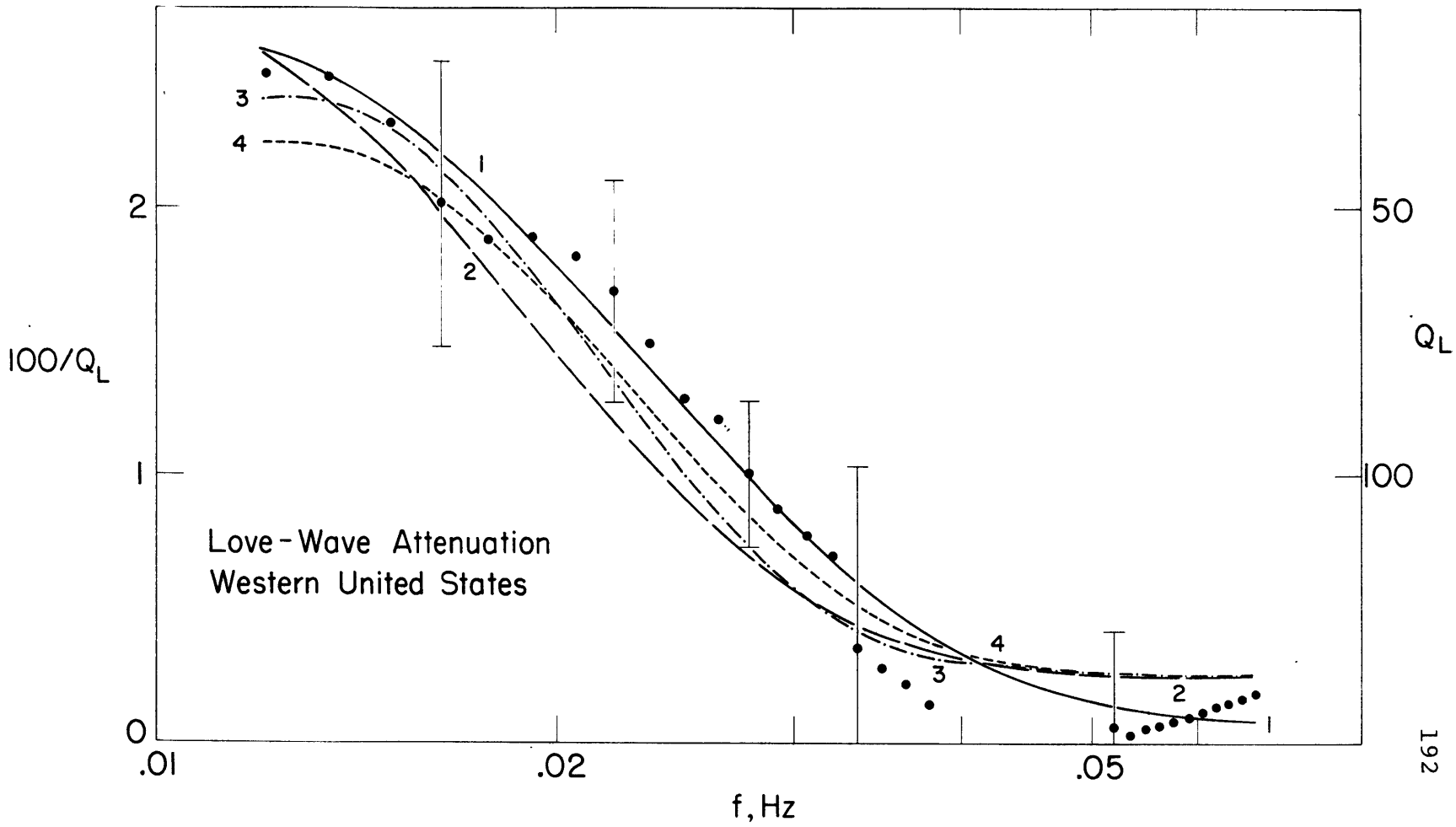
Love - Wave Attenuation
Western United States
100/Q_L
Q_L
f, Hz
.01
.02
.05
0
1
2
50
100
1
2
3
4

Unequivocal, however, is the rapid transition from high to very low Q ($20 < Q_\beta < 35$) at some depth (roughly 50 to 80 km) in the upper mantle. From the rate of damping of torsional oscillations of the earth and the attenuation of long-period surface waves along great-circle paths, it may be presumed that below some depth z_1(200 km, say), $Q_\beta^{-1}(z)$ must decrease with depth beneath the western U.S. The set of observations given in Table 4.3, however, places no constraint on precisely what z_1 should be or how rapidly Q_β^{-1} must decrease with depth below z_1. In the terminology of the new global tectonics, however, we might venture that between LON and TUC the lithosphere is about 60 km thick and the asthenosphere is at least 150 km thick.

The Rayleigh-wave attenuation predicted by model 1 is not a good fit to observations (see Figure 4.8). A search for a frequency-independent $Q_\beta^{-1}(z)$ that satisfies both Love and Rayleigh-wave attenuation produced models like that shown as model 2 in Figure 4.6a. Model 2 predicts values of Q_L^{-1} and Q_R^{-1} respectively greater than and less than observed for frequencies greater than .05 Hz (Figures 4.7 and 4.8). This is not surprising, but rather indicates that losses under pure compression are not negligible near the earth's surface.

A more serious failing of model 2 is that for frequencies between .023 and .028 Hz, the model predicts values of Q_L^{-1} and Q_R^{-1} respectively less than and greater than

Figure 4.8 Rayleigh-wave attenuation predicted by Q_β^{-1} models, western United States. The numbers next to theoretical curves of $Q_R^{-1}(f)$ correspond to those of the $Q_\beta^{-1}(z,f)$ models of Figure 4.6. Observed Rayleigh-wave attenuation, with selected error bars, is also shown. Note semi-log scale.

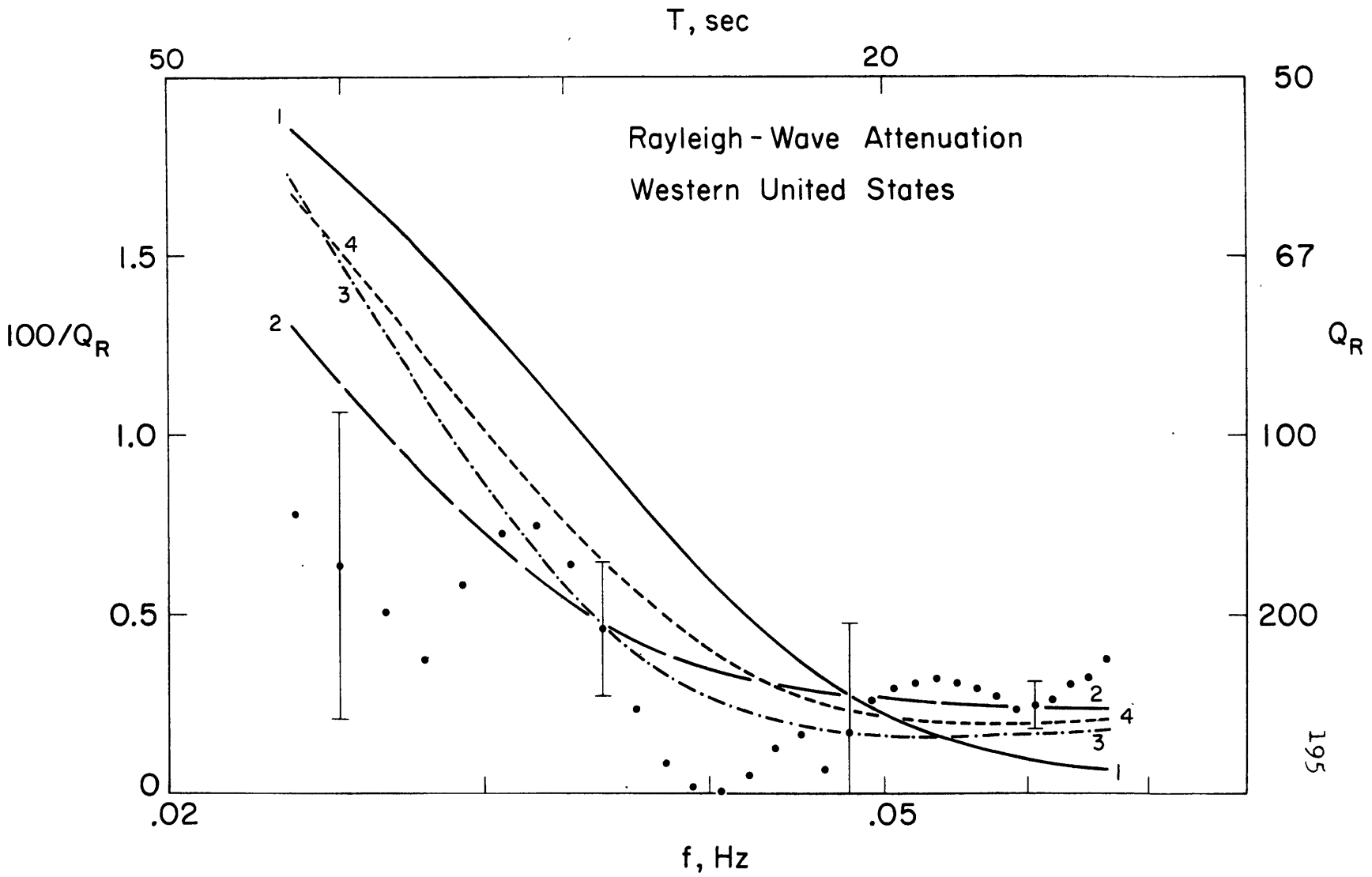
T, sec
50
20
Rayleigh - Wave Attenuation
Western United States
1
2
3
4
1.5
1.0
0.5
0
100/Q_R
67
100
200
Q_R
.02
.05
f, Hz

observed. Furthermore, the discrepancies exceed the supposed uncertainties. This failing, which we shall see is not restricted to frequency-independent models, cannot be due to the neglect of compressive losses; Q_K^{-1} would have to be negative to correct the differences between model and measurement shown in Figures 4.7 and 4.8. The problem may be put simply: at frequencies between .023 and .028 Hz, Q_L^{-1} is measured to be roughly twice Q_R^{-1}, while all models of attenuation for this region (using the phase-velocity partial derivatives calculated from a reasonable facsimile of the true velocity structure) predict Q_L^{-1} comparable to (and usually less than) Q_R^{-1} for the same range of frequencies. Among all models considered, none was able to fit both Love and Rayleigh wave Q^{-1} for $.023 < f < .028$ Hz. We are thus left with the conclusion that either Q_β^{-1} is not isotropic in the upper mantle beneath the United States or that the surface waves in this frequency range are strongly affected by some mode-dependent, but undetected, phenomenon such as lateral refraction or higher-mode interference.

Ellipsoidal magma-pockets preferentially oriented with their major axis in the horizontal plane have been proposed (Shimozuru, 1963a,b; Takeuchi et al., 1968) as the cause of an anisotropy in mantle shear-wave velocity beneath Japan. Aki and Kaminuma (1963) suggested such an anisotropy to account for a discrepancy between Love and Rayleigh-wave phase velocities (cf. Aki, 1968).

A similar anisotropy in the western U.S., involving oblate-spheroidal pockets of melt oriented with one major axis vertical and the minor axis roughly NE-SW (e.g. NW trending dikes), might explain both the discrepancy between Love-and Rayleigh-wave attenuation and the observed differences between SV and SH attenuation (see section 3.5.1). The data, however, do not warrant further pursuit of this point.

Because the measurements of Love-wave attenuation extend to longer periods than do those of Rayleigh waves, we place greater emphasis in all following discussions on Q_L^{-1} between frequencies of .01 and .03 Hz than on Q_R^{-1} in the range .023 to .028 Hz. The need for careful determinations of Q_R^{-1} in the western United States at periods greater than 43 seconds, of course, cannot be overstated.

As mentioned above, the requirement that Q_β^{-1} be everywhere independent of frequency is neither reasonable nor necessary. It is anticipated that near the earth's surface, and perhaps throughout the lithosphere. Q_β^{-1} is frequency-independent. This follows from laboratory observations of the independence of Q_β^{-1} on frequency for rocks at low pressure (e.g. Attewell and Ramana,1966) and on Walsh's (1966) explanation of this phenomenon as frictional losses at the surfaces of cracks, which are expected to be closed by the application of an effective

pressure of a few kilobars. The presence of fluid in the cracks might extend to the upper mantle the depth at which such an effective pressure is reached (Gordon and Davis, 1968). In much of the mantle, and certainly in the asthenosphere, Q_β^{-1} is likely to be a function of frequency. From the discussion of Chapter 2, wherever the asthenosphere is a site of partial melting the attenuation may be treated as arising from one or more relaxation processes.

If Q_β^{-1} is allowed to depend on frequency as well as depth, then measurements of the damping of surface waves do not constrain the depths to regions of high or low attenuation. Two models of $Q_\beta^{-1}(z,f)$ which roughly fit Love-wave attenuation and Rayleigh-wave attenuation ($f > .03$ Hz) are shown in Figure 4.6b(see also Figures 4.7 and 4.8). In model 3, a relaxation Rx(.1,8) (see Chapter 2) is postulated for the depth range 85 to 350 km. In model 4, a relaxation Rx(.1,20) is confined to the depth interval 60 to 160 km. From these and similar models in which a single relaxation process controls attenuation over some depth interval in the upper mantle (and Q_β^{-1} is frequency-independent elsewhere) we conclude: (1) if the zone in which the relaxation occurs is specified, the parameters of the relaxation (relaxation strength, relaxation time) may be determined. (2) The relaxation time is a decreasing function of the depth to the top of the relaxation zone. (3) The relaxation time must lie

roughly in the range 25 to 150 sec; the corresponding depth to the top of the relaxation zone is in the approximate range 60 to 90 km.

4.6.2 East-central United States

There is also a fairly wide range of Q_β^{-1} models that can fit surface-wave attenuation in east-central United States. The technique used for generating models to match the data set given in Tables 4.5 and 4.6 was the same as in the previous section except that the (isotropic) velocity-model of McEvilly (1964) was used to calculate the phase-velocity partial derivatives to be substituted in equations (4.7) and (4.8). Several possible models of Q_β^{-1} for east-central U.S. are given in Figure 4.9; the values of Q_L^{-1} and Q_R^{-1} predicted by these models are compared with observed values in Figures 4.10 and 4.11, respectively. The fit is, for all models, within the stated uncertainties except for the longest-period Love waves (a consequence of the unusually small 'error' for Q_L^{-1} at these frequencies, particularly f = .0178 Hz; i.e. theoretical $Q_L^{-1}(f)$ curves are constrained in the inversion procedure to pass through $100/Q_L = .539$ at f = .0178 Hz).

If Q_β^{-1} is assumed to be independent of frequency throughout the crust and upper mantle, then a model such as model 5 (Figure 4.9) is required. In model 5, Q_β is

Figure 4.9 Some models of Q_β^{-1}, east-central United States. In model 5, Q^{-1} is everywhere independent of frequency. In models 6 and 7, Q^{-1} within the 'asthenosphere' is controlled by a relaxation process and Q^{-1} outside the asthenosphere is frequency-independent. The parameters of the relaxation are $\Delta\mu = .032$, $\tau = 20$ sec in model 6; $\Delta\mu = .037$, $\tau = 10$ sec in model 7.

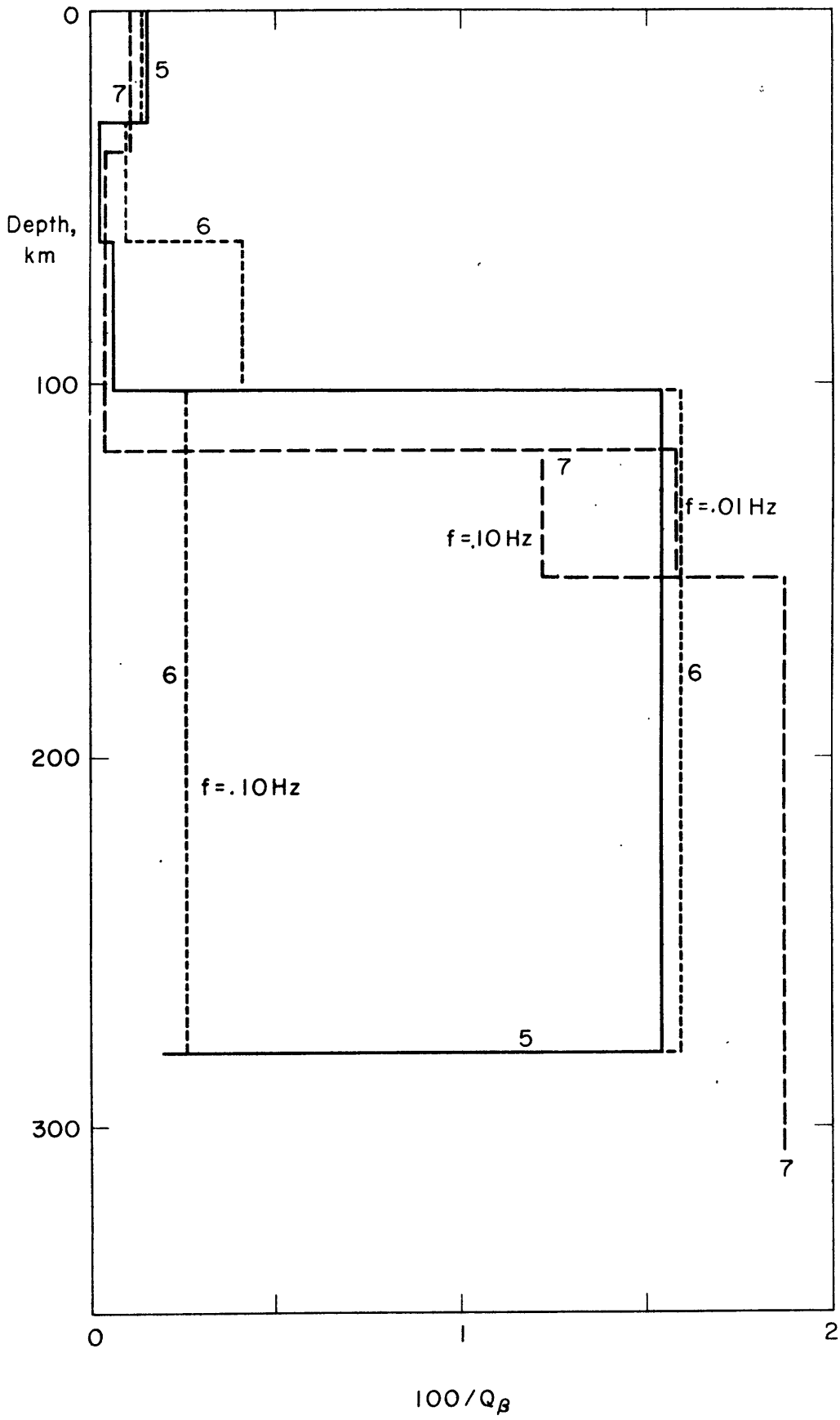
0
100
200
300
Depth, km
5
7
6
7
f=.01 Hz
f=.10 Hz
6
6
f=.10 Hz
5
7
0
1
2
100/Qβ

Figure 4.10 Love-wave attenuation predicted by Q_β^{-1} models, east-central United States. Numerals correspond to the numbered Q_β^{-1} models of Figure 4.9. Observed Love-wave attenuation, including selected error bars, is shown for comparison. Note semi-log scale.

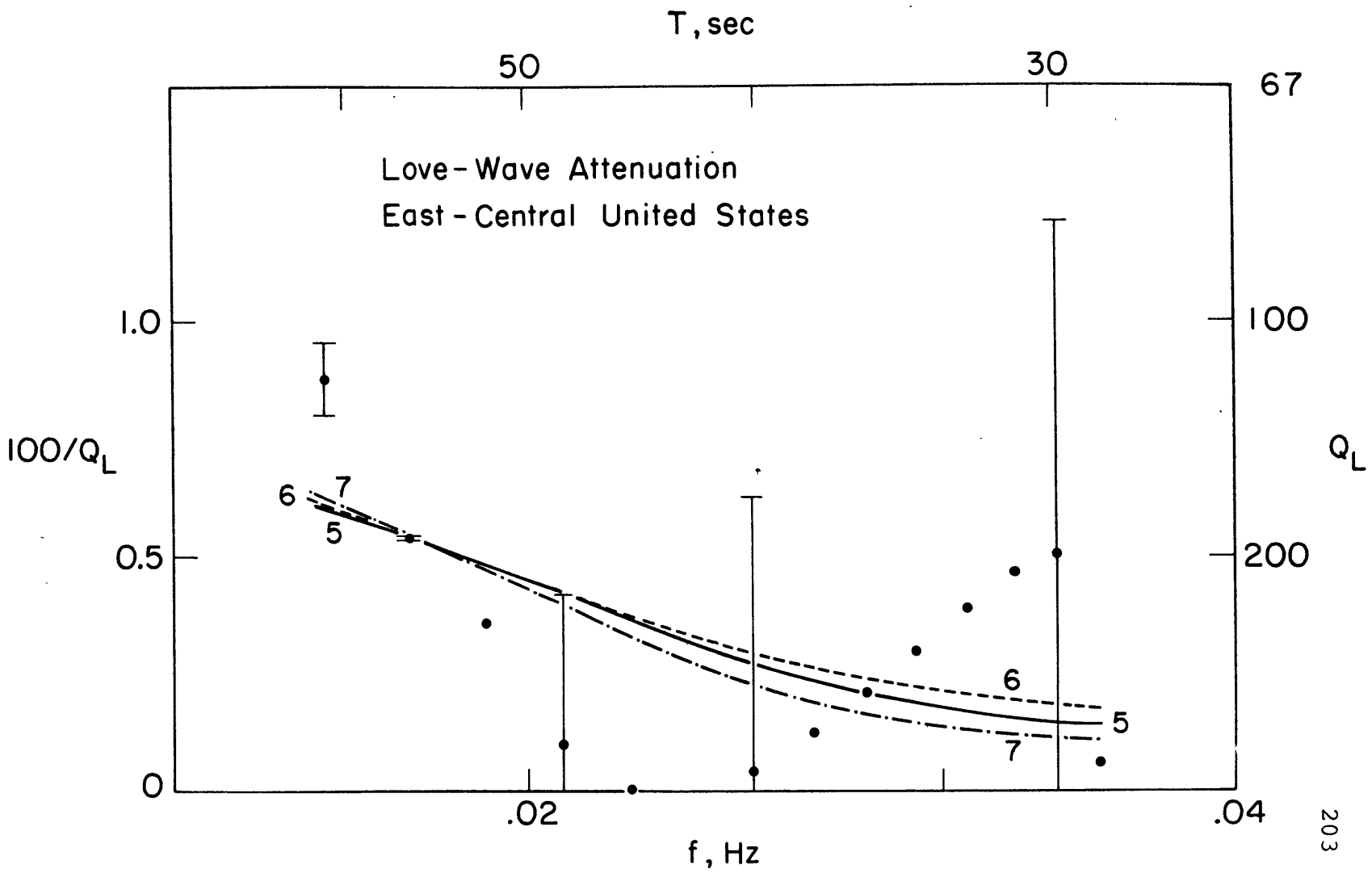
T, sec
50
30
67
Love-Wave Attenuation
East-Central United States
1.0
100
100/Q_L
Q_L
6
7
5
0.5
200
6
5
7
0
.02
.04
f, Hz

Figure 4.11 Rayleigh-wave attenuation predicted by Q_β^{-1} models, east-central United States. Numbers adjacent to theoretical curves correspond to numbers of the Q_β^{-1} models (Figure 4.9). Observed $Q_R^{-1}(f)$, with selected error bars, are also given. Note semi-log scale.

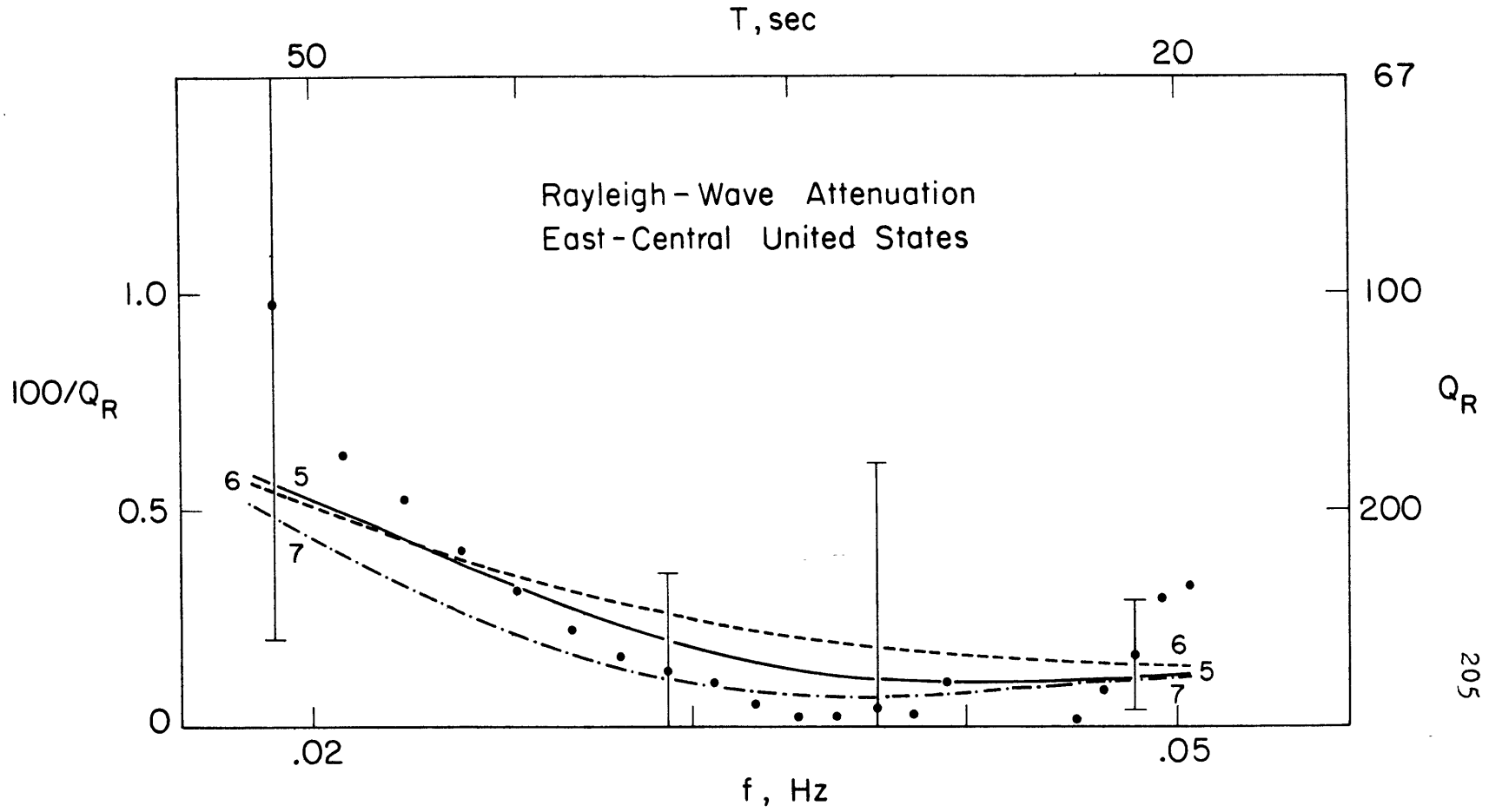
T, sec
50
20
67
Rayleigh - Wave Attenuation
East - Central United States
1.0
100
100/Q_R
Q_R
0.5
200
6
5
7
6
5
7
0
.02
.05
f, Hz

on the order of 1000 in the uppermost 100 km (and decreases with depth in the top 60 km), but Q_β equals about 65 between 100 and 280 km (i.e. within the most pronounced 'low-velocity' layer of McEvilly's velocity models). Comparison of model 5 with models 1 and 2 (Figure 4.6a) would lead, if we were willing to accept the notion that Q_β^{-1} is everywhere frequency-independent, to the conclusion that the lithosphere is thicker in east-central U.S. (100 km) than in western U.S. (60 to 80 km) and that attenuation in the asthenosphere is less (by a factor of 2 or 3) in east-central U.S. than in the western region.

Two equally possible Q_β^{-1} models incorporating relaxations in the asthenosphere are shown as models 6 and 7 in Figure 4.9. In model 6, a relaxation Rx(.032,20) is located between 100 and 280 km depth while Q_β^{-1} is frequency-independent above 100 km depth. In model 7, a relaxation Rx(.037,10) occurs between about 120 and 150 km depth [this depth interval roughly coincides with the 'low-velocity zone' in the model ER-2 (Green and Hales, 1968), appropriate to short-period P waves, of mantle velocity in central U.S.] ; while Q_β^{-1} is taken to be independent of frequency above and below the zone of relaxation. Note that if the relaxation is confined to a depth interval as narrow as in model 7, then the mantle below the relaxed zone must still be highly attenuating (i.e. successive iterations in the inversion process move

toward a more attenuating mantle below 150 km). The strengths of the relaxations in models 6 and 7 are considerably less (by a factor of about 3) than those of the relaxations in models 3 and 4 for the western United States. These models (6 and 7) also suggest, therefore, both that the lithosphere is thicker and that the asthenosphere is less pronounced in east-central U.S. than in western North America.

Clearly, any of a wide assortment of $Q_\beta^{-1}(z,f)$ models can satisfy equally well the surface-wave attenuation observations in east-central and western U.S., even if we restrict consideration to models with no more than four to eight free parameters and with no losses under pure compression. To further narrow the collection of possible models, we must consider independent evidence. This we do in the next chapter: travel-time delays, velocity structures, and body-wave differential attenuation measurements are combined with the surface-wave attenuation results discussed in this chapter to determine a model of the mechanical behavior of the North American upper mantle consistent with all of the above data.

Chapter 5. Synthesis and Discussion

We have measured seismic absorption in the North American mantle with several different yardsticks, each sensitive to a different integral or average of the true attenuation over a particular frequency band. In this chapter we shall combine the results of the various approaches, with the aim of producing physically plausible models of Q^{-1} consistent with all of the attenuation data. Because of the functional relationship of modulus to attenuation in a linear system, further constraints to Q^{-1} models are provided by the travel-time residuals of body waves and velocity models derived from seismic-refraction surveys. Particular attention will be focused on the western United States, both because of the abnormally high attenuation in the upper mantle there and because of the region's significance to global tectonics.

5.1 A model of Q^{-1}, western United States

Let us construct a model of Q^{-1} (z,f) appropriate to the western United States, principally the Basin and Range and Columbia Plateau provinces, based on the ideas and findings discussed in the previous three chapters. We know that the upper mantle in the western United States is probably partially molten and is characterized by high attenuation which is almost entirely the result of losses due to the shearing component of stress. The most likely

attenuation mechanism is viscous damping in the fluid phase, a mechanism that is adequately characterized as a thermally-activated relaxation, or superposition of several relaxations, of the shear stress. (If the 'effective concentration' of fluid is sufficiently great, then the damping is no longer formally equivalent to a relaxation process, though the essential features of a relaxation are retained.) Thus Q^{-1} should be frequency-dependent (as should the shear modulus), a result corroborated in Chapter 3.

A model of attenuation in the western United States is constrained by at least the following input: (1) Q_L^{-1} and Q_R^{-1} as given in Tables 4.2 and 4.3; (2) an estimate of the total attenuation of vertically incident shear-waves (f=.1 Hz) as implied by Figure 3.3; (3) the boundaries and the velocity decrease of the 'low-velocity zone' for short-period (f= 1 Hz) compressional waves.

The total attenuation of a shear wave vertically incident in the western United States is clearly at least as large as the <u>difference</u> in attenuation of (vertically incident) shear waves between western and east-central United States. Let us set $\delta t_S^* = 0$ in east-central U.S. Then from Figure 3.3, a conservative <u>lower bound</u> for δt_S^* (f= .1 Hz) in the Basin and Range province is +7 sec. (If we had set $\delta t_S^* = 0$ at FLO, say, then we would have $\delta t_S^* = +14$ at TUC, +19 at LON.) This lower bound is still a

large number. If the zone of high attenuation is confined to a layer 100 km thick, then $\delta t_S^* = +7$ sec (for vertical incidence) at f=.1 Hz implies that $Q_\beta = 10$ at f=.1 Hz within such a layer.

The existence throughout most of western North America of a well-defined low-velocity zone for both shear and compressional waves has been accepted for some time and has been cited as evidence for partial melting in the upper mantle (see Section 2.1). If the low-velocity zone is a locus of partial melting, then the low velocities are consequences both of shear relaxations due to viscous dissipation in the melt phase and of (frequency-independent) decreases in the elastic moduli of the solid phase due to thermal expansion of the crystal lattice. Separation of these two effects, unless one of the two is negligible or unless the velocities (moduli) are measured over the entire frequency range, requires an arbitrary assumption. We shall assume that the sharp decrease in velocity beneath a higher-velocity 'lid' is due to a relaxation process, and that the shear modulus is partially relaxed at all depths between the base of the 'lid' and the depth at which the velocity again equals the velocity in the 'lid'. In the Basin and Range and Columbia Plateau provinces, the zone of relaxed shear-modulus appropriate to a frequency of 1 Hz is presumed to extend from about 60 to 160 km (Johnson, 1967; Julian, 1970). [In at least parts of the Basin and

Range province, the 'lid' has an abnormally low velocity and may not even be present (Archambeau et al., 1969; Julian, 1970); partial melting extending to depths as shallow as the base of the crust has been suggested.] The decrease in compressional velocity (at f= 1 Hz) associated with the relaxation is taken to be 0.2 km/sec (this is roughly the mean of the velocity decreases in Julian's models NTS N1 and NTS N3), which amounts to a relaxation strength $\Delta\mu$ of about 0.1. It is further presumed that the peak frequency of such a relaxation is in excess of 10 Hz, so that the shear modulus at f = 1 Hz is approximately equal to the relaxed modulus.

It is necessary then to assumed that at least one additional relaxation process operates in the asthenosphere in order to satisfy the attenuation of surface waves and of long-period body waves. As was shown in Chapter 4, a single shear-relaxation in the upper mantle can explain the attenuation of Love and Rayleigh waves in the western United States. The parameters of such a relaxation are such, however, as to predict δt_S^* less than 7 sec for S waves of frequency 0.1 Hz (δt_S^* = 3.5 sec for model 3, 0.6 sec for model 4). For a single relaxation, confined to a depth interval of 100 km or less, to give δt_S^* = 7 sec at f = 0.1 Hz requires that the relaxation strength be greater than or equal to 0.2 (with equality only if the relaxation-peak frequency is 0.1 Hz). If there were such a relaxation operative between 60 and 160 km depth, then

the attenuation of surfaces waves in the period range 20 to 40 seconds would be much greater than is observed (Figures 4.1 and 4.2); e.g. at f=.03 Hz, $100/Q_L \geq 1.5$ and $100/Q_R \geq 2.5$. We are therefore forced to conclude that most of the attenuation of 10-sec S-waves takes place deeper than 100 or 150 km.

A model of $Q_\beta^{-1}(z,f)$ consistent with all of the above considerations is given in Figure 5.1 and Table 5.1. The essential features of the model are as follows: (1) Attenuation is small in the uppermost 60 km. The decrease in Q_β^{-1} with depth in this zone, though suggested by results of the inversion procedure discussed in Chapter 4, is not statistically significant. Q_K^{-1} is non-zero only in the uppermost 30 km (this to better match Q_L/Q_R in the period range 15 to 20 sec), in line with the notion that attenuation in this region is due to frictional dissipation at the surfaces of microcracks (Walsh, 1966). Note that the ratio $Q_\mu/Q_K = 3$ corresponds approximately to $Q_\beta/Q_\alpha = 2$. Such a ratio was found by Press (1964) for Lg and Pg waves in the crust near the Nevada Test Site, though he attributed some of the P-wave energy loss to mode conversion. (2) In the 'low-velocity zone' between about 60 and 160 km, attenuation is the result of a superposition of two relaxations of equal strength. The higher frequency ($2\pi\tau = .05$ sec) relaxation produces sharp decreases in compressional and shear velocities

Figure 5.1 A relaxation model of $Q_\beta^{-1}(z,f)$, western United States. Q_β^{-1} is independent of frequency above 60 km, and depends on frequency as shown in the inserts (semi-log scale) for the two layers deeper than 60 km. $100/Q_\beta$ is plotted as a function of depth z for two specific frequencies.

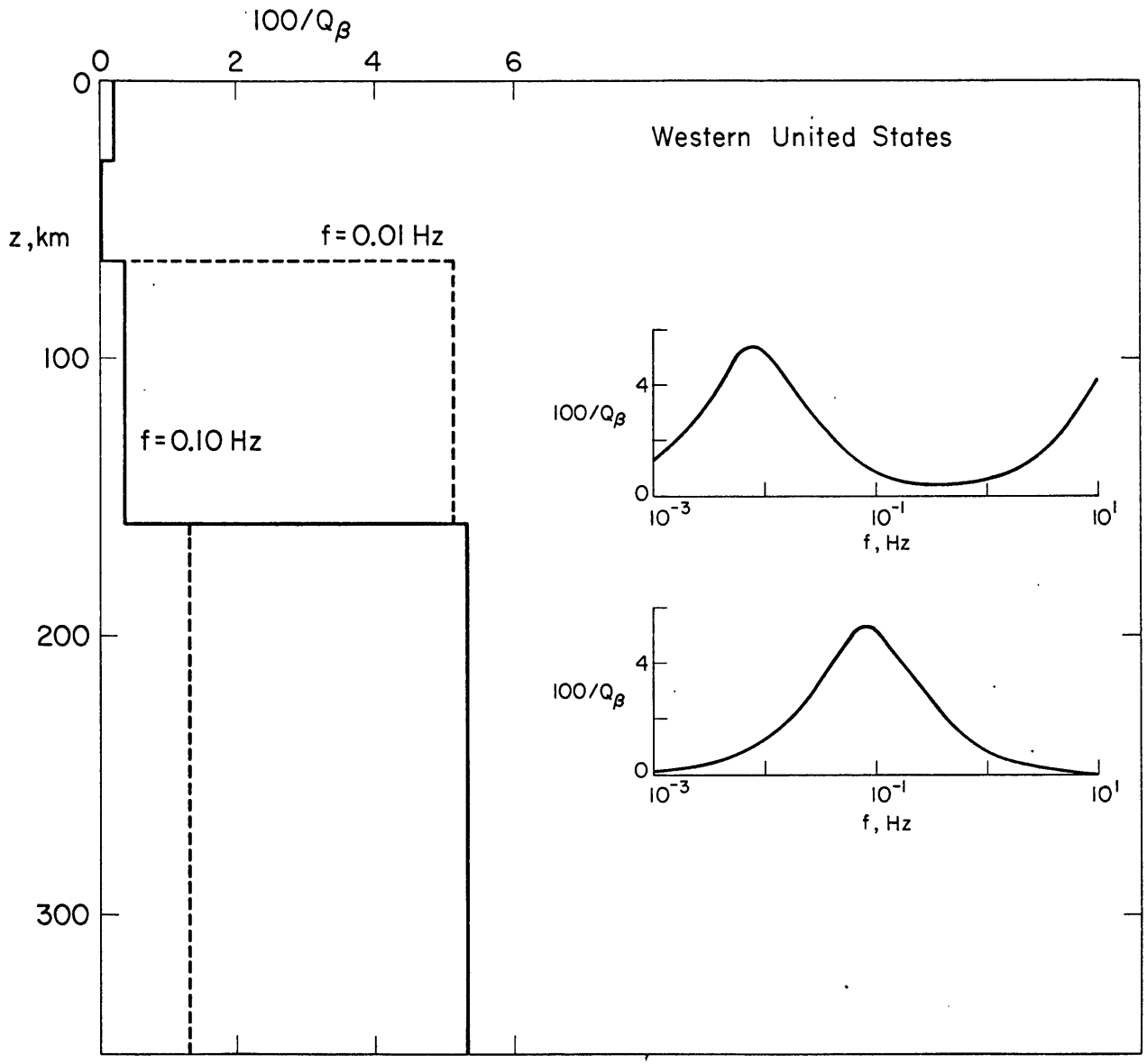
100/Qβ
0
2
4
6
0
Western United States
z, km
f = 0.01 Hz
100
f = 0.10 Hz
200
300
100/Qβ
4
0
10^-3
10^-1
10^1
f, Hz
100/Qβ
4
0
10^-3
10^-1
10^1
f, Hz

Table 5.1

A model of Q^{-1}, western United States

Layer	Thickness km	$100/Q_\mu$	$100/Q_K$
1	29	0.1	0.3
2	35	0.01	0
3	96	Rx(0.1,.008)+Rx(0.1,20)	0
4	190	Rx(0.1,2)	0

Note: Rx($\Delta\mu$, τ) indicates that attenuation is given by

$$100/Q_\mu = \frac{100\,\Delta\mu}{(1-\Delta\mu)^{\frac{1}{2}}} \quad \frac{2\pi f\tau}{1+(2\pi f\tau)^2}$$

where f is frequency.

(0.18 and 0.24 km/sec, respectively, at 1 Hz) at the top of the layer. The lower frequency relaxation ($2\pi\tau = 125$ sec) accounts for the observed attenuation of surface waves. (3) Below 160 km, a single relaxation ($2\pi\tau = 12.5$ sec) is sufficient to account for most of the attenuation of long-period ($f \simeq 0.1$ Hz) shear waves. The lower boundary of this fourth layer, which we shall call the 'lower asthenosphere' to distinguish it from the 'upper asthenosphere' between 60 and 160 km, is located at a depth of 350 km in the model; this depth is not well-determined and may, in fact, lie anywhere in the range 250 to 400 km. It should be remembered, however, that the product $h \cdot \Delta\mu$, where h is the layer thickness and $\Delta\mu$ the strength of the relaxation in the layer, is roughly fixed by the value of δt_S^*.

The model of Table 5.1 may be checked against measured attenuation in several ways. The predicted surface-wave attenuation is shown in Figure 5.2, together with the observations of Q_L^{-1} and Q_R^{-1} as given in Tables 4.3 and 4.4. The fit of the model is quite satisfactory, except perhaps for Q_R^{-1} between .0235 and .030 Hz. (The discrepancy between Q_L^{-1} and Q_R^{-1} in this frequency range was noted in section 4.6.1.) Although not shown in Figure 5.2, the predicted Rayleigh-wave attenuation, which peaks ($100/Q_R = 2.7$) at $f = .014$ Hz, is quite large for frequencies less than .03 Hz. Efforts to confirm or disprove the

Figure 5.2 Attenuation of Love and Rayleigh waves, western United States. Theoretical curves, predicted by the relaxation model of Table 5.1, are compared to measured values (circles), taken from Tables 4.3 and 4.4.

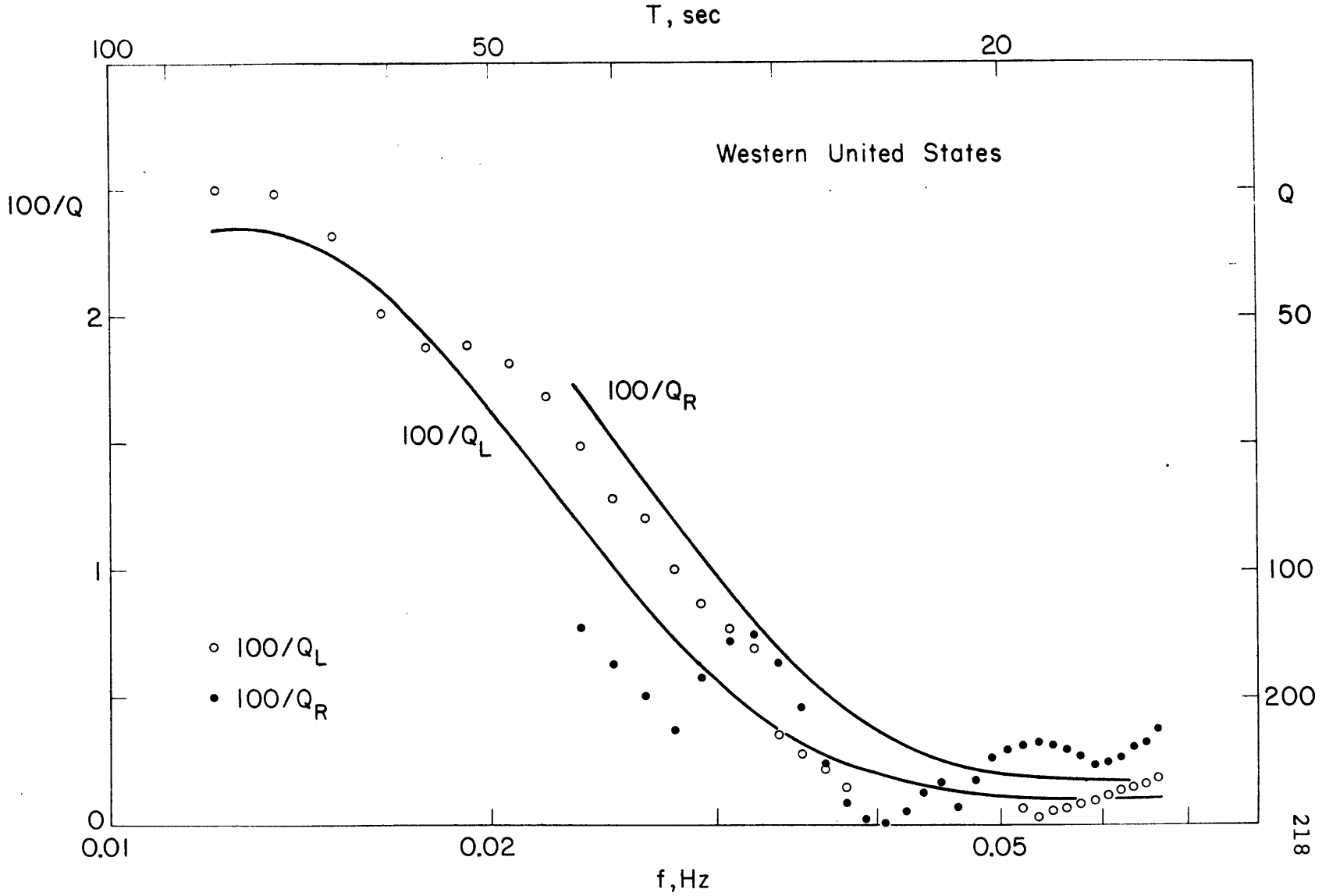
T, sec
100
50
20
Western United States
100/Q
Q
2
1
0
50
100
200
100/Q_R
100/Q_L
○ 100/Q_L
• 100/Q_R
0.01
0.02
0.05
f, Hz
218

validity of these values should be encouraged. (See also the discussion on possible anisotropy of Q^{-1} in Chapter 6.)

The predicted body-wave attenuation and travel-time delay (for vertical incidence) are given as functions of frequency in Figure 5.3. At f = 0.1 Hz, $\delta t_S^* = 7.4$ sec, in agreement with our (conservative) estimate. [Note that, while δt_S^* does indeed depend on frequency, its value lies within 15% of 7 sec at all frequencies in the band over which shear-wave spectral ratios were determined (section 3.3); thus the assumption that the slopes of the spectral ratios are independent of frequency over the frequency band should not introduce serious error.] Travel-time residuals, which are monotonically decreasing functions of frequency, are comparable in magnitude but somewhat lower (as we expect, see following section) than the <u>difference</u> in travel-time delays between western and central United States (Hales and Roberts, 1970; Cleary and Hales, 1966). It is possible, in theory, to test Figure 5.3 by measuring the variation of P- or S-wave travel-time delay with frequency; such variations are probably not resolvable, however, using present techniques. At f = 1 Hz, $100/Q_\alpha = .3$ throughout the asthenosphere and $\delta t_P^* = 0.38$ sec. This value of differential attenuation is equivalent to a body-wave magnitude 0.16 (f = 1 Hz) lower than at a station overlying a non-attenuating lower mantle. While the results of section

Figure 5.3 Differential attenuation and travel-time delay predicted by Q_β^{-1} model, western United States. (a) δt^*, for P and S waves, versus frequency (semi-log scale). (b) Travel-time delay δt, for P and S waves, versus frequency. Both δt^* and δt are evaluated relative to an unrelaxed upper mantle.

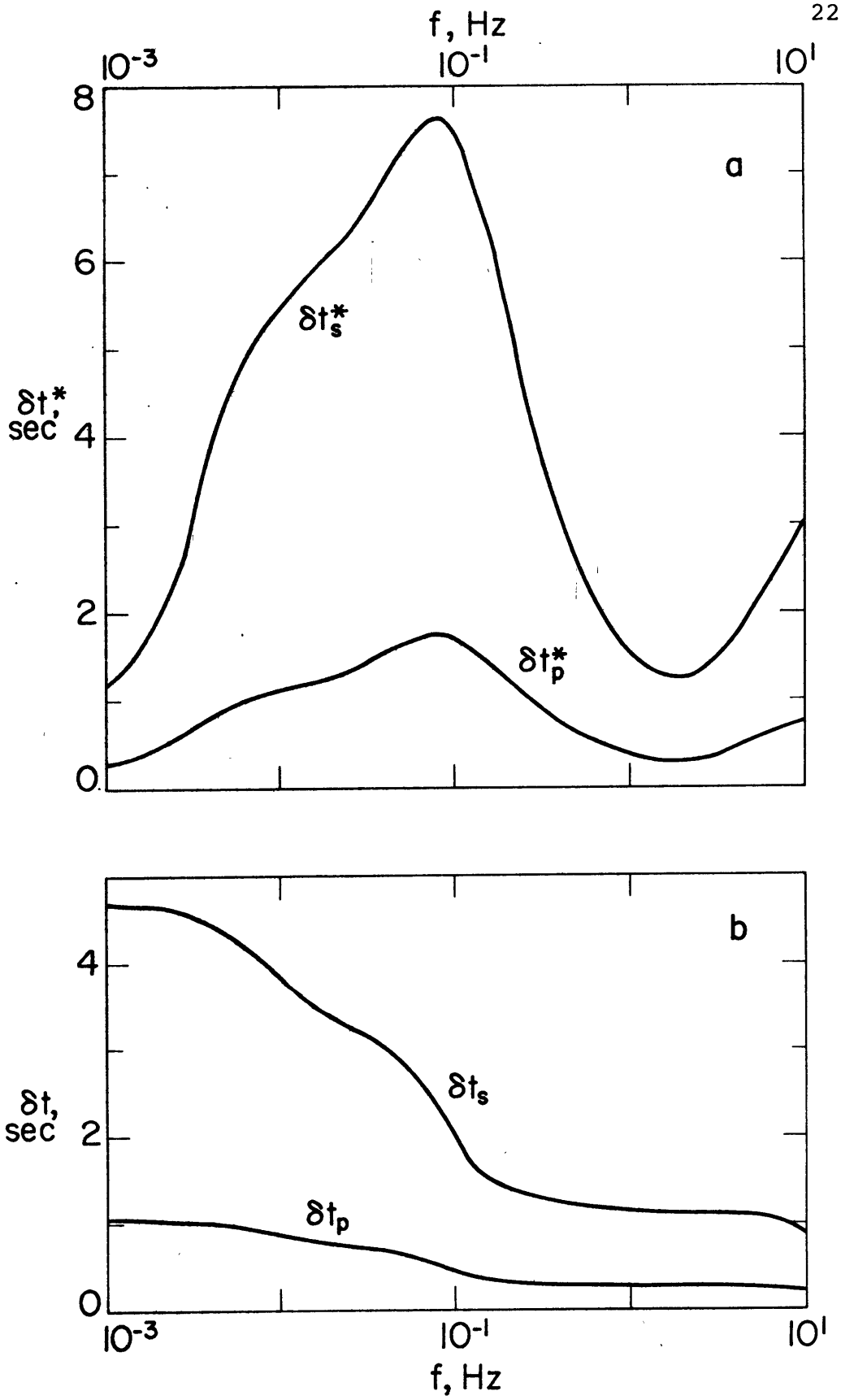
f, Hz
10-3
10-1
10¹
8
6
4
2
0
δt*, sec
δt*s
δt*p
a
δt, sec
δts
δtp
b
f, Hz

3.5.3 suggest that the attenuation of short-period (f = 1 Hz) P waves in the Basin and Range province may be greater than predicted by the model of Figure 5.1, the model should be treated as an average over several provinces. Certainly Figures 3.3 and 3.5, for instance, imply that attenuation beneath some stations exceeds that given by the model.

The relaxation model of Figure 5.1 predicts that the shear modulus is frequency-dependent. In particular, for frequencies less than about .01 Hz, μ is at least partially relaxed at all depths between 60 and (roughly) 350 km. This is shown in Figure 5.4a, where shear velocity as predicted by the relaxation model is plotted versus depth for f = .01 and .003 Hz. For simplicity, an unrelaxed velocity of 4.6 km/sec is assumed for the entire depth range 30 to 350+ km. For comparison, two recent models (Toksöz et al., 1967; Kanamori, 1970a) of the shear-velocity structure in tectonic regions of the earth are also given. These models, generated to fit phase and group velocities of long-period (f = .003 to .010 Hz) Love and Rayleigh waves for purely 'tectonic' paths, may or may not accurately represent the upper mantle of western North America. The essential point is that the relaxation model, while not designed to describe the velocity as a function of depth, is consistent with the major features of the 'tectonic' models: a sharp decrease in shear velocity

Figure 5.4 Some comparisons of the relaxation model of Q_β^{-1} with additional data. (a) Shear velocity, at frequencies of .003 and .01 Hz, predicted by the relaxation model (unrelaxed velocity = 4.6 km/sec, 60 to 350 km) compared with 'tectonic' models of Toksöz et al. (1967) and Kanamori (1970a). (b) P-wave attenuation, at a frequency of 3 Hz, predicted by the relaxation model compared with the attenuation model of Archambeau et al. (1969).

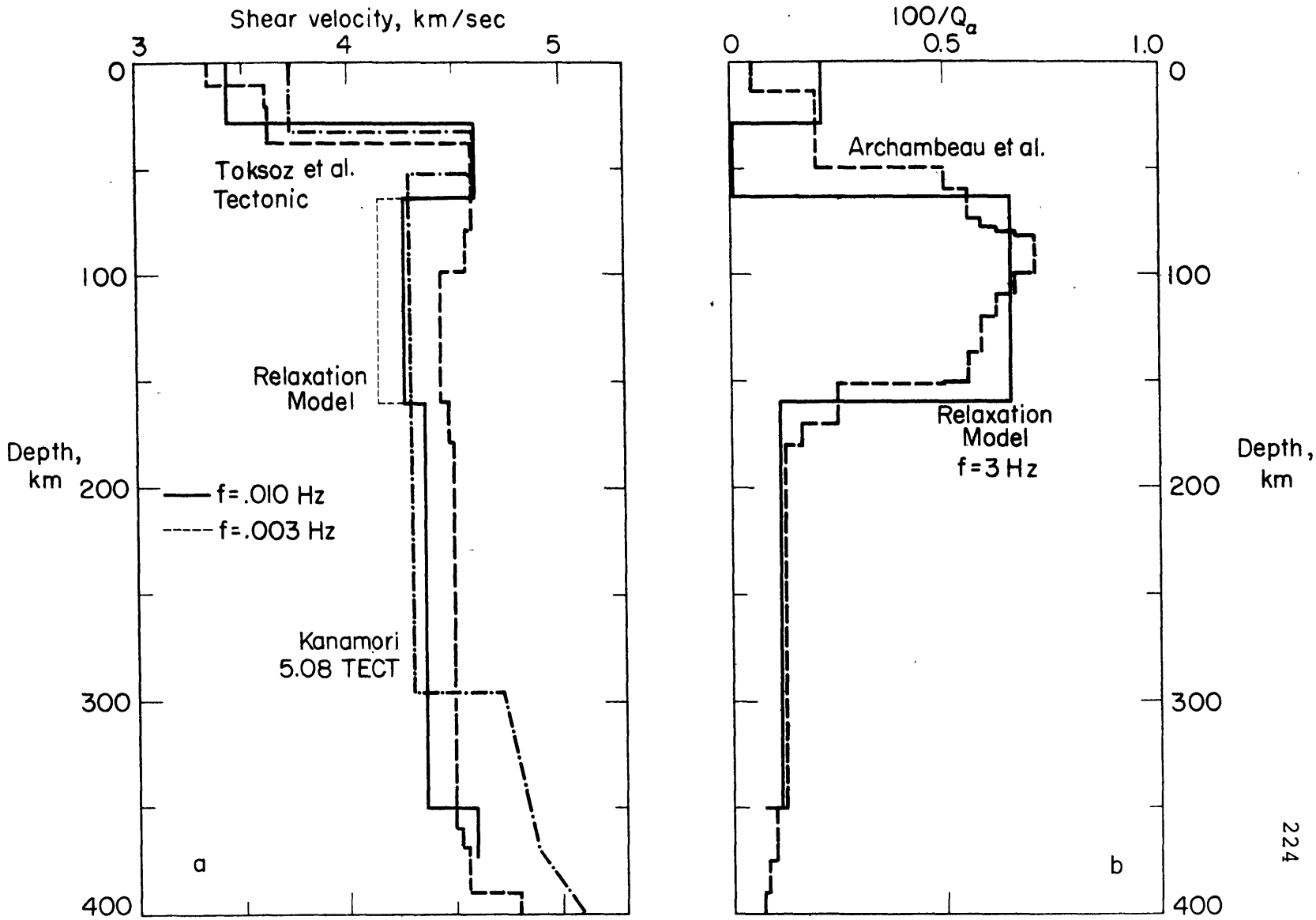
Shear velocity, km/sec
3
4
5
0
100
200
300
400
Depth, km
Toksoz et al.
Tectonic
Relaxation
Model
f=.010 Hz
f=.003 Hz
Kanamori
5.08 TECT
a
100/Q$_\alpha$
0
0.5
1.0
Archambeau et al.
Relaxation
Model
f=3 Hz
b

at some depth in the range 50 to 80 km; a small increase in velocity at a depth near 160 km; and a larger increase in velocity at a depth of 300 km or greater (this increase is deep enough in the model of Toksöz et al., though not in the model of Kanamori, to be associated with the olivine-spinel transition). At seismic periods sufficiently shorter than 100 sec, the shear-wave velocity will be essentially unrealxed below 160 km. Thus Kovach and Robinson (1969), using $dt/d\Delta$ of S waves in the approximate period-range 10 to 25 sec, found the 'low-velocity' in the Basin and Range province to extend from 50 to about 180 km.

A further test of the relaxation model is shown in Figure 5.4b, where the predicted attenuation of high-frequency (f = 3 Hz) P-waves is compared to the Q_α model of Archambeau et al.(1969) for the western United States (they give 2-5 Hz as the frequency range for which their model is appropriate). While the precise value of Q_α^{-1} in the depth interval 60 to 160 km is controlled by the (somewhat arbitrary) value of the relaxation time of the higher-frequency relaxation, still the close similarity (at least below 60 km) of Q_α^{-1} determined by Archambeau and his co-workers is heartening. (At depths shallower than 60 km, neither we nor Archambeau et al. have much control on Q_α^{-1}.)

If the relaxation processes of our attenuation model are the result of partial melting in the asthenosphere, then

we may apply equations (2.4) to estimate the physical properties of the fluid phase. A relaxation strength of 0.1 implies $c(\alpha)/\alpha = 0.5$, where c and α are the fluid concentration and the aspect ratio of the melt pockets, respectively. Furthermore, relaxation times of .008, 2, and 20 sec correspond to $\eta / \alpha = 1.1 \times 10^{10}$, 2.4×10^{12}, and 2.4×10^{13} poise, respectively. As has been emphasized earlier, the quantities c, α and η are not uniquely determined by the relaxation parameters. Nonetheless, we may hazard a guess at plausible values.

Between 60 and 160 km, a partial melt with c(total) = .01, $\eta = 2 \times 10^{8}$ poise, and fluid inclusions of two distinct shapes ($\alpha = 2 \times 10^{-2}$ and $\alpha = 1 \times 10^{-5}$) is consistent with both the relaxation model and our expectations of how molten material might be distributed in the mantle. (Also consistent are any set of parameters equal to the above multiplied by a fixed constant less than perhaps 5 or 10.) The viscosity, while somewhat higher than values observed for molten lavas on the earth's surface (Clark, 1966), is not out of line with estimates of the viscosity of molten rock at pressures near 100 kb (Murase and Suzuki, 1966). A melt model with two inclusion-populations of very different aspect ratios is reminiscent of the discussion of the ice-brine system (section 2.3.2). One might postulate that 'melt' behaves differently at different grain boundaries (e.g. olivine-olivine, olivine-pyroxene, etc.), completely 'wetting' some

boundaries while only partially wetting others, but there is no way to test such an idea at present.

Between 160 and 350 km, if the total fluid concentration is equal to the concentration in the overlying layer (60 to 160 km), then c = ,01 implies $\alpha = 2 \times 10^{-2}$ and $\eta = 5 \times 10^{10}$ poise. (This amounts to a 'mapping' of the relaxation Rx (.1,.008) to Rx (.1,2) on going from the upper to the lower asthenosphere; i.e. a shift to lower frequencies because of the higher viscosity in the lower layer. Does the same 'mapping' then apply to the lower-frequency relaxation in the upper asthenosphere; is there a second relaxation, with $\tau \simeq 5 \times 10^3$ sec, between 160 and 350 km?) Such an increase in viscosity of the fluid probably cannot be explained as due merely to the increase in pressure, but might be related to the stability of free water or some other volatile. An alternative hypothesis is that the viscosity of the fluid phase remains very nearly constant throughout the depth range 60 to 350 km. In that case, the total concentration or viscous inclusions below 160 km equals 5×10^{-5} ($\alpha = 1 \times 10^{-4}$). It is clear that, while we have resolved none of the ambiguity in interpreting our relaxation model for attenuation in western United States, the consequences of the model for studies of volcanism and tectonics of the region are significant.

When considering the relaxation model proposed for the western United States, one should keep several points in

mind: (1) The notion that observed seismic attenuation in the mantle is the result of thermally-activated relaxation processes is not new (see Gordon and Nelson, 1966; Jackson, 1969a; Nur and Simmons, 1969; Goetze, 1969; Nur, 1971). Most previous studies, however, were based on the premise of spherical symmetry and were constrained by a data set less complete than that considered here. The interpretive value of such studies is questionable. (2) A necessary, but not sufficient, condition for partial melting in the asthenosphere, if the considerations of Chapter 2 are approximately correct, is that seismic attenuation in the asthenosphere be almost entirely due to one or more relaxations of the shear component of stress. Thus the conclusion that the proposed relaxation-model fits all available attenuation data for the western United States is consistent with partial melting in that region but does not prove that a partial melt, in the usual sense, exists. For instance, viscous grain-boundary relaxation-peaks of strength greater than 0.1 have been observed at sub-solidus temperatures in polycrystalline metals, salts, oxides, and at least two silicates (see Jackson, 1969b; Goetze, 1969; Jackson and Anderson, 1970). Whether we might wish to call the viscous-inclusions 'grain boundaries' or 'melt pockets' does not affect, however, our use of equations (2.3) and (2.4); cf. section 2.3.3. (3) The model of Table 5.1, even were it approximately

correct in its major features, is a gross simplification. If the asthenosphere is indeed partially molten, then such quantities as the amount and distribution of melt and the viscosity of the fluid no doubt vary continuously along both vertical (i.e. with temperature and pressure) and horizontal directions. Even the idea that viscosity is proportional to $e^{H/RT}$, for some activation energy H, while a more realistic approach than assuming viscosity constant within layers 100 to 200 km thick, does not hold for many silicate liquids (Clark, 1966). Attenuation models more complicated than the relaxation model of Table 5.1, however, are not justified by existing seismic data though may eventually be required as information on the physical state and rheology of rock systems at high temperatures and pressures becomes available.

In summary, both the shear modulus and the attenuation in shear in the upper mantle of western North America appear to depend upon frequency in ways which are consistent with simple models for the physical behavior of partial melts. The mantle displays some viscous character to depths as great as 350 km. The asthenosphere, viewed as the zone within which the shear modulus at very low frequencies is abnormally small, is thus seen to be at least 300 km thick beneath western North America. [It is possible that at frequencies less than those of seismic waves, further relaxations occur either above 60 km depth or

deeper than 350 km. Walcott (1970), for instance, estimated from the isostatic rebound of the Lake Bonneville region that the lithosphere in the Basin and Range province is only 20 km thick.] Thus equating the asthenosphere to the 'low-velocity zone', particularly if the velocities are those of short-period body waves, may be quite misleading.

5.2 Lateral variation of some properties of the asthenosphere

The model of attenuation developed in the preceding section constitutes an average $Q_\beta^{-1}(z,f)$ for much of western North America. But the details of the attenuation structure vary laterally, reflecting lateral changes in temperature, composition, or microstructure. Using the relaxation model of attenuation given in Table 5.1 as a guide, we attempt in this section to unravel some of the regional variations in those physical properties which affect the mechanical behavior of a partially molten asthenosphere.

5.2.1 The relaxation in the lower asthenosphere

Let us adopt the following hypothesis: the Q_β^{-1} structure beneath any point in the western United States (and perhaps the rest of the continent as well) is similar to the relaxation model of Table 5.1 except that the particular parameters ($\Delta\mu$, τ) of each of the three relaxations are considered unknown. How may these parameters, which we expect will show regional variations, be determined? Clearly we should not use as constraints any measurements which average over too great a horizontal distance; this probably rules out surface-wave velocity or attenuation as important input. Vertically averaged information, however, should preserve most lateral variations. Thus travel-time delays and differential attenuation of

body waves are vital pieces of data.

In section 5.1, we distinguished between an upper and a lower asthenosphere. Most of the attenuation of long-period teleseismic P and S waves occurs in the lower asthenosphere, while most of the delay (due to relaxation of the shear modulus) of short-period body waves takes place in the upper asthenosphere. [Most of the total delay of short-period P waves can also be attributed to the 'low-velocity zone', i.e. to the depth interval 100 to 200 km (Hales et al., 1968).] Let us focus on the (single) relaxation process in the lower asthenosphere. Beneath any given seismograph-station, attenuation in the lower asthenosphere is completely specified by the two parameters ($\Delta\mu$, τ) of the relaxation. To determine $\Delta\mu$ and τ , we need to find two independent observables that are functions of both parameters. Measurement of attenuation (δt^*, say) at two distinct frequencies would serve this purpose. In effect, such information is contained in the spectral ratio, over a finite frequency-band, of two body waves; but the relatively small bandwidth and the perturbations introduced by crustal layering and lateral inhomogeneities probably preclude the use of the spectral ratios of Chapter 3 to determine $\delta t^*_S(f)$ or $\delta t^*_P(f)$. Measurement of δt^*_S and δt^*_P at the same frequency (e.g. 0.1 Hz), however, does not determine $\Delta\mu$ and τ since, if all attenuation is associated with the shear component of

stress, δt_S^* and δt_P^* contain (in principle) the same information. Thus, we shall make use, in addition to δt_S^* and δt_P^* of the travel-time delay δt_S of long period shear waves, in particular that fraction of the delay due to the relaxation process in the lower asthenosphere. In the discussion to follow it will be assumed that (1) a single relaxation-process in the lower asthenosphere controls δt_P^* and δt_S^* and contributes some portion of δt_S; (2) the remainder of the S-wave delay is attributable to effects the magnitude of which may be estimated.

The travel-time delays of S waves to most North American seismograph-stations have been determined by Hales and co-workers (Doyle and Hales, 1967, Hales and Roberts, 1970). These values, corresponding to first motion of long-period S waves, are appropriate to a frequency of about 0.1 Hz (or perhaps slightly higher); though the dominant frequency of the waves used was typically somewhat lower, .05 to .07 Hz (Doyle and Hales, 1967). A positive travel-time delay is due to lower-than average shear-velocity in the crust or upper mantle. The low velocity may be attributed to several possible causes: (1) high temperatures, (2) one or more relaxation processes with relaxation times (τ) less than about 2 sec, (3) a crust thicker than average, (4) chemical or mineralogical composition. How may we isolate that portion of the travel-time delay which arises from a relaxation in the lower asthenosphere?

We shall assume that the travel-time delay δt_P of short-period P waves consists of only two parts: (1) the delay, which we shall call $\delta t_P'$, due to passage through the 'low-velocity zone' (in the upper asthenosphere), which is primarily the consequence of at least one relaxation (due to partial melting, say) which peaks at a frequency in excess of 10 Hz; (2) the delay, which we shall call $\delta t_P''$, due to temperature-induced changes in the elastic moduli associated with thermal expansion in the crystalline lattice of the solid portions of the entire upper mantle. (We require δt_P, $\delta t_P'$, and $\delta t_P''$ to be non-negative; this is satisfied by adding a constant to all values as reported in the literature, of δt_P at stations of interest.) The term $\delta t_P'$ may be calculated if the P-wave velocity structure of the mantle has been determined by seismic-refraction experiments. We then presume $\delta t_P'' = \delta t_P - \delta t_P'$ is non-negative. Both the high-frequency relaxations in the upper asthenosphere and the temperature-induced changes in the shear modulus of the solid mantle affect δt_S ($f \simeq 0.1$ Hz); let us call the respective contributions $\delta t_S'$ and $\delta t_S''$. The relations among $\delta t_S'$, $\delta t_S''$, $\delta t_P'$, and $\delta t_P''$ are given in Appendix 4. Note that we have neglected, largely out of ignorance, contributions to δt_P arising from compositional differences (i.e. different crustal thickness, different upper-mantle mineralogy, etc.). If relative changes in P- and S-wave

velocity due to such a composition difference are similar to changes that might be produced by a (fictional) difference in temperature, then our conclusions below are unaffected; if not, then our estimate of the S-wave delay attributable to a relaxation process in the lower asthenosphere will be in error.

Implicit in the use of the equations given in Appendix 4 is the presumption that δt_P and δt_S are reasonably well known. Such a presumption is not, in fact, valid. All of the several published tabulations of travel-time delays employed shallow earthquakes or explosions as sources; most of these events were located near lithospheric plates downthrust into the asthenosphere at island-arc regions. The effect of plates on the travel-times of body waves from shallow events near island arcs is large and direction-dependent (Davies and McKenzie, 1969; Toksöz et al., 1971); this effect introduces some bias to most station travel-time delays reported to date.

In an effort to circumvent this bias, δt_P at WWSSN stations in the United States was determined using deep-focus South American earthquakes. For each of 16 earthquakes in the period January 1964 through January 1967, the travel-time delays, relative to the Jeffreys-Bullen travel-time tables, at United States stations were taken from the Bulletin of the International Seismological Centre. Every earthquake used was deeper than 530 km,

was of magnitude 4.3 or greater, and was recorded (i.e. P-wave arrivals were reported) by at least two WWSSN stations in the United States. The mean value of δt_p, together with standard deviation, at each station is given in Table 5.2. Values of δt_p taken from several frequently cited compilations (Carder et al., 1966; Cleary and Hales, 1966; Herrin and Taggart, 1968) are also included. (Note that these δt_p values differ slightly from those originally reported. Since travel-time delays are usually known only to within addition of a constant, we have subtracted from each delay a 'baseline' value, common to every entry in a given column; the 'baseline' for each column was selected so that the average delay equals zero at those 15 stations covered by all four studies.)

It is expected that the travel-time residuals of Carder et al. (1966) most closely approximate those that would be determined if deep-earthquakes in several scattered regions were used as sources. This is because none of the sources used by Carder and co-workers was situated near a downthrust plate; all sources were nuclear explosions located either in the Pacific basin or in the interior of a continent. Comparison of the δt_p values, which represent an average over several propagation-directions, of Carder et al.(1966) and the values determined using deep-focus earthquakes in South America suggest anomalously large delays are associated with the

Table 5.2. Travel-time delays of short-period P waves at WWSSN stations in the United States.

Station	δt_P, sec			
	Deep earthquakes, S. America	Carder et al.	Cleary-Hales	Herrin-Taggart
AAM	-1.0 ± .3[a]	-0.9	-.24	-.26
ALQ	0.3 ± .6	0.1	.32	-.02
ATL	-0.6 ± .2	-0.2		-.21
BKS	0.3 ± .4	0.2[c]	.32	.59
BLA	0.3 ± .5	0.1	-.42	-.28
BOZ	0.8	0.2		-.50
COR	0.9 ± .3	1.0	.79	.73
DAL	-0.5	-0.6	-.02	.07
DUG	0.6 ± .3	0.0	.22	-.10
FLO	-1.7	-0.5	-.89	-.78
GEO	-0.1	-0.5	-.42	-.13
GOL	0.4 ± .2	-0.5	.30	.00
GSC	0.9		-.58	
JCT	-0.2 ± .7			
LON	-0.1 ± .7		.04	-.23
LUB	-0.9	0.4	-.04	-.31
RCD	-0.3 ± .1	0.4	-.06	.05
SCP	0.6 ± 1.1	-0.3	-.14	-.37
TUC	-0.1 ± .5	0.3	.25	.08
WES	0.4 ± .2	0.3	.01	.66

Table 5.2 (continued).

baseline[b]	-0.2	0.3	-.06	.25

[a] standard deviation (4 or more determinations)

[b] must be added to each entry in column to agree with published values

[c] this value is actually for station BRK

Rocky Mountain region (compare delays in the two columns at RCD, GOL, LUB, DUG, and BOZ) and perhaps the Appalachians (SCP?). The total range of δt_P values in the several previously published studies is less than for the delays obtained from the deep earthquakes; this range would be reduced in the latter compilation if data were averaged over a wider range of azimuths.

The scheme for determining the parameters $\Delta\mu$ and τ of the relaxation in the lower asthenosphere, given δt_S^*, δt_P^*, δt_S, $\delta t_P'$, and δt_P, is outlined in Appendix 4. There are 14 seismograph stations in the United States at which the required five quantities are known or can be estimated. Values of the first four of these quantities at those stations are given in Table A4.1 of Appendix 4. We have calculated $\Delta\mu$ and τ at each station using three different tabulations of δt_P: (1) those determined from deep South American earthquakes, (2) those of Carder et al. (1966), and (3) those of Herrin and Taggart (1968). (The requirement that δt_P be non-negative requires that we add a constant to every entry in each column of Table 5.2: 1.0 sec to the deep-earthquake residuals; 0.9 sec to the residuals of Carder et al., and 0.85 sec to the residuals of Herrin and Taggart. Any residuals still negative after this correction were arbitrarily set equal to zero. See Appendix 4 for a discussion of the 'baseline ambiguity'.) The relaxation parameters and s^2, a

measure of the ability of a single relaxation to fit the data (see Appendix 4), are given in Table 5.3.

Differences between values of $\Delta\mu$ and τ at a given station for different δt_P give some illustration of the dependence of the relaxation parameters on the input. In general, $\Delta\mu$ is most sensitive to δt_S (corrected), and is about equally sensitive to δt_S^* and 4 δt_P^*. [See equations (A4.12) through (A4.14), Appendix 4.] We may think of $\bar{\tau}$ as being determined by the relative magnitudes of δt_S and δt_S^* (or δt_P^*). If δt_S^* and δt_P^* are considered fixed, then decreasing the corrected value of δt_S (i.e. the delay which we attribute to a relaxation in the lower asthenosphere), say by using a larger value of δt_P, generally results in a larger τ. Thus large changes in the adopted value of δt_P at a station can profoundly affect $\Delta\mu$ and τ (see, for example, stations BOZ, DUG, GEO, LUB, and WES). Furthermore, none of the three sets of data used to determine the relaxation parameters in Table 5.3 is internally consistent. We should have used δt_S from deep South American earthquakes in trial 1; and values of δt_S^* and δt_P^* averaged over several propagation directions would have been more appropriate for trials 2 and 3. We are limited, however, by the data at hand. The values of $\Delta\mu$ and τ in Table 5.3 should therefore be considered approximate and subject to possible further change as improved attenuation and travel-time data become available.

Table 5.3 Relaxation parameters for the lower asthenosphere

Station	Trial 1 δt_p from deep earthquakes			Trial 2 δt_p from Carder et al.			Trial 3 δt_p from Herrin and Taggart		
	$\Delta\mu$	τ sec	s^2	$\Delta\mu$	τ sec	s^2	$\Delta\mu$	τ sec	s^2
AAM	.15	2.75	.0013	.15	2.75	.0013	.09	1.54	.0122
ALQ	.18	1.74	.0086	.18	1.39	.0086	.19	1.25	.0089
BKS	.08	.55	.0102	.09	.50	.0125	.07	.59	.0087
BOZ	.12	1.41	.0005	.16	.73	.0007	.21	.48	.0010
COR	.10	.95	.0000	.10	.95	.0000	.12	.67	.0000
DUG	.31	6.65	.0007	.16	1.20	.0003	.17	1.06	.0003
FLO	.02	0.	.0035	.01	0.	.0009	.02	0.	.0032
GEO	.27	4.41	.0008	.18	1.82	.0004	.21	2.91	.0005
LON	.36	4.60	.0038				.28	2.84	.0026
LUB	.14	.41	.0002	.07	1.91	.0000	.11	.55	.0000
RCD	.08	1.56	.0164	.08	1.56	.0163	.08	1.56	.0164
SCP	.07	1.56	.0080	.11	1.35	.0000	.11	1.31	.0000
TUC	.23	1.42	.0136	.22	1.70	.0137	.23	1.45	.0136
WES	.14	1.52	.0293	.45	7.66	.0000	.14	1.52	.0292

5.2.2 Lateral variation of temperature and other properties

We may regard the compilation of Table 5.3 as a map, on a rather gross scale, of the physical properties of the lower asthenosphere. In this section, values of $\Delta\mu$ and τ in Table 5.3 are interpreted to imply lateral variation of melt concentration, fluid viscosity, and temperature in a partially melted asthenosphere. Considerable speculation and simplification will be necessary; the results should be viewed as illustrative rather than definitive.

In Figure 5.5 is shown the relaxation strengths for trial 1; i.e. using δt_p as determined from deep earthquakes in South America. If our very simple notion that thickness and depth of the asthenosphere are constant, then $\Delta\mu$ is very roughly equal (using equation 2.4) to $.2c/\alpha$. If we further presume, for no justifiable reason, that α is constant, then Figure 2.3 may be regarded as a map of melt concentration in the lower asthenosphere. The line $\Delta\mu = 0.2$ corresponds to $c = \alpha$; taking $\alpha = 2 \times 10^{-2}$, for instance (see section 5.1), would imply that the melt concentration exceeds 2% in the asthenosphere beneath the Basin and Range and Columbia Plateau provinces.

The relaxation time τ is approximately proportional to the melt viscosity. Let us assume that the functional dependence of η on temperature T is of the form

Figure 5.5 Lateral variation of the strength $\Delta\mu$ of the relaxation process in the lower asthenosphere of the United States. Data used to determine $\Delta\mu$ were those of Table A4.1 and the P-wave delays determined from deep earthquakes. The dashed lines represent (approximately) the contour $\Delta\mu = .2$.

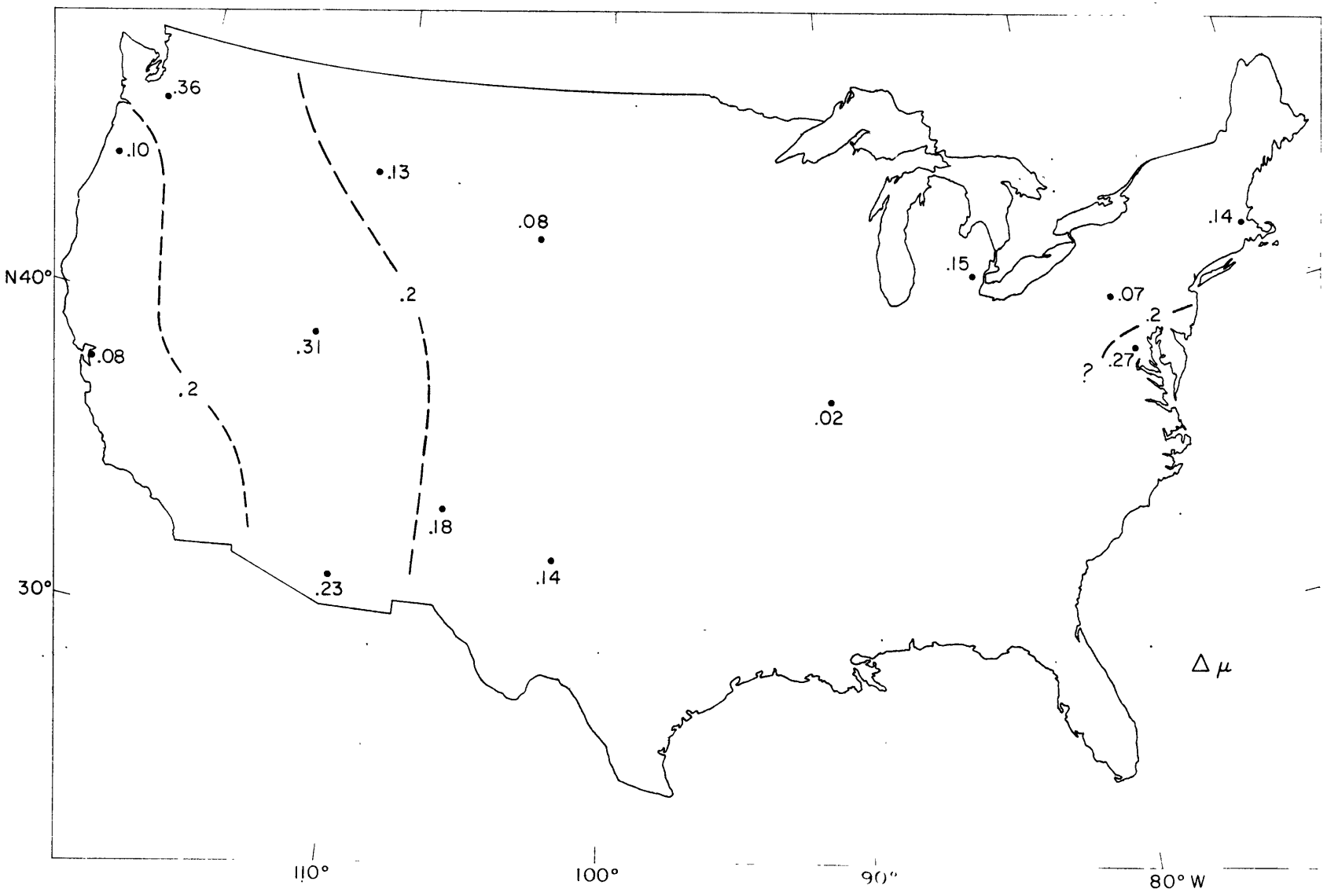
.36
.10
.13
.08
.15
.14
.07
.2
.2
.31
.08
.2
.27
?
.02
.18
.14
.23
30°
N40°
Δμ
110°
100°
90°
80° W

$$\eta(T) = \eta_o \, e^{H/RT} \qquad (5.1)$$

where η_o and H are constants. Then if we have obtained relaxation times τ_1 and τ_2 for the lower-asthenosphere relaxation beneath stations 1 and 2, the temperatures T_1 and T_2 in the asthenosphere beneath the respective stations are related by

$$\frac{1}{T_1} - \frac{1}{T_2} = \frac{R}{H} \ln \left(\frac{\tau_1}{\tau_2} \right) \qquad (5.2)$$

Use of (5.2) to obtain temperatures is restricted by several assumptions in addition to those stated in section 5.2.1: (1) The relaxations in the asthenosphere beneath stations 1 and 2 occur at the same depth (loosely, over the same depth range). This requirement is made because H is a function of pressure; in the most simple relationship, H increases linearly with pressure. (2) The aspect ratio of fluid inclusions in the lower asthenosphere is the same for stations 1 and 2. This important assumption has no justification other than simplicity. (3) Lateral differences in η (i.e. τ) are attributed only to temperature variations; such other variables as composition must remain fixed. This is a weak assumption; it is discussed more fully below. (4) To obtain the absolute values of temperature beneath all stations, the value of T beneath one station must be assumed.

A correction to (5.2) must be made when the relaxation strength $\Delta\mu$ is relatively large. This is because of the shift in the relaxation-peak frequency, relative to that predicted by equation (2.4), when c/α is of the order of 1 or greater (see section 2.3.1; also Figure 2.4). If τ_0 is the relaxation time given by (2.4) and τ is the 'relaxation' time of the self-consistent, generalized Walsh model, then an approximate rule-of-thumb for the relationship between τ and τ_0 is

$$\ln (\tau / \tau_0) = 1.4 \Delta\mu \quad ; \qquad (5.3)$$

i.e. if α and η are considered fixed, then as c is varied the relative changes in τ and $\Delta\mu$ are given roughly by (5.3). The relaxation times in Table 5.3 correspond to τ ; the proper relaxation-time to substitute in (5.2) is τ_0.

Using (5.3) and (5.2), temperatures in the lower asthenosphere were computed for the three sets of $\Delta\mu$ and τ listed in Table 5.3. These temperatures are given in Table 5.4. For each set of relaxation parameters, two activation energies were used in equation (5.2). The value of 57 kcal/mole is the activation energy (at 1 bar pressure) for grain-boundary relaxation in forsterite (Jackson, 1969b); it is also very near the value of 52 kcal/mole that Euler and Winkler (1957) obtained for the

Table 5.4. Temperature in the lower asthenosphere from relaxation parameters.

Station	Trial 1		Trial 2		Trial 3	
	T_1[a]	T_2[b]	T_1	T_2	T_1	T_2
	°K		°K		°K	
AAM	1700[c]	1700[c]	1700[c]	1700[c]	1700[c]	1700[c]
ALQ	1751	1722	1777	1732	1735	1715
BKS	1868	1768	1881	1772	1801	1742
BOZ	1767	1728	1846	1759	1847	1759
COR	1806	1744	1806	1744	1793	1738
DUG	1636	1672	1789	1737	1749	1721
GEO	1669	1687	1747	1720	1654	1680
LON	1678	1690			1665	1685
LUB	1914	1785	1727	1711	1815	1747
RCD	1748	1720	1748	1720	1697	1699
SCP	1748	1720	1769	1729	1720	1708
TUC	1781	1734	1761	1725	1726	1711
WES	1760	1725	1641	1675	1708	1703

[a] calculated assuming H = 57 kcal/mole in (5.2)

[b] calculated assuming H = 134 kcal/mole in (5.2)

[c] assumed

activation energy controlling viscosity (at 1 bar pressure) in molten basalt (natural and synthetic) of a fairly wide composition-range [atomic ratio (Si + Al)/ O = .40 to .43]. The value of 134 kcal/mole is the activation energy for viscous flow in liquid silica (Bockris et al., 1955). Both because of the increase in effective activation-energy with pressure and because the composition of the melt, if melting in the lower asthenosphere contributes to the generation of basalt, is no less silicic than basalt, we may treat the former value of activation energy as a lower bound.

Suppose we adopt literally a set of temperature values from Table 5.4. In Figure 5.6, for instance we have plotted temperatures for trial 2 (H = 57 kcal/mole). The highest values of temperature appear to be associated with the Rocky Mountain and Pacific Border regions. Particular values of temperature are uncertain, due not only to errors in $\Delta\mu$ and τ but to uncertainty in H and in the assumed temperature at the reference station (AAM in Table 5.4); however the trend of temperature differences in Figure 5.4 is reasonably accurate if all our assumptions are correct. From the discussion of the preceding paragraph, the range of temperature is probably no larger than that in Figure 5.6 (for the same travel-time and attenuation input); i.e. about 240°K. Julian (1970) noted that lateral differences in temperature, at a depth of 350 to 400 km, of this magnitude might explain observed variations in the

Figure 5.6 Lateral variation of temperature in the lower asthenosphere of the United States. Values of temperature, given in units of degrees Kelvin, are roughly appropriate to a depth of 250 km. Data used to determine T were those of Table A4.1, the P-wave delays of Carder et al. (1966), and an assumed activation energy for viscosity of 57 kcal/mole. Some very approximate contours of temperature are shown as dashed lines.

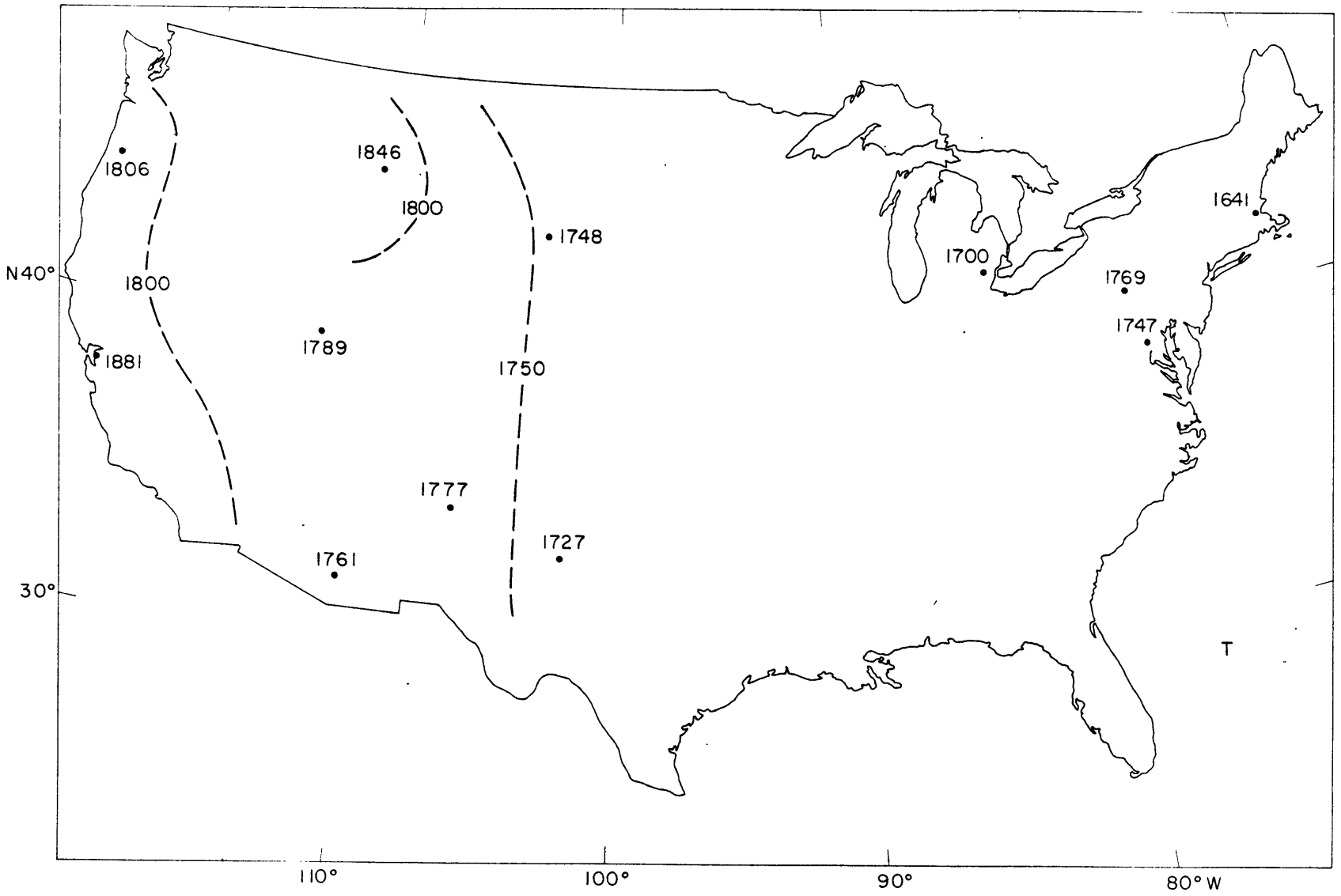
1806
1846
1800
1748
1800
1700
1641
1769
1747
1789
1881
1750
1777
1727
1761
T
N40°
30°
110°
100°
90°
80° W

depth to the '400-km discontinuity' in western North America. The spacing of values in Figure 5.6 is too large to be of much use at this stage in testing hypotheses of mantle tectonics; one might speculate, however, that the high temperatures beneath BKS and COR are related to a late-Tertiary lithosphere-subduction zone near the western coast of North America (e.g. Atwater, 1970).

Lateral variation of temperature in the mantle such as that indicated in Figure 5.6 should affect other physical properties. High temperature is generally related to high heat-flux at the surface; it is doubtful, though, whether temperature differences no larger than 100°K in the lower asthenosphere (150 to 350 km) could be resolved by surface measurements of heat-flow, which is much more sensitive to conditions in the upper crust. The temperature variations and melt concentrations given, say, in Figures 5.6 and 5.5, because of their effect on density, might be expressed in surface topography or long-wavelength gravity anomalies. If the relative density-decrease upon melting is 10 percent, then a melt concentration of 2 percent (see above) amounts to a relative density change of -.002. If such a difference were uniform within a layer 200 km thick (i.e. the lower asthenosphere), the lithosphere would be elevated (relative to a solid lower asthenosphere) by .4 km. Similarly, adopting a value of $3 \times 10^{-5}\ {}^{o}K^{-1}$ for the coefficient of (volume) thermal expansion, a temperature increase of 100°K should, by isostasy, raise the lithosphere .6 km.

Thus some of the elevation of the Rocky Mountains and adjacent plateau regions may be compensated by decreased density in the lower asthenosphere.

In principle, both $\Delta\mu$ and τ in Table 5.3 contain information on temperature. We expect that, other variables held fixed, $\Delta\mu$ increases with increasing temperature. Thus it is an apparent contradiction that some stations with low (high) temperature in Table 5.4 show high (low) $\Delta\mu$ in Table 5.3 (in the trial-1 set, for instance, see BKS, COR, LUB, GEO, LON). How may such a contradiction be explained? To some extent, errors and inconsistencies (see above) in our input-data are to blame. It is worth noting that the 'contradictions' at GEO and LUB are much less pronounced when the (presumably better-determinted) δt_p values of Carder et al. are adopted than when the delays determined from deep earthquakes, at roughly a single azimuth, are used. Observe also that the total spread in temperatures in Table 5.4 is less for trial 2 than 1 and less for trial 3 than 2; this is probably a consequence of the larger data-base used in the Herrin-Taggart study than in the other two.

It is possible that the 'discrepancies' between T (Table 5.4) and $\Delta\mu$ (Table 5.3) at many stations are real. In that case one or more of our assumptions is in error. (1) The assumption that a single relaxation can fit travel-time delays and attenuation is clearly not reasonable at

several stations listed in Table 5.3 (i.e. those for which the error s^2 is relatively large). (2) The assumption that the asthenosphere is uniform in thickness may be incorrect. In that case, while values of τ in Table 5.3 remain unchanged, the listed values of $\Delta\mu$ are actually proportional (approximately) to $h \cdot \Delta\mu$, where h is the (laterally variable) thickness of the lower asthenosphere. Thus a large (small) value of $\Delta\mu$ might mean a thick (thin) asthenosphere instead of abnormally high (low) temperatures. (3) It is highly probable that the composition of the melt varies laterally, even if the composition of the asthenosphere as a whole is uniform. In many binary and ternary liquid-silicate systems, the activation energy for viscous flow is linear with composition (mole fraction) over certain composition-ranges (Mackenzie, 1957; Bottinga and Weill, 1970). The molar composition of the melt phase in a partially molten mantle is, no doubt, a function of melt concetration (i.e. of temperature). Thus use of a single fixed activation-energy (even if the depth of the relaxation beneath all stations is the same, a dubious presumption) may lead to considerable error in the estimate of temperature. Furthermore, the role of water or other volatiles may be crucial. Suppose there is a small amount of water throughout the asthenosphere. In regions where the temperature is barely above the solidus, the melt concentration (and thus

$\Delta\mu$) is small. Because most of the water will be present in the melt phase, the concentration of water in the melt will be relatively high. This will drastically decrease the melt viscosity (see Shaw, 1963). On the other hand, where the melt concentration is large, the water will be a relatively minor phase so the viscosity of the melt will not be too different from the anhydrous value. (An argument similar to this was advanced by Ringwood, 1969, to support the hypothesis of wet melting from a stability standpoint.) Such an explanation could account for the pattern of $\Delta\mu$ and η (i.e. τ) in western United States (see Table 5.3): At COR and BKS, $\Delta\mu$ is relatively low while the apparent temperature (Table 5.4) is quite high (relative to stations in the Basin and Range province, say). It might be that the high 'temperatures' (as interpreted from low viscosities) are due to the presence of water, perhaps in abnormally large amounts (due to subduction of water-saturated sediments at an adjacent trench?).

We have seen how the functional relationships among travel-time delays and differential attenuation may be used to estimate properties of a partially melted mantle. In order of decreasing reliability, these properties are the relaxation time τ , the relaxation strength $\Delta\mu$, and

the temperature T in the lower asthenosphere. With the usual ambiguity, $\Delta\mu$ and τ may be further used to estimate the concentration, viscosity, and geometrical arrangement of the melt phase. These physical properties, however, can be determined to an accuracy no better than that of the data used as input. Thus the large uncertainties presently associated with attenuation and delay determinations and the unknown dependence on temperature of fluid viscosity in partially melted mantle-rocks greatly limit the quantitative application of many of the ideas discussed above.

Chapter 6. Concluding Remarks

Models of the spatial dependence of seismic attenuation within the earth have become more sophisticated and more complicated as further data is acquired. Such a phenomenon is not new to geophysics; on most scales of investigation the earth is a complex body. Heterogeneity however, is one of the earth's most interesting characteristics; a thoroughly uniform planet would quickly prove to be quite dull. The anelastic properties of the upper mantle, in particular, because they are so strongly controlled by temperature, fluid content, and microstructure, can be inverted to deduce the mantle's physical state.

Several different techniques to elucidate the lateral and vertical variations of Q^{-1} in the earth have been introduced and discussed in this work and applied, specifically, to North America. One such technique is the measurement of differential attenuation δt^* from the spectral ratios of long-period body waves generated by deep-focus earthquakes. Horizontal variations in δt^* can resolve, in principle, lateral changes in the vertically averaged Q^{-1} of the mantle over distances as short as a wavelength, or several tens of kilometers. Thus generating a 'map' of δt^* for a particular region can aid in determining that region's mantle-properties; the only requirement for use of this procedure is that the area have

a reasonably dense network of seismograph stations. If one could deploy his own network of seismometers, one might better understand the physics of the transition between tectonic provinces by measuring δt^* at closely-spaced intervals across the boundary between regions of high and low differential attenuation (e.g. between the Southern Rockies and the Great Plains, or perhaps between the Basin and Range province and the Sierra Nevada or Colorado Plateau provinces) or perpendicular to the strike of a zone of active rifting (e.g. the Imperial Valley-Salton trough region, or, when ocean-bottom seismometers become more readily usable, a mid-ocean ridge such as in the Gulf of California, say).

Measurement of δt^* need not be restricted to waves from deep earthquakes. Once 'station corrections' to δt^* have been determined using P and S waves from deep events, then the effect on δt^*, measured using waves from shallow earthquakes, of heterogeneous Q^{-1} near the earthquake source can be recovered. From our observations of δt_S^* from an event on the Arctic mid-ocean ridge, such an effect may be quite large. Both island arcs and oceanic ridges are excellent candidates for study using such a scheme.

Another technique employed in this work to investigate the dissipative characteristics of the North American mantle was the measurement of Love- and Rayleigh-wave attenuation over short (less than 2000 km), relatively

homogeneous paths. Surface-wave attenuation at periods longer than 40 or 50 sec is invaluable for estimating the vertical dependence of Q^{-1} in the upper mantle of a region. At shorter periods, largely because the anelastic losses of surface waves are small, the technique is limited by the effects of scattering and interference.

Seismic-wave attenuation in the mantle of North America shows a strong regional dependence. There is a broad zone of high δt^* between the Rocky Mountains and the Sierra Nevada-Cascade ranges; a smaller area of high apparent attenuation is in northeast United States. Regional patterns of δt_S^* and δt_P^* are consistent, and the relative magnitudes of P- and S-wave attenuation suggest all of the P-wave dissipation is due to losses in shear. That the high δt^* in western United States is due to low Q in the upper mantle is confirmed by the attenuation of surface waves. Models for Q_β^{-1} in western North America involve a high-Q ($Q_\beta \simeq 1000$) lithosphere some 60 to 90 km thick and an asthenosphere with $Q_\beta \simeq 20$ to 30 in the frequency range of surface waves. In east-central United States, on the other hand, the lithosphere (as seen by surface waves) is perhaps 100 to 120 km thick and Q_β (at surface-wave frequencies) in the asthenosphere is probably not less than 60 or 70.

The attenuation of seismic waves beneath western North America appears to have several further interesting

characteristics. Limited evidence from comparison of Q_L^{-1} and Q_R^{-1} and of δt^*_{SV} and δt^*_{SH} gives some suggestion that Q^{-1} in the asthenosphere of the Basin and Range and Columbia Plateau provinces may be anisotropic. SH waves propagating in the NW-SE direction are apparently attenuated more than SV waves. Similarly, the ratio Q_L^{-1}/Q_R^{-1} in the frequency range .02 to .03 Hz is too high to be explained by any isotropic Q_β^{-1} model. It is of course risky to deduce anisotropy from measurements in only one direction of propagation. Still, if the attenuation in the mantle is attributed to ellipsoidal (oblate spheroidal) pockets of magma (see below) preferentially oriented by non-hydrostatic stress, we would deduce that the minor axes of these ellipsoids are horizontal and point NE-SW. Such a minor axis should be perpendicular to the direction of compressional deviatoric stress; this direction, if presumed to be horizontal, would therefore parallel (roughly) the present direction of sea-floor spreading in the Gulf of California and on the Gorda and Juan de Fuca ridges. Thus an anisotropy of attenuation, if confirmed by further measurements along <u>different</u> directions from that employed in this study, would provide a test of hypotheses of mantle tectonic-patterns that involve western North America (e.g. Atwater, 1970).

Q^{-1} in the mantle of western United States, further, is frequency dependent. In particular, the difference in

body-wave attenuation between the Basin and Range and adjacent provinces appears to be less at frequencies near 1 Hz than at frequencies a decade lower. That Q^{-1} is a function of frequency should not be surprising. A large body of geophysical evidence supports the hypothesis that the asthenosphere of at least the western part of North America is partially molten; both theoretical and laboratory models of partially melted rock predict that attenuation and shear modulus in a partially molten asthenosphere are strongly frequency-dependent over at least some portion of the frequency-range of seismic waves.

We presume that the fluid phase in partially melted rock is concentrated at grain boundaries. Though several distinct mechanisms of attenuation are operative in a partial melt, the dissipation of elastic-wave energy at seismic frequencies is probably controlled by viscous losses within the fluid inclusions. Generalizing a mechanical model proposed by Walsh for partially melted rock, it has been shown that for 'effective' concentrations $c(\alpha)/\alpha$, where $c(\alpha)$ is the volume concentration of inclusions of aspect ratio α, less than about unity the attenuation and shear modulus in the (partially molten) asthenosphere are adequately described by a superposition of one or more relaxation processes. The parameters of the relaxations are controlled by the viscosity, concentration, and geometrical arrangement of the melt.

Based upon the above theoretical considerations, a relaxation model for $Q^{-1}(z,f)$ in western United States was constructed. In the model, a lithosphere about 60 km thick overlies an asthenosphere that may be as thick as 300 km and must be vertically inhomogeneous. The model was designed to fit measured surface-wave attenuation, an estimate of the total attenuation of vertically incident shear-waves from δt_S^* values, and the approximate dimensions and velocity decrease of the 'low-velocity' zone determined from travel-times of short-period P waves. In addition, the model is consistent with published 'tectonic' models of the shear-velocity structure obtained from long-period surface waves and with attenuation models for short-period P waves. In all, the model satisfies a wide range of data spanning roughly a factor of 1000 in frequency.

There are many ways this model may be further tested. The foremost test will be the measurement of attenuation, preferably at frequencies and strain amplitudes appropriate to seismic waves, in partially melted rocks, particularly the ultrabasic rocks thought to comprise the upper mantle. A great number of the statements made above depend upon our particular phenomenological model for the mechanical behavior of a partial melt. If this model is incorrect, many of our interpretations will require alteration.

The relaxation model for Q^{-1} may also be tested by

seismic means. Of particular help would be a network of reliable, broad-band seismometers such as are currently being developed. The synthesis of body waves, over a wide frequency band and over the approximate distance-range 10 to 30 degrees, might prove to unravel simultaneously some of the elastic and anelastic properties of the upper mantle. The proposed model of Q^{-1} in western United States could be used as a starting point for such a study. The relaxation model may be tested and improved at lower frequencies by the suggestion of Liu and Archambeau (1970) that the periods of the earth's free oscillations might be measurably shifted in a region with upper-mantle Q^{-1} as high as in the Basin and Range province.

Because δt^* is a function of position, the parameters of the relaxations in the asthenosphere must also change laterally. Variations in the strength of a relaxation may be interpreted (with ambiguity) to give the regional dependence of the concentration of melt. Differences in the peak frequency of a relaxation may be interpreted, with several additional assumptions, to yield the lateral variation of temperature. The unknown dependence of the relaxation time on such other variables as major-element composition and concentration of volatiles makes absolute values of temperature subject to considerable uncertainty. It may nonetheless be concluded that temperature differences in the lower asthenosphere (at a depth near 250 km, say)

need be no larger than 100 to 200°K, with the highest temperatures beneath the Rocky Mountain and Pacific Border regions, to explain differences in the relaxation time obtained from travel-time delays and differential attenuation.

References

Aki, K., Seismological evidences for the existence of soft thin layers in the upper mantle under Japan, J. Geophys. Res., 73, 585-594, 1968.

Aki, K., and K. Kaminuma, Phase velocity of Love waves in Japan, 1, Love waves from the Aleutian shock of March 9, 1957, Bull. Earthquake Res. Inst. Univ. Tokyo, 41, 243-259, 1963.

Aki, K., and K.L. Larner, Interpretation of spectral amplitude distribution and phase-delay anomaly of P waves observed at LASA (abstract), Eos, Trans. Amer. Geophys. Union, 50, 244,.1969.

Aki, K., and K.L. Larner, Surface motion of a layered medium having an irregular interface due to incident plane SH waves, J. Geophys. Res., 75, 933-954, 1970.

Alexander, S.S., Surface wave propagation in the western United States, Ph.D. thesis, California Institute of Technology, Pasadena, 242 pp., 1963.

Anderson, D.L., Latest information from seismic observations, in The Earth's Mantle, ed. by T.F. Gaskell, Academic Press, New York, 355-420, 1967.

Anderson, D.L., and C.B. Archambeau, The anelasticity of the earth, J. Geophys. Res., 69, 2071-2084, 1964.

Anderson, D.L., A. Ben-Menahem, and C.B. Archambeau, Attenuation of seismic energy in the upper mantle, J. Geophys. Res., 70, 1441-1448, 1965.

Anderson, D.L., and B.R. Julian, Shear velocities and elastic parameters of the mantle, J. Geophys. Res.,

74, 3281-3286, 1969.

Anderson,D.L., and C. Sammis, Partial melting in the upper mantle, Phys. Earth. Planet. Interiors, 3, 41-50, 1970.

Anderson, D.L., and H. Spetzler, Partial melting and the low-velocity zone, Phys. Earth. Planet. Interiors, 4, 62-64, 1970.

Archambeau, C.B., E.A. Flinn, and D.G. Lambert, Fine structure of the upper mantle, J. Geophys. Res., 74, 5825-5865, 1969.

Asada, T., and K. Takano, Attenuation of short period P waves in the mantle, J. Phys. Earth, 11, 25-34, 1963.

Attewell, P.B., and Y.V. Ramana, Wave attenuation and internal friction as functions of frequency in rocks, Geophysics, 31, 1049-1056, 1966.

Atwater, T., Implications of plate tectonics for Cenozoic tectonic evolution of western North America, Geol. Soc. Am. Bull., 81, 3513-3536, 1970.

Backus, G., and F. Gilbert, The resolving power of gross earth data, Geophys. J. Roy. Astron. Soc., 16, 169-205, 1968.

Backus, G., and F. Gilbert, Uniqueness in the inversion of inaccurate gross earth data, Phil. Trans. Roy. Soc. London, Ser A., 266, 123-192, 1970.

Barazangi, M., and B. Isacks, Lateral variations of seismic wave attenuation in the upper mantle above the inclined earthquake zone of the Tonga island arc (abstract), Eos, Trans. Amer. Geophys. Union, 51, 780, 1970.

Basham, P.W., Canadian magnitudes of earthquakes and nuclear explosions in south-western North America, Geophys. J. Roy. Astron. Soc., 17, 1-13, 1969.

Båth, M., and A. López-Arroyo, Attenuation and dispersion of G waves, J. Geophys. Res., 67, 1933-1942, 1962.

Ben-Menahem, A., S.W. Smith, and T.L. Teng, A procedure for source studies from spectrums of long-period seismic body waves, Bull. Seism. Soc. Am., 55, 203-235, 1965.

Berckhemer, H., and K.H. Jacob, Investigation of the dynamical process in earthquake foci by analyzing the pulse shape of body waves, Ber. Inst. Meteor. Geophys., Univ. Frankfurt/Main, 13, 85 pp., 1968.

Berg, J.W., Jr., L. Trembly, D.A. Emilia, J.R. Hutt, J.M. King, L.T. Long, W.R. McKnight, S.K. Sarmah, R. Souders, J.V. Thiruvathukal, and D.A. Yossler, Crustal refraction profile, Oregon coast range, Bull. Seism. Soc. Am., 56, 1357-1362, 1966.

Biot, M.A., Theory of propagation of elastic waves in a fluid-saturated porous solid, 1, Low-frequency range, J. Acoust. Soc. Am., 28, 168-178, 1956a.

Biot, M.A., Theory of propagation of elastic waves in a fluid-saturated porous solid, 2, Higher frequency range, J. Acoust. Soc. Am., 28, 179-191, 1956b.

Birch, F., Elasticity of igneous rocks at high temperatures and pressures, Bull. Geol. Soc. Am., 54, 263-286, 1943.

Birch, F., The velocity of compressional waves in rocks to 10 kilobars, part 1, J. Geophys. Res., 65, 1083-1102, 1960.

Birch, F., Compressibility; elastic constants, in Handbook of Physical Constants, ed. by S.P. Clark, Jr., Geol. Soc. Am. Memoir 97, pp. 97-173, 1966.

Birch, F., Interpretations of the low-velocity zone, Phys. Earth Planet. Interiors, 3, 178-181, 1970.

Blackwell, D.D., Heat-flow determinations in the northwestern United States, J. Geophys. Res., 74, 992-1007, 1969.

Bockris, J.O'M., J.D. Mackenzie, and J.A. Kitchener, Viscous flow in silica and binary liquid silicates, Trans. Faraday Soc., 51, 1734-1748, 1955.

Boore, D.M., Love waves in nonuniform wave guides: finite difference calculations, J. Geophys. Res., 75, 1512-1527, 1970.

Bottinga, Y., and D.F. Weill, Viscosity of anhydrous silicate melts (abstract), Eos, Trans. Amer. Geophys. Union, 51, 439, 1970.

Brace, W.F., J.B. Walsh, and W.T. Frangos, Permeability of granite under high pressure, J. Geophys. Res., 73, 2225-2236, 1968.

Caner, B., W.H. Cannon, and C.E. Livingstone, Geomagnetic depth sounding and upper mantle structure in the Cordillera region of western North America, J. Geophys. Res., 72, 6335-6351, 1967.

Carder, D.S., D.W. Gordon, and J.N. Jordan, Analysis of surface focus travel times, Bull. Seism. Soc. Am., 56, 815-840, 1966.

Chander, R., L.E. Alsop, and J. Oliver, On the synthesis of shear-coupled PL waves, Bull. Seism. Soc. Am.,

58, 1849-1877, 1968.

Chandra, U., Analysis of body-wave spectra for earthquake energy determination, Bull. Seism. Soc. Am., 60, 539-563, 1970a.

Chandra, U., The peru-Bolivia border earthquake of August 15, 1963, Bull. Seism. Soc. Am., 60, 639-646, 1970b.

Chang, A.C., Love waves and the crust-upper mantle structure of the southwestern United States, Ph.D. thesis, Rice University, Houston, Texas, 85 pp., 1968.

Chinnery, M.A., and M.N. Toksöz, P-wave velocities in the mantle below 700 km, Bull. Seism. Soc. Am., 57, 199-226, 1967.

Clark, S.P., Jr., Viscosity, in Handbook of Physical Constants, ed. by S.P. Clark, Jr., Geol. Soc. Am. Memoir 97, p. 299, 1966.

Cleary, J., Analysis of the amplitudes of short-period P waves recorded by Long Range Seismic Measurements stations in the distance range 30° to 102°, J. Geophys. Res., 72, 4705-4712, 1967.

Cleary, J., and A.L. Hales, An analysis of the travel times of P waves to North American stations, in the distance range 32° to 100°, Bull. Seism. Soc. Am., 56, 467-489, 1966.

Clowes, R.M. and E.R. Kanasewich, Seismic attenuation and the nature of reflecting horizons within the crust, J. Geophys. Res., 75, 6693-6705, 1970.

Combs, J.B., Terrestrial heat flow in north central United States, Ph.D. thesis, Massachusetts Institute of

Technology, Cambridge, 317 pp., 1970.

Davies, D., and D.P. McKenzie, Seismic travel-time residuals and plates, Geophys. J. Roy. Astron. Soc., 18, 51-63, 1969.

Dehlinger, P., E.F. Chiburis, and M.M. Collver, Local travel-time curves and their geologic implications for the Pacific northwest states, Bull. Seism. Soc. Am., 55, 587-607, 1965.

Demenitskaya, R.M., and A.M. Karasik, Magnetic data confirm that the Nansen-Amundsen basin is of normal oceanic type, in Continental Margins and Island Arcs, ed. by W.H. Poole, Geological Survey of Canada Paper 66-15, Department of Mines and Technical Surveys, 191-196, 1966.

Dorman, L.M., Anelasticity and the spectra of body waves, J. Geophys. Res., 73, 3877-3883, 1968.

Doyle, H.A., and A.L. Hales, An analysis of the travel times of S waves to North American stations, in the distance range 28° to 82°, Bull. Seism. Soc. Am., 57, 761-771, 1967.

Duda, S.J., The earthquake volume, Bull. Seism. Soc. Am., 60, 1479-1489, 1970.

Eshelby, J.D., The determination of the elastic field of an ellipsoidal inclusion, and related problems, Proc. Roy. Soc., Ser. A, 241, 376-396, 1957.

Euler, R., and H.G.F. Winkler, On the viscosities of rock- and silicate-melts (in German), Glastech. Ber., 30,

325-332, 1957.

Ewing, M., and F. Press, Determination of crustal structure from phase velocity of Rayleigh waves, Part III: the United States, Bull. Geol. Soc. Am., 70, 229-244, 1959.

Fairborn, J.W., Shear wave velocities in the lower mantle, Bull. Seism. Soc. Am., 59, 1983-1999, 1969.

Fedotov, S.A., The absorption of transverse seismic waves in the upper mantle and energy classification of near earthquakes of intermediate focal depth, Bull. Acad. Sci. USSR, Geophys. Ser.,English Transl., no. 6, 509-520, 1963.

Fedotov, S.A., and S.A. Boldyrev, Frequency dependence of the body-wave absorption in the crust and upper mantle of the Kuril-Island chain, Bull. Acad. Sci. USSR, Geophys. Ser., English. Transl., no. 9, 553-562, 1969.

Fenneman, N.M., Physiography of Western United States, McGraw-Hill, New York, 534 pp., 1931.

Fenneman, N.M., Physiography of Eastern United States, McGraw-Hill, New York, 714 pp., 1938.

Frantti, G.E., Attenuation of P_n waves from offshore Maine explosions, Bull. Seism. Soc. Am., 55, 417-423, 1965.

Goetze, C., High temperature elasticity and anelasticity of polycrystalline salts, Ph.D. thesis, Harvard University, Cambridge, Massachusetts, 90 pp., 1969.

Gordon, R.B., and L.A. Davis, Velocity and attenuation of seismic waves in imperfectly elastic rock, J. Geophys. Res., 73, 3917-3935, 1968.

Gordon, R.B., and C.W. Nelson, Anelastic properties of the earth, Rev. Geophys., 4, 457-474, 1966.

Gorshkov, G.S., On some theoretical problems of volcanology, Bull. Volcanol., 19, 103-113, 1958.

Green, R.W.E., and A.L. Hales, The travel times of P waves to 30° in the central United States and upper mantle structure, Bull. Seism. Soc. Am., 58, 267-289, 1968.

Greenfield, R.J., and R.M. Sheppard, The Moho depth variations under the LASA and their effect on $dT/d\Delta$ measurements, Bull. Seism. Soc. Am., 59, 409-420, 1969.

Gutenberg, B., Variations in physical properties within the earth's crustal layers, Am. J. Science, Daly volume, 243-A, 285-312, 1945a.

Gutenberg, B., Amplitudes of surface waves and magnitudes of shallow earthquakes, Bull. Seism. Soc. Am., 35, 3-12, 1945b.

Gutenberg, B., Amplitudes of P, PP, and S and magnitude of shallow earthquakes, Bull. Seism. Soc. Am., 35, 57-69, 1945c.

Gutenberg, B., Attenuation of seismic waves in the earth's mantle, Bull. Seism. Soc. Am., 48, 269-282, 1958.

Guyton, J.W., Systematic deviations of magnitude from body waves at seismograph stations in the United States, in Proceedings of the VESIAC Conference on Seismic Event Magnitude Determination, VESIAC Rept. 4410-71-X, 111-126, 1964.

Hagiwara, T., A note on the theory of the electromagnetic seismograph, Bull. Earthquake Res. Inst., Tokyo Univ., 36, 139-164, 1958.

Hales, A.L., J.R. Cleary, H.A. Doyle, R. Green, and J. Roberts, P-wave station anomalies and the structure of the upper mantle, J. Geophys. Res., 73, 3885-3896, 1968.

Hales, A.L., and H.A. Doyle, P and S travel time anomalies and their interpretation, Geophys. J. Roy. Astron. Soc., 13, 403-415, 1967.

Hales, A.L., and J.L. Roberts, The travel times of S and SKS, Bull. Seism. Soc. Am., 60, 461-489, 1970.

Harkrider, D.G., Surface waves in multilayered elastic media, 1, Rayleigh and Love waves from buried sources in a multilayered elastic half-space, Bull. Seism. Soc. Am., 54, 627-679, 1964.

Haskell, N.A., Crustal reflection of plane P and SV waves, J. Geophys. Res., 67, 4751-4767, 1962.

Healy, J.H., and D.H. Warren, Explosion studies in North America, in The Earth's Crust and Upper Mantle, ed. by P.J. Hart, Amer. Geophys. Un. Geophys. Mon. 13, Washington, D.C., 208-220, 1969.

Herrin, E., Regional variations of P-wave velocity in the

upper mantle beneath North America, in The Earth's Crust and Upper Mantle, ed. by P.J. Hart, Amer. Geophys. Un. Geophys. Mon. 13, Washington, D.C. 242-246, 1969.

Herrin E., and J. Taggart, Regional variations in P travel times, Bull. Seism. Soc. Am., 58, 1325-1337, 1968.

Hershey, A.V., The elasticity of an isotropic aggregate of anisotropic cubic crystals, J. Appl. Mech. 21, 236-240, 1954.

Hirasawa, T., and K. Takano, Differential attenuation of P waves as derived from a Hindu-Hush earthquake, J. Phys. Earth, 14, 49-57, 1966.

Ibrahim, A.K. and O.W. Nuttli, Travel-time curves and upper-mantle structure from long period S waves, Bull. Seism. Soc. Am., 57, 1063-1092, 1967.

Ichikawa, M., and P.W. Basham, Variations in short-period records from Canadian seismograph stations, Can. J. Earth. Sci., 2, 510-542, 1965.

Isacks, B., Focal mechanisms of earthquakes in western South America (abstract), Eos, Trans. Amer. Geophys. Union, 51, 355, 1970.

Isacks, B., J. Oliver, and L.R. Sykes, Seismology and the new global tectonics, J. Geophys. Res., 73, 5855-5899,

1968.

Jackson, D.D., Elastic relaxation model for seismic wave attenuation in the earth, Phys. Earth Planet. Interiors, 2, 30-34, 1969a.

Jackson, D.D., Grain-boundary relaxations and the attenuation of seismic waves, Ph.D. thesis, Massachusetts Institute of Technology, Cambridge, 136 pp., 1969b.

Jackson, D.D., and D.L. Anderson, Physical mechanisms of seismic-wave attenuation, Rev. Geophys., 8, 1-63, 1970.

James, D.E., T.J. Smith, and J.S. Steinhart, Crustal structure of the middle Atlantic states, J. Geophys. Res., 73, 1983-2007, 1968.

Johnson, L.R., Array measurements of P velocities in the upper mantle, J. Geophys. Res., 72, 6309-6325, 1967.

Johnson, L.R., Array measurements of P velocities in the lower mantle, Bull. Seism. Soc. Am., 59, 973-1008, 1969.

Johnson, S.H., and R.W. Couch, Crustal structure in the north Cascade Mountains of Washington and British Columbia from seismic refraction measurements, Bull. Seism. Soc. Am., 60, 1259-1269, 1970.

Julian, B.R., Regional variations in upper mantle structure beneath North America, Ph.D. thesis, California Institute of Technology, Pasadena, 208 pp., 1970.

Julian, B.R., and D.L. Anderson, Travel times, apparent velocities and amplitudes of body waves, Bull. Seism.

Soc. Am., 58, 339-366, 1968.

Kaminuma, K., and T. Hirasawa, The phase velocity of Love waves from an Iranian earthquake, (in Japanese), Zisin, Ser. 2, 17, 139-147, 1964.

Kanamori, H., Spectrum of P and PcP in relation to the mantle-core boundary and attenuation in the mantle, J. Geophys. Res., 72, 559-571, 1967a.

Kanamori, H., Spectrum of short-period core phases in relation to the attenuation in the mantle, J. Geophys. Res., 72, 2181-2186, 1967b.

Kanamori, H., Attenuation of P waves in the upper and lower mantle, Bull. Earthq. Res. Inst., Tokyo Univ., 45, 299-312, 1967c.

Kanamori, H., Velocity and Q of mantle waves, Phys. Earth Planet. Interiors, 2, 259-275, 1970a.

Kanamori, H., Mantle beneath the Japanese arc, Phys. Earth Planet. Interiors, 3, 475-483, 1970b.

Katsumata, M., The effect of seismic zones upon the transmission of seismic waves (in Japanese), Kenshin Ziho, 25, 89-95, 1960.

Kê, T.S., Experimental evidence of the viscous behavior of grain boundaries in metals, Phys. Rev., 71, 533-546, 1947.

Kê, T.S., Viscous slip along grain boundaries and diffusion of zinc in alpha-brass, J. Appl. Phys., 19, 285-290, 1948.

Kell, G.S., Volume properties of ordinary water, in Handbook of Chemistry and Physics, 51st ed., 1970-1971, ed. by R.C. Weast, Chemical Rubber Co., Cleveland, Ohio, p. F5, 1970.

Khattri, K.N., Focal mechanism of the Brazil deep focus earthquake of November 3, 1965, from the amplitude spectra of isolated P waves, Bull. Seism. Soc. Am., 59, 691-704, 1969.

Knopoff, L., Q, Rev. Geophys., 2, 625-660, 1964.

Kovach, R.L., and D.L. Anderson, Attenuation of shear waves in the upper and lower mantle, Bull. Seism. Soc. Am., 54, 1855-1864, 1964.

Kovach, R.L., and R. Robinson, Upper mantle structure in the Basin and Range province, western North America, from the apparent velocities of S waves, Bull. Seism. Soc. Am., 59, 1653-1665, 1969.

Krŏner, E., Calculation of elastic constants of polycrystals from the constants of single crystals (in German), Z. Phys., 151, 504-518, 1958.

Krŏner, E., Elastic moduli of perfectly disordered composite materials, J. Mech. Phys. Solids, 15, 319-329, 1967.

Kumazawa, M., and O.L. Anderson, Elastic moduli, pressure derivatives, and temperature derivatives of single-crystal olivine and single-crystal forsterite, J. Geophys. Res., 74, 5961-5972, 1969.

Kurita, T., Attenuation of short-period P-waves and Q in

the mantle, J. Phys. Earth, 16, 61-78, 1968.

Kushiro, I., Y. Syono, and S. Akimoto, Melting of a peridotite nodule at high pressures and high water pressures, J. Geophys. Res., 73, 6023-6029, 1968.

Lambert, I.B., and P.J. Wylie, Stability of hornblende and a model for the low velocity zone, Nature, 219, 1240-1241, 1968.

Lambert, I.B., and P.J. Wylie, Low-velocity zone of the earth's mantle: incipient melting caused by water, Science, 169, 764-766, 1970.

Larner, K.L., Near-receiver scattering of teleseismic body waves in layered crust-mantle models having irregular interfaces, Ph.D. thesis, Massachusetts Institute of Technology, Cambridge, 274 pp., 1970.

Levenberg, K., A method for the solution of certain non-linear problems in least squares, Quart. Appl. Math., 2, 164-168, 1944.

Liu, H.P., and C.B. Archambeau, The effect of anelasticity on the periods of the earth's free oscillations, paper delivered at the National Fall Meeting of the American Geophysical Union, San Francisco, California, December 10, 1970.

Lliboutry, L., Sea-floor spreading, continental drift and lithosphere sinking with an asthenosphere at melting point, J. Geophys. Res., 74, 6525-6540, 1969.

Long, L.T., and J.W. Berg, Jr., Transmission and attenuation of the primary seismic wave, 100 to 600 km, Bull.

Seism. Soc. Am., 59, 131-146, 1969.

Lybimova, Ye.A., Heat flow and the dynamics of the earth's interior, Bull. Acad. Sci. USSR, Phys. Solid Earth, English Trans., no. 5, 273-280, 1970.

Mackenzie, J.D., The discrete ion theory and viscous flow in liquid silicates, Trans. Faraday Soc., 53, 1488-1493, 1957.

Marquardt, D.W., An algorithm for least-squares estimation of nonlinear parameters, J. Soc. Indust. Appl. Math., 11, 431-441, 1963.

McEvilly, T.V., Central U.S. crust-upper mantle structure from Love and Rayleigh wave phase velocity inversion, Bull. Seism. Soc. Am., 54, 1997-2015, 1964.

McGinley, J.R., Jr., and D.L. Anderson, Relative amplitudes of P and S waves as a mantle reconnaissance tool, Bull. Seism. Soc. Am., 59, 1189-1200, 1969.

Mikumo, T., and T. Kurita, Q distribution for long-period P waves in the mantle, J. Phys. Earth, 16, 11-29, 1968.

Mitronovas, W., B. Isacks, and L. Seeber, Earthquake locations and seismic wave propagation in the upper 250 km of the Tonga island arc, Bull. Seism. Soc. Am., 59, 1115-1135, 1969.

Molnar, P., and J. Oliver, Lateral variations of attenuation in the upper mantle and discontinuities in the lithosphere, J. Geophys. Res., 74, 2648-2682, 1969.

Mooney, H.M., Upper mantle inhomogeneity beneath New Zealand: seismic evidence, J. Geophys. Res., 75,

285-309, 1970.

Murase, T., and T. Suzuki, Ultrasonic velocity of longitudinal waves in molten rocks, J. Fac. Sci., Hokkaido Univ., Ser. 7, 2, 273-285, 1966.

Nagamune, T., Y. Yokoyama, and M. Suga, Attenuation of short period P waves observed at relatively short epicentral distances, inferred from unified magnitude determinations, Geophys. Mag., 33, 257-269, 1967.

National Earthquake Information Center, Seismicity of the Arctic region, map NEIC 3020, 1970.

Nemethy, G., and H.A. Scheraga, Structure of water and hydrophobic bonding in proteins, 1, A model for the thermodynamic properties of liquid water, J. Chem. Phys., 36, 3382-3400, 1962.

Nur, A., Viscous phase in rocks and the low-velocity zone, J. Geophys. Res., 76, in press, 1971.

Nur, A., and G. Simmons, The effect of viscosity of a fluid phase on velocity in low porosity rocks, Earth Planet. Sci. Letters, 7, 99-108, 1969.

Nuttli, O.W., and B.A. Bolt, P-wave residuals as a function of azimuth, 2, Undulations of the mantle low-velocity layer as an explanation, J. Geophys. Res., 74, 6594-6602, 1969.

Oliver, J., On the long-period character of shear waves, Bull. Seism. Soc. Am., 51, 1-12,1961.

Oliver, J., and B. Isacks, Deep earthquake zones, anomalous structures in the upper mantle, and the lithosphere, J. Geophys. Res., 72, 4259-4275, 1967.

Pakiser, L.C., and I. Zietz, Transcontinental crustal and upper-mantle structure, Rev. Geophys., 3, 505-520, 1965.

Piccirelli, R., and T.A. Litovitz, Ultrasonic shear and compressional relaxation in liquid glycerol, J. Acous. Soc. Am., 29, 1009-1020, 1957.

Press, F., Some implications on mantle and crustal structure from G waves and Love waves, J. Geophys. Res., 64, 565-568, 1959.

Press, F., Seismic wave attenuation in the crust, J. Geophys. Res., 69, 4417-4418, 1964.

Reitzel, J.S., D.I. Gough, H. Porath, and C.W. Anderson III, Geomagnetic deep sounding and upper mantle structure in the western United States, Geophys. J. Roy. Astron. Soc., 19, 213-235, 1970.

Ringwood, A.E., Composition and evolution of the upper mantle, in The Earth's Crust and Upper Mantle, ed. by P.J. Hart, Amer. Geophys. Un., Geophys. Mon. 13, 1-17, 1969.

Roller, J.C., and W.H. Jackson, Seismic wave propagation in the upper mantle: Lake Superior, Wisconsin, to central Arizona, J. Geophys. Res., 71, 5933-5941, 1966.

Romney, C., B.G. Brooks, R.H. Mansfield, D.S. Carder, J.N. Jordan, and D.W. Gordon, Travel times and amplitudes of principal body phases recorded from GNOME,

Bull. Seism. Soc. Am., 52, 1057-1074, 1962.

Roy, R.F., D.D. Blackwell, E.R. Decker, Continental heat flow, paper presented at The Nature of the Solid Earth, a symposium in honor of Professor Francis Birch, Cambridge, Massachusetts, April, 1970.

Roy, R.F., E.R. Decker, D.D. Blackwell, and F. Birch, Heat flow in the United States, J. Geophys. Res., 73, 5207-5221, 1968.

Sacks, I.S., Distribution of absorption of shear waves in South America and its tectonic significance, Carnegie Institution Yearbook, 67, 339-344, 1969.

Sato, R., and A.F. Espinosa, Dissipation in the earth's mantle and rigidity and viscosity in the earth's core determined from waves multiply reflected from the mantle-core boundary, Bull. Seism. Soc. Am., 57, 829-856, 1967.

Satô, Y., Attenuation, dispersion, and the wave guide of the G waves, Bull. Seism. Soc. Am., 48, 231-251, 1958.

Shaw, H.R., Obsidian-H_2O viscosities at 1000 and 2000 bars in the temperature range 700° to 900°C, J. Geophys. Res., 68, 6337-6343, 1963.

Shimozuru, D., On the possibility of the existence of the molten portion in the upper mantle of the earth, J. Phys. Earth, 11, 49-55, 1963a.

Shimozuru, D., Geophysical evidences for suggesting the existence of molten pockets in the earth's upper mantle, Bull. Volcanol., 26, 181-194, 1963b.

Simmons, G., and R.F. Roy, Heat flow in North America, in The Earth's Crust and Upper Mantle, ed. by P.J. Hart, Amer. Geophys. Un., Geophys. Mon. 13, Washington, D.C., 78-81, 1969.

Skinner, B.J., Thermal expansion, in Handbook of Physical Constants, ed. by S.P. Clark, Jr., Geol. Soc. Am. Memoir 97, p. 94, 1966.

Smith, C.S., Grains, phases, and interfaces: an interpretation of microstructure, Trans. A.I.M.E., 175, 15-51, 1948.

Solomon, S.C., and M.N. Toksöz, Lateral variation of attenuation of P and S waves beneath the United States, Bull. Seism. Soc. Am., 60, 819-838, 1970.

Spetzler, H., and D.L. Anderson, The effect of temperature and partial melting on velocity and attenuation in a simple binary system, J. Geophys. Res., 73, 6051-6060, 1968.

Steinhart, J.S., and R.P. Meyer, Explosion Studies of Continental Structure, University of Wisconsin, 1956-1959, Carneige Institution of Washington Publication 622, 409 pp., 1961.

Sumner, R.D., Attenuation of earthquake generated P waves along the western flank of the Andes, Bull. Seism. Soc. Am., 57, 173-190, 1967.

Sutton, G.H., W. Mitronovas, P.W. Pomeroy, Short-period seismic energy radiation patterns from underground nuclear explosions and small-magnitude earthquakes,

Bull. Seism. Soc. Am., 57, 249-267, 1967.

Sykes, L.R., The seismicity of the Arctic, Bull. Seism. Soc. Am., 55, 519-536, 1965.

Sykes, L.R., Seismological evidence for transform faults, sea floor spreading, and continental drift, in The History of the Earth's Crust, ed. by R.A. Phinney, Princeton University Press, New Jersey, 120-150, 1968.

Takeuchi, H., Y. Hamano, and Y. Hasegawa, Rayleigh- and Love-wave discrepancy and the existence of magma pockets in the upper mantle, J. Geophys. Res., 73, 3349-3350, 1968.

Teng, T.L., Body wave and earthquake source studies, Ph.D. thesis, California Institute of Technology, Pasadena, 205 pp., 1966.

Teng, T.L., Attenuation of body waves and the Q structure of the mantle, J. Geophys. Res., 73, 2195-2208, 1968.

Teng, T.L., Correction to a paper by Ta-liang Teng, "Attenuation of body waves and Q structure of the mantle," J. Geophys. Res., 74, 6720-6721, 1969.

Teng, T.L.,and A. Ben-Menahem, Mechanism of deep earthquakes from spectrums of isolated body-wave signals, 1, The Banda Sea earthquake of March 21, 1964, J. Geophys. Res., 70, 5157-5170, 1965.

Toksöz, M.N., A. Ben-Menahem, and D.G. Harkrider, Determination of source parameters of explosions and earthquakes

by amplitude equalization of seismic surface waves, 1, Underground nuclear explosions, J. Geophys. Res., 69, 4355-4366, 1964.

Toksöz, M.N., M.A. Chinnery, and D.L. Anderson, Inhomogeneities in the Earth's mantle, Geophys. J. Roy. Astron. Soc., 13, 31-59, 1967.

Toksöz, M.N., J.W. Minear, and B.R. Julian, Temperature field and geophysical effects of a downgoing slab, J. Geophys. Res., 76, in press, 1971.

Tryggvason, E., Dissipation of Rayleigh wave energy, J. Geophys. Res., 70, 1449-1455, 1965.

Tsai, Y.-B., and K. Aki, Simultaneous determination of the seismic moment and attenuation of seismic surface waves, Bull. Seism. Soc. Am., 59, 275-287, 1969.

Tsujiura, M., Frequency analysis of seismic waves 1, Bull. Earthquake Res. Inst., Tokyo Univ., 44, 873-891, 1966.

Tsujiura, M., Regional variation of P wave spectrum (1), Bull. Earthquake Res. Inst., Tokyo Univ., 47, 613-633, 1969.

Ubbelohde, A.R., Melting and Crystal Structure, Clarendon Press, Oxford, 325 pp., 1965.

Unger, J.D., Melting of granite under effective confining pressure, M.S. thesis, Massachusetts Institute of Technology, Cambridge, 42 pp., 1967.

Utsu, T., Variations in spectra of P waves recorded at Canadian Arctic seismograph stations, Can. J. Earth. Sci., 3, 597-621, 1966a.

Utsu, T., Regional differences in absorption of seismic waves in the upper mantle as inferred from abnormal distributions of seismic intensities, J. Fac. Sci., Hokkaido Univ., Ser. 7, 2, 359-374, 1966b.

Utsu, T., Anomalies in seismic wave velocity and attenuation associated with a deep earthquake zone 1, J. Fac. Sci., Hokkaido Univ., Ser. 7, 3, 1-25, 1967.

Utsu, T., and H. Okada, Anomalies in seismic wave velocity and attenuation associated with a deep earthquake zone 2, J. Fac. Sci., Hokkaido Univ., Ser. 7, 3, 65-84, 1968.

Vaišnys, J.R., Propagation of acoustic waves through a system undergoing phase transformations, J. Geophys. Res., 73, 7675-7683, 1968.

Vogt, P.R., and N.A. Ostenso, Magnetic and gravity profiles across the Alpha cordillera and their relation to Arctic sea-floor spreading, J. Geophys. Res., 75, 4925-4937, 1970.

Vvedenskaya, A.V., and L.M. Balakina, Double refraction in the earth's mantle, Bull. Acad. Sci. USSR, Geophys. Ser., English Transl., no. 8, 814-819, 1959.

Wadati, K., and T. Hirono, Magnitude of earthquakes-especially of near, deep-focus earthquakes, Geophys. Mag., 27, 1-10, 1956.

Wadati, K., T. Hirono, and T. Yumura, On the attenuation of S-waves and the structure of the upper mantle in the region of the Japanese Islands, Pap. Met.

Geophys., 20, 49-78, 1969.

Walcott, R.I., Flexural rigidity, thickness, and viscosity of the lithosphere, J. Geophys. Res., 75, 3941-3954, 1970.

Walsh, J.B., Seismic wave attenuation in rock due to friction, J. Geophys. Res., 71, 2591-2599, 1966.

Walsh, J.B., Attenuation in partially melted material, J. Geophys. Res., 73, 2209-2216, 1968.

Walsh, J.B., A new analysis of attenuation in partially melted rock, J. Geophys. Res., 74, 4333-4337, 1969.

Ward, R.W., and M.N. Toksöz, Causes of regional variation of magnitudes, Bull. Seism. Soc. Am., in press, 1971.

Warren, D.H., A seismic-refraction survey of crustal structure in central Arizona, Geol. Soc. Am. Bull., 80, 257-282, 1969.

Whitcomb, J.H., and D.L. Anderson, Reflection of P'P' seismic waves from discontinuities in the mantle, J. Geophys. Res., 75, 5713-5728, 1970.

Woolard, G.P., and J.C. Rose, International Gravity Measurements, Geophysical and Polar Research Center, Univ. Wisconsin, Madison, 518 pp., 1963.

Wu, T.T., The effect of inclusion shape on the elastic moduli of a two-phase material, Intern. J. Solids Structures, 2, 1-8, 1966.

Wyss, M., and J.N. Brune, Seismic moment, stress, and source dimensions for earthquakes in the California-Nevada region, J. Geophys. Res., 73, 4681-4694, 1968.

York, D., Least-squares fitting of a straight line, Can. J. Phys., 44, 1079-1086, 1966.

Zener, C.M., Elasticity and Anelasticity of Metals, University of Chicago Press, Illinois, 170 pp., 1948.

Appendix 1. Wu's treatment of the elastic moduli of two-phase materials

Consider a single inclusion, in the shape of an ellipsoid, of one (elastic, isotropic) material embedded in a matrix of a second (elastic, isotropic) material. If the matrix is subjected to a uniform strain ε^{o}_{ij} at infinity, then the strain ε_{ij} within the inclusion is uniform and is a function only of ε^{o}_{ij}, the elastic constants of matrix and inclusion, and the shape of the inclusion (Eshelby, 1957). When the axes of the ellipsoid coincide with the coordinate axes, we may write

$$\varepsilon_{ij} = T_{ijpg} \quad \varepsilon^{o}_{pg} \qquad \text{(A1.1)}$$

(Wu, 1966), where T_{ijpg} are the components of a fourth-order tensor.

Now consider a composite material, consisting of isolated ellipsoidal inclusions of one material (with elastic constants K_2 and μ_2) within a continuous matrix of another material (with elastic constants K_1 and μ_1). Suppose further that the inclusions are randomly oriented and are of dimensions smaller than any characteristic length of interest. Then the composite may be treated as macroscopically isotropic with two elastic constants, say K and μ. If the volume concentration of the inclusion

phase is not small, then it is presumed that the strain within any single inclusion due to a uniform strain applied to the composite at infinity is still given by (A1.1), but with the elastic constants of the matrix replaced by those of the composite in the appropriate expressions for T_{ijpg}. This is the 'self-consistent approximation', first applied (in somewhat different form) to the problem of the elasticity of polycrystalline aggregates by Hershey (1954) and Krŏner (1958).

If at the boundaries (presumed to be at infinity) of the composite a uniform surface traction is applied, then the total elastic energy may be written (Wu, 1966) both in terms of the elastic constants of the composite and in terms of the constants of matrix and inclusion (the latter involves computing an orientation average of the inclusion strain). When the applied stress at infinity is, respectively, pure compression or simple shear then equating the two expressions for elastic energy gives implicit tensor formulas (2.5) for the macroscopic moduli (all of the resulting orientation-averages of components T_{ijpg} can be written, conveniently, in terms of T_{iijj} and T_{ijij}, which are both independent of orientation). If the inclusions are oblate spheroids of aspect ratio α, then the scalar forms T_{iijj} and T_{ijij} depend only on α, K_2, μ_2, K, and μ (Wu, 1966). In particular:

$$T_{iijj} = \frac{3F_1}{F_2} \qquad \text{(A1.2)}$$

$$T_{ijij} - \frac{1}{3} T_{iijj} = \frac{2}{F_3} + \frac{1}{F_4} + \frac{F_4F_5 + F_6F_7 - F_8F_9}{F_2F_4}$$

where

$$F_1 = 1 + A\left[\tfrac{3}{2}(g+\phi) - R(\tfrac{3}{2}g + \tfrac{5}{2}\phi - \tfrac{4}{3})\right]$$

$$F_2 = 1 + A\left[1 + \tfrac{3}{2}(g+\phi) - R(\tfrac{3}{2}g + \tfrac{5}{2}\phi)\right] + B(3-4R)$$

$$+ \tfrac{1}{2}A\,(A + 3B)\,(3 - 4R)\left[g + \phi - R(g - \phi + 2\phi^2)\right]$$

$$F_3 = 1 + \tfrac{1}{2}A\left[-\frac{1+\alpha^2}{\alpha^2}\,g + R(2 - \phi + \frac{1+\alpha^2}{\alpha^2}\,g)\right]$$

$$F_4 = 1 + \tfrac{1}{4}A\left[3\phi + g - R(g - \phi)\right]$$

$$F_5 = A\left[-g + R(g + \phi - \tfrac{4}{3})\right] + B\phi(3 - 4R)$$

$$F_6 = 1 + A\left[1 + g - R(g + \phi)\right] + B(1 - \phi)\,(3 - 4R)$$

$$F_7 = 2 + \tfrac{1}{4}A\left[9\phi + 3g - R(5\phi + 3g)\right] + B\phi\,(3-4R)$$

$$F_8 = A\left[1 - \tfrac{3}{2}\phi - \tfrac{1}{2}g + \tfrac{1}{2}R(5\phi + g - 4)\right] + B(1 - \phi)(3 - 4R)$$

$$F_9 = A\left[-g + R(g - \phi)\right] + B\phi\,(3 - 4R)$$

$$A = \frac{\mu_2}{\mu} - 1$$

$$B = \frac{1}{3}\left(\frac{K_2}{K} - \frac{\mu_2}{\mu}\right)$$

$$R = \frac{3\mu}{3K + 4\mu}$$

$$\phi = \frac{\alpha}{(1 - \alpha^2)^{3/2}} \left[\cos^{-1}\alpha - \alpha(1 - \alpha^2)^{\frac{1}{2}}\right]$$

$$g = \frac{\alpha^2}{1 - \alpha^2}(3\phi - 2).$$

When the inclusions are not of uniform shape, then an additional average is required in computing the contribution of the inclusions to the total elastic energy. In that case, equations (2.6) supplant (2.5).

Appendix 2. Complete compilation of surface-wave propagation parameters, western and east-central United States.

The ten tables to follow present individual determinations, for all events studied, of phase velocity, group velocity, and apparent attenuation-coefficient for Love and Rayleigh waves along the LON-TUC and RCD-ATL paths. In addition, average propagation-parameters are given for each of the two propagation-directions for the LON-TUC path. The numbering of events follows the listing in Tables 4.1 and 4.2.

In the following tables, F is the frequency (in Hz), C is the phase velocity (in km/sec), U is the group velocity (in km/sec), GAMMA or G is the attenuation coefficient (i.e. k* in the text), and SD is the standard deviation.

LON TO TUC

RAYLEIGH WAVE VERTICAL

EVENT 1

F	C	U	GAMMA
0.0250	3.740	3.532	-0.115E-03
0.0264	3.726	3.478	-0.629E-04
0.0278	3.711	3.422	0.233E-04
0.0292	3.694	3.383	0.132E-03
0.0307	3.678	3.303	0.234E-03
0.0321	3.662	3.341	0.305E-03
0.0335	3.646	3.326	0.352E-03
0.0349	3.632	3.321	0.297E-03
0.0364	3.624	3.318	0.201E-03
0.0378	3.613	3.233	0.156E-03
0.0392	3.596	3.221	0.140E-03
0.0406	3.582	3.232	0.138E-03
0.0421	3.569	3.237	0.141E-03
0.0435	3.557	3.205	0.138E-03
0.0449	3.544	3.078	0.689E-04
0.0463	3.523	2.963	0.374E-04
0.0478	3.503	2.898	0.623E-04
0.0492	3.480	2.856	0.124E-03
0.0506	3.459	2.865	0.161E-03
0.0521	3.439	2.849	0.205E-03
0.0535	3.419	2.821	0.264E-03
0.0549	3.401	2.837	0.276E-03
0.0563	3.384	2.847	0.297E-03
0.0578	3.368	2.865	0.316E-03
0.0592	3.355	2.880	0.295E-03
0.0606	3.342	2.835	0.349E-03
0.0620	3.327	2.832	0.401E-03
0.0635	3.315	2.930	0.354E-03
0.0649	3.307	3.028	0.350E-03
0.0663	3.301	3.094	0.419E-03

EVENT 3

F	C	U	GAMMA
0.0163	3.784	3.647	0.404E-04
0.0178	3.772	3.622	0.825E-04
0.0192	3.759	3.605	0.114E-03
0.0206	3.748	3.589	0.128E-03
0.0220	3.736	3.565	0.134E-03
0.0235	3.725	3.532	0.141E-03
0.0249	3.712	3.503	0.149E-03
0.0263	3.699	3.509	0.155E-03
0.0277	3.690	3.548	0.160E-03
0.0291	3.684	3.563	0.174E-03
0.0306	3.677	3.527	0.179E-03
0.0320	3.668	3.466	0.214E-03
0.0334	3.658	3.446	0.260E-03
0.0348	3.649	3.423	0.290E-03
0.0362	3.638	3.354	0.271E-03
0.0377	3.625	3.285	0.242E-03
0.0391	3.610	3.230	0.230E-03
0.0405	3.594	3.185	0.252E-03
0.0419	3.576	3.164	0.270E-03
0.0434	3.562	3.142	0.300E-03
0.0448	3.547	3.057	0.357E-03

EVENT 4

F	C	U	GAMMA
0.0366	3.649	3.040	0.620E-04
0.0380	3.622	3.059	0.935E-04
0.0395	3.599	3.089	0.104E-03
0.0409	3.578	3.095	0.122E-03
0.0424	3.559	3.073	0.143E-03
0.0438	3.540	3.030	0.155E-03
0.0452	3.520	2.983	0.157E-03
0.0467	3.500	2.953	0.152E-03
0.0481	3.480	2.943	0.146E-03
0.0495	3.462	2.947	0.139E-03
0.0510	3.445	2.964	0.131E-03
0.0524	3.431	2.989	0.128E-03
0.0538	3.418	2.964	0.146E-03
0.0553	3.403	2.891	0.185E-03
0.0567	3.386	2.857	0.219E-03
0.0581	3.371	2.857	0.243E-03
0.0596	3.356	2.856	0.253E-03
0.0610	3.343	2.854	0.248E-03
0.0625	3.329	2.844	0.226E-03

EVENT 5

F	C	U	GAMMA
0.0205	3.754	3.530	0.130E-03
0.0219	3.738	3.522	0.142E-03
0.0234	3.724	3.524	0.188E-03
0.0248	3.713	3.532	0.242E-03
0.0262	3.703	3.436	0.283E-03
0.0276	3.682	3.352	0.323E-03
0.0290	3.665	3.400	0.378E-03
0.0304	3.654	3.461	0.433E-03
0.0319	3.646	3.483	0.475E-03
0.0333	3.639	3.472	0.498E-03
0.0347	3.631	3.438	0.501E-03
0.0361	3.623	3.343	0.487E-03
0.0375	3.613	3.273	0.483E-03
0.0389	3.604	3.247	0.475E-03
0.0403	3.594	3.234	0.461E-03
0.0418	3.581	3.222	0.460E-03
0.0432	3.567	3.210	0.469E-03
0.0446	3.554	3.195	0.487E-03

EVENT 6

F	C	U	GAMMA
0.0278	3.707	3.555	-0.161E-03
0.0292	3.699	3.531	-0.262E-04
0.0306	3.690	3.495	0.855E-04
0.0321	3.680	3.462	0.131E-03
0.0335	3.670	3.396	0.142E-03
0.0349	3.655	3.273	0.229E-03
0.0363	3.635	3.209	0.298E-03
0.0378	3.617	3.234	0.270E-03
0.0392	3.603	3.212	0.262E-03
0.0406	3.585	3.137	0.283E-03
0.0420	3.567	3.120	0.330E-03
0.0435	3.551	3.111	0.405E-03

WESTERN U. S.

LON TO TUC

LOVE WAVE

EVENT 2

F	C	U	GAMMA
0.0165	4.225	3.987	0.385E-03
0.0179	4.204	3.974	0.393E-03
0.0194	4.186	3.959	0.389E-03
0.0208	4.169	3.955	0.379E-03
0.0222	4.154	3.960	0.363E-03
0.0237	4.142	3.963	0.341E-03
0.0251	4.132	3.960	0.313E-03
0.0266	4.122	3.951	0.285E-03
0.0280	4.112	3.941	0.263E-03
0.0294	4.103	3.937	0.259E-03
0.0309	4.095	3.938	0.280E-03
0.0323	4.088	3.940	0.326E-03
0.0337	4.082	3.932	0.391E-03
0.0352	4.075	3.908	0.461E-03
0.0366	4.067	3.871	0.526E-03
0.0380	4.059	3.830	0.579E-03

EVENT 3

F	C	U	GAMMA
0.0163	4.324	4.003	0.177E-03
0.0178	4.294	3.971	0.231E-03
0.0192	4.268	3.963	0.270E-03
0.0206	4.245	3.957	0.297E-03
0.0220	4.225	3.932	0.307E-03
0.0235	4.204	3.886	0.297E-03
0.0249	4.183	3.812	0.270E-03
0.0263	4.158	3.652	0.235E-03
0.0277	4.122	3.546	0.176E-03
0.0291	4.089	3.545	0.970E-04
0.0306	4.060	3.532	0.727E-05
0.0320	4.033	3.445	-0.838E-04
0.0334	4.007	3.307	-0.321E-03
0.0348	3.971	3.261	-0.377E-03
0.0362	3.936	3.223	-0.421E-03
0.0377	3.902	3.200	-0.432E-03
0.0391	3.871	3.202	-0.395E-03
0.0405	3.843	3.241	-0.311E-03
0.0419	3.821	3.401	-0.183E-03
0.0434	3.811	3.625	-0.493E-04
0.0448	3.808	3.740	0.367E-04
0.0462	3.806	3.768	0.906E-04
0.0476	3.805	3.767	0.136E-03
0.0490	3.804	3.744	0.184E-03
0.0505	3.802	3.690	0.227E-03
0.0519	3.798	3.578	0.242E-03
0.0533	3.789	3.424	0.219E-03
0.0547	3.776	3.329	0.197E-03
0.0561	3.763	3.315	0.190E-03
0.0576	3.751	3.341	0.190E-03
0.0590	3.740	3.406	0.192E-03
0.0604	3.733	3.514	0.190E-03
0.0618	3.729	3.644	0.174E-03
0.0633	3.729	3.748	0.151E-03
0.0647	3.730	3.735	0.148E-03
0.0661	3.729	3.639	0.185E-03

EVENT 4

F	C	U	GAMMA
0.0194	4.215	4.082	0.441E-03
0.0208	4.203	4.055	0.483E-03
0.0223	4.194	4.036	0.460E-03
0.0237	4.182	3.986	0.412E-03
0.0251	4.169	3.956	0.352E-03
0.0266	4.156	3.850	0.268E-03
0.0280	4.134	3.669	0.183E-03
0.0294	4.103	3.663	0.135E-03
0.0309	4.085	3.707	0.112E-03
0.0323	4.064	3.655	0.962E-04
0.0337	4.037	3.506	-0.238E-03
0.0352	4.011	3.464	-0.293E-03
0.0366	3.985	3.393	-0.359E-03
0.0380	3.957	3.321	-0.437E-03
0.0395	3.928	3.285	-0.512E-03
0.0409	3.901	3.279	-0.573E-03
0.0424	3.876	3.292	-0.620E-03
0.0438	3.854	3.300	-0.631E-03
0.0452	3.833	3.292	-0.587E-03
0.0467	3.814	3.282	-0.512E-03
0.0481	3.795	3.257	-0.418E-03
0.0495	3.776	3.231	-0.327E-03
0.0510	3.758	3.240	-0.267E-03
0.0524	3.742	3.255	-0.218E-03
0.0538	3.728	3.248	-0.159E-03
0.0553	3.713	3.247	-0.116E-03
0.0567	3.700	3.257	-0.920E-04
0.0581	3.688	3.266	-0.736E-04
0.0596	3.676	3.279	-0.629E-04
0.0610	3.666	3.266	-0.240E-04
0.0625	3.655	3.232	0.341E-04
0.0639	3.644	3.218	0.731E-04
0.0653	3.634	3.220	0.935E-04
0.0668	3.624	3.224	0.960E-04

EVENT 7

F	C	U	GAMMA
0.0121	4.524	4.186	0.325E-03
0.0135	4.496	4.193	0.337E-03
0.0149	4.457	4.160	0.304E-03
0.0163	4.434	4.131	0.262E-03
0.0178	4.402	4.023	0.228E-03
0.0192	4.368	3.900	0.192E-03
0.0206	4.325	3.813	0.172E-03
0.0220	4.287	3.757	0.156E-03
0.0235	4.247	3.622	0.114E-03
0.0249	4.199	3.517	0.777E-04

WESTERN U.S.

LCN TO TLC

RAYLEIGH WAVE VERTICAL

F	C	SD	U	SD	G*10**4	SD
0.0164	3.784		3.647		0.404	
0.0178	3.772		3.622		0.825	
0.0192	3.759		3.605		1.140	
0.0207	3.751	0.004	3.559	0.042	1.290	0.014
0.0221	3.737	0.001	3.543	0.030	1.380	0.057
0.0235	3.724	0.001	3.528	0.006	1.645	0.332
0.0249	3.722	0.016	3.522	0.017	0.920	1.852
0.0264	3.709	0.015	3.474	0.037	1.250	1.749
0.0278	3.697	0.014	3.467	0.100	0.863	2.054
0.0292	3.685	0.015	3.467	0.091	1.644	1.664
0.0307	3.675	0.015	3.460	0.072	2.329	1.468
0.0321	3.664	0.014	3.437	0.066	2.812	1.474
0.0335	3.653	0.014	3.409	0.065	3.130	1.503
0.0349	3.642	0.012	3.362	0.080	3.292	1.185
0.0364	3.634	0.011	3.248	0.137	2.638	1.547
0.0378	3.618	0.005	3.215	0.094	2.499	1.484
0.0392	3.602	0.005	3.199	0.065	2.434	1.451
0.0406	3.587	0.007	3.176	0.061	2.512	1.365
0.0421	3.571	0.009	3.162	0.069	2.688	1.346
0.0435	3.555	0.010	3.133	0.075	2.934	1.472
0.0449	3.541	0.015	3.076	0.087	2.725	1.828
0.0463	3.511	0.016	2.958	0.007	0.947	0.810
0.0478	3.491	0.016	2.920	0.032	1.041	0.592
0.0492	3.471	0.013	2.901	0.064	1.315	0.106
0.0506	3.452	0.010	2.914	0.070	1.460	0.212
0.0520	3.435	0.006	2.917	0.099	1.665	0.544
0.0535	3.418	0.001	2.891	0.101	2.050	0.834
0.0549	3.402	0.001	2.864	0.038	2.305	0.643
0.0563	3.385	0.001	2.852	0.007	2.590	0.552
0.0577	3.369	0.002	2.861	0.006	2.795	0.516
0.0592	3.356	0.001	2.868	0.017	2.740	0.297
0.0606	3.342	0.001	2.844	0.013	2.985	0.714
0.0620	3.328	0.001	2.838	0.008	3.135	1.237
0.0634	3.315		2.930		3.540	
0.0649	3.307		3.028		3.560	
0.0663	3.301		3.094		4.190	

WESTERN U.S.

LCN TO TUC

LOVE WAVE

F	C	SD	U	SD	G*10**4	SD
0.0121	4.524		4.186		3.250	
0.0135	4.496		4.193		3.370	
0.0150	4.457		4.160		3.040	
0.0164	4.326	0.104	4.039	0.078	2.747	1.046
0.0178	4.298	0.099	3.989	0.029	2.840	0.944
0.0192	4.258	0.079	3.975	0.076	3.230	1.129
0.0207	4.235	0.067	3.943	0.100	3.327	1.314
0.0221	4.214	0.056	3.919	0.120	3.215	1.272
0.0235	4.193	0.044	3.859	0.173	2.910	1.272
0.0249	4.171	0.029	3.802	0.216	2.532	1.217
0.0264	4.145	0.020	3.814	0.154	2.627	0.254
0.0278	4.123	0.011	3.711	0.198	2.073	0.483
0.0292	4.098	0.008	3.708	0.197	1.637	0.847
0.0307	4.080	0.018	3.718	0.202	1.331	1.376
0.0321	4.062	0.028	3.669	0.246	1.108	2.083
0.0335	4.042	0.038	3.563	0.309	-0.560	3.893
0.0349	4.019	0.052	3.524	0.320	-0.697	4.615
0.0364	3.995	0.066	3.475	0.322	-0.847	5.298
0.0378	3.972	0.079	3.430	0.318	-0.967	5.851
0.0392	3.899	0.040	3.243	0.059	-4.535	0.827
0.0406	3.872	0.041	3.260	0.027	-4.420	1.853
0.0421	3.848	0.039	3.346	0.077	-4.015	3.090
0.0435	3.832	0.030	3.455	0.229	-3.401	4.113
0.0449	3.820	0.018	3.502	0.315	-2.751	4.410
0.0463	3.810	0.006	3.508	0.342	-2.107	4.261
0.0478	3.800	0.007	3.493	0.359	-1.410	3.917
0.0492	3.790	0.020	3.469	0.361	-0.715	3.613
0.0506	3.780	0.031	3.450	0.317	-0.200	3.493
0.0520	3.770	0.040	3.409	0.228	0.120	3.253
0.0535	3.758	0.043	3.334	0.124	0.300	2.673
0.0549	3.744	0.045	3.287	0.058	0.405	2.213
0.0563	3.731	0.045	3.286	0.041	0.490	1.994
0.0577	3.719	0.045	3.303	0.053	0.582	1.864
0.0592	3.708	0.045	3.341	0.090	0.645	1.802
0.0606	3.699	0.047	3.385	0.175	0.830	1.513
0.0620	3.692	0.052	3.426	0.290	1.040	0.989
0.0634	3.686	0.060	3.463	0.373	1.120	0.551
0.0649	3.681	0.068	3.458	0.362	1.207	0.385
0.0663	3.676	0.074	3.419	0.292	1.405	0.629

WESTERN U.S.

TUC TO LON

RAYLEIGH WAVE VERTICAL

EVENT 8

F	C	U	GAMMA
C.C235	3.764	3.572	0.160E-03
0.0249	3.751	3.523	0.157E-03
0.0264	3.737	3.441	0.160E-03
C.C278	3.717	3.404	0.205E-03
0.0292	3.7C1	3.359	0.287E-03
0.C306	3.680	3.235	0.349E-03
0.0321	3.655	3.146	0.320E-03
0.0335	3.628	3.C76	0.189E-03
C.C349	3.599	3.016	0.252E-04
C.C363	3.571	2.963	-0.139E-03
C.C378	3.532	2.973	-0.393E-03
C.C392	3.5C6	2.919	-0.5C0E-03
0.0406	3.480	2.898	-0.533E-03
C.0420	3.457	2.894	-0.530E-03
0.0435	3.435	2.893	-0.5C8E-03
0.0449	3.414	2.861	-0.464E-03
C.C463	3.393	2.841	-0.398E-03
0.0477	3.373	2.868	-0.284E-03
0.C492	3.357	2.897	-0.186E-03
C.C5C6	3.342	2.880	-0.114E-03
0.0520	3.327	2.849	-0.59CE-04
C.C534	3.312	2.821	-0.214E-04
0.C549	3.296	2.803	-0.727E-05
0.0563	3.281	2.796	-0.108E-04
C.C577	3.267	2.787	-0.170E-04
0.0591	3.254	2.769	-0.167E-04
C.C606	3.240	2.750	-0.170E-04
C.C620	3.226	2.736	-0.242E-04
0.0634	3.213	2.714	-0.316E-04
C.C648	3.200	2.684	-0.315E-04
0.0663	3.186	2.655	-0.322E-04

EVENT 9

F	C	U	GAMMA
0.0248	3.767	3.449	0.226E-03
C.C262	3.747	3.353	0.794E-04
0.0277	3.720	3.298	0.417E-05
0.0291	3.698	3.304	0.125E-04
C.0305	3.677	3.284	0.162E-04
0.0319	3.657	3.287	0.236E-04
C.0333	3.640	3.279	0.341E-05
0.0347	3.623	3.269	-0.401E-04
0.C362	3.608	3.320	-0.505E-04
0.C376	3.598	3.371	-0.281E-04
0.C390	3.590	3.318	-0.228E-04
C.C404	3.577	3.169	-0.489E-04
0.0418	3.558	3.049	-0.627E-04
C.C432	3.537	2.997	-0.347E-04
C.C447	3.516	2.945	0.563E-04
0.0461	3.494	2.880	0.190E-03
0.0475	3.470	2.823	0.285E-03
C.C489	3.446	2.789	0.304E-03
0.0503	3.423	2.829	0.260E-03
C.C518	3.4C5	2.915	0.217E-03
C.C532	3.392	2.960	0.196E-03
C.C546	3.379	2.966	0.175E-03
C.C560	3.367	2.967	0.148E-03
0.0574	3.356	2.984	0.107E-03
C.C588	3.346	3.021	0.602E-04
C.C603	3.339	3.007	0.422E-04

EVENT 10

F	C	U	GAMMA
C.C348	3.689	3.317	-0.457E-04
C.C362	3.673	3.294	-C.996E-04
0.C377	3.656	3.252	-0.142E-03
0.C391	3.639	3.234	-0.161E-03
C.C405	3.622	3.199	-0.163E-03
C.C419	3.599	3.104	-0.826E-04
C.C434	3.580	3.069	0.130E-05
0.0448	3.560	3.009	0.562E-04
C.0462	3.539	3.008	0.118E-03
0.0476	3.522	3.082	0.215E-03
C.C490	3.509	3.148	0.315E-03
C.C5C5	3.498	3.192	0.377E-03
C.C519	3.490	3.246	0.370E-03
C.C533	3.484	3.295	0.311E-03
C.C547	3.479	3.315	0.238E-03
0.0561	3.475	3.292	0.160E-03
C.C576	3.469	3.202	0.812E-04
C.C590	3.461	3.102	0.410E-04
C.C604	3.450	3.041	0.618E-04
C.C618	3.439	2.988	0.119E-03
C.C633	3.426	2.945	0.18CE-03
C.C647	3.414	2.919	0.228E-03
C.C661	3.401	2.902	0.27CE-03

WESTERN U.S.

TUC TO LON

LOVE WAVE

EVENT 8

F	C	U	GAMMA
C.C1C7	4.458	4.046	0.471E-04
C.C121	4.403	4.022	0.484E-04
C.C135	4.359	4.025	0.862E-04
0.C150	4.326	4.044	0.130E-03
C.C164	4.300	4.012	0.153E-03
0.C178	4.272	3.923	C.160E-03
0.C192	4.240	3.874	0.185E-03
C.02C7	4.213	3.885	0.225E-03
0.0221	4.190	3.884	C.250E-03
C.C235	4.170	3.844	0.246E-03
0.C249	4.148	3.783	0.224E-03
C.0264	4.124	3.729	0.203E-03
C.C278	4.101	3.680	0.189E-03
0.0292	4.076	3.619	0.177E-03
0.C3C6	4.050	3.549	0.163E-03
C.0321	4.023	3.482	0.151E-03
C.C335	3.995	3.419	0.152E-03
C.C349	3.966	3.364	0.171E-03
0.0363	3.937	3.341	0.209E-03
0.0378	3.906	3.313	0.201E-03
C.C392	3.881	3.289	0.146E-03
C.0406	3.855	3.212	0.676E-04
C.0420	3.827	3.165	-0.183E-04
0.0435	3.801	3.195	-0.997E-04
0.0449	3.779	3.236	-0.171E-03
C.C463	3.760	3.267	-0.218E-03
C.C477	3.744	3.286	-0.222E-03
0.C492	3.729	3.296	-0.179E-03
C.C5C6	3.716	3.346	-0.105E-03
0.C520	3.706	3.421	-0.360E-04
0.C534	3.699	3.433	-0.705E-06
C.0549	3.691	3.399	0.138E-04
0.0563	3.682	3.370	0.220E-04
C.C577	3.673	3.348	0.305E-04
0.C591	3.665	3.333	0.398E-04
C.C606	3.656	3.324	0.481E-04
C.C620	3.647	3.319	0.551E-04
0.0634	3.639	3.313	0.632E-04
C.C649	3.631	3.303	0.754E-04
C.C663	3.623	3.291	0.912E-04

EVENT 9

F	C	U	GAMMA
C.C106	4.506	4.100	0.155E-03
C.C121	4.453	4.074	C.226E-03
C.C135	4.403	4.043	0.268E-03
0.C149	4.369	4.020	0.302E-03
C.C163	4.335	4.010	0.329E-03
0.C177	4.307	3.989	0.336E-03
C.C191	4.280	3.923	0.311E-03
C.C2C6	4.250	3.824	0.266E-03
C.C220	4.215	3.749	0.227E-03
C.C234	4.182	3.715	0.199E-03
C.C248	4.151	3.699	0.18CE-03
C.C262	4.124	3.672	0.179E-03
C.C277	4.096	3.579	0.211E-03
0.0291	4.063	3.490	0.256E-03
C.0305	4.031	3.451	0.232E-03
C.0319	4.000	3.368	0.283E-03
C.0333	3.965	3.252	0.276E-03

EVENT 10

F	C	U	GAMMA
C.C149	4.336	4.050	0.247E-03
C.0163	4.309	3.984	0.240E-03
C.C178	4.276	3.922	0.241E-03
0.0192	4.247	3.914	0.273E-03
C.C2C6	4.222	3.896	0.320E-03
C.C220	4.198	3.867	0.368E-03
C.0235	4.176	3.844	0.409E-03
C.C249	4.155	3.821	0.429E-03
C.0263	4.134	3.795	0.423E-03
0.C277	4.115	3.776	0.404E-03
C.C291	4.096	3.759	0.385E-03
C.03C6	4.079	3.784	0.379E-03
C.0320	4.066	3.867	0.396E-03
C.C334	4.060	3.886	0.371E-03
0.0348	4.051	3.827	0.312E-03
C.C362	4.041	3.771	0.247E-03
C.0377	4.028	3.722	0.189E-03
0.0391	4.016	3.695	0.136E-03
C.C4C5	4.002	3.646	0.989E-04
C.C419	3.988	3.503	0.430E-04
C.0434	3.965	3.360	0.102E-04
C.0448	3.941	3.327	-0.260E-05
0.0462	3.919	3.325	0.752E-05
C.C476	3.898	3.327	0.236E-04
C.0490	3.879	3.323	0.529E-04
C.C505	3.861	3.319	0.916E-04
C.C519	3.843	3.325	0.132E-03

WESTERN U.S.

TUC TC LCN

RAYLEIGH WAVE VERTICAL

F	C	SD	U	SD	G*10**4	SD
0.0235	3.764		3.572		1.600	
0.0249	3.759	0.011	3.486	0.052	1.915	0.488
0.0264	3.742	0.007	3.396	0.062	1.197	0.570
0.0278	3.718	0.002	3.350	0.075	1.046	1.420
0.0292	3.699	0.002	3.331	0.039	1.497	1.941
0.0307	3.678	0.002	3.259	0.035	1.826	2.353
0.0321	3.656	0.001	3.215	0.100	1.718	2.096
0.0335	3.634	0.008	3.174	0.143	0.962	1.312
0.0349	3.637	0.046	3.195	0.166	-0.202	0.394
0.0364	3.617	0.051	3.184	0.206	-0.964	0.443
0.0378	3.595	0.062	3.190	0.209	-1.877	1.867
0.0392	3.577	0.068	3.147	0.217	-2.279	2.455
0.0406	3.559	0.073	3.083	0.171	-2.483	2.531
0.0421	3.537	0.074	3.013	0.110	-2.251	2.642
0.0435	3.516	0.075	2.981	0.094	-1.805	2.842
0.0449	3.496	0.075	2.937	0.074	-1.172	3.004
0.0463	3.474	0.075	2.908	0.086	-0.267	3.150
0.0478	3.454	0.076	2.920	0.135	0.720	3.103
0.0492	3.436	0.077	2.937	0.180	1.443	2.861
0.0506	3.420	0.078	2.958	0.190	1.743	2.565
0.0520	3.406	0.081	2.994	0.205	1.760	2.174
0.0535	3.395	0.086	3.013	0.236	1.619	1.688
0.0549	3.383	0.091	3.013	0.254	1.352	1.274
0.0563	3.372	0.097	3.005	0.245	0.991	0.953
0.0577	3.362	0.101	2.981	0.207	0.571	0.654
0.0592	3.352	0.103	2.957	0.178	0.282	0.400
0.0606	3.341	0.105	2.927	0.164	0.290	0.410
0.0620	3.329	0.150	2.856	0.178	0.474	1.013
0.0634	3.316	0.150	2.825	0.163	0.742	1.496
0.0649	3.304	0.151	2.797	0.166	0.982	1.835
0.0663	3.290	0.152	2.773	0.174	1.189	2.137

TUC TO LCN

LOVE WAVE

F	C	SD	U	SD	G*10**4	SD
0.0107	4.482	0.034	4.073	0.038	1.010	0.763
0.0121	4.428	0.035	4.048	0.037	1.372	1.256
0.0135	4.383	0.035	4.034	0.013	1.771	1.286
0.0150	4.344	0.022	4.038	0.016	2.263	0.878
0.0164	4.315	0.018	4.002	0.016	2.407	0.880
0.0178	4.285	0.019	3.944	0.038	2.457	0.881
0.0192	4.256	0.021	3.904	0.026	2.563	0.646
0.0207	4.228	0.019	3.868	0.039	2.703	0.476
0.0221	4.201	0.013	3.832	0.074	2.817	0.756
0.0235	4.176	0.006	3.800	0.075	2.847	1.102
0.0249	4.151	0.004	3.767	0.063	2.777	1.329
0.0264	4.127	0.006	3.731	0.061	2.683	1.345
0.0278	4.104	0.010	3.677	0.099	2.680	1.183
0.0292	4.078	0.017	3.619	0.134	2.727	1.050
0.0307	4.053	0.024	3.589	0.168	2.747	1.082
0.0321	4.029	0.033	3.560	0.252	2.767	1.226
0.0335	4.006	0.048	3.499	0.315	2.663	1.098
0.0349	4.008	0.060	3.581	0.326	2.415	0.997
0.0364	3.988	0.074	3.543	0.303	2.280	0.269
0.0378	3.966	0.086	3.506	0.288	1.950	0.085
0.0392	3.947	0.095	3.476	0.279	1.410	0.071
0.0406	3.927	0.104	3.415	0.306	0.782	0.151
0.0421	3.906	0.114	3.325	0.238	0.120	0.438
0.0435	3.881	0.116	3.275	0.117	-0.447	0.777
0.0449	3.858	0.115	3.281	0.064	-0.842	1.228
0.0463	3.838	0.112	3.296	0.041	-1.052	1.595
0.0478	3.819	0.109	3.306	0.029	-0.992	1.737
0.0492	3.803	0.106	3.309	0.019	-0.630	1.640
0.0506	3.787	0.102	3.332	0.019	-0.067	1.390
0.0520	3.773	0.097	3.372	0.068	0.480	1.188
0.0535	3.699		3.433		-0.007	
0.0549	3.691		3.399		0.138	
0.0563	3.682		3.370		0.220	
0.0577	3.673		3.348		0.305	
0.0592	3.665		3.333		0.398	
0.0606	3.656		3.324		0.481	
0.0620	3.647		3.319		0.551	
0.0634	3.639		3.313		0.632	
0.0649	3.631		3.303		0.754	
0.0663	3.623		3.291		0.912	

EAST - CENTRAL L.S.

RCD TC ATL

RAYLEIGH WAVE VERTICAL

EVENT 12

F	C	U	GAMMA
0.0206	4.074	3.831	0.389E-05
0.0220	4.054	3.724	0.195E-04
0.0234	4.026	3.622	0.331E-04
0.0249	4.000	3.556	0.508E-04
0.0263	3.971	3.499	0.706E-04
0.0277	3.942	3.439	0.854E-04
0.0291	3.912	3.386	0.107E-03
0.0305	3.883	3.352	0.123E-03
0.0320	3.855	3.327	0.128E-03
0.0334	3.829	3.318	0.118E-03
0.0348	3.805	3.347	0.102E-03
0.0362	3.786	3.368	0.906E-04

EVENT 14

F	C	U	GAMMA
0.0193	4.083	3.823	0.240E-03
0.0207	4.067	3.815	0.275E-03
0.0222	4.046	3.708	0.268E-03
0.0236	4.020	3.644	0.258E-03
0.0250	3.996	3.605	0.229E-03
0.0264	3.970	3.515	0.171E-03
0.0279	3.941	3.437	0.115E-03
0.0293	3.909	3.379	0.619E-04
0.0307	3.881	3.337	0.715E-05
0.0322	3.850	3.234	-0.578E-04
0.0336	3.816	3.154	-0.101E-03
0.0350	3.782	3.124	-0.110E-03
0.0364	3.751	3.103	-0.105E-03
0.0379	3.721	3.076	-0.932E-04
0.0393	3.692	3.054	-0.738E-04
0.0407	3.664	3.044	-0.441E-04
0.0422	3.639	3.048	-0.444E-05
0.0436	3.617	3.063	0.352E-04
0.0450	3.596	3.075	0.683E-04
0.0465	3.578	3.080	0.968E-04
0.0479	3.561	3.078	0.123E-03
0.0493	3.544	3.065	0.148E-03
0.0507	3.529	3.052	0.170E-03

EVENT 15

F	C	U	GAMMA
0.0193	4.081	3.811	0.137E-04
0.0207	4.057	3.734	-0.804E-05
0.0221	4.033	3.662	-0.224E-04
0.0235	4.005	3.562	-0.458E-04
0.0250	3.973	3.472	-0.574E-04
0.0264	3.940	3.405	-0.573E-04
0.0278	3.906	3.359	-0.412E-04
0.0292	3.874	3.346	0.210E-05
0.0307	3.846	3.339	0.598E-04
0.0321	3.820	3.311	0.114E-03
0.0335	3.794	3.259	0.165E-03
0.0349	3.767	3.219	0.216E-03
0.0364	3.741	3.215	0.264E-03
0.0378	3.719	3.166	0.327E-03
0.0392	3.693	3.118	0.393E-03

EVENT 16

F	C	U	GAMMA
0.0192	4.066	3.755	0.213E-03
0.0206	4.039	3.681	0.162E-03
0.0220	4.012	3.639	0.133E-03
0.0235	3.986	3.592	0.870E-04
0.0249	3.959	3.542	0.536E-04
0.0263	3.933	3.482	0.316E-04
0.0277	3.904	3.420	0.375E-05
0.0292	3.876	3.387	-0.280E-04
0.0306	3.849	3.342	-0.709E-04
0.0320	3.822	3.259	-0.121E-03
0.0334	3.791	3.186	-0.153E-03
0.0348	3.760	3.137	-0.173E-03
0.0363	3.730	3.093	-0.190E-03
0.0377	3.700	3.060	-0.200E-03
0.0391	3.672	3.045	-0.194E-03
0.0405	3.645	3.033	-0.168E-03
0.0420	3.620	3.026	-0.127E-03
0.0434	3.597	3.041	-0.892E-04
0.0448	3.577	3.069	-0.562E-04
0.0462	3.559	3.086	-0.148E-04
0.0476	3.543	3.088	0.365E-04

EAST - CENTRAL U.S.

RCC TC ATL

LOVE WAVE

EVENT 11

F	C	U	GAMMA
0.0235	4.357	3.744	-0.567E-05
0.0249	4.316	3.714	0.161E-04
0.0263	4.277	3.683	0.402E-04
0.0277	4.241	3.653	0.688E-04
0.0291	4.207	3.619	0.102E-03
0.0306	4.174	3.580	0.138E-03
0.0320	4.142	3.553	0.169E-03
0.0334	4.113	3.558	0.185E-03

EVENT 12

F	C	U	GAMMA
0.0206	4.426	3.984	-0.371E-04
0.0220	4.392	3.869	-0.781E-04
0.0234	4.350	3.752	-0.107E-03
0.0249	4.308	3.686	-0.117E-03
0.0263	4.267	3.641	-0.110E-03
0.0277	4.229	3.605	-0.924E-04
0.0291	4.192	3.577	-0.672E-04
0.0305	4.158	3.559	-0.380E-04
0.0320	4.127	3.549	-0.918E-05
0.0334	4.098	3.554	0.124E-04
0.0348	4.073	3.576	0.183E-04

EVENT 13

F	C	U	GAMMA
0.0164	4.574	3.978	0.106E-03
0.0178	4.518	3.952	0.768E-04
0.0192	4.469	3.932	0.651E-04
0.0207	4.427	3.908	0.669E-04
0.0221	4.388	3.861	0.866E-04
0.0235	4.350	3.794	0.122E-03
0.0249	4.311	3.724	0.175E-03
0.0264	4.272	3.667	0.232E-03
0.0278	4.235	3.625	0.284E-03
0.0292	4.199	3.584	0.332E-03
0.0306	4.164	3.541	0.379E-03
0.0320	4.131	3.506	0.417E-03
0.0335	4.099	3.495	0.431E-03

EVENT 14

F	C	U	GAMMA
0.0164	4.521	4.014	0.120E-03
0.0179	4.471	3.947	0.761E-04
0.0193	4.425	3.909	0.450E-04
0.0207	4.384	3.863	0.178E-04
0.0222	4.344	3.796	-0.659E-05
0.0236	4.304	3.746	-0.279E-04
0.0250	4.266	3.715	-0.395E-04
0.0264	4.231	3.683	-0.469E-04
0.0279	4.198	3.644	-0.534E-04
0.0293	4.164	3.622	-0.610E-04
0.0307	4.135	3.604	-0.572E-04
0.0322	4.107	3.588	-0.458E-04
0.0336	4.082	3.572	-0.315E-04

Appendix 3. On the inversion of surface-wave attenuation: the over-determined problem.

Suppose we have a set $\{b_i;\ i=1,\ m\}$ of m independent measurements of surface-wave (i.e. normal-mode) attenuation. Assume a $Q_\beta^{-1}(z)$ model consisting of n layers within each of which Q_β^{-1} is constant, independent of frequency. Let $\{x_j;\ j=1,\ n\}$ be that model. If $x_j^2 << 1$ for all j, then (Anderson and Archambeau, 1964) each observation b_i is a linear combination of the x_j:

$$\sum_{j=1}^{n} a_{ij}\, x_j = b_i \qquad i = 1,2,\ldots,m$$

or, in matrix notation,

$$A\,\underline{x} = \underline{b} \qquad \text{(A3.1)}$$

where A is a known, mxn matrix, and $\underline{x}$ and $\underline{b}$ are column matrices with n and m rows, respectively. When $m > n$, then (A3.1) is over-determined and may be solved by the customary method of least squares. That is, requiring the squared vector norm

$$s^2 = \left\| A\,\underline{x} - \underline{b} \right\|^2$$

to be a minimum leads to the relation

$$A^T A \underline{x} = A^T \underline{b} \qquad \text{(A3.2)}$$

which may be solved directly for $\underline{x}$ once $\underline{b}$ is given. (A^T is the transpose of A.)

There is no assurance, however, that the least-squares solution is physically plausible, i.e. that $x_j > 0$ for every layer j. And, indeed, in practice (A3.2) is usually unstable for attenuation problems (see also Knopoff, 1964), producing oscillating solutions in which, for most j, x_j and x_{j+1} are large in magnitude and opposite in sign. We therefore use a modification of (A3.2), sometimes called the method of 'damped least squares'(Levenberg, 1944; Marquardt, 1963), which has been used with considerable success in the numerical solution of non-linear problems. In particular, Julian (1970) recently employed the technique to obtain compressional-velocity models from travel-time data.

Assume an initial model $\underline{x}_0$ and define

$$\underline{\xi} = \underline{x} - \underline{x}_0 \qquad \text{(A3.3)}$$

$$\underline{\beta} = \underline{b} - A \underline{x}_0$$

We now seek to determine $\underline{\xi}$, the solution to

$$A\,\underline{\xi} = \underline{\beta} \tag{A3.4}$$

subject to the additional constraint that $\underline{x} = \underline{x}_o + \underline{\xi}$ be not too different from $\underline{x}_0$. This may be satisfied by requiring that our choice of $\underline{\xi}$ be such as to minimize

$$\sigma^2 = \left\| A\,\underline{\xi} - \underline{\beta} \right\|^2 + \alpha \left\| \underline{\xi} \right\|^2 \tag{A3.5}$$

The parameter α may be chosen freely, and is usually selected so that the two terms in the right-hand side in (A3.5) are comparable in magnitude. The requirement that σ^2 be a minimum leads to the well-posed problem

$$(A^T A + \alpha\, I_n)\,\underline{\xi} = A^T \underline{\beta} \tag{A3.6}$$

where I_n is the nxn identity matrix. Solution of (A3.6), together with (A3.3), leads to a model $\underline{x}$ that 'fits' the observations better than $\underline{x}_0$; i.e.

$$\left\| A\,\underline{x} - \underline{b} \right\|^2 \leq \left\| A\,\underline{x}_o - \underline{b} \right\|^2$$

(e.g. Levenberg, 1944). We note in passing that such a model $\underline{x}$ depends upon $\underline{b}$, $\underline{x}_0$, and α.

In practice, we have adopted the following procedure: (1) Assume a starting model $\underline{x}_0$. (2) Choose ξ_j (j=1,n) such that

$$\frac{\partial}{\partial \xi_k}\left[\sum_{i=1}^{m} w_i \left(\sum_{j=1}^{n} a_{ij}\xi_j - \beta_i\right)^2 + \alpha \sum_{j=1}^{n} \xi_j^2\right] = 0 \qquad k=1,\ldots,n$$

where a_{ij} are the components of the matrix A. This is equivalent to minimizing σ^2 in (A3.5), except for the weighting function w_i (i=1,m), taken equal to the reciprocal of the variance of the measurement error for the quantity b_i. (3) Calculate $\underline{x} = \underline{x}_0 + \underline{\xi}$. (4) Repeat (2) and (3) with $\underline{x}$ as the new starting model until either (a) $\left|a_{ij}\, x_j - b_i\right|^2 < 1/w_i$ for all i, or (b) $x_j < 0$ for some j.

Now let us suppose that x_j ($=Q_\beta^{-1}(z)$, z in layer j) is a function of frequency in some of the layers, i.e. $x_j = G_j(f)$, where G_j has a known functional form and depends explicitly on a small number of unknown parameters. The dependence of G_j on these parameters is not in general linear, however, so incorporation of the unknowns directly into the damped-least-squares scheme is not possible. Rather a suitable search process may be used for those parameters upon which G_j depends non-linearly or, alternatively, $G_j(f)$ may be approximated (Backus and Gilbert, 1968) by some linear combination of unknowns (e.g. a polynomial in f).

To illustrate, let us postulate a simple relaxation in layer j = r; i.e.

$$x_j \equiv G_j(f) = c_1 \frac{c_2 f}{1 + (c_2 f)^2}$$

for $j = r$. Clearly, $G_j(f, c_1, c_2)$ is linear in c_1 but not in c_2. Let us fix c_2. Now define

$$p_{ij} = \begin{cases} a_{ij} \dfrac{c_2 f_i}{1+(c_2 f_i)^2} & j = r \\ a_{ij} & \text{otherwise} \end{cases}$$

$$u_j = \begin{cases} c_1 & j = r \\ x_j & \text{otherwise} \end{cases}$$

where f_i is the frequency of the ith surface wave (normal mode). Then (A3.1) may be written in the form

$$P\,\underline{u} = \underline{b}$$

which can be solved in the manner outlined earlier, with some modifications.

As before, assume an initial model $\underline{u}_0$, (equivalently, $\underline{x}_0$). Let

$$\underline{v} = \underline{u} - \underline{u}_o$$

$$\underline{\xi} = \underline{x} - \underline{x}_o$$

$$\underline{\beta} = \underline{b} - P\,\underline{u}_o$$

Then requiring the quantity

$$\sigma^2 = \left\| P\,\underline{v}(f_o) - \underline{\beta} \right\|^2 + \alpha \left\| \underline{\xi}(f_o) \right\|^2$$

to be a minimum for some fixed frequency f_0 yields the relations

$$(P^T P + \alpha Q)\, \underline{v} = P^T \underline{\beta} \qquad \text{(A3.7)}$$

where the diagonal, nxn matrix Q is given by

$$q_{ij} = \begin{cases} \dfrac{c_2 f_i}{1+(c_2 f_i)^2}\, \delta_{ij} & j = r \\ \delta_{ij} & \text{otherwise} \end{cases}$$

and δ_{ij} is the (n-dimensional) Kronecker delta. Solving (A3.7) gives $\underline{v}$ and thus $\underline{x}$. This solution $\underline{x}$ depends upon the data $\underline{b}$, and upon c_2, $\underline{u}_0$, α and f_0. By choosing a second c_2, repeating the above steps, judiciously selecting yet another c_2, etc., it is possible to determine a 'best' value for c_2 and the resulting solution $\underline{x}$.

Appendix 4. Determination of relaxation parameters from travel-time delays and differential attenuation.

We wish to determine the relaxation strength $\Delta\mu$ and the relaxation time τ of a hypothetical relaxation-process in the lower asthenosphere, assuming that the differential attenuation δt_P^* and δt_S^* of long-period P and S waves, the travel-time delays δt_P and δt_S of, respectively, short-period P waves and long-period S waves, and the delay $\delta t_P'$ introduced to the travel time of a short-period P wave due only to passage (at vertical incidence) through the 'low-velocity zone' (as constrained by seismic-refraction data) are all known. Define $\delta t_P''$, $\delta t_S'$, and $\delta t_S''$ as in section 5.2. Let us then first express $\delta t_S'$ and $\delta t_S''$ in terms of $\delta t_P'$ and $\delta t_P''$.

If the 'low-velocity zone' (as 'seen' by short-period waves) is vertically homogeneous (not a bad assumption considering the uncertainties involved in deducing the parameters of a low-velocity layer from travel-time data) and is attributable to a single relaxation with peak frequency greater than 10 Hz, then we may write

$$\delta t_S' = \frac{h_1}{\beta_1}\left[(1-\Delta\mu_1)^{-1/2} - 1\right] \qquad (A4.1)$$

where h_1 is the thickness of the 'low-velocity zone' (as defined by short-period P waves), β_1 is the unrelaxed

shear-wave velocity in that zone, and the strength of the relaxation in the zone is given by

$$\Delta\mu_1 = \frac{3}{4}\left(\frac{\alpha_1}{\beta_1}\right)^2 \left[1 - \left(1 + \frac{\alpha_1\,\delta t'_P}{h_1}\right)^{-2}\right] . \qquad \text{(A4.2)}$$

α_1 is the unrelaxed P-wave velocity in the 'low-velocity zone', and is normally equated to the P-wave velocity in the 'lid'. Note that when $\Delta\mu_1$ is small relative to unity,

$$\delta t'_S \simeq \frac{3}{4}\left(\frac{\alpha_1}{\beta_1}\right)^3 \delta t'_P .$$

It is presumed that contributions to $\delta t''_P$ are confined to some depth interval (of thickness h_2) over which elastic properties at very high frequencies (i.e. frequencies above any relaxation-peak frequencies) are uniform. Then

$$\delta t''_S = h_2 \left\{ \left[\beta_2 + \left(\frac{\partial\beta}{\partial T}\right)_P \Delta T\right]^{-1} - \beta_2^{-1} \right\} \qquad \text{(A4.3)}$$

where β_2 is the (unrelaxed) shear-velocity that the layer would have if $\Delta T = 0$ and the 'temperature difference'

(relative to a mantle with $\delta t''_p = 0$) is given by

$$\Delta T = \frac{\alpha_2}{\left(\frac{\partial \alpha}{\partial T}\right)_p} \left[\left(1 + \frac{\alpha_2 \, \delta t''_p}{h_2} \right)^{-1} - 1 \right] . \qquad \text{(A4.4)}$$

The partial derivatives of velocity with respect to temperature (at constant pressure) may be taken from published ultrasonic measurements. [We have used the VRH values calculated for polycrystalline forsterite by Kumazawa and Anderson (1969).] It may seem grossly improper to assume that ΔT, α_2 and β_2 are constant throughout the depth interval h_2 over which temperature-induced lateral changes in velocity are significant. However, note that when

$$- \left(\frac{\partial \beta}{\partial T}\right)_p \frac{\Delta T}{\beta} \ll 1 \qquad \text{(A4.5)}$$

(which holds for $T < 1000^{\circ}K$), then

$$\delta t''_S \simeq - \left(\frac{\partial \beta}{\partial T}\right)_p \frac{h_2 \, \Delta T}{\beta_2^2} . \qquad \text{(A4.6)}$$

Further, if

$$-\left(\frac{\partial \alpha}{\partial T}\right)_P \frac{\Delta T}{\alpha_2} \ll 1 \qquad \text{(A4.7)}$$

then

$$\delta t''_S \simeq \left(\frac{\alpha_2}{\beta_2}\right)^2 \frac{\left(\frac{\partial \beta}{\partial T}\right)_P}{\left(\frac{\partial \alpha}{\partial T}\right)_P} \delta t''_P \,. \qquad \text{(A4.8)}$$

We may approximate the upper mantle by a stack of layers within each of which velocity and temperature are constant. If (A4.5) and (A4.7) hold within each layer, then (A4.8) is still valid for the mantle as a whole as long as Poisson's ratio is approximately constant in the upper mantle and the derivatives of velocity with respect to temperature are approximately independent of pressure and temperature (this latter requirement is probably not strictly valid). Thus, from (A4.6), the quantities h_2 and ΔT in (A4.3) may be considered, respectively, the sum of the thicknesses of all layers in which lateral temperature-variations affect travel-time delays and the average (weighted by layer thickness) temperature excess, relative to an upper mantle for which $\delta t''_S = 0$, within these layers.

Suppose that δt_S has been suitably corrected by subtracting $\delta t_S'$ and $\delta t_S''$, given respectively by equations (A4.1) and (A4.3). Then the three quantities δt_S, $\delta t_S''$, and $\delta t_P''$ (all evaluated at roughly the same frequency) over-determine the two parameters $\Delta\mu$ and τ. We thus resort to a variation of the method of least squares to evalute these two parameters.

In terms of $\Delta\mu$ and τ, δt_S, δt_S^* (see equation 3.6) and δt_P^* may be written.

$$\delta t_S = \frac{h}{\beta_U}\left\{\left[1 - \frac{\Delta\mu}{1+(\omega\tau)^2}\right]^{-1/2} - 1\right\} \qquad \text{(A4.9)}$$

$$\delta t_S^* = \frac{\pi h}{\beta_U}\left[1 - \frac{\Delta\mu}{1+(\omega\tau)^2}\right]^{-1/2} \frac{\Delta\mu}{(1-\Delta\mu)^{1/2}} \frac{\omega\tau}{1+(\omega\tau)^2} \qquad \text{(A4.10)}$$

and

$$\delta t_P^* = \frac{4\pi h}{3\alpha_U}\left[1 - \frac{4}{3}\left(\frac{\beta_U}{\alpha_U}\right)^2 \frac{\Delta\mu}{1+(\omega\tau)^2}\right]^{-1/2} \left[\frac{\beta(\omega)}{\alpha(\omega)}\right]^2 \frac{\Delta\mu}{(1-\Delta\mu)^{1/2}} \frac{\omega\tau}{1+(\omega\tau)^2} \qquad \text{(A4.11)}$$

In writing (A4.9) through (A4.11) it has been assumed that the relaxation is uniform throughout a layer (the lower

asthenosphere) of thickness h; β_u and α_u are the unrelaxed shear-wave and compressional-wave velocities [we have taken $\beta_u = \beta_2 + \left(\partial\beta/\partial T\right)_P \Delta T$; similarly for α_u] ; $\beta(\omega)$ and $\alpha(\omega)$ are the shear-wave and compressional-wave velocities at the angular frequency ω , where $\omega/2\pi \simeq .1$ Hz.

If we make the approximate substitution

$$\frac{\beta(\omega)}{\alpha(\omega)} \simeq \frac{\beta_u}{\alpha_u}$$

in (A4.11), then each of the relations (A4.9) through (A4.11) may be rewritten to yield $\Delta\mu$ explicitly:

$$\Delta\mu = \left[1 + (\omega\tau)^2\right] \left\{1 - \left(1 + \frac{\beta_u}{h}\,\delta t_s\right)^{-2}\right\} \qquad \text{(A4.12)}$$

$$\equiv \Delta M_1$$

$$\Delta\mu = \left[1 + (\omega\tau)^2\right] \left\{\frac{1 + \frac{(\omega\tau)^2}{2} - \sqrt{\left[1 + \frac{(\omega\tau)^2}{2}\right]^2 - \left[1 + (\omega\tau)^2 - \left(\frac{\pi h}{\beta_u\,\delta t_s^*}\right)^2 (\omega\tau)^2\right]}}{1 + (\omega\tau)^2 - \left(\frac{\pi h}{\beta_u\,\delta t_s^*}\right)^2 (\omega\tau)^2}\right\} \qquad \text{(A4.13)}$$

$$\equiv \Delta M_2$$

and

$$\Delta\mu = \left[1+(\omega\tau)^2\right]\left\{\frac{1+\frac{4}{3}\left(\frac{\beta_v}{\alpha_v}\right)^2+(\omega\tau)^2-\sqrt{\left[1+\frac{4}{3}\left(\frac{\beta_v}{\alpha_v}\right)^2+(\omega\tau)^2\right]^2-\frac{16}{3}\left(\frac{\beta_v}{\alpha_v}\right)^2\left[1+(\omega\tau)^2-\frac{4}{3}\left(\frac{\beta_v}{\alpha_v}\right)^2\left(\frac{\pi h}{\alpha_v \delta t_p^*}\right)^2(\omega\tau)^2\right]}}{\frac{8}{3}\left(\frac{\beta_v}{\alpha_v}\right)^2\left[1+(\omega\tau)^2-\frac{4}{3}\left(\frac{\beta_v}{\alpha_v}\right)^2\left(\frac{\pi h}{\alpha_v \delta t_p^*}\right)^2(\omega\tau)^2\right]}\right\} \qquad \text{(A4.14)}$$

$$\equiv \Delta M_3$$

Assume τ is known. Then choose $\Delta\mu$ such that

$$s^2(\Delta\mu) = \sum_{i=1}^{3}(\Delta\mu - \Delta M_i)^2$$

is a minimum. (This criterion will give a 'best' estimate of $\Delta\mu$ only if $\Delta\mu$ is a normally-distributed random variable. Such is almost certainly not the case.) This is clearly satisfied by

$$\Delta\mu = \frac{1}{3}\sum_{i=1}^{3}\Delta M_i$$

Note that $s^2 = s^2(\Delta\mu, \tau)$. Thus we may change τ, recompute $\Delta\mu$ such that s^2 is minimized, and repeat this two-step sequence in some systematic fashion (we employed a binary-search routine) until we find $\Delta\mu$ and τ such that $s^2(\Delta\mu, \tau)$ is a minimum with respect to both parameters.

The quantities δt_S^*, δt_P^*, δt_S, $\delta t_P'$ and $\delta t_S'$

at the 14 U.S. stations studied are given in Table A4.1. Values of δt_S are from Hales and Roberts (1970). Values of $\delta t_P'$ were calculated from the compressional-velocity models indicated. At BKS and COR, because no mantle velocity-structures have yet been reported for California or western Oregon, we have assumed $\delta t_P'$ beneath these stations equals the average at other stations in western United States. [Nuttli and Bolt (1969) have proposed a rather extreme model, based on the azimuthal variation of travel-time residuals, for the low-velocity zone beneath California; we choose, however, not to adopt their model because the predicted value of $\delta t_P'$ (2.2 sec) at BKS seems high.] Values of $\delta t_S'$ were calculated using equations (A4.2) and (A4.1), with $\alpha_1 = 8.2$ km/sec and $\beta_1 = 4.6$ km/sec (if $\Delta T = 0$), and h_1 obtained from the compressional-velocity structure. Following the discussion of section 5.1, the parameter h in equations (A4.12) through (A4.14) was taken equal to 200 km.

Equations (A4.12) through (A4.14) presume knowledge of the absolute values of δt_S, δt_S^* and δt_P^*. In fact these quantities are known only to within addition of a constant; the 'baselines' are uncertain. Nonetheless these baselines must be estimated. We might, for instance, subtract from each value of δt_S the lowest value reported. This would be reasonable if the lowest delay-value were well-known; such is not the case. We have therefore

Table A4.1. Travel-time delays and differential attenuation used to compute relaxation parameters.

Station	δt_S^* sec	δt_P sec	δt_S sec	$\delta t_P'$ sec	$\delta t_S'$ sec
AAM	11.8	1.9	.99	.04[c]	.17
ALQ	8.8	4.7	5.31	.20[d]	.93
BKS	4.9	0[b]	6.46	.21[e]	.97
BOZ	11.2	1.9	6.14	.15[f]	.70
COR	7.0	1.5	6.57	.21[e]	.97
DUG	11.3	3.0	4.85	.15[f]	.70
FLO	0[b]	0[b]	1.85	.05[g]	.22
GEO	15.6	3.0	2.82	.04[c]	.18
LON	16.8	5.3	3.59	.31[h]	1.39
LUB	5.6	1.2	4.10	.19[d]	.88
RCD	3.8	3.2	0[b]	.20[f]	.92
SCP	8.6	1.9	2.73	.04[c]	.17
TUC	11.2	6.2	5.87	.30[h,i]	1.35
WES	18.2	3.8	3.23	.04[c]	.18
Baseline[a]	-8.0	-2.2	-4.20		

[a] must be added to each entry in column to agree with values as published or reported earlier

[b] calculated value negative; value set equal to zero for calculation of relaxation parameters

Table A4.1 (continued)

[c] model NC 1, Julian (1970)

[d] model NTS E1, Julian (1970)

[e] assumed (see text)

[f] model NTS NE1, Julian (1970)

[g] model ER 2, Green and Hales (1968)

[h] model NTS N3, Julian (1970), unrelaxed velocity = 8.0 km/sec

[i] similar to $\delta t_P^* = .28$ in model CIT204, Johnson (1967)

allowed some leeway in the choice of baselines, varying them until the average value of s^2 for our station-set appeared to be roughly a minimum. A crude constraint was that variations in δt_S^* and δt_P^* (and in δt_S and δt_P) baselines be approximately in the ratio of 4 to 1 (see section 3.5.2, also Hales and Roberts, 1970). The final baselines chosen are shown in Table A4.1. Note that a few of the values of δt_S, δt_S^* and δt_P^*, even after subtracting respective baselines, are still negative. This is attributed to measurement error; residuals with such negative values are arbitrarily set equal to zero.

Biographical Note

A product of the post-war baby boom, the author spent the days of his callow youth in megalopolis, California. It seemed only natural that he should gravitate toward what he thought the local epitome of erudition, California Institute of Technology. A nascent fascination with earth lore was there nurtured within the sepulchral walls of the Seismological Laboratory. Bachelor in geophysics in hand, this lad joined the eastern exodus in 1966, missing by one scant year the knell of the drill sergeant. With time out for love and time out for frivolity, the latter engendered in part by the opulent bestowals of the National Science and Hertz Foundations, the author eventually settled upon this present work. Fringe benefits of the trek include:

S.C. Solomon and M.N. Toksöz, On the density distribution in the moon, Phys. Earth Planet. Interiors, 1, 475-484, 1968.

S.C. Solomon and S. Biehler, Crustal structure from gravity anomalies in the southwest Pacific, J. Geophys. Res., 74, 6696-6701, 1969.

S.C. Solomon and M.N. Toksöz, Lateral variation of attenuation of P and S waves beneath the United States, Bull. Seismol. Soc. Am., 60, 819-838,1970.

S.C. Solomon, R.W. Ward, and M.N. Toksöz, Earthquake and explosion magnitudes: The effect of lateral variation

of seismic attenuation, to appear in the proceedings of the ARPA Symposium on Long-Period Multi-Azimuth Analysis, Woods Hole, Massachusetts, July 22-23, 1970.

S.C. Solomon, Surface-wave attenuation and partial melting in the asthenosphere (abstract), EOS, Trans. Amer. Geophys. Un., 51, 781, 1970.